

SHEAR WAVE

ECHOCARDIOGRAPHY

Mihai Strachinaru | THESIS

SHEAR WAVE ECHOCARDIOGRAPHY

Mihai Strachinaru

SHEAR WAVE ECHOCARDIOGRAPHY

Thesis

to obtain the degree of Doctor from the
Erasmus University Rotterdam
by command of the
rector magnificus

Prof.dr. R.C.M.E. Engels

and in accordance with the decision of the Doctorate Board.

The public defence shall be held on

Wednesday the 15th of January 2020 at 11:30 hrs

by

Mihai Strachinaru

born in Iasi, Romania

Erasmus University Rotterdam



DOCTORAL COMMITTEE:

Promotor: Prof.Dr.ir. A.F.W. van der Steen

Other members: Prof. Dr. P.P.T de Jaegere
Prof. Dr. Jan D'hooge
Prof. Dr. W.A. Helbing

Copromotors: Dr. ir. H.J. Vos
Dr. M.L. Geleijnse

CONTENT

Chapter 1	Introduction	7
PART 1		
Chapter 2	A simple, fast and reproducible echocardiographic approach to grade left ventricular diastolic function.	41
Chapter 3	Relation between E/e' ratio and NT-proBNP levels in elderly patients with symptomatic severe aortic stenosis	59
Chapter 4	Determinants of changes in pulmonary artery pressure in patients with severe aortic stenosis treated by transcatheter aortic valve implantation	77
Chapter 5	In depth echocardiographic analysis of left atrial function in healthy adults using speckle tracking echocardiography and volumetric analysis.	95
Chapter 6	The mitral annular displacement by two-dimensional speckle tracking: a new tool in evaluating the left atrial function	113
Chapter 7	Repeated Echocardiograms do not provide Incremental Prognostic Value to Single Echocardiographic Assessment in Minimally Symptomatic Patients with Chronic Heart Failure: Results of the Bio-SHiFT Study	135
PART 2		
Chapter 8	Cardiac Shear Wave Elastography Using a Clinical Ultrasound System.	157
Chapter 9	Reproducibility of Natural Shear Wave Elastography Measurements.	179
Chapter 10	Naturally occurring shear waves in healthy volunteers and hypertrophic cardiomyopathy patients.	207
Chapter 11	Local myocardial stiffness variations identified by high frame rate shear wave echocardiography.	227
Chapter 12	Myocardial stretch post atrial contraction in healthy volunteers and hypertrophic cardiomyopathy patients.	247
Chapter 13	High Frame Rate echoPIV can Measure the High Velocity Diastolic Flow Patterns.	269
Chapter 14	DISCUSSION	275
	SUMMARY	299
	SAMENVATTING	307
	List of publications	317
	PhD portofolio	325
	Curriculum Vitae	331
	Acknowledgement	335



1

Introduction

Heart failure is a clinical syndrome defined by the presence of typical symptoms (breathlessness, fatigue, ankle swelling), induced by an underlying functional cardiac abnormality, that results in an insufficient pump function or high intracardiac pressures at rest or during exertion¹. Despite numerous advances in the prevention, diagnosis and treatment of cardiac disease that lead to dysfunction, heart failure still prevails in 1-2% of the adult population in high income countries, and up to 10% of people over 70 years of age, and accounts for high rates of mortality and hospitalization²⁻⁴.

However, recognizing the disease at this stage may be too late for possibly attempting a curative treatment that would restore the normal cardiac function. Before the clinical symptoms set on, patients do have unrecognized structural or functional abnormalities that prelude heart failure^{5,6}. Demonstrating such a structural (myocardial disease, valvular heart disease, etc.) or functional abnormality in the heart is thought to be essential to the early diagnosis and treatment. In the very early stages of the disease, such abnormality can be subtle or completely absent at rest, and present only during exertion, eliciting complicated investigations¹.

1. SYSTOLIC AND DIASTOLIC FUNCTION

It is very difficult to strictly define cardiac function^{1,7}. More than a simple pump, the heart is a very active organ, adapting its shape and activity to the needs of the body, and even interacting with other organs and systems via endocrine secretions. For a long time researchers have tried to understand the inner workings of this fascinating organ that is essentially keeping us alive⁸.

Contraction and relaxation of the cardiac myocyte are active processes, meaning that coupling and uncoupling of the myofibril bridges needs adenosine triphosphate (ATP)^{9,10}. Ischemia for example, thus the lack of ATP production, first impedes the active muscular relaxation and is manifested by acute diastolic dysfunction. Any prolonged ischemia would eventually also affect the systolic function¹¹.

The first aspect that is evident is the forward pump function, in other words, how much blood could be sent forward into the body, and how good this flow can be adapted to the needs of the body. This is a raw description of what we presently understand by systolic function¹².

The other side of the heart function is being able to adequately accommodate the filling flow coming from the body or the lungs, without limiting or obstructing the continuity of this flow. This is the diastolic function of the heart^{9,10,12}.

Much like the forward pump function, it is not only about the change in volume allowing a certain amount of blood to fill the cavities before the next ejection. It is also about the heart's ability to do this at an adequate rate and with minimal pressure rise, since the extracardiac inflow system is a low-pressure system without unidirectional valves. This means that any excessive rise in pressure would reflect backwards and limit the filling^{9,10,12}. Furthermore, the diastolic function varies in time, since it is conditioned by numerous active and passive factors.

2. CARDIAC CYCLE

The dynamic relation between contraction and relaxation, filling and emptying of the heart, represents a continuum that has been studied extensively and is named the cardiac cycle, arbitrarily divided in electrical, mechanical or volumetric aspects that do not perfectly superpose as there are interactions and overlapping between these aspects¹³. The temporal relationship of the events during this continuum is classically represented in the Wigger's diagram (Figure 1):

It is important to note that the pressure and volume continuously vary during this cycle, with the exception of a few time intervals where at least one of these variables remains stable. For example, the only period when there is very little variation in pressure and volume is the end of diastasis, i.e., right before the atrial contraction. Also, during the isovolumetric periods very rapid build or decrease in pressure occurs without volume change, leading to rapid variation in parietal distension forces¹²⁻¹⁷.

To make this variability even more complex, the heart continuously interacts with the rest of the body through very complex regulation of the contractility (variation in heart rate and inotropic state), preload and load dependent increase in contractility (Frank Starling law), and afterload^{12,14-16}.

3. HEART SOUNDS

Heart sounds have been among the first physical signs investigated by modern semiology.^{12,18-23} Heart sounds are audible vibrations induced by the heart. The most

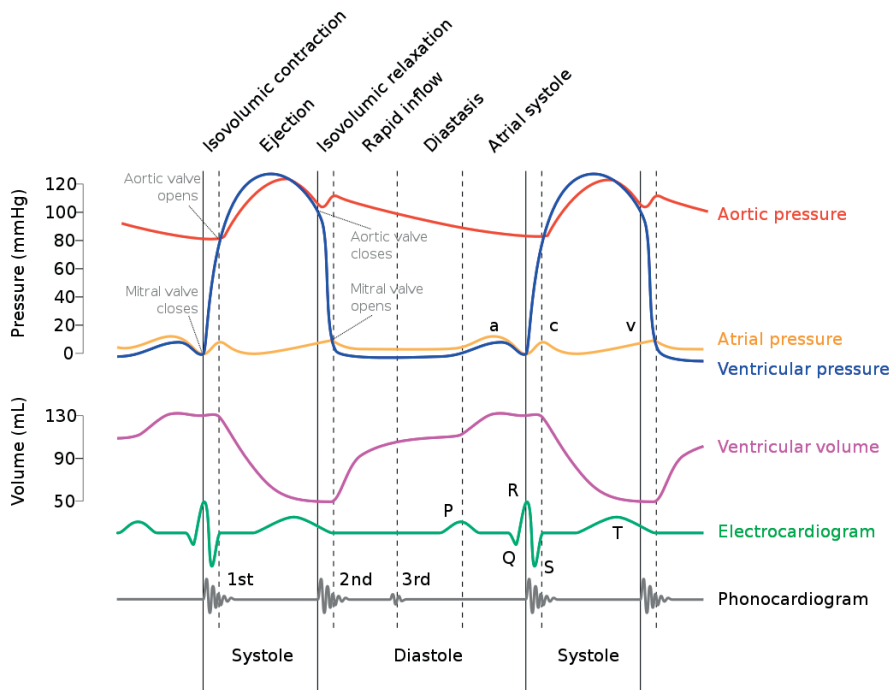


Figure 1. Classic Wigger's diagram for the left heart (Wiggers Diagram 2.svg. (2017, October 9). Wikimedia Commons, the free media repository. Retrieved 14:46, March 27, 2019 from https://commons.wikimedia.org/w/index.php?title=File:Wiggers_Diagram_2.svg&oldid=262202428). The heart cycle and the relation between ECG, heart sounds, volume and pressure in the left ventricle. Systole and diastole are defined according to the valve events. The diastole is further subdivided into isovolumetric relaxation, early filling, diastasis and atrial systole. The isovolumetric contraction is an early systolic event.

important components of these sounds are the valvular components, although other sounds may participate^{12,18,19} (turbulence of the blood flow, vibration of the heart walls, vibration of the aorta because of flow). In its turn, the valvular component is formed mainly by the closing of one heart valve, closely followed by the closing and opening of the other valves, in a sequence that is determined by the electrical activation and difference in pressures between the left and the right heart¹².

The first heart sound (S1) is mainly composed of the mitral valve closure, followed closely by tricuspid valve closure and successive opening of the pulmonary and aortic valves (M-T-P-A). Reciprocally, the second heart sound (S2) is formed by the closing of the aortic valve, followed by closure of the pulmonary and opening of the tricuspid and mitral valve (A-P-T-M)^{12,19}. The respective closing sound is provoked by the reverberation of the blood as the column of blood suddenly decelerates and is blocked by the valve^{18,19}.

The relation of the heart sounds with the flow and motion events in the left heart is depicted in Figure 2. Notice the presence of the two isovolumetric periods, between the closure of the mitral valve and opening of the aortic and respectively closure of the aorta and opening of the mitral valve. During these times pressure is changing rapidly, but volume remains virtually constant^{12,17}. Also notice that the isovolumetric contraction is slightly shorter than the relaxation. Also, as already noted by several authors, the closing of the mitral valve happens a lot later in relation to the QRS complex R wave on the electrocardiogram (ECG) than theoretically considered in the classical Wigger diagram^{13,20-23}.

Several studies looked at the delay between the actual valve snapping and the phonocardiography (PCG) tracing^{24,25}. This delay is expected to be short because of the velocity of sound in the tissue (1540 m/s in soft tissue²⁶), and was demonstrated to range under 3 ms for modern echocardiographic systems²⁴. In other words, any other event generated by the closing of the mitral or aortic valves should be seen as synchronous to the onset of the respective heart sounds. As will be seen in this thesis, the closing of the valves is a natural source of vibrations in the heart that can be analyzed and used to investigate the stiffness of the muscle.

4. QUANTIFYING THE HEART FUNCTION

The study of the evolution of intracavitary pressure during the cardiac cycle provides information about the dynamic relationship between preload (incoming pressure and volume), afterload (resistance to ejection) and chamber properties: contractility and compliance^{12,14,17}. During diastole, the heart remains closed with regard to the great arteries because the superior arterial diastolic pressure keeps the ventriculo-arterial valves closed¹². Compliance is the ability of the heart to distend and increase its inner volume simultaneous to the increase of transmural pressure^{12,17}. It is reciprocal to elastance, which would be the tendency of the heart to recoil to its initial volume after removing a distending force^{14,15,17}.

These last two reciprocal elastic properties of the cardiac chambers are very interesting, because although they are still influenced by loading conditions, they represent the inner properties of the heart walls. Diseases that affect directly the elastic properties of the heart muscle lead to a pathological reaction to incoming flow. Diastolic dysfunction of the ventricles however is the result of a combination of one or more factors: impaired relaxation (active process), reduction in the elastic recoil (restoring forces) and increased wall stiffness (structural damage)^{12,16}.

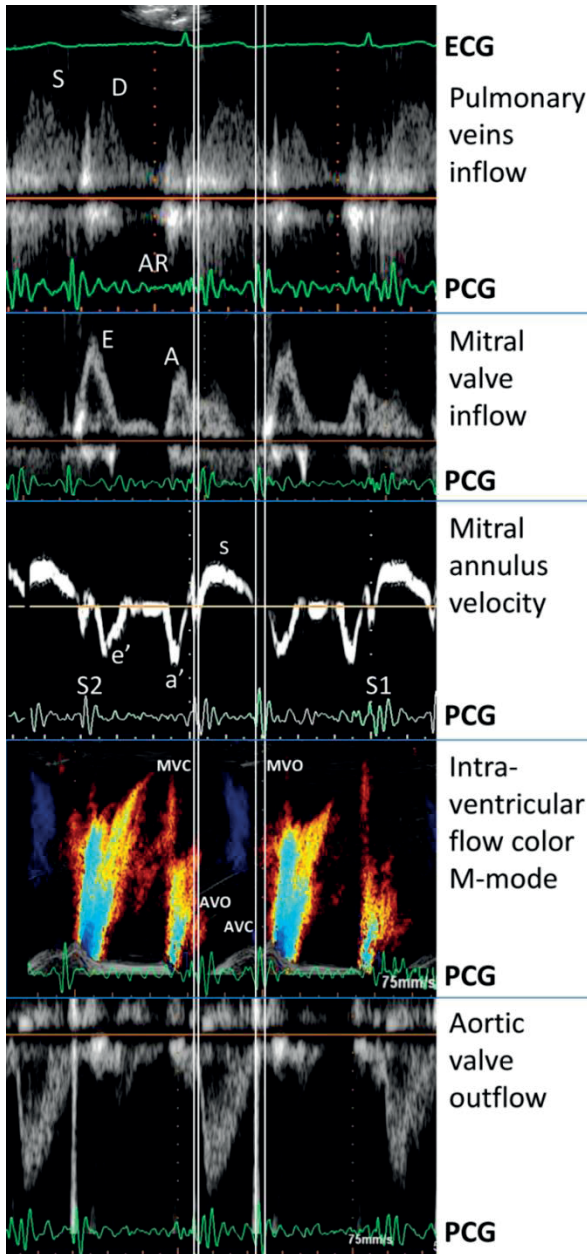


Figure 2. Relation between heart sounds and the events during the cardiac cycle in the left ventricle of a normal volunteer (Source: personal collection). Phonocardiography signal is amplified and unfiltered in order to increase sensitivity at the cost of an excess noise. The heart sounds are clearly defined (S1 and S2). The valvular events are marked with vertical lines, corresponding to the valve opening or closing clicks on the Doppler tracings (MVO: mitral valve opening; MVC: mitral valve closing; AVO: aortic valve opening; AVC: aortic valve closure). As has already been observed, mitral valve closure occurs much later than the peak of the QRS complex as presented in the Wigger diagram. Note also that isovolumetric contraction is shorter than the isovolumetric relaxation. In the upper panel the pulmonary venous inflow into the left atrium, with a forward systolic (S) and diastolic (D) phase and an atrial reversal (AR). Below the mitral inflow, with rapid filling (E) and atrial contraction (A). On the next panel, the medial annulus velocity measured with pulsed wave Tissue Doppler. The negative diastolic velocities e' and a' , corresponding to the filling phases during diastole, as well as the positive velocity in systole s' are visible. During the isovolumetric periods, velocity spikes correspond to the valvular events. Below is the color M-mode inflow of the left ventricle during diastole, and the aortic outflow in systole.

ECG: electrocardiogram; PCG: phonocardiogram.

The main parameter presently needed to classify heart failure patients is the left ventricle ejection fraction (LVEF= the relative volumetric variation to the maximal diastolic volume). According to the latest guidelines¹, it separates patients in three groups, from those with normal or preserved LVEF (LVEF \geq 50%), those with mid-range LVEF (LVEF

between 40-49%), and those with clearly reduced LVEF (LVEF<40%). In patients with preserved LVEF it is accepted that the diastolic dysfunction is the main cause for heart failure. There is however overlap between these groups, as patients with reduced LVEF also have diastolic dysfunction and patients with preserved LVEF have subtle abnormalities in the forward pump function that cannot be detected by measuring the LVEF¹.

Initially the heart function was characterized by using invasive pressure/volume loops, which can have a limited application in patients undergoing other invasive procedures, but cannot be used systematically in other patients^{12,14,17}. Invasive measurements remain the reference and gold standard for the evaluation of diastolic function¹⁶. Unfortunately, even the pressure/volume loops have their own limitations and are subject to a large variability, especially with loading conditions, but also with heart rate, chamber volume or inotropic state¹⁷. Another disadvantage would be that the elastic properties of the heart wall are indirectly calculated from the diastolic slope of the pressure/volume curve. This induces another possible error, if the tangent line is not a perfect fit. Moreover, given the indirect nature of this determination, this type of investigation gives global estimation of the elastic properties of the heart chambers, while ignoring local variations in stiffness¹⁷.

Noninvasive imaging on the other hand allows to precisely define deformation (change in shape and volume) and flow between cardiac chambers or between the heart and the great arteries^{1,7,27}.

Echocardiography is the first-line imaging investigation of the heart because of its low cost, repeatability, ease of access and lack of complications. It has been so in the last 50 years, and we owe to this method the largest part of our present-day understanding of *in-vivo* heart mechanics, physiology and pathology²⁸.

In real life volumes can be measured with acceptable precision in echocardiography. With present day 3D application, their change can be followed throughout systole and diastole⁷. However, measuring **the systolic heart function** with echocardiography is not simple. Simple volume changes cannot offer insight into the contractile forces needed to obtain it, nor the mechanical stress imposed to the left ventricular wall in the process. Extensive research has been directed recently to defining and establishing new parameters for the pump function that would perform better than the classical LVEF²⁹⁻³⁵. Even more so, LVEF precise measurements have moved more in the field of alternate imaging modalities such as magnetic resonance imaging (MRI) and computed tomography scanning (CT)^{27,36}.

The diastolic function can also be estimated with echocardiography. As we cannot directly measure the intracavitary pressures, the measurements rely on indices of flow in order to derive the pressure gradient between two cardiac chambers and between the heart and the body via its natural connections. This type of surrogate measure tries to replace the pressure sensor used in the gold standard pressure/volumes loops^{12,17}. As further detailed in the following chapter, tissue motion and deformation can also be estimated with echocardiography and integrated into the assessment of the diastolic function.

5. PRESENT DAY ALGORITHMS FOR DIASTOLIC FUNCTION EVALUATION WITH ECHOCARDIOGRAPHY

Although CMR and nuclear imaging may be used to estimate the filling rate of the left ventricle, the best modality of investigating the diastole is echocardiography, which is highly feasible, harmless, low cost, and can be used repetitively for follow-up¹⁶. Several indices of flow, as well as 2D measurements and tissue deformation form the basis of the present-day algorithm for diastolic function evaluation (Table 1 and Figure 2).

Table 1. Echocardiographic parameters of diastolic function (Adapted from Nagueh et al 2016)

Variable	Method	Abnormal values
E wave peak velocity (cm/s)	Pulsed wave Doppler mitral inflow	
A wave peak velocity (cm/s)	Pulsed wave Doppler mitral inflow	
E/A ratio	Pulsed wave Doppler mitral inflow	
MV DT	Pulsed wave Doppler mitral inflow	< 160 ms or > 200ms
e' peak velocity (cm/s)	Pulsed wave TDI mitral annulus	< 7 cm/s medial < 10 cm/s lateral
E/e'		14
LA index volume (mL/BSA)	Simpson biplane or 3D volume	> 34 mL/m ²
S wave velocity	Pulsed wave Doppler pulmonary veins	
D wave velocity	Pulsed wave Doppler pulmonary veins	
S/D	Pulsed wave Doppler pulmonary veins	S<D
AR duration	Pulsed wave Doppler pulmonary veins	AR>A
Vp (cm/s)	Color M-mode of mitral inflow	> 45 cm/s
E/Vp	Color M-mode of mitral inflow	≥ 2.5
TR velocity (m/s)	Continuous wave Doppler TR	>2.8 m/s

The approach to diastolic function assessment according to the latest guidelines comprises a few successive steps¹⁶: confirmation of the diastolic dysfunction, estimation of the LV filling pressures and of the degree of severity (degree of dysfunction).

Diastolic dysfunction is present if more than half of the following parameters meet the cut-off values: annular e' velocity septal < 7 cm/s and lateral < 10 cm/s; $E/\text{average } e' > 14$; LA volume index > 34 mL/m²; peak TR velocity > 2.8 m/s¹⁶. Diastolic function is normal if more than half the parameters do not meet the cut-off, but the result can also fall into the grey zone, where precisely half of the parameters meet the cutoff value³⁷.

If diastolic dysfunction is present, grading is performed according to a complicated algorithm¹⁶ (Figure 3).

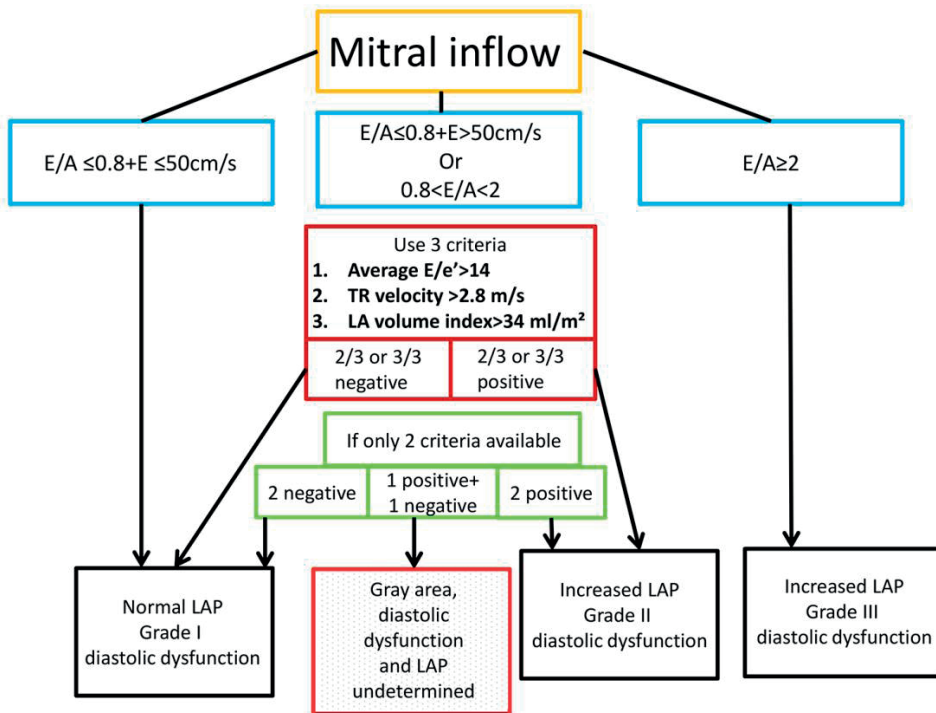


Figure 3. The algorithm for grading the diastolic function of the left ventricle according to the latest guidelines¹⁶ (Amended from Nagueh et al 2016, p.1335). In spite of the multiple parameters available, precise non-invasive determination of the diastolic pressures is currently impossible, and in certain conditions the diastolic function cannot be determined (“grey area”). LA: left atrium; LAP: left atrial pressure; TR: tricuspid valve regurgitation maximal velocity.

Beside these algorithms, new methods have been used to estimate the diastolic function: diastolic strain rate during the isovolumetric relaxation or early diastole, untwisting rate, and LA systolic strain^{7,16,27}. These modalities present several technical challenges making their reproducibility in real life insufficient for clinical use¹⁶. Diastolic strain rate displays a significant variability depending on the ultrasound system and the software used for analysis. LV untwisting depends on correct identification of the apical short

axis and is strongly influenced by loading conditions. LA strain remains challenging in patients with marked LA enlargement and important areas of echo dropout at the interatrial septum and pulmonary veins¹⁶.

Therefore, current echocardiographic evaluation of the diastolic function is based on the algorithm presented in Figure 3. This approach needs multiple parameters, and leaves room for undetermined situations. Recent multicenter studies have proven that the correlations of the individual indices with the intracardiac pressure is overall rather poor when taken individually, and only “fairly reliable” when used as part of an algorithm³⁸.

Invasive and non-invasive imaging estimate the diastolic function by looking at the consequences of the interaction between the elastic properties of the wall, pre-charge, post-charge and active relaxation, being also influenced by the relation between intra-pericardial and intrathoracic pressure.

We currently have no clinical modality to directly investigate the myocardial tissue elastic properties, which are primarily modified in disease states.

6. DEFORMATION, TISSUE ELASTIC PROPERTIES, STRESS AND STRAIN

The elasticity of a tissue refers to its property to deform reversibly under stress. Deformation of a tissue occurs under internal or external forces³⁹⁻⁴⁰. The deformation forces are different with respect to their direction (Figure 4).

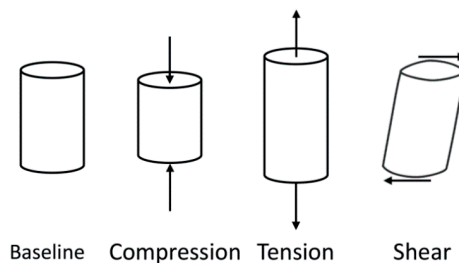


Figure 4. General deformation forces acting on a material (adapted after Wells RG 2013, p.885). Compression and tension are generated by opposite vectors acting in line with the longitudinal axis. Shear forces are induced by opposite vectors, but this time transversal to the longitudinal axis line.

These can be compression or tension forces (perpendicular on the surface) or shear forces (parallel to the surface). These forces induce a stress, defined as the force normalized to the area over which the force is exerted, or

$$\text{Stress} = \sigma = \frac{F}{A}. \quad (1)$$

Stress induces strain, which is the deformation per unit of length, or

$$\text{Strain} = \epsilon = \frac{\Delta L}{L}. \quad (2)$$

Plotting the stress σ versus the strain ϵ , as the deforming force applied is increased, produces a stress-strain diagram for the respective material. Generally elastic materials follow a sigmoid deformation (strain) curve when subjected to stress (tension), starting with a linear portion where relatively little deformation occurs. The last part of the sigmoid curve corresponds to the failure (rupture) of the material³⁹. Materials behave elastically if the strain disappears when the stress is removed (as do tissues), or plastically if the strain does not return to zero after removing the stress (permanent deformation).

Important properties of the material can be deduced from the stress/strain diagram, such as the elasticity modulus. If the deformation is relatively small, involving only the first linear portion of the curve, the relationship is described by Hooke's law³⁹:

$$\sigma = E \epsilon. \quad (3)$$

The coefficient E in this equation describes the relation between longitudinal deformation and strain of a homogeneous isotropic material (material whose properties are similar in all direction of deformation) and is called Young's modulus or elasticity modulus. Another important constant describing the properties of a given homogeneous material is the Poisson's ratio (ν). It is a measure of the Poisson's effect, in which a material that is stretched tends to get thinner in a direction transversal to the direction of deformation³⁹, i.e.

$$\nu = - \frac{\text{transversal strain}}{\text{axial strain}}. \quad (4)$$

If we consider simultaneous deformation in all spatial directions (volume change under pressure = compression), we have to introduce a new constant κ , known as bulk modulus. It is a measure of how a volume change relates to the compression in a material:

$$\kappa = - \frac{\Delta P}{\Delta V/V} = \frac{E}{3(1-2\nu)}. \quad (5)$$

The reciprocal of the bulk modulus is called the compressibility of the material. An ideal incompressible material would have an infinite bulk modulus (the denominator in

equation (5) becomes 0). In such a material the Poisson's ratio resulting from equation (5) $\nu = \frac{1}{2}$.

If the deformation forces act as opposite transversal vectors as depicted in Figure 4, the material is subjected to *shearing stress* (τ). The resulting deformation is a *shearing strain* (γ). Plotting τ versus γ will result in a shear stress-strain diagram for the respective material. As for normal (linear) stress and strain, the initial portion of the shear stress-strain diagram is a straight line. For this type of deformation equation (3) can be written:

$$\tau = G \gamma \quad (6)$$

This is equivalent to Hooke's law above, yet now for shearing stress and strain, and the constant G in this equation is called the *shear modulus*. Combining equations (1)-(6) will give us a relationship between the constants we introduced so far: E , ν and G :

$$G = \frac{E}{2(1-\nu)} \quad (7)$$

Materials whose properties depend upon the direction of the force are defined as anisotropic. An important form of anisotropic materials are the fiber-reinforced composite materials. This type of materials represents the closest the myocardial tissue⁴⁰.

Tissue is an elastic material that has much higher bulk compression modulus than shear modulus. Its Poisson's ratio is very close to 0.5 (it is nearly incompressible). Therefore, the relation between E and G resulting from equation (7) is approximately $E=3 G$ ³⁹. Soft tissues however are not perfectly elastic materials, as they display a viscoelastic behavior⁴⁰, that also varies nonlinearly with shear rate⁴¹. Adding this to their fiber-reinforced composite structure makes that live tissue needs very complex simulation models to study its behavior.

The result is that different soft tissues have different stiffness, and the same tissue can have a different stiffness under different stress conditions (hyperelasticity)^{41,43,44}. Deposition of excessive collagen (fibrosis) into a tissue is thought to induce an increase in stiffness (Figure 5)^{40,45,46}.

The *in vivo* elastic properties of the heart chambers are influenced by several components: an active component due to muscle contraction, a parietal tension derived from Laplace's law (this conditions the hyperelastic behavior of the myocardium) and an inert elasticity of the fully relaxed wall. The instantaneous value of myocardial stiffness is the

result of the interaction between these dynamic and static components, at any given moment during the heart cycle⁴⁷.

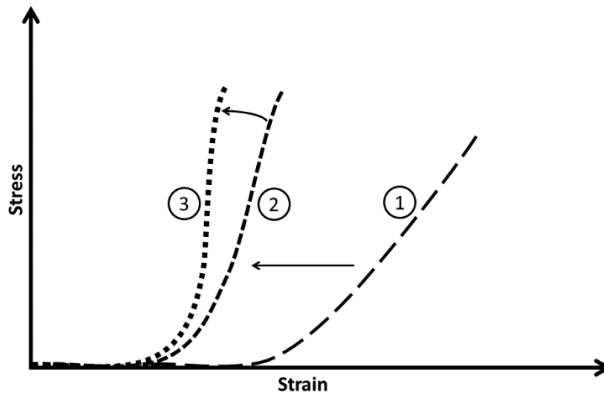


Figure 5. Relationship between shearing stress and shearing strain in the cardiac relaxed muscle (Source: personal collection), as resulting from experimental studies⁴⁴⁻⁴⁶: 1: normal conditions, the relation is more linear; 2: a stiffer muscle would have a more vertical slope; 3: in very stiff myocardium, the relationship follows a sigmoid curve, with an initial milder slope, followed by a very steep one. This sigmoid appearance is due to hyperelasticity (stiffness is not constant; it is a function of the applied stress^{41,43,44}). In normal conditions, the myocardium would never get to the point of material failure.

In the heart, diastolic deformation is induced by relatively low-pressure systems (the atria) and is restricted in the end by pressure equilibrium (the higher the equilibrium pressure the steeper the curve, see Figure 5), conditioned by the maximum distensibility of the heart walls. This in turn is dependent on cavity size, wall thickness, elastic/hyperelastic properties of the myocardium, and the pericardium⁴³⁻⁴⁶.

The passive elastic behavior of the myocardium when subjected to a multidimensional stress (similar to the *in vivo* conditions) is dependent on the bulk modulus κ and shear modulus G . These material-specific constants influence for example the propagation velocity of mechanical waves in the myocardium³⁹.

7. MECHANICAL WAVES AND ELASTOGRAPHY

Sound (and ultrasound) is a longitudinal wave, i.e. a succession of rarefactions and compressions propagating in the same direction as the local particle vibration. Opposite to this, particle vibration induced by a shear wave has a direction that is perpendicular to the direction of propagation^{42,48} (Figure 6). The propagation velocity of bulk shear waves in a material is related to the square root of the shear modulus G ⁴², whereas the speed of sound is proportional to the square root of the bulk modulus κ .

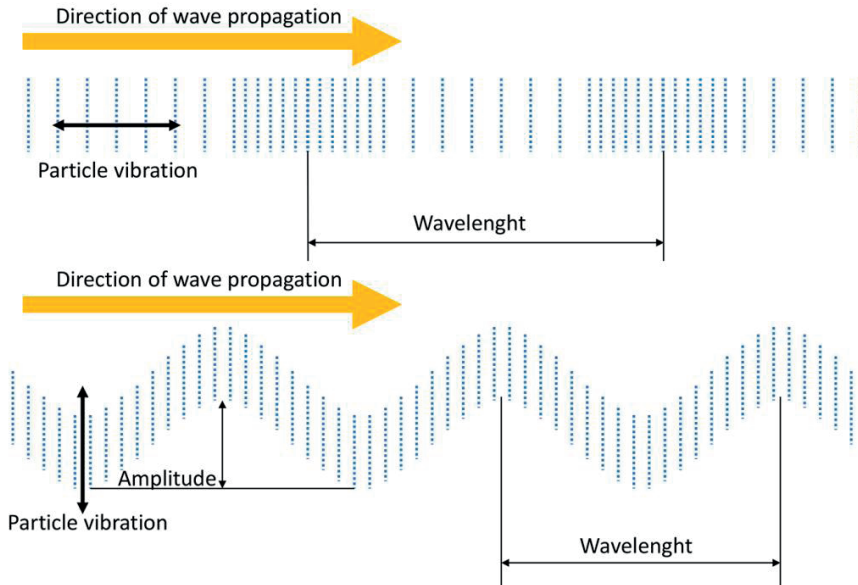


Figure 6. Longitudinal waves versus shear waves (source: personal collection). Longitudinal waves (upper panel) are formed by a succession of rarefactions and compressions propagating longitudinally, the local particle vibration being in line with the direction of propagation of the wave. Shear waves (lower panel) have a particle vibration that is perpendicular to their direction of propagation. This induces a local oscillation that has an amplitude (or a specific velocity of transversal displacement) and a specific wavelength.

Elastography is a relatively new direction in medical diagnosis aiming to display the biomechanical property of elasticity of a tissue^{42,48}. It relies in general on following a transient shear deformation that propagates in the tissue as shear waves. The generating force may be mechanical pressure or vibration, naturally occurring physiological motion or induced by a focused acoustic radiation force at a controlled depth. The internal shear deformation resulting from the applied external or internal force can be measured with an imaging method (ultrasound or MRI)⁴². If the external force varies slowly as in the case of probe palpation for parenchymatous organs it is considered quasi-static, and cannot provide direct quantification. By using dynamic forces, as vibrations or impulses, precise quantification becomes possible. Vibration is mostly used in MRI studies, where a continuous harmonic vibration is applied at the body surface^{42,48}. The usual approach in ultrasound elastography is tracking the shear wave that is induced by acoustic radiation force⁴².

The idea to use ultrasound for detecting the elastic properties of a tissue relies on the difference in propagation velocity between sound (ultrasound), which is between 1350-1600 m/s in soft tissue, and shear deformation waves which have a velocity range of 1-10 m/s^{42,48}.

By following the deformation induced by shear waves along a certain distance, usually along an M-mode line, we can determine the velocity of the shear wave, and thus indirectly the tissue stiffness (Figure 7).

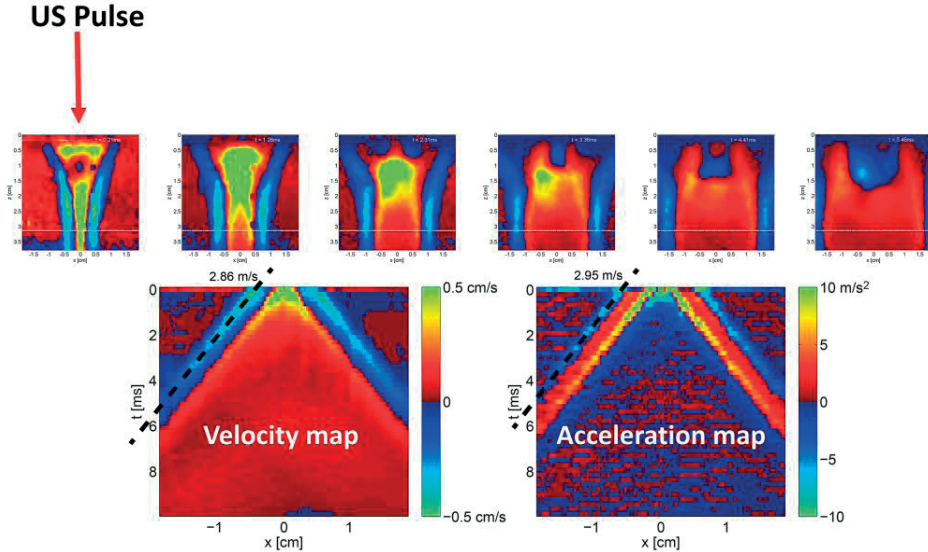


Figure 7. Shear wave induced by acoustic radiation force (US pulse) into a tissue phantom (modified from Vos et al 2016)⁴⁹. The shear wave propagates away from the focus region. Adding an M-mode line (dotted horizontal line in the upper panels) allows to reconstruct a velocity map (lower panel left). This can be converted to acceleration maps (lower panel right), where automatic tracking of the shear wave propagation is easier. The slope of this color pattern (dotted oblique lines in the lower panels) represents the propagation velocity of the shear wave.

Given the velocity range of the shear waves (1-10 m/s), in order to image their propagation we need a very fast image sampling rate, allowing to capture the wave as it travels in the tissue.

8. HIGH FRAME RATE IN ECHOCARDIOGRAPHY

A classical echography image (frame) is formed by successively scanning and adding adjacent lines (line-by-line scanning)⁵⁰. Frame rate represents the frequency at which each new full sector frame can be displayed. The main factor conditioning the frame rate in ultrasound imaging is the velocity of sound and the number of ultrasound transmissions needed to make the frame. At a depth of 15 cm in the apical window a return-trip takes about 200 μ s. So, at this depth, 5000 pulses could be emitted and analyzed every second. In order to reconstruct a 2D sector of 90° with one line per degree, we need 90

return-trips, thus $90 \times 200 \mu\text{s} = 18 \text{ ms}$. This means on average that around 50 frames can be created per second, giving a sufficient temporal resolution for the global major events visible in 2D, even more so as the human eye only can follow up to about 30 Hz frame rate. Of course, such a frame rate may prove largely insufficient when trying to image faster events, as already known in pulsed wave Doppler imaging where detection of high velocities may be hampered by aliasing.

The only way to increase the frame rate is by lowering the number of pulses required to construct a single frame. In a classical clinical ultrasound system, this can be achieved by decreasing the opening of the field-of-view, and thus preserving spatial resolution, or by reducing the line density at the cost of spatial resolution but potentially preserving the field-of-view⁵¹.

Another approach, already in use in currently-available systems is multiline acquisition (MLA). This means that several lines (their number constitutes the "MLA factor") are reconstructed from a single broader transmit beam, at the cost of a lower spatial resolution and lower signal-to-noise ratio⁵¹.

In tridimensional echocardiography, in addition to MLA techniques, retrospective gating is used. That means that the imaging volume is divided into subsectors, that are combined over several (usually 2 to 6) cardiac cycles in order to restore the full volume image at the best resolution achievable.

Research is presently directed to other ultrasound modalities allowing reconstructing images from sparse full-sector broad beams (plane or diverging unfocused beams). This allows for very high frame rates (maximum possible for the given depth), but with a lower spatial resolution and lower contrast than line-based scanning. In order to overcome this aspect, spatial compounding was proposed, by using a few number of transmit events from slightly different angles, thus limiting the frame rate but drastically improving resolution and contrast. However, as compared to focused beams, plane wave and diverging wave imaging make harmonic imaging very difficult, because the energy of the large beams generate lower amounts of harmonics⁵¹.

The possibility of reaching very high frame rates has until now remained in the field of echocardiography. High frame rate in MRI still refers to rates of around 50-60 frames/second⁵². However, due to the technological limitations (the need for the very strong coherent magnetic field generation), MRI does not yet seem able to reach the portability, ease of use and bedside characteristics of echocardiography. In the field of computed

tomography, obtaining higher frame rates has not been a goal, but rather an optimal compromise between frame rate and radiation dose⁵³.

9. TISSUE CHARACTERIZATION WITH ECHOCARDIOGRAPHY?

One of the important questions in heart imaging is precisely defining the type of tissue we are investigating. This means for example being able to differentiate a tumorous mass from the normal myocardium, a benign from a malignant tumor, normal from infarcted myocardium, or diagnose the presence of an infiltrative diffuse disease of the myocardium. This method is referred to as tissue characterization⁵⁴. This is mainly done today with MRI^{27,36,54}, though not exclusively, since computed tomography and nuclear imaging also provide information on tissue.

By using ultrasound reflection imaging alone, in the standard fashion used to make clinical echocardiography images, precise tissue characterization cannot be achieved. Some differences can be found in the signal intensity, as denser tissues are usually stronger reflectors, giving a high intensity signal, by reflecting a higher amount of the ultrasound wave at the interface with the surrounding structures. Also fluid gives an absence of echoes and a lens effect. Differences have been evoked between the speckle patterns of the cardiac muscle that would be suggestive for certain disease states, like the "granular sparkling" in cardiac amyloidosis⁵⁵. It is however not specific, and highly dependent on the echocardiography system and image settings. It is thus currently impossible for clinical cardiac ultrasound applications to determine with reasonable sensitivity and specificity the nature of two adjacent soft tissues with similar density.

Clinical tissue characterization by echocardiography is in great need of finding and exploiting other active phenomena, sufficiently different from the imaging forming one (as is the case for MRI), that could be detected and measured with ultrasound.

10. CHALLENGES OF SHEAR WAVE ELASTOGRAPHY OF THE HEART

Clinical tissue characterization by ultrasound is presently possible in various parenchymatous organs by elastography. Elastography by using shear wave imaging is already in use for numerous clinical applications, like liver fibrosis and breast, thyroid, prostate, kidney and lymph node imaging⁴². Several research groups have used external sources to induce shear waves in the myocardium⁵⁶⁻⁶⁴, demonstrating that diastolic myocardial stiffness can be determined using ultrasonic shear wave imaging^{63,64}. However it is not

clear if such investigation could be carried out reliably in everyday clinical patients, as the signal in these images can be quite noisy.

By using high frame rate experimental systems, it has been noted that during very short periods of the cardiac cycle, pulsatile waves would travel on the heart⁶⁵⁻⁶⁸, and these waves are caused by the impulse of the snapping valve on the mitral and aortic annuli which propagates within the cardiac wall (Figure 8).

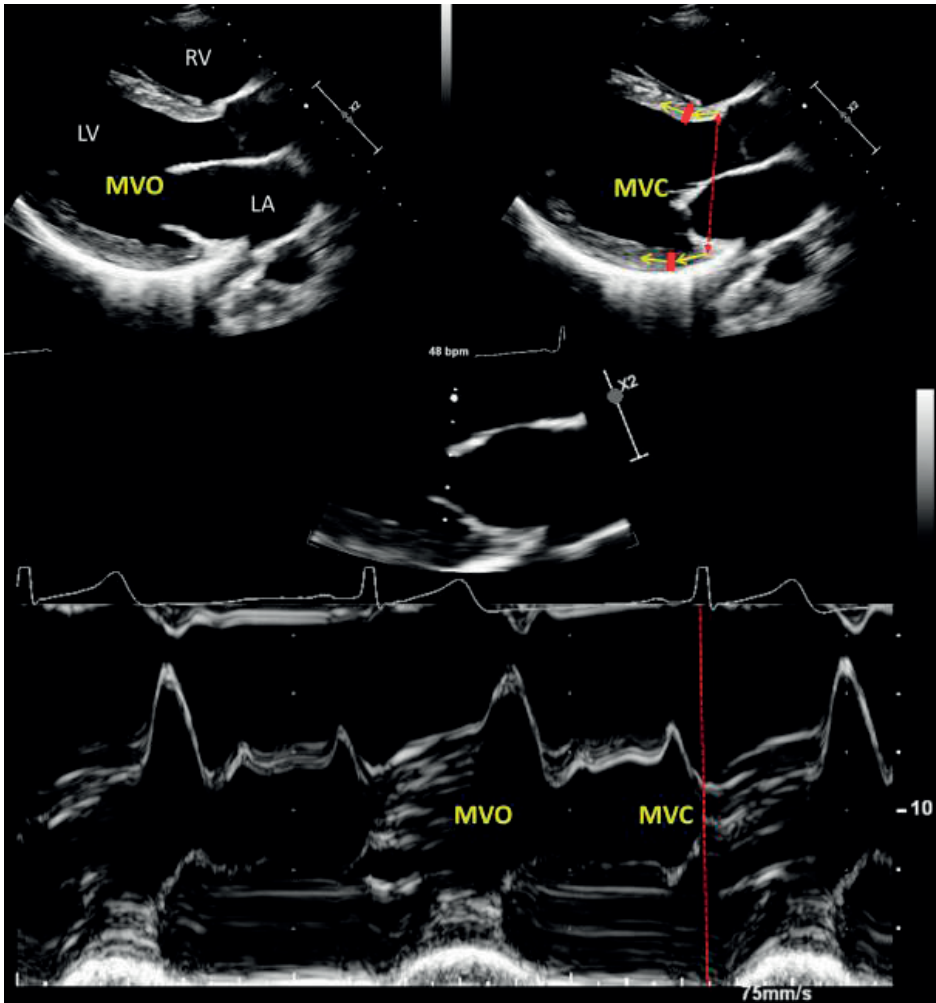


Figure 8. Theoretical model of the shear waves generated by the closure of the valves (source: personal collection). Upper panel: parasternal long axis view, with mitral valve open (MVO, left hand side image) and mitral valve closed (MVC, right hand side image). The closure of the mitral valve (lower panel, M-mode at the tips of the mitral valve as demonstrated in the central zoomed panel) induces a shear wave (red bands) appearing at the valvular annulus and coursing to the apex of the LV (yellow arrows).

Later studies demonstrated this type of waves to be a variation of Lamb waves⁶⁰⁻⁶², thus elastic waves that propagate in a medium with velocities that are theoretically dependent on the elastic properties of that medium⁶⁸⁻⁷¹. Such naturally-occurring shear waves could thus be tracked in order to investigate the stiffness of the cardiac tissue, as will be shown in this thesis.

These waves can even be seen as very brief events in classical color M-mode tracings (Figure 9). Color Tissue Doppler is a Duplex mode that has the advantage of coupling information on both local tissue velocity variation and effective tissue motion as visible on the underlying 2D/M-mode⁷²⁻⁷³. However, the preliminary observations using regular clinical systems and relatively low frame rates could not link these TDI events to naturally-occurring shear waves⁷².

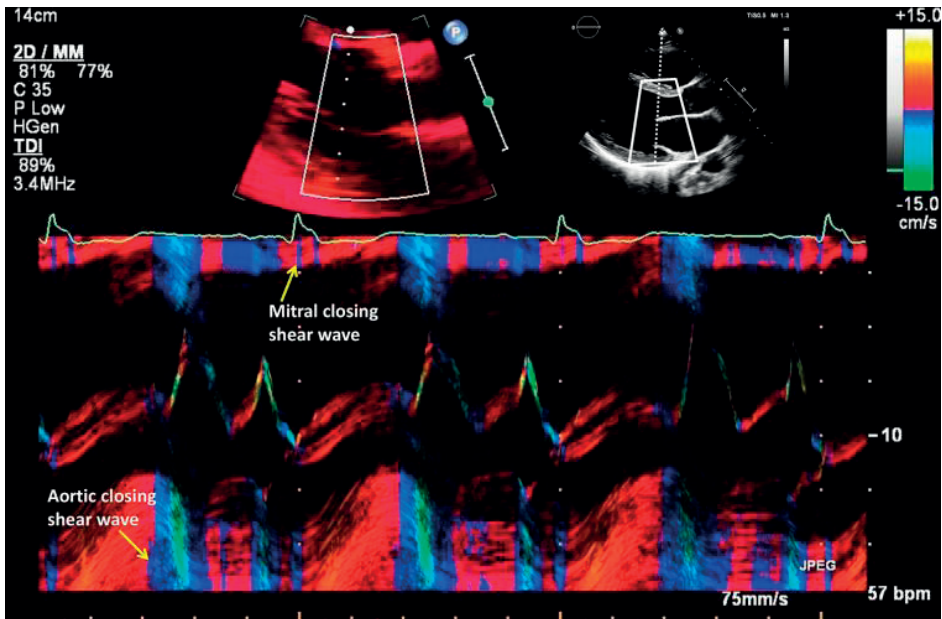


Figure 9. Clinical color TDI duplex mode in a normal volunteer (source: personal collection), with the TDI window focused on the left ventricle walls and the mitral valve (upper left and right panels). The M-mode line is traced through the mitral valve tips (upper panels). In the lower panel very short events can be visualized at the level of the LV walls at the closing of the aortic valve (not depicted in this image, but happening just before the opening of the mitral valve in M-mode) and just after the closing of the mitral valve (mitral valve shear wave).

A translation from research to a clinical application of shear wave imaging in the heart presents numerous challenges, that are discussed further.

- Theoretical and conceptual challenges

Although in other organs it has been possible to demonstrate that shear wave imaging can clearly discriminate pathology from normal tissue, allowing a noninvasive elastography of various organs, this is not yet as clear for the heart. One could assume that shear wave velocity should increase with increasing tissue stiffness, either diffusely in the whole heart or locally in case of myocardial scar. But the question is whether this difference in velocity is large enough to be exploited for clinical purposes.

The amplitude of the deformation (Figure 6) induced by the shear wave (the amplitude of the wave) should be large enough to be detected by the ultrasound system (velocity amplitude for a TDI system). Also, the frequency of these waves should be sufficiently high allowing a relatively short wavelength that can be measured precisely⁶⁵⁻⁶⁹.

- Imaging challenges

The heart is situated deeply in the thorax, at a distance ranging from 5 cm in the parasternal view up to 10-20 cm in the apical position⁷. To overcome the inherent attenuation of the ultrasound, lower-frequency probes are used to ensure penetration, yet also providing lower spatial resolution. Nonetheless, patient-specific attenuation can limit the imaging depth⁵⁰.

Also, large linear probes cannot fit between the intercostal spaces, the classical technical solution being the use of phased-array probes (Figure 10). This type of probes can cover a larger sector than the footprint of the probe itself, at the cost of a worse resolution in the far field as the lines diverge⁵⁰. Also, as explained earlier, the beam needs to cover a relative wide sector in order to achieve high frame rates, which also reduces penetration depth⁵¹.

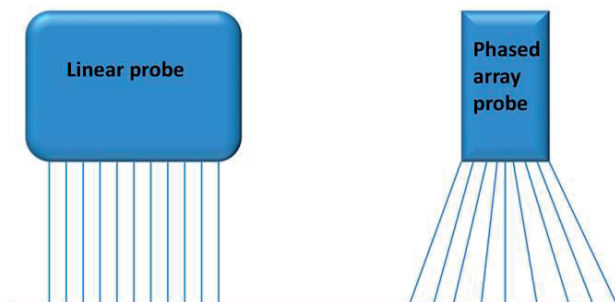


Figure 10. Difference between a linear probe and a phased-array probe (source: personal collection). Linear probes emit and receive along parallel lines. Near field and far field have the same width⁵⁰. Phased-array probes emit along slightly diverging lines, making the far field much wider than the near field, and the total opening much larger than the probe footprint. This also means that the resolution in the far field is significantly lower but can be improved by focusing.

A compromise has to be found between probe size and field of view, frequency and penetration depth, frame rate and image resolution. Until now, no clinical ultrasound application exists for cardiac elastography.

MRI has also been experimentally used for shear wave elastography of the heart^{74,75}, with promising results, but a clinical MRI cardiac elastography is not yet implemented.

- Physiological challenges

The heart is continuously moving with respect to the surrounding organs and the chest wall, displaying a complex tridimensional motion (rotation, translation, shortening and lengthening). Also, during the periods when the heart is relatively stationary or does not change volume, there is continuous variation in the intraparietal tension due to contraction/relaxation or flow exchange. Therefore the stiffness itself, hence the shear modulus, varies in time throughout the cardiac cycle^{76,77}, thus also changing the instantaneous shear wave velocity.

The behavior of the shear waves in the heart wall, be them externally induced or naturally-occurring, is not yet completely understood⁷⁷. The optimal position in which these waves would be visible is not clear, given the relation between their direction of propagation and the direction of local particle vibration, as presented above (Figure 6).

Also, mainly for the naturally-occurring shear waves, the closing of the heart valves happens during very short periods of the heart cycle in which other mechanical and electrical phenomena take place (see Chapter 2 and 3 of the Introduction). A challenge lies in separating these events from the shear waves themselves, which high frame rate imaging should be capable of distinguishing based on the exact timing of phenomena.

- Technical challenges

High frame rate imaging generates large amounts of data. Treating this data in real-time and constructing an image for live feed-back is currently impossible on any clinical ultrasound system by lack of computation power and too slow data flow. Also, adapted storage space with very fast access should be available. On the other hand, as stated above, the human eye can only interpret frame rates up to 30 Hz, indicating that the high frame rate data needs to be converted in-line to useful information with a refresh rate of 30 Hz at most.

Offline post processing needs fast data transfer and ideally automated tracking software in order to decrease measurement errors. Such software does not yet exist for cardiac applications.

- Clinical challenge

For clinicians the most important question is to show that there is actual benefit in quantifying shear waves velocities, and that it provides better sensitivity and/or specificity or it facilitates early recognition of a cardiac condition. Actually showing this benefit needs a large study population and a longitudinal design, as there is no noninvasive gold standard.

11. THESIS OUTLINE

In an effort to overcome the numerous challenges cited above, this thesis aims to prove that high frame rate echocardiography and cardiac shear wave imaging is feasible and can be used in order to detect local stiffness of the heart walls which would be clinically relevant. It is not the purpose of this thesis to propose a new engineering solution, since the scientific effort was more directed towards the clinical and pathophysiological perspective. Taking advantage of an unforeseen technical ability of a clinical ultrasound system, allowing us to readily reach a compromise between most of the aforementioned challenges, we aim to demonstrate the importance and the clinical message of shear wave imaging in the heart.

The thesis is divided into two main parts. The first part represents a series of clinical investigations covering the present day echocardiographic estimation of the diastolic function, aiming to demonstrate the unanswered questions or grey areas in the estimation of the diastolic function of the left ventricle. The second part presents a new way of looking at the diastolic properties of the left ventricle, by using high frame rate imaging, trying to fill in the gaps of our present algorithms.

Part one: clinical studies defining the challenge in assessing the diastolic function with present-day non-invasive methods.

In **Chapter 2** we discuss the present day algorithm for the grading of diastolic function, endorsed by the American Society of Echocardiography and European Association of Echocardiography (ASE/EAE) and compare it with a local modified algorithm.

One of the key parameters in diastology is the E/e' ratio. It represented a revolution in our understanding of the diastolic function based on more than filling patterns and flow indices. In **Chapter 3** we investigate the correlation between the septal, lateral and average E/e' ratio and the value of the N-terminal pro-hormone of brain natriuretic peptide (NT-proBNP) in a group of two-hundred-fifty consecutive symptomatic patients with severe aortic stenosis.

Elevated pulmonary artery pressure (PAP) is directly related to the diastolic function and is a strong predictor of adverse prognosis^{1,16}. In **Chapter 4** we assess the relation between PAP and clinical and echocardiographic parameters in the same group of elderly patients with severe aortic stenosis, and search for the determinants of the change in PAP after transcatheter aortic valve implantation (TAVI).

Left atrial size has been used as an important marker of diastolic function/dysfunction. Left atrial volume and function are considered more important than linear size. They are also important indices in our algorithms for diastolic function assessment. Left atrial dimensions and volume have been a matter of debate, leading to significant changes in the latest guidelines for chamber quantification⁷. This is investigated in **Chapter 5**.

Left atrial function can be studied not only by volume change, Doppler flow or TDI velocities, but also by annulus displacement, which may have an important role in the end-diastolic filling and generate sudden traction forces on the atrioventricular annulus and LV walls. **Chapter 6** looks at this pulling force of the left atrium on the mitral annulus from the left atrial perspective.

In clinical practice imaging is only a part of a very complex array of elements allowing estimation of the prognosis in heart failure patients. In **Chapter 7** we study the prognostic value of the echocardiographic parameters of diastolic dysfunction in the detection of clinical events in stable heart failure patients.

Part two: translational research for a new way of looking at the diastolic function of the heart, by using high frame rate imaging.

In **Chapter 8** we define and explain the method used, and validate it *in vitro* by using tissue phantoms.

Chapter 9 analyses the reproducibility and variability of the method. The results obtained with the clinical scanner (our method) and with an experimental system capable of reaching significantly higher frame rates are compared.

Shear waves should be able to detect a difference in myocardial stiffness, differentiating between normal and pathologically stiff myocardium. This is investigated in **Chapter 10**, in patients having diffuse myocardial disease.

By using shear wave elastography it is possible to resolve different tissue elastic properties. A local variation in stiffness has not yet been studied *in vivo*. In **Chapter 11** we investigated shear wave propagation in patients with myocardial scar.

The mitral annulus displacement with atrial contraction induces a wave-like phenomenon into the LV walls that was also proposed as a measure of left ventricular stiffness. By using our high frame rate TDI method in **Chapter 12** we investigate the wave-like pattern which travels over the interventricular septum after atrial contraction in patients with hypertrophic cardiomyopathy compared with healthy volunteers.

As described in the previous chapters, the stiffness of the heart is dynamic, and varies among others with the filling conditions. Intracardiac flow in diastole can also be followed by using high frame rate imaging. In **Chapter 13** we describe a new tracking algorithm of fluid dynamics in the left ventricle during diastole, taking advantage of the abilities of high frame rate echocardiography, this time using an experimental system able to image in 2D at very high frame rates (above 1000Hz), with full sector opening, adding a new perspective to our understanding of the diastolic function.

The overall results of the work are discussed in **Chapter 14**, with an overview of the future research and possible clinical applications, and a summary is provided afterwards.

REFERENCES

1. Ponikowski P, Voors AA, Anker SD, Bueno H, Cleland JGF, Coats AJS, Falk V, González-Juanatey JR, Harjola VP, Jankowska EA, Jessup M, Linde C, Nihoyannopoulos P, Parissis JT, Pieske B, Riley JP, Rosano GMC, Ruilope LM, Ruschitzka F, Rutten FH, van der Meer P; ESC Scientific Document Group. 2016 ESC Guidelines for the diagnosis and treatment of acute and chronic heart failure: The Task Force for the diagnosis and treatment of acute and chronic heart failure of the European Society of Cardiology (ESC) Developed with the special contribution of the Heart Failure Association (HFA) of the ESC. *Eur Heart J*. 2016;37(27):2129-2200. doi: 10.1093/eurheartj/ehw128.
2. Mosterd A, Hoes AW. Clinical epidemiology of heart failure. *Heart*. 2007;93(9):1137-46.
3. Bleumink GS, Knetsch AM, Sturkenboom MC, Straus SM, Hofman A, Deckers JW, Witteman JC, Stricker BH. Quantifying the heart failure epidemic: prevalence, incidence rate, lifetime risk and prognosis of heart failure The Rotterdam Study. *Eur Heart J*. 2004;25(18):1614-9.
4. van Riet EE, Hoes AW, Limburg A, Landman MA, van der Hoeven H, Rutten FH. Prevalence of unrecognized heart failure in older persons with shortness of breath on exertion. *Eur J Heart Fail*. 2014;16(7):772-7. doi: 10.1002/ejhf.110.
5. Wang TJ, Evans JC, Benjamin EJ, Levy D, LeRoy EC, Vasan RS. Natural history of asymptomatic left ventricular systolic dysfunction in the community. *Circulation*. 2003;108(8):977-82.
6. SOLVD Investigators, Yusuf S, Pitt B, Davis CE, Hood WB Jr, Cohn JN. Effect of enalapril on mortality and the development of heart failure in asymptomatic patients with reduced left ventricular ejection fractions. *N Engl J Med*. 1992;327(10):685-91.
7. Lang RM, Badano LP, Mor-Avi V, Afilalo J, Armstrong A, Ernande L, Flachskampf FA, Foster E, Goldstein SA, Kuznetsova T, Lancellotti P, Muraru D, Picard MH, Rietzschel ER, Rudski L, Spencer KT, Tsang W, Voigt JU. Recommendations for cardiac chamber quantification by echocardiography in adults: an update from the American Society of Echocardiography and the European Association of Cardiovascular Imaging. *Eur Heart J Cardiovasc Imaging*. 2015;16(3):233-70. doi: 10.1093/ehjci/jev014.
8. Bernard C. Lecture on the physiology of the heart and its connections with the brain, delivered at the Sorbonne, the 27th March, 1865. Tr. By J.S. Morel, Savannah, Purse.
9. Hall AC, Guyton, JE. *Textbook of medical physiology* (11th ed.). 2005; Philadelphia: W.B. Saunders. p. 106.
10. Pocock, Gillian. *Human Physiology* (Third ed.). 2006; Oxford University Press. p. 85.
11. Detry JM. The pathophysiology of myocardial ischaemia. *Eur Heart J*. 1996;17 Suppl G:48-52.
12. Lilly LS. *Pathophysiology of Heart Disease*. Philadelphia, PA: Lippincott Williams & Wilkins; 2011, pp 1-42, 220-248.
13. Mitchell JR, Wang JJ. Expanding application of the Wiggers diagram to teach cardiovascular physiology. *Adv Physiol Educ*. 2014;38(2):170-5. doi: 10.1152/advan.00123.2013
14. Gaasch WH, Battle WE, Oboler AA, Banas JS Jr, Levine HJ. Left ventricular stress and compliance in man. With special reference to normalized ventricular function curves. *Circulation*. 1972;45(4):746-62.
15. Maksuti E, Carlsson M, Arheden H, Kovács SJ, Broomé M, Ugander M. Hydraulic forces contribute to left ventricular diastolic filling. *Sci Rep*. 2017 Mar 3;7:43505. doi: 10.1038/srep43505.

16. Nagueh SF, Smiseth OA, Appleton CP, Byrd BF 3rd, Dokainish H, Edvardsen T, Flachskampf FA, Gilbert TC, Klein AL, Lancellotti P, Marino P, Oh JK, Popescu BA, Waggoner AD. Recommendations for the Evaluation of Left Ventricular Diastolic Function by Echocardiography: An Update from the American Society of Echocardiography and the European Association of Cardiovascular Imaging. *Eur Heart J Cardiovasc Imaging*. 2016;17(12):1321-1360.
17. Moscucci M, Grossman W. *Grossman's Cardiac Catheterization, Angiography and Intervention*. 8th ed. Philadelphia, PA: Lippincott Williams & Wilkins; 2013, pp. 467-486.
18. Turner JW. Observations on the Causes of the Sounds Produced by the Action of the Heart. *Trans Med Chir Soc Edinb*. 1828;3(Pt 1):205-229.
19. Leatham A. Splitting of the first and second heart sounds. *Lancet*. 1954;267(6839):607.
20. Goetz WA, Lansac E, Lim HS, Weber PA, Duran CM. Left ventricular endocardial longitudinal and transverse changes during isovolumic contraction and relaxation: a challenge. *Am J Physiol Heart Circ Physiol*. 2005;289(1):H196-201.
21. Golde D, Burstin L. Systolic phases of the cardiac cycle in children. *Circulation*. 1970;42(6):1029-36.
22. Konofagou EE, Provost J. Electromechanical wave imaging for noninvasive mapping of the 3D electrical activation sequence in canines and humans in vivo. *J Biomech*. 2012;45(5):856-64. doi: 10.1016/j.jbiomech.2011.11.027.
23. Costet A, Provost J, Gambhir A, Bobkov Y, Danilo P Jr, Boink GJ, Rosen MR, Konofagou EE. Electro-mechanical wave imaging of biologically and electrically paced canine hearts in vivo. *Ultrasound Med Biol*. 2014;40(1):177-87. doi: 10.1016/j.ultrasmedbio.2013.08.019
24. Walker A, Olsson E, Wranne B, Ringqvist I, Ask P. Time delays in ultrasound systems can result in fallacious measurements. *Ultrasound Med Biol*. 2002;28(2):259-63.
25. Curtiss EI, Matthews RG, Shaver JA. Mechanism of normal splitting of the second heart sound. *Circulation*. 1975;51(1):157-64.
26. Azhari H. *Basics of biomedical ultrasound for engineers*. Hoboken, NJ: John Wiley & Sons; 2010, p. 313.
27. Telles F, Marwick TH. Imaging and Management of Heart Failure and Preserved Ejection Fraction. *Curr Treat Options Cardiovasc Med*. 2018;20(11):90. doi: 10.1007/s11936-018-0689-9.
28. Edler I, Lindström K. The history of echocardiography. *Ultrasound Med Biol*. 2004;30(12):1565-644.
29. Reisner SA, Lysyansky P, Agmon Y, Mutlak D, Lessick J, Friedman Z. Global longitudinal strain: a novel index of left ventricular systolic function. *J Am Soc Echocardiogr* 2004;17:630 – 633.
30. Dalen H, Thorstensen A, Aase SA, Ingul CB, Torp H, Vatten LJ, Stoylen A. Segmental and global longitudinal strain and strain rate based on echocardiography of 1266 healthy individuals: the HUNT study in Norway. *Eur J Echocardiogr* 2010;11:176–183.
31. Voigt JU, Pedrizzetti G, Lysyansky P, Marwick TH, Houle H, Baumann R, Pedri S, Ito Y, Abe Y, Metz S, Song JH, Hamilton J, Sengupta PP, Kolias TJ, d'Hooge J, Aurigemma GP, Thomas JD, Badano LP. Definitions for a common standard for 2D speckle tracking echocardiography: consensus document of the EACVI/ASE/Industry Task Force to standardize deformation imaging. *Eur Heart J Cardiovasc Imaging* 2015;16:1 –11.

32. Yingchoncharoen T, Agarwal S, Popovic ZB, Marwick TH. Normal ranges of left ventricular strain: a meta-analysis. *J Am Soc Echocardiogr* 2013;26:185–191.
33. Mignot A, Donal E, Zaroui A, Reant P, Salem A, Hamon C, Monzy S, Roudaut R, Habib G, Lafitte S. Global longitudinal strain as a major predictor of cardiac events in patients with depressed left ventricular function: a multicenter study. *J Am Soc Echocardiogr* 2010;23:1019–1024.
34. Stanton T, Leano R, Marwick TH. Prediction of all-cause mortality from global longitudinal speckle strain: comparison with ejection fraction and wall motion scoring. *Circ Cardiovasc Imaging* 2009;2:356–364.
35. Haugaa KH, Dejagaard LA. Global Longitudinal Strain: Ready for Clinical Use and Guideline Implementation. *J Am Coll Cardiol*. 2018;71(18):1958-1959. doi: 10.1016/j.jacc.2018.03.015.
36. Messroghli DR, Moon JC, Ferreira VM, Grosse-Wortmann L, He T, Kellman P, Mascherbauer J, Nezafat R, Salerno M, Schelbert EB, Taylor AJ, Thompson R, Ugander M, van Heeswijk RB, Friedrich MG. Clinical recommendations for cardiovascular magnetic resonance mapping of T1, T2, T2* and extracellular volume: A consensus statement by the Society for Cardiovascular Magnetic Resonance (SCMR) endorsed by the European Association for Cardiovascular Imaging(EACVI). *J Cardiovasc Magn Reson*. 2017;19(1):75. doi: 10.1186/s12968-017-0389-8.
37. van Dalen BM, Strachinaru M, van der Swaluw J, Geleijnse ML. A simple, fast and reproducible echocardiographic approach to grade left ventricular diastolic function. *Int J Cardiovasc Imaging*. 2016. DOI 10.1007/s10554-015-0832-6
38. Lancellotti P, Galderisi M, Edvardsen T, Donal E, Goliash G, Cardim N, Magne J, Laginha S, Hagendorff A, Haland TF, Aaberge L, Martinez C, Rapacciuolo A, Santoro C, Ilardi F, Postolache A, Dulgheru R, Mateescu AD, Beladan CC, Deleanu D, Marchetta S, Auffret V, Schwammenthal E, Habib G, Popescu BA. Echo-Doppler estimation of left ventricular filling pressure: results of the multicentre EACVI Euro-Filling study. *Eur Heart J Cardiovasc Imaging*. 2017;18(9):961-968. doi: 10.1093/ehjci/jex067.
39. Beer F, Johnston R, Dewolf J, Mazurek, D. *Mechanics of materials*. 2009; New York: McGraw-Hill companies. P 51-58.
40. Wells RG. Tissue mechanics and fibrosis. *Biochimica et Biophysica Acta (BBA) - Molecular Basis of Disease*. 2013; 1832(7):884-890.
41. Storm C, Pastore JJ, MacKintosh FC, Lubensky TC, Janmey PA. Nonlinear elasticity in biological gels. *Nature*. 2005;435(7039):191-4.
42. Shiina T, Nightingale KR, Palmeri ML, Hall TJ, Bamber JC, Barr RG, Castera L, Choi BI, Chou YH, Cosgrove D, Dietrich CF, Ding H, Amy D, Farrokh A, Ferraioli G, Filice C, Friedrich-Rust M, Nakashima K, Schafer F, Sporea I, Suzuki S, Wilson S, Kudo M. WFUMB guidelines and recommendations for clinical use of ultrasound elastography: Part 1: basic principles and terminology, *Ultrasound Med Biol*. 2015;41:1126-47. doi: 10.1016/j.ultrasmedbio.2015.03.009
43. Haddad SM, Samani A. A novel micro-to-macro approach for cardiac tissue mechanics. *Comput Methods Biomech Biomed Engin*. 2017;20(2):215-229.
44. Holzapfel GA, Ogden RW. Constitutive modelling of passive myocardium: a structurally based framework for material characterization. *Philos Trans A Math Phys Eng Sci*. 2009;367(1902):3445-75. doi: 10.1098/rsta.2009.0091.

45. Weber KT. Cardiac interstitium in health and disease: the fibrillar collagen network. *J Am Coll Cardiol.* 1989;13(7):1637-52.
46. Villari B, Campbell SE, Hess OM, Mall G, Vassalli G, Weber KT, Kraysenbuehl HP. Influence of collagen network on left ventricular systolic and diastolic function in aortic valve disease. *J Am Coll Cardiol.* 1993;22(5):1477-84.
47. Strachinaru M, Bosch JG, van Gils L, van Dalen BM, Schinkel AFL, van der Steen AFW, de Jong N, Michels M, Vos HJ, Geleijnse ML. Naturally occurring shear waves in healthy volunteers and hypertrophic cardiomyopathy patients. *Ultrasound Med Biol.* 2019. doi: 10.1016/j.ultrasmed-bio.2019.04.004.
48. Parker KJ, Dooley MM, Rubens DJ. Imaging the elastic properties of tissue: the 20 year perspective. *Phys Med Biol.* 2011;56(1):R1-R29. doi: 10.1088/0031-9155/56/1/R01.
49. Vos HJ, van Dalen BM, Heinonen I, Bosch JG, Sorop O, Duncker DJ, van der Steen AF, de Jong N. Cardiac Shear Wave Velocity Detection in the Porcine Heart. *Ultrasound Med Biol.* 2017. pii: S0301-5629(16)30412-4. doi: 10.1016/j.ultrasmedbio.2016.11.015.
50. Stoylen A. Basic ultrasound for clinicians. http://folk.ntnu.no/stoylen/strainrate/Basic_ultrasound.
51. Cikes M, Tong L, Sutherland GR, D'hooge J. Ultrafast cardiac ultrasound imaging: technical principles, applications, and clinical benefits, *JACC Cardiovasc Imaging.* 2014;7:812-23. doi: 10.1016/j.jcmg.2014.06.004.
52. Coolen BF, Abdurrachim D, Motaal AG, Nicolay K, Prompers JJ, Strijkers GJ. High frame rate retrospectively triggered Cine MRI for assessment of murine diastolic function. *Magn Reson Med.* 2013;69(3):648-56. doi: 10.1002/mrm.24287.
53. Abbara S, Blanke P, Maroules CD, Cheezum M, Choi AD, Han BK, Marwan M, Naoum C, Norgaard BL, Rubinshtein R, Schoenhagen P, Villines T, Leipsic J. SCCT guidelines for the performance and acquisition of coronary computed tomographic angiography: A report of the society of Cardiovascular Computed Tomography Guidelines Committee: Endorsed by the North American Society for Cardiovascular Imaging (NASCI). *J Cardiovasc Comput Tomogr.* 2016;10(6):435-449. doi: 10.1016/j.jcct.2016.10.002.
54. Sharma V, Binukrishnan S, Schoepf UJ, Ruzsics B. Myocardial tissue characterization with magnetic resonance imaging. *J Thorac Imaging.* 2014;29(6):318-30. doi: 10.1097/RTI.0000000000000053.
55. Di Nunzio D, Recupero A, de Gregorio C, Zito C, Carerj S, Di Bella G. Echocardiographic Findings in Cardiac Amyloidosis: Inside Two-Dimensional, Doppler, and Strain Imaging. *Curr Cardiol Rep.* 2019;21(2):7. doi: 10.1007/s11886-019-1094-z.
56. Bouchard RR, Hsu SJ, Wolf PD, Trahey GE. In vivo cardiac, acoustic-radiation-force-driven, shear wave velocimetry. *Ultrason Imaging.* 2009;31(3):201-13.
57. Pernot M, Couade M, Mateo P, Crozatier B, Fischmeister R, Tanter M. Real-time assessment of myocardial contractility using shear wave imaging. *J Am Coll Cardiol.* 2011;58(1):65-72. doi: 10.1016/j.jacc.2011.02.042.
58. Hollender PJ, Wolf PD, Goswami R, Trahey GE. Intracardiac echocardiography measurement of dynamic myocardial stiffness with shear wave velocimetry. *Ultrasound Med Biol*, vol. 38, pp. 1271-1283, 2012.

59. Song P, Zhao H, Urban MW, Manduca A, Pislaru SV, Kinnick RR, Pislaru C, Greenleaf JF, Chen S. Improved shear wave motion detection using pulse-inversion harmonic imaging with a phased array transducer, *IEEE Trans Med Imaging*, 2013;32:2299–2310
60. Urban MW, Pislaru C, Nenadic IZ, Kinnick RR, Greenleaf JF. Measurement of viscoelastic properties of in vivo swine myocardium using lamb wave dispersion ultrasound vibrometry (LDUV). *IEEE Trans Med Imaging*. 2013;32(2):247-61. doi: 10.1109/TMI.2012.2222656.
61. Urban MW, Qiang B, Song P, Nenadic IZ, Chen S, Greenleaf JF. Investigation of the effects of myocardial anisotropy for shear wave elastography using impulsive force and harmonic vibration. *Phys Med Biol*. 2016;61(1):365-82. doi: 10.1088/0031-9155/61/1/365.
62. Vejdani-Jahromi M, Freedman J, Nagle M, Kim YJ, Trahey GE, Wolf PD. Quantifying Myocardial Contractility Changes Using Ultrasound-Based Shear Wave Elastography. *J Am Soc Echocardiogr*. 2017;30(1):90-96. doi: 10.1016/j.echo.2016.10.004.
63. Villemain O, Correia M, Khraiche D, Podetti I, Meot M, Legendre A, Tanter M, Bonnet D, Pernot M. Myocardial Stiffness Assessment Using Shear Wave Imaging in Pediatric Hypertrophic Cardiomyopathy. *JACC Cardiovasc Imaging*. 2017. pii: S1936-878X(17)30888-4. doi: 10.1016/j.jcmg.2017.08.018.
64. Villemain O, Correia M, Mousseaux E, Baranger J, Zarka S, Podetti I, Soulat G, Damy T, Hagège A, Tanter M, Pernot M, Messas E. Myocardial Stiffness Evaluation Using Noninvasive Shear Wave Imaging in Healthy and Hypertrophic Cardiomyopathic Adults. *JACC Cardiovasc Imaging*. 2018. pii: S1936-878X(18)30140-2. doi: 10.1016/j.jcmg.2018.02.002
65. Kanai H, Yonechi S, Susukida I, Koiwa Y, Kamada H, Tanaka M. Onset of pulsatile waves in the heart walls at end-systole, *Ultrasonics*. 2000;38:405-11.
66. Kanai H. Propagation of spontaneously actuated pulsive vibration in human heart wall and in vivo viscoelasticity estimation. *IEEE Trans Ultrason Ferroelectr Freq Control*, 52 2005:52:1931–1942.
67. Kanai H. Visualization of propagation of pulse vibration along the heart wall and imaging of its propagation speed. *Conf Proc IEEE Eng Med Biol Soc*. 2006;1:699-702.
68. Kanai H. Propagation of vibration caused by electrical excitation in the normal human heart. *Ultrasound Med Biol*. 2009;35(6):936-48. doi: 10.1016/j.ultrasmedbio.2008.12.013.
69. Brekke B, Nilsen LC, Lund J, Torp H, Bjastad T, Amundsen BH, Støylen A, Aase SA. Ultra-high frame rate tissue Doppler imaging, *Ultrasound Med Biol*. 2014;40:222-31. doi: 10.1016/j.ultrasmedbio.2013.09.012.
70. Konofagou EE, D'hooge J, Ophir J. Myocardial elastography--a feasibility study in vivo. *Ultrasound Med Biol*. 2002 Apr;28(4):475-82.
71. Konofagou E, Lee WN, Luo J, Provost J, Vappou J. Physiologic cardiovascular strain and intrinsic wave imaging, *Annu Rev Biomed Eng*. 2011;13:477-505.
72. Aase SA, Torp H, Støylen A. Aortic valve closure: relation to tissue velocities by Doppler and speckle tracking in normalsubjects. *Eur J Echocardiogr*. 2008;9(4):555-9. doi: 10.1093/ejecho-card/jen120.
73. Sutherland GR, Bijnens B, McDicken WN. Tissue Doppler Echocardiography: Historical Perspective and Technological Considerations, *Echocardiography*. 1999;16:445-453.

74. Elgeti T, Steffen IG, Knebel F, Hättasch R, Hamm B, Braun J, Sack I. Time-Resolved Analysis of Left Ventricular Shear Wave Amplitudes in Cardiac Elastography for the Diagnosis of Diastolic Dysfunction. *Invest Radiol*. 2016;51(1):1-6. doi: 10.1097/RLI.0000000000000198.
75. Liu Y, Royston TJ, Klatt D, Lewandowski ED. Cardiac MR elastography of the mouse: Initial results. *Magn Reson Med*. 2016;76(6):1879-1886. doi: 10.1002/mrm.26030.
76. Couade M, Pernot M, Messas E, Bel A, Ba M, Hagege A, Fink M, Tanter M. In vivo quantitative mapping of myocardium stiffening and transmural anisotropy during the cardiac cycle, *IEEE Trans Med Imaging*, 2011;30:295–305
77. Voigt JU. Direct Stiffness Measurements by Echocardiography: Does the Search for the Holy Grail Come to an End?. *JACC Cardiovasc Imaging*. 2018 Mar 9. pii: S1936-878X(18)30185-2. doi: 10.1016/j.jcmg.2018.02.004.

PART 1



A large, bold, dark grey number '2' is positioned on the right side of the page. It is partially overlaid by a solid grey rectangular shape that extends from the top right corner towards the center.

A simple, fast and reproducible echocardiographic approach to grade left ventricular diastolic function

Based on:

van Dalen BM, **Strachinaru M**, van der Swaluw J, Geleijnse ML. *A simple, fast and reproducible echocardiographic approach to grade left ventricular diastolic function*. Int J Cardiovasc Imaging. 2016; 32(5):743-52.

ABSTRACT

The American Society of Echocardiography and European Association of Echocardiography (ASE/EAE) have published an algorithm for the grading of diastolic function. However, the ability to use this algorithm effectively in daily clinical practice has not been investigated. We hypothesized that in some patients it may be difficult to grade diastolic dysfunction with this scheme, since there may be discrepancies in the assessed parameters. The aim of the current study was to test the feasibility of the ASE/EAE algorithm and to compare this with a new Thoraxcenter (TXC) algorithm. The ASE/EAE and TXC algorithms were applied to 200 patients. The ASE/EAE algorithm starts with assessment of diastolic myocardial wall velocities and left atrial (LA) volumes with subsequent assessment of E/A ratio, E-wave deceleration time and pulmonary venous flow. The TXC algorithm reverses these steps, uses LA dimension instead of volume and does not include a Valsalva manoeuvre and pulmonary venous flow. Due to inconsistencies between diastolic myocardial wall velocities and LA volumes and a not covered E/A ratio in the range of 1.5–2 it was not possible to classify 48 % of patients with the ASE/EAE algorithm, as opposed to only 10 % by the TXC algorithm. LA volume was always needed in the ASE/EAE algorithm. In only 64 % of patients LA size was necessary by the TXC algorithm. When LA volume would have been used instead of LA dimension, grading of LV diastolic function would have been different in only 2 % of patients without apparent improvement. Assessment of LA dimension was considerably faster than LA volume. The TXC algorithm to grade LV diastolic dysfunction was compared to the ASE/EAE algorithm simpler, faster, better reproducible and yields a higher diagnostic outcome.

INTRODUCTION

Heart failure is a major public health problem in developed countries [1]. Left ventricular (LV) diastolic dysfunction is one of the important mechanisms responsible for symptoms in patients with heart failure, irrespective of the presence or severity of systolic LV dysfunction [2]. It has been well established that diastolic dysfunction and filling pressures can be assessed by two-dimensional and Doppler echocardiography [3, 4]. The American Society of Echocardiography and European Association of Echocardiography (ASE/EAE) have published a guideline for the echocardiographic assessment of diastolic function in various clinical conditions [5]. This ASE/EAE guideline contains a practical algorithm for grading diastolic dysfunction (Fig. 1a). The ASE/EAE authors claimed that this algorithm was an important predictor of all-cause mortality in an earlier large cross-sectional survey [6]. However, the ability to use this algorithm effectively in daily clinical practice has not been investigated. We hypothesized that in some patients it may be difficult to grade diastolic dysfunction with this scheme, since there may be discrepancies in the assessed parameters. Therefore, the aim of this study was to test the feasibility of the ASE/EAE algorithm and to compare this with a newly proposed Thoraxcenter (TXC) algorithm (Fig. 1b).

METHODS

Study participants

The study population consisted of 200 consecutive patients (mean age 52 ± 15 year, 49 % female) referred for echocardiography in both a tertiary referral center ($n = 85$, Erasmus University Medical Center, Rotterdam, The Netherlands) and a smaller non-academical general hospital ($n = 115$, Sint Franciscus Gasthuis, Rotterdam, The Netherlands). Assessment of LV diastolic function had to be part of the echocardiography protocol and patients had to be in sinus rhythm. Athletes (international or national level of participation for at least 2 years) were excluded, as well as patients with hypertrophic cardiomyopathy, more than mild valvular disease, and a history of cardiac surgery.

In order to obtain a cut-off value for the ratio of peak early filling velocity (E) over mitral annulus early diastolic wave velocity (Em), 100 healthy control subjects (mean age 46 ± 14 year, female 49 %) in sinus rhythm, without hypertension, diabetes, or regular use of medication for cardiovascular disease, and with normal left atrial dimensions, LV dimensions, and LV ejection fraction were studied. Control subjects were recruited from our department (personnel) or were family members or friends. The institutional review board approved the study.

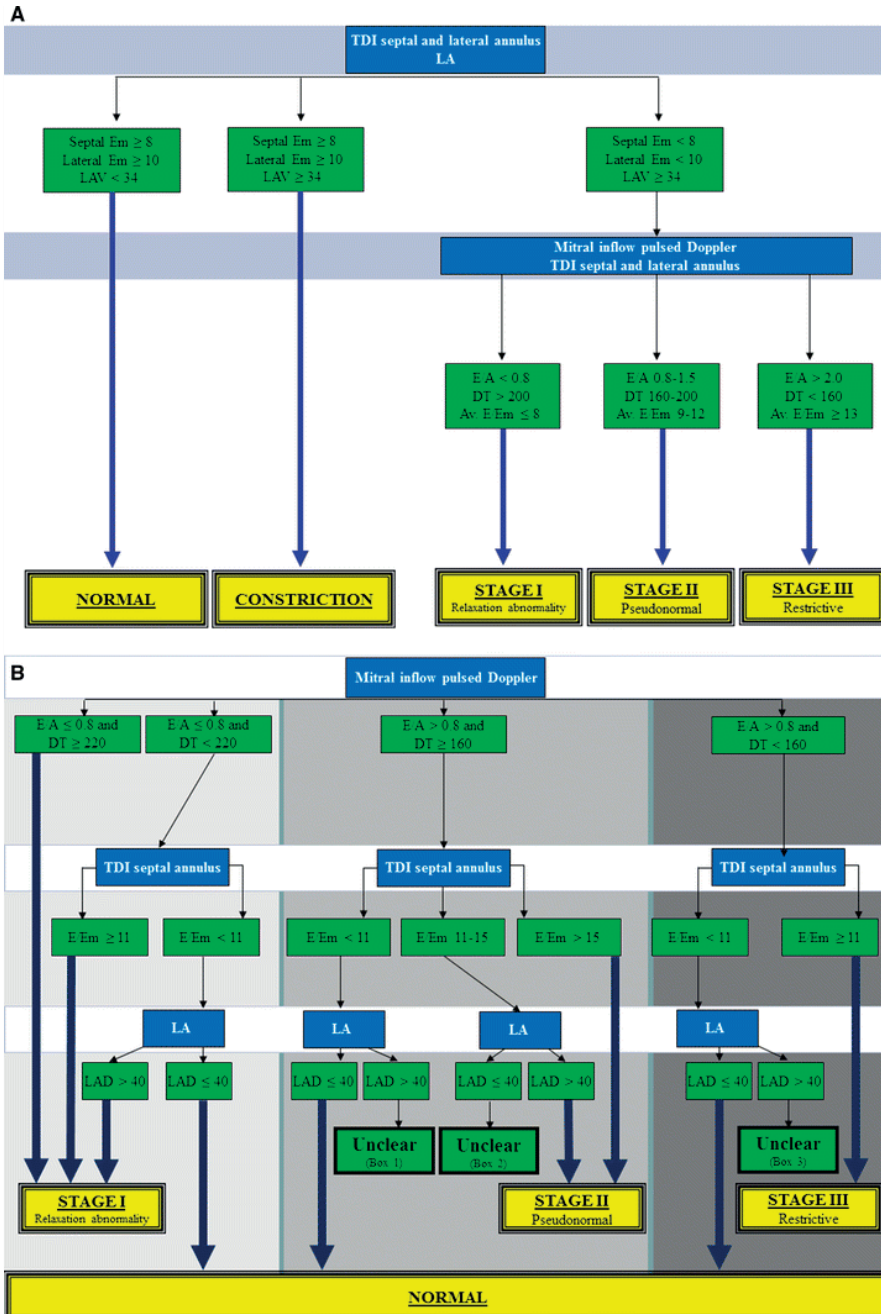


Figure 1. A. Grading of left ventricular diastolic function according to the ASE/EAE algorithm; **B.** Grading of left ventricular diastolic function according to TXC algorithm. E peak early filling velocity, A peak late filling velocity, DT E-velocity deceleration time, Em velocity of the mitral annulus early diastolic wave, TDI tissue Doppler imaging, LA left atrium, LAD left atrial dimension, LAV left atrial volume, Av averaged (from septal and lateral measurements)

Echocardiography

Two-dimensional grayscale harmonic images were obtained in the left lateral decubitus position using a commercially available ultrasound system (iE33, Philips, Best, The Netherlands), equipped with a broadband (1–5 MHz) S5-1 transducer (frequency transmitted 1.7 MHz, received 3.4 MHz). All echocardiographic measurements were averaged from three heartbeats. Left atrial (LA) dimension was measured as the anterior-posterior diameter in an end-systolic parasternal image. LA volume was calculated using the bi-plane area-length formula and indexed for body surface area [7]. From the mitral-inflow pattern, E and peak late (A) filling velocities, E/A ratio, and E-velocity deceleration time (DT) were measured. Tissue Doppler imaging was applied by placing the sample volume at the side of the medial (septal Em) and lateral annulus (lateral Em) in an apical 4-chamber view [8]. For the ASE/EAE algorithm both septal and lateral Em were needed, whereas for the TXC algorithm only septal Em was mandatory. Gain and filter settings were adjusted as needed to eliminate background noises and to allow for a clear tissue signal. To acquire the highest tissue velocities, the angle between the Doppler beam and the longitudinal motion of the investigated structure was adjusted to a minimal level. Em was recorded end-expiratory at a sweep speed of 100 mm/s.

Grading LV diastolic dysfunction

Two algorithms were used to grade diastolic dysfunction. The ASE/EAE algorithm was based on the scheme published in 2009 [5]:

- When septal Em was ≥ 8 cm/s, lateral Em ≥ 10 cm/s and/or LA volume < 34 ml/m² diastolic function was graded as normal.
- Since athletes were excluded, septal Em ≥ 8 cm/s, lateral Em ≥ 10 cm/s and/or LA volume ≥ 34 ml/m² suggested constriction, although other clinical variables should be considered as well in that case.
- When septal Em was < 8 cm/s, lateral Em < 10 cm/s and/or LA volume ≥ 34 ml/m² diastolic function was graded abnormal.

When it was not possible to grade diastolic dysfunction due to discrepancies in the assessed parameters, the exact reason was registered.

The newly proposed TXC algorithm was primarily based on the same study by Redfield et al. [6] that was used as the basis of the ASE/EAE algorithm. However, it starts with assessment of the E/A ratio and DT. Further subdivision was based on the E/Em ratio (using Em septal) and when necessary on LA dimension (rather than volume). E/Em ratio in the 100 healthy control subjects was 7.2 ± 1.9 , leading to a cut-off value of 11 (mean \pm 2SD).

- When the mitral E/A ratio was ≤ 0.8 and DT ≥ 220 ms diastolic function was graded as relaxation abnormality.

- When E/A ratio was ≤ 0.8 but DT was relatively short (< 220 ms) for relaxation abnormality, E/Em and LA dimension were used to differentiate between normal diastolic function (E/Em < 11 and LA ≤ 40 mm), and relaxation abnormality (E/Em ≥ 11 or E/Em < 11 but LA > 40 mm).
- When E/A ratio was > 0.8 and DT ≥ 160 ms, again E/Em and LA dimension were used to differentiate between normal diastolic function (E/Em < 11 and LA ≤ 40 mm), and pseudonormal diastole (E/Em 11–15 and LA > 40 mm or E/Em > 15).
- A short DT (< 160 ms) suggested restrictive filling. However, in healthy adolescents and young adults, there may be a marked contribution of active LV relaxation to LV filling, resulting in a short DT that resembles a restrictive LV filling pattern. Yet, in these subjects E/Em was supposed to be < 11 and LA dimension ≤ 40 mm.

In 50 randomly selected subjects the time needed to (offline) measure LA dimension and volume were assessed.

Statistical analysis

Continuous variables are presented as mean \pm SD and compared using Student's t test. In the 50 randomly selected subjects in whom the time needed to measure LA dimension and volume were assessed, reproducibility of measurements were tested. Measurement variability was calculated as the mean per cent error, defined as the absolute difference between the two sets of measurements, divided by the mean of the measurements.

RESULTS

Characteristics of the study population

In Table 1, the clinical and echocardiographic characteristics of the study population are shown. In 96 (48 %) patients it was possible to grade LV diastolic function by both algorithms. In only 2 out of these 96 patients there was a discrepant classification of LV diastolic function. According to clinical parameters such as age and final diagnosis, the newly proposed algorithm seemed to be correct in one patient (patient number 1, Table 2), while this is less obvious in the other patient, although both may be disputed. In the remaining 94 patients there was agreement with respect to classification of LV diastolic function by both algorithms. Normal diastole, relaxation abnormality, pseudonormal diastole and restrictive diastole in these latter 94 patients were found in 60, 19, 16, and 5 %, respectively.

Table 1. Clinical and echocardiographic characteristics of the study population

	Patients (n = 200)	Controls (n = 100)
Age (year)	52 ± 15	46 ± 14
Male, n (%)	101 (51)	51 (51)
Body surface area (m ²)	1.9 ± 0.2	1.9 ± 0.2
Heart rate, beats/min	74 ± 11	72 ± 15
Systolic blood pressure (mmHg)	126 ± 18	122 ± 15
Diastolic blood pressure (mmHg)	77 ± 9	71 ± 10
Indication echocardiography, n (%)		
<i>First echocardiogram</i>	68 (34)	
Chest pain	11 (6)	
Dyspnea	24 (12)	
Paroxysmal atrial fibrillation	8 (4)	
Cardiac murmur	8 (4)	
Post myocardial infarction	13 (7)	
Syncope/sudden cardiac death	4 (2)	
<i>Follow-up</i>	132 (66)	
Post myocardial infarction	31 (15)	
Heart failure	39 (19)	
Valve disease	27 (14)	
Miscellaneous	35 (17)	
Diastolic echocardiographic characteristics		
Left atrial dimension (mm)	41 ± 6	30 ± 5
Normalized left atrial volume (ml/m ²)	31.3 ± 10.4	23.1 ± 5.4
E-wave velocity (cm/s)	79 ± 20	66 ± 16
A-wave velocity (cm/s)	72 ± 18	52 ± 16
E/A ratio	1.1 ± 0.5	1.2 ± 0.5
E-velocity deceleration time, ms	203 ± 50	180 ± 36
Em septal (cm/s)	8.1 ± 2.7	9.6 ± 2.6
E/Em ratio	9.8 ± 4.6	7.2 ± 1.9

Values represent mean ± standard deviation. E-wave velocity = peak early phase filling velocity, A-wave velocity = peak late filling velocity, Em peak early diastolic wave velocity

Table 2. Patients with discrepant classification of left ventricular diastolic function by both algorithms

Number	LV diastolic function		Age (year)	Sex	Indication echocardiography	Clinical diagnosis	E/A ratio	E-velocity deceleration time (ms)	Em septal (cm/s)	E/Em ratio	Left atrial dimension (mm)	Normalized left atrial volume (ml/m ²)
	ASE/EAE	TXC										
1	Normal	Pseudonormal	73	Female	Follow-up mild aortic regurgitation	HFPEF	1.9	181	9.4	11.3	42	33
2	Relaxation abnormality	Normal	69	Male	Chest pain	4 year post MI, good systolic LVF	0.7	199	5.8	6.9	36	35

E/A ratio ratio of peak early over peak late filling, velocity, *Em* peak early diastolic wave velocity, *HFPEF* heart failure with preserved ejection fraction, *MI* myocardial infarction, *LV* left ventricular function, *ASE/EAE* American Society of Echocardiography and European Association of Echocardiography algorithm, *TXC* thoraxcenter algorithm

Feasibility of both algorithms to grade diastolic dysfunction

It was not possible to grade LV diastolic function in 48 % of patients by the ASE/EAE algorithm. In contrast, only 10 % of the patients were not classified by the newly proposed TXC algorithm ($P < 0.001$). The reasons for failure to qualify LV diastolic function are shown in Table 3. When there was failure to grade LV diastolic function by the ASE/EAE algorithm, moderate to severe LV diastolic function (according to the TXC algorithm) was relatively abundant: normal diastole, relaxation abnormality, pseudonormal diastole and restrictive diastole were seen in 32, 26, 32, and 10 % of patients, respectively.

Table 3. Reasons for failure to classify left ventricular diastolic function

ASE/EAE algorithm, n (%)	
Normal Em but increased left atrial volume*	16 (8)
Decreased Em but normal left atrial volume	47 (24)
Decreased Em and increased left atrial volume but E/A ratio 1.5–2.0	7 (4)
Decreased Em and increased left atrial volume but discrepant E/A ratio and DT	27 (14)
Total	97 (48)
TXC algorithm, n (%)	
Normal E/A, DT and E/Em but increased left atrial dimension (Unclear Box 1**)	12 (6)
Normal E/A, DT and left atrial dimension but E/Em in “gray zone” (Unclear Box 2**)	5 (3)
Normal E/A and E/Em but short DT and increased left atrial dimension (Unclear Box 3**)	2 (1)
Total	19 (10)

E/A ratio ratio of peak early over peak late filling velocity, *DT* E-velocity deceleration time, *Em* peak early diastolic wave velocity, *DT* E-velocity deceleration time. *ASE/EAE* American and European Associations of Echocardiography, *TXC* thoraxcenter

* No constriction, ** According to Fig. 1b

Feasibility of both algorithms was also tested for the control group. It was not possible to grade LV diastolic function in 18 % of the controls by the ASE/EAE algorithm, mainly due to discrepancy between E_m and LA volume (normal E_m but increased LA volume in 4 % and decreased E_m but normal LA volume in 10 %). Classification by the TXC algorithm was not possible in 4 % of the controls (2 in “Unclear Box 1”, 1 in “Unclear Box 2”, 1 in “Unclear Box 3”).

Use of LA dimension versus LA volume

In the total group of patients there was discrepancy in 11 patients (6 %) with respect to the cut-off values of LA dimension (40 mm) and volume (34 ml/m^2) used in the different algorithms. In 3 patients LA volume was $\geq 34 \text{ ml/m}^2$ whereas LA dimension was $< 40 \text{ mm}$. On the other hand, in 8 patients LA dimension was $\geq 40 \text{ mm}$ whereas LA volume was $< 34 \text{ ml/m}^2$.

LA volume was per protocol always needed to qualify LV diastolic function in the ASE/EAE algorithm. In 128 patients (64 %) LA size was necessary to classify LV diastolic function by the TXC algorithm. When LA volume (cut-off value 34 ml/m^2) would have been used instead of LA dimension (cut-off value 40 mm), grading of LV diastolic function by the TXC algorithm would have been different in only 3 patients (2 %) (Table 4). In two patients (patient number 1 and 3, Table 4), classification of LV diastolic function changed from unclear to normal, which in both patients may be correct. In the other patient (patient number 2, Table 4), use of LA dimension led to the seemingly correct diagnosis of pseudonormal LV diastolic function.

Table 4. Patients with different classification of left ventricular diastolic function when left atrial volume ($\geq 34 \text{ ml/m}^2$) was used instead of left atrial dimension ($\geq 40 \text{ mm}$)

Number	LV diastolic function		Age (year)	Sex	Indication echocardiography	Clinical diagnosis	E/A ratio	E-velocity deceleration time (ms)	Em septal (cm/s)	E/Em ratio	Left atrial dimension (mm)	Normalized left atrial volume (ml/m^2)
	LA dimension	LA volume										
1	Unclear (box 1*)	Normal	26	Male	Chest pain	Normal	1.0	169	9.7	7.6	45	28
2	Pseudonormal	Unclear (box 2*)	57	Male	Follow-up heart failure	DCM	0.9	170	4.5	11.6	47	32
3	Unclear (box 1*)	Normal	69	Male	Chest pain	Normal	0.9	216	7.7	9.3	43	29

E/A ratio ratio of peak early over peak late filling velocity, E_m peak early diastolic wave velocity, DCM dilated cardiomyopathy. * According to Fig. 1b

Finally, assessment of LA dimension ($6 \pm 4 \text{ s}$) was considerably faster as compared to assessment of LA volume ($40 \pm 12 \text{ s}$, $P < 0.001$).

Reproducibility

There was agreement between both observers in all subjects with respect to grading of LV diastolic function, irrespective of the algorithm used. The intra- and inter-observer variability of E/A ratio, DT, Em and E/Em were 4.8 ± 4.2 and 5.0 ± 4.4 %, 7.8 ± 5.2 and 8.4 ± 4.5 %, 5.0 ± 5.1 and 5.1 ± 4.4 %, and 5.9 ± 5.3 and 6.1 ± 4.9 %, respectively. Reproducibility of LA dimension was better as compared to LA volume: intra- and inter-observer variability 4.8 ± 4.0 and 5.8 ± 4.2 % versus 8.8 ± 6.3 and 9.1 ± 5.9 %, respectively.

DISCUSSION

The most important conclusion of the current study is that in daily practice it is not possible to feasibly use the algorithm endorsed by ASE/EAE for grading LV diastolic function. On the other hand, the proposed TXC algorithm did allow assessment of LV diastolic function in 90 % of consecutive patients in sinus rhythm in an efficient manner.

A gold standard of LV diastolic function is lacking in the current study. However, the ASE/EAE algorithm also had never been validated against an invasive evaluation of LV diastolic function, although it is based on numerous studies that did use invasive standards. Nevertheless, both algorithms are based on these same landmark studies. Importantly, it should be noted that in the 48 % of patients with possible grading of diastolic function with both algorithms, no essential differences were found. Therefore, it seems unlikely that the newly proposed TXC algorithm would have different prognostic power compared to the ASE/EAE algorithm.

Background of the ASE/EAE algorithm

The ASE and EAE have put commendable efforts in the publication in 2009 of a guideline for the echocardiographic assessment of diastolic function. It is an impressive document providing direction in this difficult aspect of echocardiography. Although it should be noted that the algorithm for qualification of diastolic function published in this guideline is supposed to be used in harmony with other potentially relevant parameters, the algorithm on itself does include several problems and inefficiencies.

Discrepancy between parameters (e.g. Em and LA volume or E/A ratio and DT) was the most important reason for failure to classify LV diastolic function. Also, an E/A ratio in the range of 1.5–2.0 is not covered in the algorithm, leading to unfeasibility to qualify some patients. In more recent studies, E/A ratio >1.5 was used as an indicator of stage III diastolic dysfunction [9, 10].

Septal and lateral Em and LA volume direct the primary differentiation between normal and abnormal LV diastolic function in the ASE/EAE algorithm to qualify LV diastolic function. The scientific background of the decision to create the algorithm in this manner was not fully elucidated in the paper in which the ASE/EAE algorithm was presented [5]. In the paper it was stated that the algorithm was based on findings of a large cross-sectional survey by Redfield et al. [6]. In this survey a combination of data from mitral inflow (E/A ratio and DT), tissue Doppler imaging (E/Em ratio) and pulmonary venous flow was used to qualify LV diastolic function. LV diastolic function was categorized as: *normal*; *mild* dysfunction, defined as impaired relaxation without evidence of increased filling pressures; *moderate* dysfunction, defined as impaired relaxation associated with moderate elevation of filling pressures or pseudonormal filling; and *severe* dysfunction, defined as advanced reduction in compliance or (reversible or fixed) restrictive filling. Redfield et al. based this classification on earlier publications by Nishimura [11] and Ommen et al. [12]. The study by Nishimura was a review from 1997, focusing on mitral inflow velocity curve patterns. Ommen et al. found the septal E/Em ratio to be the single best parameter for predicting mean LV diastolic pressure. However, from these studies, there seems to be no solid evidence in favour of using septal *and* lateral Em and in particular LA volume for the primary differentiation between normal and abnormal LV diastolic function. In fact, in 63 out of 200 patients in our study (see Table 3) there was a discrepancy between Em and LA volume, making it impossible to qualify LV diastolic function with this algorithm.

In the ASE/EAE algorithm, a cut-off value of 34 ml/m² was chosen to differentiate between normal and abnormal LV diastolic function. The decision to choose this cut-off value was supported in the ASE/EAE paper by a reference to a review by Abhayaratna et al. [13]. However, the only studies identified by Abhayaratna et al. that found a LA volume of 34 ml/m² to be the discriminatory threshold, were one case control study of atrial fibrillation in hypertrophic cardiomyopathy patients [14] and one study of subjects without a history of congenital heart disease, treatment with pacemaker implantation, valvular surgery, or cardiac transplantation, undergoing general medical consultation [15]. In the other 12 studies identified in this review cut-off values for LA volume ranging from 27 to 68 ml/m² were found, depending on the study population and the chosen endpoints. Furthermore, in the recommendation paper by Lang et al. [7], a LA volume >29 ml/m² was already considered abnormal, although this cut-off value has recently been adjusted to >34 ml/m² [16].

Background of the newly proposed TXC algorithm

For optimal application in daily clinical practice, any algorithm for qualification of LV diastolic function should be simple, fast and reproducible. The ASE/EAE scheme in-

cludes diastolic parameters that are more difficult to measure (less feasible) such as pulmonary venous flow. There is currently no evidence that assessment of these parameters is clinically relevant in a sense that they have independent incremental value over the more robust parameters for the assessment of LV filling pressures or overt heart failure. Therefore, in order to be as simple, fast and reproducible as possible, the newly proposed TXC algorithm did not include these LV diastolic function parameters.

Even more in-line with the aforementioned study by Redfield et al. [6], our algorithm starts with assessment of E/A ratio and DT. Since DT is normally between 160 and 220 ms [17] we used 220 ms as a cut-off value, instead of the 200 ms used in the ASE/EAE algorithm.

The E/Em ratio is known to correlate well with LV filling pressures [8]. Although either side of the mitral annulus can be used, septal E/Em has been shown to provide better diagnostic utility [18, 19], most likely because it is easier to align the tissue Doppler beam with the septal wall. For reasons of efficiency we decided therefore to use only the septal E/Em ratio. In two landmark papers in the field of E/Em ratio assessment [8, 12], different cut-off values for abnormal E/Em ratio have been reported. Ommen et al. [12] concluded that a septal E/Em ratio <8 suggests normal LV filling pressure, whereas >15 was highly specific for elevated LA pressure. Even though Nagueh et al. [8] found lateral Em to be slightly higher than septal Em, a lateral E/Em ratio >10 was already associated with increased LA pressure. Therefore, we have decided to define a normal value for E/Em ratio for our own department. Since E/Em was 7.2 ± 1.9 in healthy control subjects, a cut-off value of 11 (mean \pm 2SD) was chosen.

Increased LA size is associated with adverse cardiovascular outcomes [20] since it is a marker of increased LA pressure over time [21]. A large volume of prior clinical and research work used the two-dimensional derived antero-posterior linear LA dimension obtained from the parasternal long-axis view, making this the standard for linear LA measurement [7]. Evaluation of the LA in the antero-posterior dimension assumes that a consistent relationship is maintained between the antero-posterior dimension and all other LA dimensions as the atrium enlarges, which is sometimes not the case [7, 22]. Expansion of the LA in the antero-posterior dimension may for example be constrained by the thoracic cavity between the sternum and the spine. Therefore, it has been advocated to use 2D (or even 3D) volumes rather than the antero-posterior dimension although data that show the superiority of LA volumes are rather sparse [23, 24, 25, 26, 27, 28, 29, 30]. Nevertheless, in the present study we found that use of LA volume instead of LA dimension in the newly proposed TXC algorithm, would lead to a different classification of LV diastolic function in only 2 % of patients, without any evidence that it improves

the correct classification of diastolic function. Since measurement of LA dimension was considerably faster and better reproducible as compared to LA volume measurement, we have chosen to still use LA dimension in the routine application of grading of diastolic function. A Framingham Heart Study cohort of 1099 subjects between the ages of 20 and 45 years old who were not obese, were of average height and were without cardiovascular disease, identified an anteroposterior LA dimension of 27–40 mm as the normal range [31]. Therefore, we have chosen to use an anteroposterior LA dimension of 40 mm as a cut-off value.

Limitations

Validation of the new TXC algorithm against clinical outcome would be ideal. Yet, this was beyond the scope of the current paper but may be investigated in future studies. In order to represent daily clinical practice and to optimize feasibility of the new TXC scheme, further subdivision of abnormal diastolic function was only based on E/A ratio, DT, E/Em and LA dimension. In other words, although potentially helpful when there is discrepancy between different parameters, the relatively less used parameters “time difference between the pulmonary venous flow atrial reversal velocity waveform and mitral A-wave duration (Ar–A)” and “change of the E/A ratio with Valsalva maneuver (Val Δ E/A)” were not used. In future studies the incremental values of these variables should be shown before routine application may be advised. Also, when evaluating LV diastolic function, one may want to consider other echocardiographic variables such as the extent of LV hypertrophy, ejection fraction, ischemic wall motion abnormalities, and pulmonary pressure estimates. However, again, to optimize feasibility these parameters were not incorporated in the TXC algorithm, but of course each clinician should be free to use such variables as well when deemed necessary.

CONCLUSION

Assessment of LV diastolic function is an essential part of most echocardiograms, in particular when heart failure is suspected. The newly proposed TXC algorithm to grade LV diastolic dysfunction is compared to the ASE/EAE algorithm simpler, faster, better reproducible and yields a higher diagnostic outcome. Simpler because use of LA size was less needed (64 vs. 100 %) and when needed a dimension rather than a volume was measured, only the septal mitral annular velocity was measured and less useful parameters such as pulmonary venous flow and use of a Valsalva maneuver were not included in the algorithm. It is faster because of the aforementioned arguments and for example the diagnosis of LV relaxation abnormality requires only 2 measures (E/A ratio and DT) rather than 5 measures (E/A ratio, DT, septal Em, lateral Em and LA volume) in the ASE/

EAE algorithm. It is better reproducible because the intra- and inter-observer variability of the LA dimensions was lower compared to the LA volume and less parameters are involved. Finally, it yields better feasibility because a straight forward diastolic grade was defined in 90 % rather than 52 % of patients.

REFERENCES

1. Zarrinkoub R, Wettermark B, Wandell P et al (2013) The epidemiology of heart failure, based on data for 2.1 million inhabitants in Sweden. *Eur J Heart Fail* 15:995–1002
2. AlJaroudi WA, Alraies MC, Halley C et al (2013) Incremental prognostic value of diastolic dysfunction in low risk patients undergoing echocardiography: beyond Framingham score. *Int J Cardiovasc Imaging* 29:1441–1450
 Matsushita K, Minamishima T, Goda A et al (2015) Comparison of the reliability of E/E' to estimate pulmonary capillary wedge pressure in heart failure patients with preserved ejection fraction versus those with reduced ejection fraction. *Int J Cardiovasc Imaging* 31:1497–1502
3. Oh JK, Hatle L, Tajik AJ et al (2006) Diastolic heart failure can be diagnosed by comprehensive two-dimensional and Doppler echocardiography. *J Am Coll Cardiol* 47:500–506
4. Nagueh SF, Appleton CP, Gillebert TC et al (2009) Recommendations for the evaluation of left ventricular diastolic function by echocardiography. *J Am Soc Echocardiogr* 22:107–133
5. Redfield MM, Jacobsen SJ, Burnett JC Jr et al (2003) Burden of systolic and diastolic ventricular dysfunction in the community: appreciating the scope of the heart failure epidemic. *JAMA* 289:194–202
6. Lang RM, Bierig M, Devereux RB et al (2005) Recommendations for chamber quantification: a report from the American Society of Echocardiography's Guidelines and Standards Committee and the Chamber Quantification Writing Group, developed in conjunction with the European Association of Echocardiography, a branch of the European Society of Cardiology. *J Am Soc Echocardiogr* 18:1440–1463
7. Nagueh SF, Middleton KJ, Kopelen HA et al (1997) Doppler tissue imaging: a noninvasive technique for evaluation of left ventricular relaxation and estimation of filling pressures. *J Am Coll Cardiol* 30:1527–1533
8. Gillebert TC, De Pauw M, Timmermans F (2013) Echo-Doppler assessment of diastole: flow, function and haemodynamics. *Heart* 99:55–64
9. Kuwaki H, Takeuchi M, Chien-Chia Wu V et al (2014) Redefining diastolic dysfunction grading: combination of E/A ≤ 0.75 and deceleration time >140 ms and E/epsilon' ≥ 10 . *JACC Cardiovasc Imaging* 7:749–758
10. Nishimura RA, Tajik AJ (1997) Evaluation of diastolic filling of left ventricle in health and disease: doppler echocardiography is the clinician's rosetta stone. *J Am Coll Cardiol* 30:8–18
11. Ommen SR, Nishimura RA, Appleton CP et al (2000) Clinical utility of doppler echocardiography and tissue doppler imaging in the estimation of left ventricular filling pressures: a comparative simultaneous doppler-catheterization study. *Circulation* 102:1788–1794
12. Abhayaratna WP, Seward JB, Appleton CP et al (2006) Left atrial size: physiologic determinants and clinical applications. *J Am Coll Cardiol* 47:2357–2363
13. Yamaguchi K, Tanabe K, Tani T et al (2006) Left atrial volume in normal Japanese adults. *Circ J* 70:285–288
14. Tsang TS, Barnes ME, Gersh BJ et al (2002) Left atrial volume as a morphophysiological expression of left ventricular diastolic dysfunction and relation to cardiovascular risk burden. *Am J Cardiol* 90:1284–1289

15. Lang RM, Badano LP, Mor-Avi V et al (2015) Recommendations for cardiac chamber quantification by echocardiography in adults: an update from the American Society of Echocardiography and the European Association of Cardiovascular Imaging. *J Am Soc Echocardiogr* 28(1–39):e14
16. Khouri SJ, Maly GT, Suh DD et al (2004) A practical approach to the echocardiographic evaluation of diastolic function. *J Am Soc Echocardiogr* 17:290–297
17. Srivastava PM, Burrell LM, Calafiore P (2005) Lateral vs medial mitral annular tissue Doppler in the echocardiographic assessment of diastolic function and filling pressures: which should we use? *Eur J Echocardiogr* 6:97–106
18. Strachinaru M, van Dalen BM, Van Mieghem N et al (2015) Relation between E/e' ratio and NT-proBNP levels in elderly patients with symptomatic severe aortic stenosis. *Cardiovasc Ultrasound* 13:29
19. Tsang TS, Barnes ME, Gersh BJ et al (2003) Prediction of risk for first age-related cardiovascular events in an elderly population: the incremental value of echocardiography. *J Am Coll Cardiol* 42:1199–1205
20. Simek CL, Feldman MD, Haber HL et al (1995) Relationship between left ventricular wall thickness and left atrial size: comparison with other measures of diastolic function. *J Am Soc Echocardiogr* 8:37–47
21. Lester SJ, Ryan EW, Schiller NB et al (1999) Best method in clinical practice and in research studies to determine left atrial size. *Am J Cardiol* 84:829–832
22. Lim TK, Ashrafian H, Dwivedi G et al (2006) Increased left atrial volume index is an independent predictor of raised serum natriuretic peptide in patients with suspected heart failure but normal left ventricular ejection fraction: implication for diagnosis of diastolic heart failure. *Eur J Heart Fail* 8:38–45
23. Pritchett AM, Jacobsen SJ, Mahoney DW et al (2003) Left atrial volume as an index of left atrial size: a population-based study. *J Am Coll Cardiol* 41:1036–1043
24. Tsang TS, Abhayaratna WP, Barnes ME et al (2006) Prediction of cardiovascular outcomes with left atrial size: is volume superior to area or diameter? *J Am Coll Cardiol* 47:1018–1023
25. Wong GC, Marcotte F, Rudski LG (2006) Impact of chronic lisinopril therapy on left atrial volume versus dimension in chronic organic mitral regurgitation. *Can J Cardiol* 22:125–129
26. Delgado V, Vidal B, Sitges M et al (2008) Fate of left atrial function as determined by real-time three-dimensional echocardiography study after radiofrequency catheter ablation for the treatment of atrial fibrillation. *Am J Cardiol* 101:1285–1290
27. Maddukuri PV, Vieira ML, DeCastro S et al (2006) What is the best approach for the assessment of left atrial size? Comparison of various unidimensional and two-dimensional parameters with three-dimensional echocardiographically determined left atrial volume. *J Am Soc Echocardiogr* 19:1026–1032
28. Marchese P, Malavasi V, Rossi L et al (2012) Indexed left atrial volume is superior to left atrial diameter in predicting nonvalvular atrial fibrillation recurrence after successful cardioversion: a prospective study. *Echocardiography* 29:276–284
29. Keenan NG, Cueff C, Cimadevilla C et al (2010) Usefulness of left atrial volume versus diameter to assess thromboembolic risk in mitral stenosis. *Am J Cardiol* 106:1152–1156

A simple, fast and reproducible echocardiographic approach to grade left ventricular diastolic function

30. Vasan RS, Larson MG, Levy D et al (1997) Distribution and categorization of echocardiographic measurements in relation to reference limits: the Framingham Heart Study: formulation of a height- and sex-specific classification and its prospective validation. *Circulation* 96:1863–1873

3

Relation Between E/e' ratio and NT-proBNP Levels in Elderly Patients with Symptomatic Severe Aortic Stenosis

Based on:

Strachinaru M, van Dalen BM, Van Mieghem N, De Jaegere PP, Galema TW, Morissens M, Geleijnse ML. *Relation between E/e' ratio and NT-proBNP levels in elderly patients with symptomatic severe aortic stenosis*. Cardiovasc Ultrasound. 2015;13(1):29

ABSTRACT

Background: Symptoms in the elderly patients with severe aortic stenosis (AS) and comorbidities seem to lack in specificity. Therefore, objective parameters for increased left ventricular(LV) filling pressures are needed. The aim of this study was to investigate the correlation between the septal, lateral and average E/e' ratio and the value of the N-terminal pro-hormone of brain natriuretic peptide (NT-proBNP).

Methods: Two-hundred-fifty consecutive symptomatic patients (mean age 80 ± 8 years, 52% men) with severe AS underwent transthoracic echocardiography and NT-proBNP measurement.

Results: in the overall population the septal E/e' ($r=0,459$, $r^2=0,21$, $P < 0,0001$), lateral E/e' ($r=0,322$, $r^2=0,10$, $P < 0,0001$), and the average E/e' ($r=0,432$, $r^2=0,18$, $P < 0,0001$) were all significantly correlated to NT-proBNP. After the exclusion of patients with confounders (more than mild aortic or mitral regurgitation, severe renal dysfunction, obesity or severe COPD) the septal E/e' ($r=0,584$, $r^2=0,34$, $P < 0,0001$), lateral E/e' ($r=0,377$, $r^2=0,14$, $P < 0,0001$), and the average E/e' ($r=0,487$, $r^2=0,24$, $P < 0,0001$) were all significantly better correlated to NT-proBNP. In obese patients no significant correlations were seen. Previous bypass surgery did not alter the correlations.

Conclusions: In elderly patients with severe symptomatic AS there is a significant correlation between the E/e' ratio and NT-proBNP, in particular after exclusion of confounders. The correlation was best for the septal E/e' ratio and was preserved in patients with a history of bypass surgery.

INTRODUCTION

Aortic stenosis (AS) is the most common valvular heart disease in the Western world and its prevalence is expected to increase due to the aging of the population¹. Current recommendations warrant the presence of symptoms in order to indicate aortic valve replacement². However, in elderly patients symptoms related to increased left ventricular (LV) filling pressures are less specific, because of the normal aging process and the multiple comorbidities³. One objective parameter of increased LV filling pressures is the echocardiographic ratio of the transmitral E-wave velocity and early diastolic velocity of the myocardium, the so called E/e' ratio⁴⁻⁷. Although the value of this ratio may be less reliable in elderly AS patients with important annular calcifications⁷, the E/e' was proven to be a strong predictor of mortality in non-operated elderly patients with AS, especially in conjunction with the N-terminal pro-hormone of brain natriuretic peptide (NT-proBNP)⁸. This hormone reflects the total burden of the disease on the LV, and has been demonstrated to have a good prognostic value in the setting of severe AS⁹⁻¹⁶.

This study sought to assess the relation between the E/e' ratio and NT-proBNP. More specifically, the values of the septal versus lateral myocardial wall derived E/e' ratio were investigated in detail.

METHODS

Patient population

After exclusion of patients with an aortic or mitral valvular prosthesis, mitral stenosis or significant areas of focal LV akinesia (defined as an akinetic region extending to at least 3 segments, involving the basal septum and/or the basal lateral wall) the study included 250 consecutive subjects (mean age 80 ± 8 years, 52% men) with symptomatic severe AS, defined as an aortic valve area less than 1 cm^2 and/or less than $0.6 \text{ cm}^2/\text{m}^2$ and available NT-proBNP level who were treated by transcatheter aortic valve replacement (TAVI).

Transthoracic echocardiography

Two-dimensional echocardiography was performed using a Philips iE33 system (Philips, Best, The Netherlands) with the patient in the left lateral decubitus position. Echocardiographic studies were performed by an independent experienced echocardiographer, blinded to the patient's clinical and biochemical status. All echocardiograms were saved as video loops or still frames in a digital database and were reanalyzed by an experienced cardiologist (MS). The LV ejection fraction cut-off value of 50% was calculated using the biplane modified Simpson rule. The mitral inflow velocity profile (E/A wave ratio, E wave

deceleration time) was assessed with pulse-wave Doppler. The early diastolic velocities at the septal and lateral annulus level were assessed with pulse-wave Tissue Doppler from a standard apical 4-chamber view.

Blood sampling

Venous blood samples were drawn from patients with AS within 30 minutes of the Doppler echocardiography study from an antecubital vein into EDTA acid Vacutainer test tubes (Mediost BV, Doesburg, The Netherlands) after 30 minutes of supine rest. Samples were placed immediately on ice, and plasma separation was performed at 4°C. For NT-proBNP determination, an electrochemiluminescence immunoassay (ProBNP Elecsys, Roche Diagnostics GmbH, Mannheim, Germany) was used. For the evaluation of renal function, serum creatinine levels were determined and glomerular filtration rate (GFR) was calculated using the 2009 CKD-EPI creatinine equation¹⁷.

Definitions of possible confounders

Impaired ejection fraction was defined as <50%. Obesity was defined as a BMI (body mass index) above 30 kg/m²¹⁸. Severe COPD was considered in GOLD class III or IV¹⁹.

Severe impairment of the renal function was defined as GFR less than 30ml/min/1.73m², present for more than 3 months, as estimated by 2009 CKD-EPI creatinine equation¹⁷. Aortic and mitral regurgitation were assessed semi quantitatively according to current guidelines for the evaluation of native valves²⁰.

Significant coronary artery disease was defined as >50% stenosis in at least one coronary artery.

Pulmonary hypertension was considered when the estimated pulmonary pressure derived from Doppler tracings of the tricuspid insufficiency was above 40mmHg.

Statistical analysis

Continuous variables are presented as means (\pm SD) if normally distributed, or otherwise by geometric means for natriuretic peptide levels. Because of the very large range of values of the natriuretic peptide and the abnormal distribution of this variable, the log₁₀ of the NT proBNP was used in the analysis. Categorical variables are presented as frequencies and percentages. Differences between similar continuous variables were assessed by the paired-samples *t* test. Multivariable linear regression was performed in order to identify the possible confounders. Correlations were computed using Pearson's method, and graphically represented with linear regression lines whenever appropriate. For nonlinear parameters, a best-fit regression line was traced, using multiple nonlinear

regression equations and choosing the most statistically significant model that fitted the data. A two-sided p value less than 0.05 was used for declaring statistical significance. All statistical analyses were performed with SPSS 21.0 software (SPSS Inc, Chicago, IL, USA).

RESULTS

The baseline characteristics of the population are shown in Table 1.

Table 1. Baseline characteristics of the study patients

Variable	Study population n=250
Age	80(±8)
Male gender	129(52%)
BMI > 30kg/m ²	52(21%)
Diabetes	69(28%)
Severe renal dysfunction	27(11%)
Atrial fibrillation	47(19%)
Coronary artery disease	138(55%)
Previous CABG	53(21%)
PCI	90(36%)
COPD GOLD 3-4	17(7%)
NYHA class I	17(7%)
NYHA class II	76(30%)
NYHA class III-IV	149(60%)
Angor	66(26%)
Syncope	18(7%)
Pulmonary hypertension	85(34%)
Ejection fraction less than 50%	60(24%)
More than mild mitral regurgitation	39(16%)
More than mild aortic regurgitation	29(12%)

Data are presented as mean ±SD or number (percentage %)

BMI= body mass index; CABG= coronary artery by-pass graft surgery; COPD= chronic obstructive pulmonary disease; GOLD = Global Initiative for Chronic Obstructive Lung Disease classification of COPD; NYHA class= New York Heart Association classification of heart failure symptoms; PCI= percutaneous coronary intervention.

All patients were symptomatic. 66 patients(26%) had angina and only 18(7%) syncope. 149(60%) were in class NYHA III and IV, 76 (30%) in class II and 17(7%) in NYHA class I. In 8 patients NYHA class could not be determined. Impaired LV function was present in 60 patients (24%). Other potential confounders were present in 139 patients (56%);, severe COPD in 17 (7%), obesity in 52 (21%), severe renal dysfunction in 27 (11%) and

significant associated mitral or aortic regurgitation or a combination of the two in 61 (24%). In Table 2 the mean values for the echocardiographic parameters and NT-proBNP data are shown.

Table 2. Echocardiographic and biological data

Maximal pressure gradient (mmHg)	73±23
Mean pressure gradient (mmHg)	44±15
Pulmonary artery pressure (mmHg)	39±13
Ejection fraction (%)	55±12
E/A ratio	1,0 ± 0,6
e' septal (cm/s)	4,6 ± 1,7
e' lateral (cm/s)	6,3 ± 2,4
e' average (cm/s)	5,5 ± 1,9
E/e' septal	20,2 ± 9,1
E/e' lateral	15,7 ± 7,2
E/e' average	17,4 ± 6,9
E-wave deceleration time (ms)	240 ± 86
N terminal pro Brain Natriuretic Peptide (pmol/l)	217, 95% CI (161,226)
Log10 N-terminal pro Brain Natriuretic Peptide	2,3(±0,6)

Data are presented as mean ±SD or number (percentage %) for normally distributed values and as geometric mean and 95% CI for NT-proBNP

The E/A ratio was 1.0 ± 0.6 , E-wave deceleration time was 240 ± 86 ms, septal E/e' was 20.2 ± 9.1 , lateral E/e' was 15.7 ± 7.2 , and average E/e' was 17.4 ± 6.9 . NT-proBNP was 271 pmol/L (95% confidence interval 161,226), Log10 NT-proBNP was 2.3 ± 0.6 .

Correlations between the diastolic parameters and NT-proBNP

As seen in Figure 1, in the overall population the septal E/e' ($r=0,459$, $r^2=0,21$, $P < 0,0001$), lateral E/e' ($r=0,322$, $r^2=0,10$, $P < 0,0001$), and the average E/e' ($r=0,432$, $r^2=0,18$, $P < 0,0001$) were all significantly correlated to NT-proBNP. Also, the E/A ratio ($r=0,230$, $r^2=0,05$, $P < 0,001$), and E-wave deceleration time ($r=-0,263$, $r^2=0,07$, $P < 0,0001$) were significantly correlated to NT-proBNP.

Influence of ejection fraction on the correlations between the E/e' ratio and NT-proBNP

In the 60 patients with impaired EF $< 50\%$ the correlation for the septal E/e' ($r=0,361$, $r^2=0,13$, $P=0,005$) and average E/e' ($r=0,377$, $r^2=0,14$, $P=0,01$) was weaker. For the lateral E/e' the correlation was even not significant ($r=0,234$, $r^2=0,05$, $P=0,13$). In the 190 patients with EF $\geq 50\%$ the septal E/e' ($r=0,426$, $r^2=0,18$, $P < 0,0001$), lateral E/e' ($r=0,277$, $r^2=0,07$, $P < 0,01$), and the average E/e' ($r=0,353$, $r^2=0,12$, $P < 0,0001$) were all significantly correlated to NT-proBNP.

Relation Between E/e' ratio and NT-proBNP Levels in Elderly Patients with Symptomatic Severe Aortic Stenosis

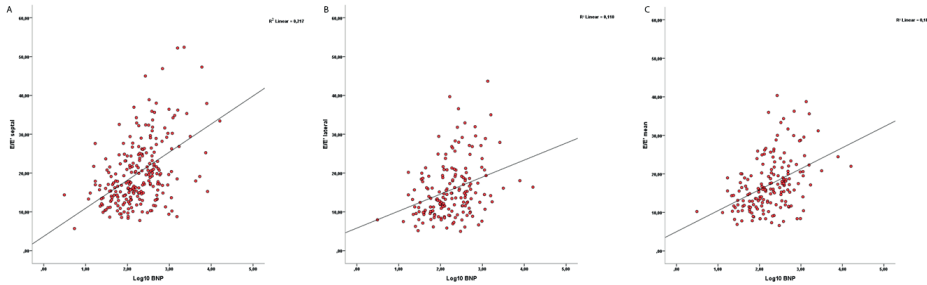


Figure 1. Correlations between E/e' ratio and Log10 NT-proBNP in the overall study population. A: septal point; B: lateral point; C: mean septal-lateral E/e'

Influence of other potential confounders on the correlations between the diastolic parameters and NT-proBNP

A multivariable linear regression model was constructed to assess the potential influence of the clinical, echocardiographic and biological factors on the correlation between E/e' ratio and NT-proBNP. On this model, the potential confounders that were identified were: severe COPD (standardized $\beta = -0,088$, $p = 0,05$), obesity (standardized $\beta = -0,092$; $p = 0,05$), significant aortic regurgitation (standardized $\beta = 0,096$; $p = 0,04$), significant mitral regurgitation (standardized $\beta = 0,148$; $p = 0,002$), altered ejection fraction (standardized $\beta = 0,314$; $p = 0,0001$) and renal dysfunction (standardized $\beta = 0,343$; $p = 0,0001$). Diabetes ($p = 0,46$), coronary artery disease ($p = 0,56$), pulmonary hypertension ($p = 0,14$), previous CABG ($p = 0,09$) did not significantly alter the correlation between E/e' and NT-proBNP.

After the exclusion of the 139 patients (56%) with more than mild aortic or mitral regurgitation, severe renal dysfunction, obesity or severe COPD there remained 111 patients (mean age 82 ± 8 years, 51% men), representing 44% of the initial group. As seen in Figure 2, the septal E/e' ($r = 0,584$, $r^2 = 0,34$, $P < 0,0001$), lateral E/e' ($r = 0,377$, $r^2 = 0,14$, $P < 0,0001$), and the average E/e' ($r = 0,487$, $r^2 = 0,24$, $P < 0,0001$) were now all significantly better correlated to NT-proBNP.

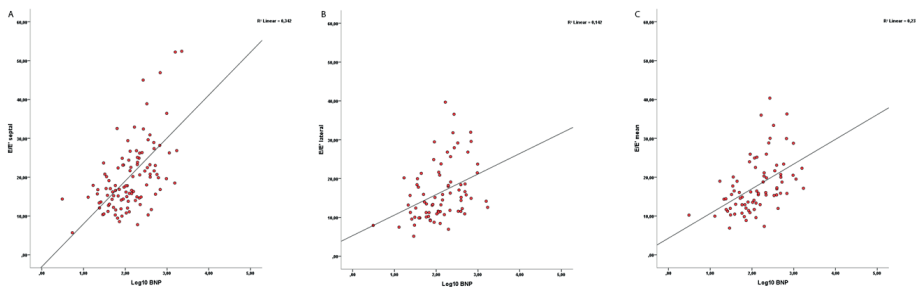


Figure 2. Correlations between E/e' ratio and Log10 NT-proBNP in the patient population without major confounders. A: septal point; B: lateral point; C: mean septal-lateral E/e'

In contrast, the level of linear correlation with the mitral E/A ratio did not change ($r=0,255$, $r^2=0,07$, $P=0,01$) and the E-wave deceleration time was not at all correlated to NT-proBNP ($r=-0,065$, $r^2=0,04$, $P=0,5$). As seen in Figure 3, the best-fit correlation lines were described by quadratic equations, with $r^2=0,12$, $P=0,002$ for the E/A ratio and non-significant results on all models for the E-wave deceleration time.

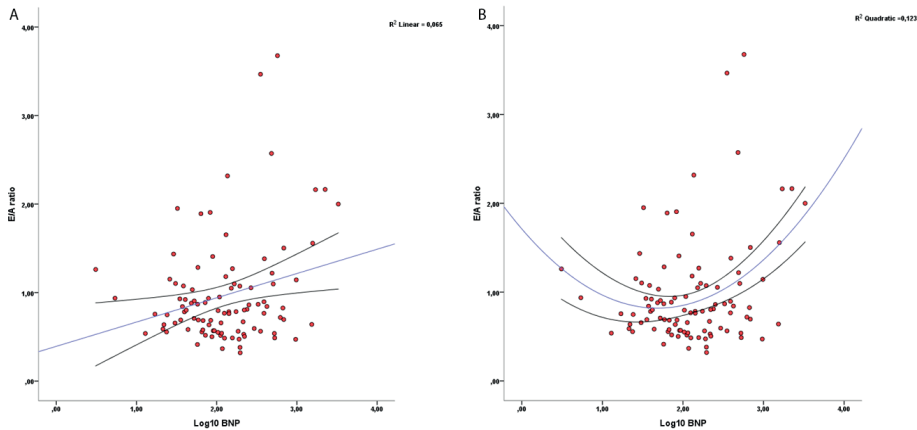


Figure 3. Correlation between E/A ratio and Log10 NT-proBNP. A: linear correlation; B: best-fit correlation line (quadratic equation). The regression lines are displayed with blue lines, and the 95% confidence intervals with black lines.

The influence of the ejection fraction on the correlation between the E/e' ratio and NT-proBNP in the confounder-free group

In the confounder-free group, the relations between E/e' and NT-proBNP were significant ($r=0,574$, $r^2=0,33$, $P<0,0001$ at the septal wall, $r=0,392$, $r^2=0,15$, $P=0,002$ for the lateral wall, and $r=0,484$, $r^2=0,23$, $P<0,0001$ for the average value) in the 93 patients with preserved EF. In the 18 patients with impaired EF all correlations were non-significant: $r=0,258$, $r^2=0,07$, $P=0,3$ for the septal wall, $r=-0,02$, $r^2=0,00$, $P=0,95$ for the lateral wall, and $r=0,058$, $r^2=0,00$, $P=0,8$ for the average value.

Correlations between the diastolic parameters and NT-proBNP in the obese patients

In the specific subgroup of 52 obese patients the septal E/e' ($r=0,260$, $r^2=0,07$, $P=0,07$), lateral E/e' ($r=0,150$, $r^2=0,02$, $P=0,37$), and the average E/e' ($r=0,237$, $r^2=0,06$, $P=0,15$) were all not significantly correlated to NT-proBNP. After exclusion of 10 patients with other confounders, the septal E/e' ($r=0,260$, $r^2=0,07$, $P=0,07$), lateral E/e' ($r=0,256$, $r^2=0,07$, $P=0,17$), and the average E/e' ($r=0,293$, $r^2=0,09$, $P=0,11$) remained not significantly correlated to NT-proBNP in the obese subgroup. The value of the NT proBNP in obese patients was

lower, with a geometrical mean of 94 pmol/l, 95% CI (81,142), compared to 217 pmol/L in the non-obese patients ($P=0.027$). In the other subgroups (COPD, renal dysfunction) a specific analysis was not possible because of the limited number of patients.

Influence of previous coronary bypass surgery on septal versus lateral E/e' assessment

In the 53 patients (68% men) with a history of coronary artery bypass graft (CABG) surgery the septal E/e' ($r=0,583$, $r^2=0,34$, $P < 0,0001$), lateral E/e' ($r=0,441$, $r^2=0,20$, $P < 0,01$), and the average E/e' ($r=0,571$, $r^2=0,33$, $P < 0,0001$) were also all significantly correlated to NT-proBNP. After exclusion of 24 patients with the previously mentioned confounders these numbers were for septal E/e' ($r=0,577$, $r^2=0,33$, $P < 0,01$), for lateral E/e' ($r=0,507$, $r^2=0,26$, $P < 0,05$), and for the average E/e' ($r=0,565$, $r^2=0,32$, $P < 0,01$).

Difference between the correlation levels of the E/e' ratio at the medial, lateral and average septal points

The level of correlation was significantly better for the septal point when compared to the lateral ($p < 0,0001$). There was also a difference favoring the septal point against the average e', but this difference did not reach a significant p value ($p=0,051$)

DISCUSSION

In this study in elderly patients with severe symptomatic AS the main findings were: 1) there is a significant correlation between the E/e' ratio and NT-proBNP, in particular in patients without obesity, severe renal dysfunction, severe COPD, or significant left-sided valvular regurgitation, 2) the correlation was best for the septal E/e' ratio, and 3) this latter correlation was preserved in patients with a history of CABG.

In elderly patients with severe AS, clinical symptoms are difficult to ascertain and less specific because of the normal aging process and the multiple comorbidities usually present in the AS patients referred for TAVI. In order to help the decision for aortic valve intervention, an objective parameter of increased LV filling pressure seems important in their evaluation. The E/e' ratio is the main stay of echocardiography to indirectly assess LV filling pressure²¹⁻²². The current guidelines recommend the use of the average E/e' ratio derived from the septal and lateral wall²²⁻²³. However, evidence for the use of the average E/e' ratio is lacking and the specific accuracy of the septal or lateral E/e' is still debated. Each of the two E/e' ratios has its specific benefits. Translational movement of the heart may less affect septal wall velocity and certainly Doppler beam angle errors are less likely to occur when septal wall velocities are measured. Also, it was shown that the

septal E/e' ratio best correlated to LV filling pressures in subjects with preserved systolic LV function²⁴ and in particular in the elderly²⁵. On the other hand, Nagueh *et al.* claimed that "the lateral E/e' ratio was easier to quantify"²⁶⁻²⁷. Obviously, a septal or lateral localized myocardial wall infarction will negatively influence the respective measurements. Therefore, patients with such abnormalities were excluded from our study.

Our study population has some important unique features. The patients were elderly with extensive aortic and mitral annular calcifications and a significant number of these patients had coronary artery disease and a history of previous CABG. Despite these characteristics a good correlation between the E/e' ratio and NT-proBNP was found. The best results were seen for the septal E/e' ratio with a correlation coefficient of 0.459. Exclusion for confounders (obesity, severe renal dysfunction, severe COPD, or significant left-sided valvular regurgitation) resulted in even better correlations. The best improvement was seen for the septal E/e' ratio with a correlation coefficient of 0.584.

The septal E/e' ratio could be superior due to the aforementioned reasons but also because of the extensive posterior mitral annular calcification that may have resulted in more problems in assessing the lateral annulus, which is a part of the posterior annular ring²⁸.

We had expected that a previous CABG with its influence on septal function²⁹⁻³⁰ would affect the accuracy of the septal E/e' ratio. Surprisingly, a history of CABG did not affect the correlation of the septal E/e' ratio with NT-proBNP.

Comparison to other studies and clinical implications

The level of correlation found between E/e' and NT-proBNP in our study in elderly patients with AS is quite similar to correlations published in the literature in general cardiac patients.³¹⁻³³ In AS little data are available^{16,34}. There is only a very small study on 29 middle-aged (65 ± 12 years) severe AS patients¹⁶. In that paper weak correlations were described between E/e' and NT-proBNP with only significant results seen for the septal E/e'. Because of the evidence in the literature^{16,25}, as well as the results of the present study and the specific practical benefits, the use of septal E/e' ratio rather than the lateral or average E/e' should be encouraged, until other sound data are available from prospective large-scale trials such as the EURO-FILLING study³⁵.

In the global population included here, the correlation between the surrogate markers of LV filling pressures remains moderate. Only about 44% of the symptomatic elderly patients with severe aortic stenosis displayed strong correlations. From a practical clinical standpoint, care should be taken in interpreting the results of the usual diastolic

function parameters in the presence of the confounders defined in this study: more than mild aortic/mitral regurgitation, severe renal impairment, severe COPD, obesity and left ventricular dysfunction.

Apart from the negative impact of impaired EF on the correlation between E/e' and NT-proBNP, the influence of obesity was striking. Even for the septal E/e' ratio no significant correlation was seen, probably because of the well-known paradoxically lower NT-proBNP levels than in normal weight patients for the same filling pressures³⁶. In such patients we can only speculate that the E/e' ratio better reflects LV filling pressures.

These findings could have an impact on the costs of medical care, since adding a NT proBNP assay to the routine evaluation is relatively expensive³⁷ and not covered by medical insurances, while E/e' ratio can be measured repetitively during each echocardiographic examination, without any supplemental risk or cost for the patient.

Study limitations

As mentioned above, the population included in this study was carefully selected by a "heart team" according to present guidelines on the management of valvular heart disease³⁸. That means first of all that they had to have clinical symptoms in association with a severe aortic stenosis in order to be considered for TAVI. An asymptomatic control group with severe aortic stenosis could have better demonstrated the role of echocardiographic data in the decision making. Such a group is difficult to constitute in an elderly population with several comorbidities.

The cross-sectional nature of the study could be a limitation in itself. However, data collection in this population was very rigorous, according to a very strict and prospectively designed protocol.

Although it demonstrates a correlation between echocardiographic and biological markers of elevated left ventricular filling pressures, it is possible that the cutoff value of 15 for the septal E/e' is too sensitive (practically all the patients having an E/e' ratio above this value, with a mean of 20 ± 9), or that all the selected patients had chronically elevated LVEDP, as reflected by the mean value of NT proBNP=217pmol/l. Unfortunately, a better cutoff point could not be determined from our data, because the LVEDP was measured in all patients during the initial phase of the intervention, before TAVI, but already on general anesthesia, which invariably leads to dramatic changes in pressures.

CONCLUSION

In elderly patients with severe symptomatic AS there is a significant correlation between the E/e' ratio and NT-proBNP, in particular after exclusion of confounders. The correlation was best for the septal E/e' ratio and was preserved in patients with a history of CABG.

REFERENCES

1. Lung B, Baron G, Butchart EG, Delahaye F, Gohlke-Ba"rwolf C, Levang OW, Tornos P, Vanoverschelde JL, Vermeer F, Boersma E, Ravaud P, Vahanian A. A prospective survey of patients with valvular heart disease in Europe: the Euro Heart Survey on Valvular Heart Disease. *Eur Heart J* 2003;24:1231–1243.
2. Nishimura R. A., Otto C. M., Bonow R. O., Carabello B. A., Erwin J. P., Guyton R. A., O'Gara P. T., Ruiz C. E., Skubas N. J., Sorajja P., Sundt T. M., Thomas J. D. 2014 AHA/ACC Guideline for the Management of Patients With Valvular Heart Disease: A Report of the American College of Cardiology/ American Heart Association Task Force on Practice Guidelines. *J Am Coll Cardiol*. 2014;63:e57-e185. doi:10.1016/j.jacc.2014.02.536.
3. Monin JL, Lancellotti P, Monchi M, Lim P, Weiss E, Piérard L, Guéret P. Risk score for predicting outcome in patients with asymptomatic aortic stenosis. *Circulation*. 2009 Jul 7;120(1):69-75. doi: 10.1161/CIRCULATIONAHA.108.808857.
4. Dal-Bianco JP, Khandheria BK, Mookadam F, Gentile F, Sengupta PP. Management of asymptomatic severe aortic stenosis. *J Am Coll Cardiol*. 2008 ;52:1279-92. doi: 10.1016/j.jacc.2008.07.020.
5. D'Agate DJ, Smith RH, Lazar JM, Doppler echocardiographic assessment of left ventricular filling pressures in elderly patients with moderate/severe aortic stenosis. *Am J Geriatr Cardiol*. 2002 ;11:173-6, 196.
6. Gjetsson P, Caidahl K, Farasati M, Odén A, Bech-Hanssen O. Preoperative moderate to severe diastolic dysfunction: a novel Doppler echocardiographic long-term prognostic factor in patients with severe aortic stenosis. *J Thorac Cardiovasc Surg*. 2005 ;129: 890-6.
7. McMurray JJ, Adamopoulos S, Anker SD, Auricchio A, Böhm M, Dickstein K, Falk V, Filippatos G, Fonseca C, Gomez-Sanchez MA, Jaarsma T, Køber L, Lip GY, Maggioni AP, Parkhomenko A, Pieske BM, Popescu BA, Rønnevik PK, Rutten FH, Schwitter J, Seferovic P, Stepinska J, Trindade PT, Voors AA, Zannad F, Zeiher A; Task Force for the Diagnosis and Treatment of Acute and Chronic Heart Failure 2012 of the European Society of Cardiology, Bax JJ, Baumgartner H, Ceconi C, Dean V, Deaton C, Fagard R, Funck-Brentano C, Hasdai D, Hoes A, Kirchhof P, Knuuti J, Kolh P, McDonagh T, Moulin C, Popescu BA, Reiner Z, Sechtem U, Sirnes PA, Tendera M, Torbicki A, Vahanian A, Windecker S, McDonagh T, Sechtem U, Bonet LA, Avraamides P, Ben Lamin HA, Brignole M, Coca A, Cowburn P, Dargie H, Elliott P, Flachskampf FA, Guida GF, Hardman S, Jung B, Merkely B, Mueller C, Nanas JN, Nielsen OW, Orn S, Parissis JT, Ponikowski P; ESC Committee for Practice Guidelines, ESC guidelines for the diagnosis and treatment of acute and chronic heart failure 2012: The Task Force for the Diagnosis and Treatment of Acute and Chronic Heart Failure 2012 of the European Society of Cardiology. Developed in collaboration with the Heart Failure Association (HFA) of the ESC. *Eur J Heart Fail*. 2012 ;14: 803-69. doi: 10.1093/eurjhf/hfs105.
8. Biner S, Rafique AM, Goykhan P, Morrissey RP, Naghi J, Siegel RJ. Prognostic value of E/E' ratio in patients with unoperated severe aortic stenosis. *JACC Cardiovasc Imaging*. 2010 ;3: 899-907. doi: 10.1016/j.jcmg.2010.07.005.
9. Casaclang-Verzosa G, Nkomo VT, Sarano ME, Malouf JF, Miller FA Jr, Oh JK. E/Ea is the major determinant of pulmonary artery pressure in moderate to severe aortic stenosis. *J Am Soc Echo-cardiogr*. 2008 ;21: 824-7. doi: 10.1016/j.echo.2007.12.002.

10. Nessmith MG, Fukuta H, Brucks S, Little WC. Usefulness of an elevated B-type natriuretic peptide in predicting survival in patients with aortic stenosis treated without surgery. *Am J Cardiol.* 2005 ;96: 1445-8.
11. Pedrazzini GB, Masson S, Latini R, Klersy C, Rossi MG, Pasotti E, Faletta FF, Siclari F, Minervini F, Moccetti T, Auricchio A. Comparison of brain natriuretic peptide plasma levels versus logistic EuroSCORE in predicting in-hospital and late postoperative mortality in patients undergoing aortic valve replacement for symptomatic aortic stenosis, *Am J Cardiol.* 2008 ;102: 749-54. doi: 10.1016/j.amjcard.2008.04.055.
12. Ben-Dor I, Minha S, Barbash IM, Aly O, Dvir D, Deksis T, Okubagzi P, Torguson R, Lindsay J, Satler LF, Pichard AD, Waksman R. Correlation of brain natriuretic peptide levels in patients with severe aortic stenosis undergoing operative valve replacement or percutaneous transcatheter intervention with clinical, echocardiographic, and hemodynamic factors and prognosis. *Am J Cardiol.* 2013 ;112: 574-9. doi: 10.1016/j.amjcard.2013.04.023
13. Philippe Pibarot, Jean G. Dumesnil, Improving Assessment of Aortic Stenosis, *J Am Coll Cardiol.* 2012;60: 169-180. doi:10.1016/j.jacc.2011.11.078
14. Bergler-Klein J, Klaar U, Heger M, Rosenhek R, Mundigler G, Gabriel H, Binder T, Pacher R, Maurer G, Baumgartner H, Natriuretic peptides predict symptom-free survival and postoperative outcome in severe aortic stenosis. *Circulation.* 2004 ;109: 2302-8.
15. Bruch C, Stypmann J, Grude M, Gradaus R, Breithardt G, Wichter T. Tissue Doppler imaging in patients with moderate to severe aortic valve stenosis: clinical usefulness and diagnostic accuracy. *Am Heart J.* 2004 ;148: 696-702.
16. Galema TW, Yap SC, Geleijnse ML, van Thiel RJ, Lindemans J, ten Cate FJ, Roos-Hesselink JW, Bogers AJ, Simoons ML. Early detection of left ventricular dysfunction by Doppler tissue imaging and N-terminal pro-B-type natriuretic peptide in patients with symptomatic severe aortic stenosis. *J Am Soc Echocardiogr.* 2008 ;21: 257-61.
17. Adeera Levin, Paul E Stevens, Summary of KDIGO 2012 CKD Guideline: behind the scenes, need for guidance, and a framework for moving forward, *Kidney International* 2013, 49–61; doi:10.1038/ki.2013.444
18. WHO. Obesity: preventing and managing the global epidemic. Report of a WHO Consultation. WHO Technical Report Series 894. Geneva: World Health Organization, 2000
19. GOLD, Global Strategy for the diagnosis, management, and prevention of chronic obstructive pulmonary disease, http://www.goldcopd.org/uploads/users/files/GOLD_Report_2014_Jan23.pdf
20. Joint Task Force on the Management of Valvular Heart Disease of the European Society of Cardiology (ESC); European Association for Cardio-Thoracic Surgery (EACTS), Vahanian A, Alfieri O, Andreotti F, Antunes MJ, Barón-Esquivias G, Baumgartner H, Borger MA, Carrel TP, De Bonis M, Evangelista A, Falk V, Jung B, Lancellotti P, Pierard L, Price S, Schäfers HJ, Schuler G, Stepinska J, Swedberg K, Takkenberg J, Von Oppell UO, Windecker S, Zamorano JL, Zembala M., Guidelines on the management of valvular heart disease (version 2012). *Eur Heart J.* 2012 Oct;33(19):2451-96. doi: 10.1093/eurheartj/ehs109.
21. Ommen SR, Nishimura RA, Appleton CP, Miller FA, Oh JK, Redfield MM, Tajik AJ., Clinical utility of Doppler echocardiography and tissue Doppler imaging in the estimation of left ventricular

- filling pressures: A comparative simultaneous Doppler-catheterization study, *Circulation*. 2000 ;102: 1788-94
22. Nagueh S F, Appleton CP, Gillebert TC, Marino PN, Oh JK, Smiseth OA, Waggoner AD, Flachskampf FA, Pellikka PA, Evangelista A. Recommendations for the Evaluation of Left Ventricular Diastolic Function by Echocardiography, *J Am Soc Echocardiogr*. 2009 ;22: 107-33. doi: 1016/j.echo.2008.11.023.
 23. Paulus W.J., Tschope C., Sanderson J.E., Rusconi C., Flachskampf F.A., Rademakers F.E. Marino P, Smiseth OA, De Keulenaer G, Leite-Moreira AF, Borbély A, Edes I, Handoko ML, Heymans S, Pezzali N, Pieske B, Dickstein K, Fraser AG, Brutsaert DL. How to diagnose diastolic heart failure: a consensus statement on the diagnosis of heart failure with normal left ventricular ejection fraction by the Heart Failure and Echocardiography Associations of the European Society of Cardiology. *Eur Heart J*. 2007; 28: 2539–2550
 24. Firstenberg MS, Levine BD, Garcia MJ, Greenberg NL, Cardon L, Morehead AJ, Zuckerman J, Thomas JD., Relationship of echocardiographic indices to pulmonary capillary wedge pressures in healthy volunteers, *J Am Coll Cardiol*. 2000 ;36: 1664-9
 25. Srivastava PM, Burrell LM, Calafiore P. Lateral vs medial mitral annular tissue Doppler in the echocardiographic assessment of diastolic function and filling pressures: which should we use? *Eur J Echocardiogr*. 2005 ;6: 97-106
 26. Nagueh SF, Middleton KJ, Kopelen HA, Zoghbi WA, Quiñones MA., Doppler tissue imaging: a non-invasive technique for evaluation of left ventricular relaxation and estimation of filling pressures, *J Am Coll Cardiol*. 1997 ;30: 1527-33
 27. Nagueh SF, Mikati I, Kopelen HA, Middleton KJ, Quiñones MA, Zoghbi WA, Doppler estimation of left ventricular filling pressure in sinus tachycardia. A new application of tissue doppler imaging, *Circulation*. 1998;98: 1644-50.
 28. Tsang W, Meineri M, Hahn RT, Veronesi F, Shah AP, Osten M, Nathan S, Russo M, Lang RM, Horlick EM, A three-dimensional echocardiographic study on aortic-mitral coupling in transcatheter aortic valve replacement, *European Heart Journal - Cardiovascular Imaging* May 2013, DOI: 10.1093/ehjci/jet058
 29. Codreanu I, Pegg TJ, Selvanayagam JB, Robson MD, Rider OJ, Dasanu CA, Jung BA, Taggart DP, Clarke K, Holloway CJ, Details of left ventricular remodeling and the mechanism of paradoxical ventricular septal motion after coronary artery bypass graft surgery, *J Invasive Cardiol*. 2011 ;23: 276-82
 30. Joshi SB, Salah AK, Mendoza DD, Goldstein SA, Fuisz AR, Lindsay J., Mechanism of paradoxical ventricular septal motion after coronary artery bypass grafting, *Am J Cardiol*. 2009;103: 212-5. doi: 10.1016/j.amjcard.2008.08.067
 31. Watanabe T, Iwai-Takano M, Oikawa M, Yamaki T, Yaoita H, Maruyama Y. Optimal noninvasive assessment of diastolic heart failure in patients with atrial fibrillation: comparison of tissue doppler echocardiography, left atrium size, and brain natriuretic peptide. *J Am Soc Echocardiogr*. 2008;21: 689-96.
 32. Mak GS, DeMaria A, Clopton P, Maisel AS. Utility of B-natriuretic peptide in the evaluation of left ventricular diastolic function: comparison with tissue Doppler imaging recordings. *Am Heart J*. 2004 ;148: 895-902.

33. Eindhoven JA, van den Bosch AE, Ruys TP, Opić P, Cuypers JA, McGhie JS, Witsenburg M, Boersma E, Roos-Hesselink JW, N-terminal pro-B-type natriuretic peptide and its relationship with cardiac function in adults with congenital heart disease, *J Am Coll Cardiol*. 2013 ;62: 1203-12. doi: 10.1016/j.jacc.2013.07.019
34. Cemri M, Arslan U, Kocaman SA, Cengel A. Relationship between N-terminal pro-B type natriuretic peptide and extensive echocardiographic parameters in mild to moderate aortic stenosis. *J Postgrad Med*. 2008 ;54: 12-6.
35. Galderisi M, Lancellotti P, Donal E, Cardim N, Edvardsen T, Habib G, Magne J, Maurer G, Popescu BA., European multicentre validation study of the accuracy of E/e' ratio in estimating invasive left ventricular filling pressure: EURO-FILLING study, *Eur Heart J Cardiovasc Imaging*. 2014;15: 810-6. doi: 10.1093/ehjci/jeu022
36. Beleigoli A, Diniz M, Nunes M, Barbosa M, Fernandes S, Abreu M, Ribeiro A, Reduced Brain Natriuretic Peptide Levels in Class III Obesity: The Role of Metabolic and Cardiovascular Factors. *Obes Facts* 2011;4: 427-432
37. Richard Troughton, G. Michael Felke2, James L. Januzzi Jr, Natriuretic peptide-guided heart failure management, *European Heart Journal* 2014; 35: 16–24. doi:10.1093/eurheartj/eh463
38. Joint Task Force on the Management of Valvular Heart Disease of the European Society of Cardiology (ESC); European Association for Cardio-Thoracic Surgery (EACTS), Vahanian A, Alfieri O, Andreotti F, Antunes MJ, Barón-Esquivias G, Baumgartner H, Borger MA, Carrel TP, De Bonis M, Evangelista A, Falk V, Iung B, Lancellotti P, Pierard L, Price S, Schäfers HJ, Schuler G, Stepinska J, Swedberg K, Takkenberg J, Von Oppell UO, Windecker S, Zamorano JL, Zembala M., Guidelines on the management of valvular heart disease (version 2012). *Eur Heart J*. 2012 Oct;33(19):2451-96. doi: 10.1093/eurheartj/ehs109

4

Determinants of changes in pulmonary artery pressure in patients with severe aortic stenosis treated by transcatheter aortic valve implantation

Based on:

Strachinaru M, MD, Ren B, van Dalen BM, Van Mieghem NM, De Jaegere PTT, van Gils L, Galema TW, Geleijnse ML. *Determinants of changes in pulmonary artery pressure in patients with severe aortic stenosis treated by transcatheter aortic valve implantation*. Revision submitted to Acta Cardiologica.

ABSTRACT

Background: Elevated pulmonary artery pressure (PAP) in patients with severe aortic stenosis (AS) is a strong predictor of adverse prognosis. This study sought to assess the relation between PAP and clinical and echocardiographic parameters in elderly patients with severe AS, as well as to identify the determinants of the change in PAP after transcatheter aortic valve implantation (TAVI).

Methods: The study included 170 subjects (age 81 ± 7 years, 45% men) with symptomatic severe AS who were treated by TAVI. They underwent a clinical evaluation and a transthoracic echocardiography before the TAVI procedure and 6 months after.

Results: In a multivariable analysis, the independent predictors for baseline PAP were the body mass index ($\beta=0,21$, $p=0,006$), COPD GOLD class ($\beta=0,20$; $p=0,009$), the E/e' ratio ($\beta=0,20$; $p=0,02$) and the degree of aortic regurgitation ($\beta=0,20$; $p=0,01$). After TAVI, there was significantly less (51% vs 29%, $p<0,0001$) pulmonary hypertension, defined as a tricuspid regurgitation velocity $\geq 2,8$ m/s. The baseline variables related to an improvement in PAP were the tricuspid regurgitation velocity ($p=0,0001$) and the E/e' ($p=0,005$). From the parameters potentially modified with TAVI, the only independent predictor of PAP variation was the change in the E/e' ratio ($\beta=0,23$; $p=0,01$).

Conclusions: Independent predictors for baseline PAP in elderly patients with symptomatic AS were the body mass index, GOLD class, the aortic regurgitation and the E/e' ratio. The baseline predictors for a change in PAP 6 months after TAVI were the baseline PAP and E/e', with only the change in the E/e' ratio being correlated to the change in PAP.

INTRODUCTION

Aortic stenosis (AS) is the most common valvular heart disease in the Western world and its prevalence is expected to increase due to the aging of the population¹. The rise in pulmonary pressure (PAP) in these patients has been clearly demonstrated as a strong predictor of worse prognosis after medical, surgical or interventional management²⁻⁴. We also know from several studies that PAP improves after relieving the valvular obstacle⁵⁻⁷. There is however little data concerning the determinants of this rise in PAP and in particular on the factors associated with post interventional improvement in PAP⁸⁻¹². This study sought to assess the relation between PAP and clinical and echocardiographic parameters in patients with severe AS, as well as to identify the determinants of improvement in PAP after transcatheter aortic valve implantation (TAVI).

METHODS

The study design was monocentric and retrospective, involving patients treated by TAVI for severe aortic stenosis between 2005 and 2014 in our institution. The study was conducted according to the principles of the Declaration of Helsinki. Retrospective clinical studies are waived for approval by our Institutional Ethical Committee. All patients have given written consent for the use of their anonymized data in this research.

Patient population

After exclusion of patients with prior aortic or mitral valvular surgery, mitral stenosis or significant areas of focal LV akinesia (defined as an akinetic region extending to at least 3 segments, involving the basal septum and/or the basal lateral wall) the study included 170 subjects (mean age 81 ± 78 years, 45% men) with symptomatic severe AS, defined as an aortic valve area less than 1 cm^2 and/or less than $0.6 \text{ cm}^2/\text{m}^2$ and/or a mean pressure gradient over 40mmHg, who were treated by TAVI. All patients underwent a clinical evaluation and a transthoracic echocardiography at baseline before the TAVI procedure and at 6 months post-TAVI.

Venous blood samples were drawn from each patient within 30 minutes of the Doppler echocardiography study after 30 minutes of supine rest. For NT-proBNP determination, an electrochemoluminescence immunoassay (ProBNP Elecsys, Roche Diagnostics GmbH, Mannheim, Germany) was used. Because of the very large range of values of the natriuretic peptide and the abnormal distribution of this variable, the log₁₀ of the NT proBNP was used in the analysis.

Transthoracic echocardiography

Two-dimensional echocardiography was performed using a Philips iE33 system (Philips, Best, The Netherlands) with the patient in the left lateral decubitus position. Echocardiographic studies were performed by an independent experienced echocardiographer, blinded to the patient's clinical status. All echocardiograms were saved as video loops or still frames in a digital database and were reanalyzed by an experienced cardiologist (MS). LV ejection fraction was calculated using the biplane modified Simpson rule. The mitral inflow velocity profile (E/A wave ratio, E wave deceleration time) was assessed with pulsed-wave Doppler. The early diastolic velocities at the septal annulus level were assessed with pulse-wave Tissue Doppler from a standard apical 4-chamber view¹³. Pulmonary artery pressure was estimated from the trans tricuspid systolic gradient. Tricuspid annular systolic excursion (TAPSE) was measured in standard apical 4-chamber view.

Each echocardiographic measurement was performed by at least two different observers: one initial by the sonographer performing the study, validated by a supervising imaging cardiologist; and a second measurement performed by MS (highly experienced imaging cardiologist), who was blinded to the clinical status of the subjects during these measurements. In case of disagreement between the two observers, a highly experienced imaging cardiologist (MG) acted as third observer and adjusted the result.

Definitions

Obesity was defined as a BMI (body mass index) above 30 kg/m²¹⁴. COPD was classified according to GOLD class¹⁵. Severe impairment of the renal function was defined as GFR less than 30ml/min/1,73m², present for more than 3 months, as estimated by the 2009 CKD-EPI creatinine equation¹⁶. Aortic and mitral regurgitation were assessed semi quantitatively according to current guidelines for the evaluation of native valves¹⁷. Pulmonary hypertension (PHT) was considered at a value of the trans tricuspid systolic gradient above 2,8m/s¹⁸. Significant coronary artery disease was defined as >50% stenosis in at least one coronary artery.

Statistical analysis

Continuous variables are presented as means (\pm SD) if normally distributed. Categorical variables are presented as frequencies and percentages. Differences between continuous variables were assessed by the paired-samples *t* test and between categorical variables by chi-square test. Univariate linear regression was used to identify the factors related to PAP level. The factors found to be significant in univariate analysis or considered relevant based on clinical data were entered into a multivariable linear regression model. The overall performance of the regression model was assessed using R²

statistics. Collinearity diagnostics and Durbin-Watson statistics were used to check the assumptions of no multicollinearity and serial independence of errors. A two-sided p value less than 0.05 was used for declaring statistical significance. All statistical analyses were performed with SPSS 21.0 software (SPSS Inc, Chicago, IL, USA).

RESULTS

The baseline characteristics of the population are shown in Table 1. All patients were symptomatic. Ten patients (6%) were in NYHA class I, 53 patients (31%) were in NYHA

Table 1: Baseline characteristics of the study patients

Variable	Study population n=170
Age	81 (± 7)
Male gender	76 (45%)
BMI > 30kg/m ²	31 (18%)
Diabetes	40 (24%)
Hypertension	91 (54%)
Severe renal dysfunction	19 (11%)
Atrial fibrillation	34 (20%)
Pacemaker before TAVI	15 (9%)
LBBB before TAVI	29 (17%)
Coronary artery disease	92 (54%)
Previous CABG	38 (22%)
Previous PCI	38 (22%)
PCI along with TAVI	19 (11%)
COPD GOLD 2-4	49 (29%)
Pulmonary hypertension	86 (51%)
NYHA class I	10 (6%)
NYHA class II	53 (31%)
NYHA class III-IV	102 (60%)
Log ₁₀ NT-proBNP	2.3 \pm 0.6
Angina	47 (27%)
Syncope	15 (9%)

Data are presented as mean \pm SD or number (percentage %)

BMI= body mass index; CABG= coronary artery by-pass graft surgery; COPD= chronic obstructive pulmonary disease; GOLD = Global Initiative for Chronic Obstructive Lung Disease classification of COPD; LBBB= left bundle branch block; NYHA class= New York Heart Association classification of heart failure symptoms; PCI= percutaneous coronary intervention; NT-proBNP= N-terminal pro Brain Natriuretic Peptide.

class II and 102 patients (60%) were in NYHA class III or IV (in 5 patients NYHA class could not be determined due to immobility). Forty-six patients (27%) had angina and 15 (9%) syncope. Significant COPD (class 2-4) was present in 49 patients (29%), obesity in 32 (18%), severe renal dysfunction in 19 (11%). Ninety-two of these patients (54%) had coronary artery disease, in 38 (22%) already treated by coronary bypass surgery and in 38 (22%) by a percutaneous intervention. In addition, a percutaneous intervention was performed along with the TAVI intervention in 19 (11%) patients. PHT was present in 86 patients (51%). A pacemaker was already present before the TAVI procedure in 15 (9%) and a complete left bundle branch block (LBBB) was diagnosed at baseline in 29 (17%).

Determinants of PHT at baseline (Table 2)

In univariate analysis, COPD class, mitral and aortic insufficiency, ejection fraction and E/e' ratio (Figure 1) were related to baseline PAP. In a multivariable analysis, the independent predictors for PHT were BMI (Beta=0,21, p=0,006), COPD GOLD class (Beta=0,20; p=0,009), aortic regurgitation (Beta=0,20; p=0,01) and the E/e' ratio (Beta=0,20; p=0,02).

Table 2: Baseline determinants of PHT

Parameter	N=170 mean±SD	Univariate analysis		Multivariable analysis	
		Beta	p	Beta	p
Age	81±7	-0,14	0,08		
Male gender		-0,08	0,28		
BMI	26±5	0,09	0,26	0,21	0,006
COPD GOLD class (0 to 4)	0,78±0,99	0,19	0,01	0,20	0,009
Mitral regurgitation (0 to 3)	1,09±0,65	0,15	0,05	0,10	0,21
Aortic regurgitation (0 to 3)	0,91±0,69	0,23	0,003	0,20	0,01
Mean transaortic gradient (mmHg)	44±15	0,09	0,23	0,11	0,20
Ejection fraction (%)	55±12	-0,21	0,006	-0,15	0,10
E/e' septal	21 ± 9	0,28	<0,0001	0,20	0,02
TAPSE baseline (mm)	20 ± 5	-0,067	0,39		
Atrial fibrillation		0,12	0,11		
LBBB at baseline		0,10	0,19		
Pacemaker at baseline		0,01	0,86		
Coronary artery disease		-0,03	0,66		
Sever renal failure		-0,13	0,11		
Diabetes		0,06	0,42		
Hypertension		-0,02	0,77		

Data are presented as mean ±SD. Significant P values (<0,05) are highlighted in bold

BMI= body mass index; CI= confidence intervals; COPD= chronic obstructive pulmonary disease; LBBB= left bundle branch block; TAPSE= tricuspid annular plane systolic excursion; SD= standard deviation

Determinants of changes in pulmonary artery pressure in patients with severe aortic stenosis treated by transcatheter aortic valve implantation

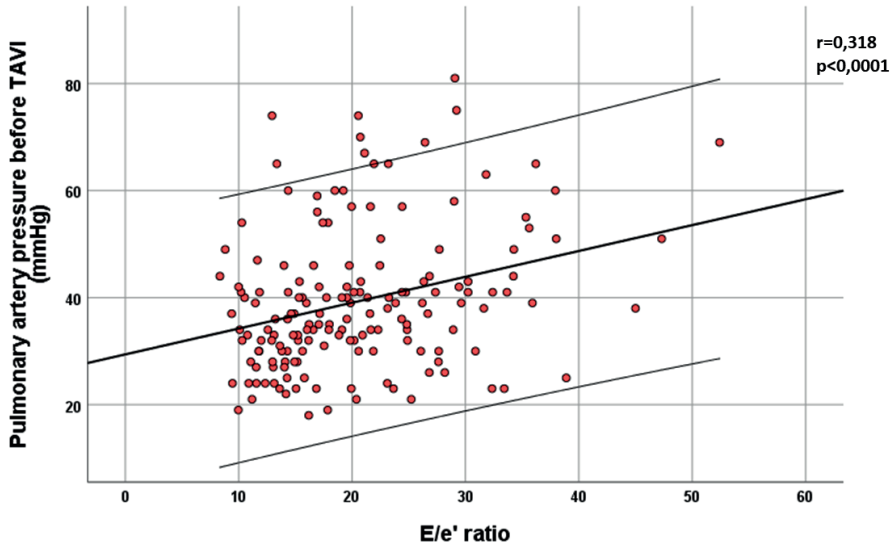


Figure 1: Correlation plot between baseline values of the E/e' ratio and the value of the pulmonary artery pressure as derived from the maximal transtricuspid gradient. A correlation line was fitted to the data (central thick line), as well as 95% confidence intervals (thin lateral lines).

Table 3: Comparison between no improvement or worsening PAP vs improved PAP

Variable	No improvement N=69	Improved N=101	p
Age	80±8	82±6	0,06
Male gender	34(49%)	42(42%)	0,32
BMI > 30kg/m ²	12(17%)	20(20%)	0,15
Diabetes	16(23%)	24(24%)	0,9
Hypertension	37(54%)	54(54%)	0,98
Severe renal dysfunction	9(13%)	10(10%)	0,52
Atrial fibrillation	16(23%)	18(18%)	0,39
Coronary artery disease	36(52%)	56(55%)	0,67
PCI along with TAVI	5(7%)	14(14%)	0,17
COPD GOLD 2-4	19(28%)	30(30%)	0,76
NYHA class I	3(4%)	7(7%)	0,48
NYHA class II	27(39%)	26(26%)	0,06
NYHA class III-IV	37(54%)	65(64%)	0,16
LVEDP	19±7	19±7	1
COPD GOLD class (0 to 4)	0,71±1	0,82±1	0,48
Mitral regurgitation (0 to 3)	1,1±0,6	1,1±0,7	1
Aortic regurgitation (0 to 3)	0,9±0,7	0,92±0,7	0,85

Table 3: Comparison between no improvement or worsening PAP vs improved PAP (continued)

Variable	No improvement N=69	Improved N=101	p
Mean transaortic gradient (mmHg)	42±15	46±15	0,09
Ejection fraction (%)	55±12	55±13	1
E/e' septal	22±10	18±7	0,005
Tricuspid regurgitation Vmax	2,6±0,4	2,9±0,5	0,0001
TAPSE baseline (mm)	19,7 ± 5	20,3 ± 5	0,44
LBBB before TAVI	13 (19%)	16 (16%)	0,61
Pacemaker present	6 (9%)	9 (9%)	0,44
Log BNP	2,4±0,5	2,3±0,6	0,24

Data are presented as mean ±SD. Significant P values (<0,05) are highlighted in bold

LVEDP= left ventricular end-diastolic pressure

Baseline predictors of improvement in pulmonary artery pressure (Table 3)

Before TAVI, 86 patients (51%) had PHT. After TAVI an improvement in PAP, defined as a decrease in trans tricuspid systolic gradient as compared to the baseline value, was noted in 101 patients (59%). No improvement or increased gradient was noted in 69 (41%). After TAVI the number of PHT patients was significantly lower (50; $p < 0.0001$) and 36 (21%) PHT patients normalized the PAP.

When comparing the baseline parameters in the group with improved trans tricuspid gradient versus the group without improvement, the only significantly different variables are the baseline value of the trans tricuspid gradient and the E/e' ratio (Figure 2).

Determinants of changes in pulmonary artery pressure in patients with severe aortic stenosis treated by transcatheter aortic valve implantation

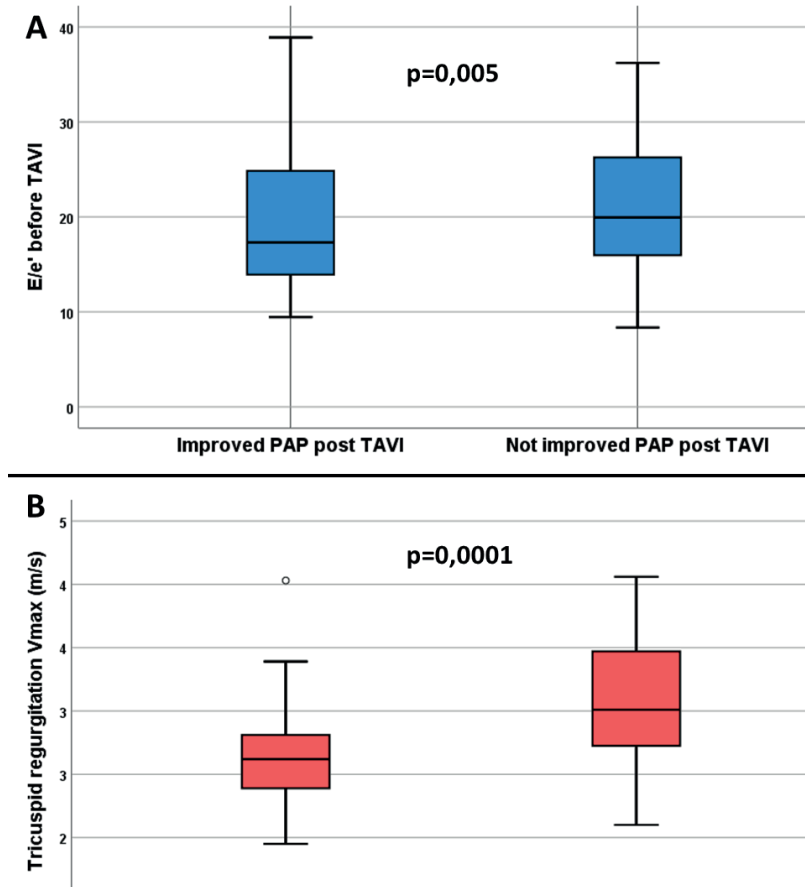


Figure 2: Comparison between the groups of patients who improved their transtricuspid gradient 6 months after TAVI implantation (left boxplots) and the ones who did not improve or increased their gradient (right boxplots). The only significantly different parameters measured at baseline (before TAVI) according to our analysis were the E/e' ratio (A) and maximal velocity of the tricuspid regurgitation (B). The higher E/e' ratio and higher transtricuspid gradient probably reflect a more advanced state of disease in the patients who did not show improvement in pulmonary artery pressure after TAVI.

Variation of clinical and echographic parameters 6 months after TAVI (Table 4)

There was a significant decrease in NYHA class, mean transaortic gradient, as well as in tricuspid regurgitation velocity. We noted a significant decrease in $\text{Log}_{10}\text{NT-proBNP}$ from $2,3 \pm 0,6$ at baseline to $2,1 \pm 0,5$ six months after TAVI ($p=0,002$). There was no significant change in the mean degree of mitral and aortic regurgitation. The E and A waves velocity increased significantly, without improvement of mean ejection fraction or E/e' ratio.

A new-onset (not present at baseline) LBBB was noticed in 67 (39%) patients. Implantation of a new pacemaker (not present at baseline) was indicated in 46 patients (27%).

Table 4: Variation of clinical and echocardiographic variables after TAVI

N=170 Variable	mean variation±SD	95% Confidence Interval		p
		Lower	Upper	
NYHA class (I to IV)	-0,9±0,8	-1,05	-0,81	<0,0001
Tricuspid regurgitation peak velocity	-0,1±0,4	-0,04	-0,16	0,001
Mean transaortic gradient (mmHg)	-35±16	-38	-33	<0,0001
Mitral regurgitation (0 to 3)	-0,05±0,6	-0,14	0,05	0,326
Aortic regurgitation (0 to 3)	-0,09±0,9	-0,24	0,05	0,198
Ejection fraction (%)	-0,03±9	-1,38	1,32	0,966
E wave amplitude (cm/s)	5±26	1,2	9,21	0,01
A wave amplitude (cm/s)	13±27	8,32	18,03	<0,0001
E/A ratio	-0,09±0,55	-0,19	0,003	0,058
E wave deceleration time (ms)	12±99	-4	28	0,147
Septal e' (cm/s)	0,24±1,6	-0,01	0,50	0,065
E/e' ratio	-0,18±7,3	-1,03	1,38	0,770
TAPSE (mm)	-0,09 ± 3	-0,59	0,42	0,733
Log ₁₀ NT-proBNP	0,13±0,5	0,05	0,20	0,002

Data are presented as mean ±SD. Significant P values (<0,05) are highlighted in bold

Right ventricular function parameters in the whole group did not change significantly (baseline TAPSE=20,03±5,4 mm; six months after TAVI the average TAPSE=20,12±5,2 mm; p=0,73).

Parameter variation as determinants of a change in PAP 6 months after TAVI (Table 5)

In univariate and multivariate analysis, only the change in E/e' ratio was a predictor of a change in PAP (Figure 3).

Table 5: Parameter variation as determinants of pulmonary artery pressure change 6 months after TAVI

N=170 Δ parameter	Mean variation±SD	Univariate analysis		Multivariable analysis	
		Beta	p	Beta	p
Δ mean transaortic gradient(mmHg)	-35±16	-0,11	0,16	-0,07	0,45
PCI with TAVI		0,09	0,25	0,02	0,86
Δ mitral regurgitation (0 to 3)	-0,10±0,58	0,09	0,22	-0,11	0,21
Δ aortic regurgitation (0 to 3)	-0,12±0,94	0,12	0,13	0,17	0,07
Δ ejection fraction(%)	0,09±8,55	-0,13	0,11	-0,01	0,96
Δ E/e' ratio	-0,04±7,36	0,27	0,001	0,23	0,01
Δ TAPSE (mm)	-0,1±3	0,09	0,19	0,01	0,84

Determinants of changes in pulmonary artery pressure in patients with severe aortic stenosis treated by transcatheter aortic valve implantation

Table 5: Parameter variation as determinants of pulmonary artery pressure change 6 months after TAVI (continued)

N=170 Δ parameter	Univariate analysis		Multivariable analysis		
	Mean variation \pm SD	Beta	p	Beta	p
New onset LBBB after TAVI		0,06	0,44	0,06	0,55
New pacemaker implantation		0,09	0,24	0,12	0,21

Data are presented as mean \pm SD. Significant P values (<0,05) are highlighted in bold

CI= confidence intervals; PCI= percutaneous coronary intervention; SD= standard deviation

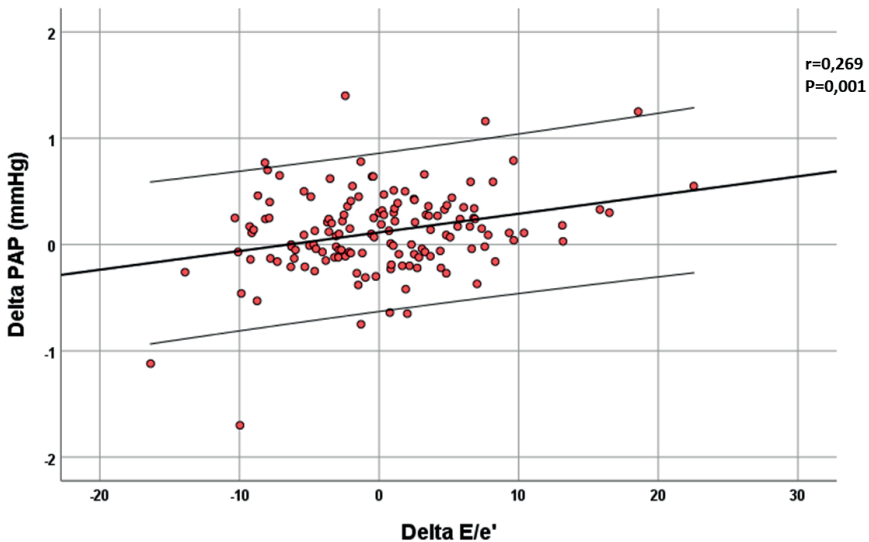


Figure 3: Correlation plot between the variation of the E/e' ratio before and after the TAVI procedure (delta E/e') and the variation of the pulmonary artery pressure (delta PAP) as derived from the maximal transtricuspid gradient. A correlation line was fitted to the data (central thick line), as well as 95% confidence intervals (thin lateral lines).

DISCUSSION

The main findings of this study in patients with severe AS treated with TAVI were: 1) the independent determinants of the baseline value of the PAP were BMI, the GOLD classification of COPD, aortic regurgitation and E/e' ratio; 2) there was a significant improvement in PAP 6 months after TAVI, with significantly less patients having PHT, 3) the baseline parameters predicting an improvement in PAP were the tricuspid regurgitation velocity and the E/e' ratio, and 4) the change in E/e' ratio was the only predictor of a change in PAP.

PHT is noted in 28-56% of the patients with AS, depending on the definition threshold^{3-4,7,9} and clinical characteristics. Elderly persons with severe AS undergoing TAVI may have several comorbidities, especially COPD, leading to a significant increase in PAP that is relatively unrelated to AS. They may also have concomitant regurgitant lesions of the left heart valves that contribute to an increase in PAP. In our study PHT was present in 51% of patients. Several factors were shown to be related to a rise in PAP in univariate analysis: the GOLD classification of COPD, mitral or aortic regurgitation, E/e' ratio, and ejection fraction. Surprisingly, the trans-aortic gradient did not reach statistical significance. Moreover, the multivariable model including these parameters yielded only four independent predictors for PHT: COPD severity, filling pressures of the left ventricle, reflected by the E/e' ratio, BMI and aortic insufficiency. This is in concordance with data already present in the literature, showing that diastolic function of the left ventricle is the main predictor of elevated PAP in severe AS¹². The role of COPD severity is obvious, especially in this elderly population in whom chronic pulmonary disease is not rare. The fact that BMI was not significant in the univariate analysis, but very significant in the multivariate cannot be explained by our statistical model, but the result is consistent with previous findings¹⁹. It could be due to the influence of the BMI on the prevalence of hypertension, diabetes and coronary artery disease (factors that were not entered in the multivariable analysis due to their lack of impact in the univariate model). Numerous publications address the prognostic role of the postprocedural paravalvular leak²⁰, but there is very little recent data on the impact of pre-procedural native valve aortic insufficiency associated to aortic stenosis²¹.

In our study, there was an overall statistically significant improvement in PAP, but only 59% really improved, and only 21% normalized the PAP. The value of the PAP was unchanged or even worsened in 41%. This may explain the little overall variation of the mean PAP. There was also a significant improvement in transaortic gradient without significant changes in the ejection fraction and the overall degree of mitral and aortic insufficiency. The effect of TAVI on the ejection fraction has indeed been reported as either neutral or positive.²²⁻²⁴ In a recent meta-analysis a non-significant trend towards a reduction in mitral regurgitation was reported²⁵, consistent with our findings. The change in aortic regurgitation is of course, very variable, depending on the baseline characteristics of each patient as well as numerous technical factors²⁶.

It has already been noted that PAP improves after successful TAVI intervention (according to VARC 2 criteria²⁰). This is most likely due to the removal of the valvular obstacle and the possible improvement in left ventricular systolic and diastolic function or valvular regurgitation. The persistence of PHT is considered to impact long term prognosis in patients with severe AS¹¹. The improvement in PAP was related to the initial value of the

PAP and the E/e' ratio. Very few studies investigated this particular matter, and only in the setting of surgical valvular replacement, but the results are similar²⁷⁻²⁸. Higher values of PAP and E/e' may suggest a more advanced disease in which the beneficial effects after TAVI may be less important. The only independent dynamic variable predicting a change in PAP after TAVI proved to be the change in the E/e' ratio.

The general clinical improvement, demonstrated by a significant decrease of the NYHA class, was reflected in echocardiography by a decrease in tricuspid regurgitation peak velocity and mean transaortic gradient (Table 4). This improvement was correlated with a similar evolution of the biomarkers of elevated intracardiac pressure, as observed in heart failure in general²⁹ and in elderly patients with aortic stenosis¹³.

After TAVI, the mitral inflow E and A waves had significantly higher amplitudes, but the E/e' ratio did not change considerably. The E/e' ratio has a paradoxical evolution: although it was a significant determinant of the baseline PAP and of the improvement in PAP, its mean value did not change significantly. There could be several explanations to the paradoxical behavior of this parameter, that does not change in spite of the significant change in PAP. One explanation may reside in an early and sustained increase in cardiac output after relieving the aortic obstacle (as reflected by the rise in E and A velocities through an unchanged mitral valve). Also, improvement of the septal e' velocity could be limited in the presence of a prosthetic valve very close to the mitral septal point. However, the role of the diastolic function as measured by the E/e' ratio is reinforced by the fact that the other main potential factors influencing the PAP (left heart valvular regurgitation, LV ejection fraction, severity of the pulmonary disease and right ventricular function) did not show any significant correlations in this study.

The debate on the optimal site of e' measurement is still going on but the septal site seems to correlate best to direct and indirect measurements of LV filling pressures^{13,30-31}.

A new-onset LBBB or the implantation of a new pacemaker did not demonstrate a significant effect on the pulmonary artery pressure in our patients, in univariate and multivariate analysis.

Clinical implications

PAP evaluation by echocardiography needs to be a part of the prognostic estimation of potential TAVI candidates^{20,32}, along with the filling pressures of the left ventricle, the two elements being interconnected. COPD and obesity remain clinical features to be considered when estimating the role of AS in the rise of PAP. The improvement in the filling pressures of the left ventricle after relieving the valvular obstacle, although

insignificant on the population level, seems to be the main factor contributing to the reduction in PAP.

Study limitations

This is a retrospective cross-sectional study, but the quality of the data was not compromised because data acquisition has been done according to a very strict prospectively defined TAVI protocol. The limited number of patients is also a potential problem in interpreting statistical models, especially when the number of variables is important. However, the level of statistical significance was sufficient to sustain our conclusions. The evaluation of PAP by echocardiography has several known limitations³³⁻³⁴ but was preferred due to its lack of risk for the patient, as compared to invasive measurements. Finally, in AS patients the evaluation of the aortic regurgitation is already difficult¹⁷. Estimating its change can be even more so, since it is a comparison of valvular regurgitation with a paraprosthetic leak.

CONCLUSION

Independent predictors for baseline PAP in elderly patients with symptomatic AS were the body mass index, GOLD class and left ventricular filling pressure reflected by the E/e' ratio. The baseline variables related to a change in PAP 6 months after TAVI were the baseline PAP and E/e', with only the change in the E/e' ratio being correlated to the change in PAP.

REFERENCES

1. Iung B, Baron G, Butchart EG, Delahaye F, Gohlke-Baerwolf C, Levang OW *et al*. A prospective survey of patients with valvular heart disease in Europe: the Euro Heart Survey on Valvular Heart Disease. *Eur Heart J* 2003;24:1231–1243.
2. Cam A, Goel SS, Agarwal S, Menon V, Svensson LG, Tuzcu EM *et al*. Prognostic implications of pulmonary hypertension in patients with severe aortic stenosis. *J Thorac Cardiovasc Surg*. 2011;142(4):800-8. doi: 10.1016/j.jtcvs.2010.12.024.
3. Zlotnick DM, Ouellette ML, Malenka DJ, DeSimone JP, Leavitt BJ, Helm RE *et al*. Effect of preoperative pulmonary hypertension on outcomes in patients with severe aortic stenosis following surgical aortic valve replacement. *Am J Cardiol*. 2013;112(10):1635-40. doi: 10.1016/j.amjcard.2013.07.025
4. Luçon A, Oger E, Bedossa M, Boulmier D, Verhoye JP, Eltchaninoff H *et al*. Prognostic implications of pulmonary hypertension in patients with severe aortic stenosis undergoing transcatheter aortic valve implantation: study from the FRANCE 2 registry. *Circ Cardiovasc Interv*. 2014;7(2):240-7. doi: 10.1161/CIRCINTERVENTIONS.113.000482
5. Tracy GP, Proctor MS, Hizny CS. Reversibility of pulmonary artery hypertension in aortic stenosis after aortic valve replacement, *Ann Thorac Surg*, 50 (1990), pp. 89–93
6. Schewel D, Schewel J, Martin J, Voigtländer L, Frerker C, Wohlmuth P *et al*. Impact of transcatheter aortic valve implantation (TAVI) on pulmonary hyper-tension and clinical outcome in patients with severe aortic valvular stenosis, *Clin Res Cardiol*. 2015;104(2):164-74. doi: 10.1007/s00392-014-0772-5
7. Ben-Dor I, Goldstein SA, Pichard AD, Satler LF, Maluenda G, Li Y *et al*. Clinical profile, prognostic implication, and response to treatment of pulmonary hypertension in patients with severe aortic stenosis, *Am J Cardiol*. 2011;107(7):1046-51. doi: 10.1016/j.amjcard.2010.11.031
8. Aragam JR, Folland ED, Lapsley D, Sharma S, Khuri SF, Sharma GV. Cause and impact of pulmonary hypertension in isolated aortic stenosis on operative mortality for aortic valve replacement in men, *Am J Cardiol*, 69 (1992), pp. 1365–1367
9. Faggiano P, Antonini-Canterin F, Ribichini F, D'Aloia A, Ferrero V, Cervesato E, *et al*. Pulmonary artery hypertension in adult patients with symptomatic valvular aortic stenosis, *Am J Cardiol*, 85 (2000), pp. 204–208
10. Ahn HS, Chang SA, Kim HK, Kim SJ, Lee SP, Park SJ *et al*. Determinants of pulmonary hypertension development in moderate or severe aortic stenosis, *Int J Cardiovasc Imaging*. 2014;30(8):1519-28. doi: 10.1007/s10554-014-0498-5
11. D'Ascenzo F, Conrotto F, Salizzoni S, Rossi ML, Nijhoff F, Gasparetto V *et al*. Incidence, predictors, and impact on prognosis of systolic pulmonary artery pressure and its improvement after transcatheter aortic valve implantation: a multicenter registry, *J Invasive Cardiol*. 2015;27(2):114-9
12. Casaclang-Verzosa G, Nkomo VT, Sarano ME, Malouf JF, Miller FA Jr, Oh JK. E/Ea is the major determinant of pulmonary artery pressure in moderate to severe aortic stenosis. *J Am Soc Echocardiogr*. 2008 ;21: 824-7. doi: 10.1016/j.echo.2007.12.002.
13. Strachinaru M, van Dalen BM, Van Mieghem N, De Jaegere PP, Galema TW, Morissens M *et al*. Relation between E/e' ratio and NT-proBNP levels in elderly patients with symptomatic severe aortic stenosis, *Cardiovasc Ultrasound*. 2015;13(1):29. doi: 10.1186/s12947-015-0021-8

14. WHO. Obesity: preventing and managing the global epidemic. Report of a WHO Consultation. WHO Technical Report Series 894. Geneva: World Health Organization, 2000
15. GOLD, Global Strategy for the diagnosis, management, and prevention of chronic obstructive pulmonary disease, <http://www.goldcopd.org/>.
16. Adeera Levin, Paul E Stevens. Summary of KDIGO 2012 CKD Guideline: behind the scenes, need for guidance, and a framework for moving forward, *Kidney International* (2013) 85, 49–61; doi:10.1038/ki.2013.444
17. Vahanian A, Alfieri O, Andreotti F, Antunes MJ, Barón-Esquivias G, Baumgartner H *et al*. Guidelines on the management of valvular heart disease (version 2012). *Eur Heart J*. 2012;33(19):2451-96. doi: 10.1093/eurheartj/ehs109.
18. Rudski LG, Lai WW, Afilalo J, Hua L, Handschumacher MD, Chandrasekaran K *et al*. Guidelines for the echocardiographic assessment of the right heart in adults: a report from the American Society of Echocardiography endorsed by the European Association of Echocardiography, a registered branch of the European Society of Cardiology, and the Canadian Society of Echocardiography. *J Am Soc Echocardiogr*. 2010;23(7):685-713; quiz 786-8. doi: 10.1016/j.echo.2010.05.010
19. Weyman AE, Davidoff R, Gardin J, Ryan T, St John Sutton M, Weissman NJ. Echocardiographic evaluation of pulmonary artery pressure with clinical correlates in predominantly obese adults, *J Am Soc Echocardiogr*. 2002;15(5):454-62.
20. Kappetein AP, Head SJ, Génèreux P, Piazza N, van Mieghem NM, Blackstone EH *et al*. Updated Standardized Endpoint Definitions for Transcatheter Aortic Valve Implantation: The Valve Academic Research Consortium-2 Consensus Document†. *J Am Coll Cardiol*. 2012;60(15):1438-1454. doi:10.1016/j.jacc.2012.09.001.
21. Honda S, Kitai T, Okada Y, Tani T, Kim K, Kaji S *et al*. Impact of aortic regurgitation on the prognosis of severe aortic stenosis. *Heart*. 2012;98(21):1591-4. doi: 10.1136/heartjnl-2012-302089.
22. Kamperidis V, Joyce E, Debonnaire P, Katsanos S, van Rosendael PJ, van der Kley F *et al*. Left ventricular functional recovery and remodeling in low-flow low-gradient severe aortic stenosis after transcatheter aortic valve implantation, *J Am Soc Echocardiogr*. 2014;27(8):817-25. doi: 10.1016/j.echo.2014.04.021.
23. Kempny A, Diller GP, Kaleschke G, Orwat S, Funke A, Radke R *et al*. Longitudinal left ventricular 2D strain is superior to ejection fraction in predicting myocardial recovery and symptomatic improvement after aortic valve implantation, *Int J Cardiol*. 2013;167(5):2239-43. doi: 10.1016/j.ijcard.2012.06.012
24. D'Andrea A, Padalino R, Cocchia R, Di Palma E, Riegler L, Scarafilo R *et al*. Effects of transcatheter aortic valve implantation on left ventricular and left atrial morphology and function, *Echocardiography*. 2015;32(6):928-36. doi: 10.1111/echo.12808
25. Sannino A, Losi MA, Schiattarella GG, Gargiulo G, Perrino C, Stabile E *et al*. Meta-analysis of mortality outcomes and mitral regurgitation evolution in 4,839 patients having transcatheter aortic valve implantation for severe aortic stenosis. *Am J Cardiol*. 2014;114(6):875-82. doi:10.1016/j.amjcard.2014.06.022.
26. O'Sullivan KE, Gough A, Segurado R, Barry M, Sugrue D, Hurley J. Is valve choice a significant determinant of paravalvular leak post-transcatheter aortic valve implantation? A systematic review and meta-analysis, *Eur J Cardiothorac Surg*. 2014;45(5):826-33. doi: 10.1093/ejcts/ezt515.

Determinants of changes in pulmonary artery pressure in patients with severe aortic stenosis treated by transcatheter aortic valve implantation

27. Tracy GP, Proctor MS, Hizny CS. Reversibility of pulmonary artery hypertension in aortic stenosis after aortic valve replacement. *Ann Thorac Surg.* 1990;50(1):89-93.
28. Tassan-Mangina S, Metz D, Nazeyllas P, Torossian F, Pop C, Bertrand J *et al.* Factors determining early improvement in mitral regurgitation after aortic valve replacement for aortic valve stenosis: a transthoracic and transesophageal prospective study, *Clin Cardiol.* 2003;26(3):127-31.
29. Klimczak-Tomaniak D, van den Berg VJ, Strachinaru M, Akkerhuis KM, Baart SJ, Caliskan K *et al.* Longitudinal patterns of NT-proBNP, troponin T and CRP in relation to the dynamics of echocardiographic parameters in heart failure patients. *Eur Heart J Cardiovasc Imaging.* 2019. pii: jez242. doi: 10.1093/ehjci/jez242.
30. Srivastava PM, Burrell LM, Calafiore P. Lateral vs medial mitral annular tissue Doppler in the echocardiographic assessment of diastolic function and filling pressures: which should we use? *Eur J Echocardiogr.* 2005;6: 97-106
31. Nagueh SF, Middleton KJ, Kopelen HA, Zoghbi WA, Quiñones MA. Doppler tissue imaging: a noninvasive technique for evaluation of left ventricular relaxation and estimation of filling pressures, *J Am Coll Cardiol.* 1997 ;30: 1527-33
32. Barbash IM, Escarcega RO, Minha S, Ben-Dor I, Torguson R, Goldstein SA *et al.* Prevalence and impact of pulmonary hypertension on patients with aortic stenosis who underwent transcatheter aortic valve replacement, *Am J Cardiol.* 2015;115(10):1435-42. doi: 10.1016/j.amjcard.2015.02.022.
33. Firstenberg MS, Levine BD, Garcia MJ, Greenberg NL, Cardon L, Morehead AJ *et al.* Relationship of echocardiographic indices to pulmonary capillary wedge pressures in healthy volunteers, *J Am Coll Cardiol.* 2000 ;36: 1664-9.
34. Naeije R, D'Alto M, Forfia PR. Clinical and research measurement techniques of the pulmonary circulation: the present and the future, *Prog Cardiovasc Dis.* 2015;57(5):463-72. doi: 10.1016/j.pcad.2014.12.003.

5

In-depth echocardiographic analysis of left atrial function in healthy adults using speckle tracking echocardiography and volumetric analysis

Based on:

van Grootel RWJ, **Strachinaru M**, Menting ME, Vletter-McGhie JS, Roos-Hesselink JW, van den Bosch AE. *In depth echocardiographic analysis of left atrial function in healthy adults using speckle tracking echocardiography and volumetric analysis*. *Echocardiography*. 2018; 35(12):1956-1965.

1 | INTRODUCTION

Assessment of the left atrium (LA) is gaining increased attention as it reflects the severity and chronicity of many different conditions and is associated with significant morbidity and mortality.¹

In the absence of valvular disease, LA volume reflects the presence of elevated left ventricular (LV) diastolic pressure and dysfunction.² LA maximum volume is the most often described parameter, but LA phasic function could be a more sensitive measure in patients with heart failure, valvular disease, and atrial fibrillation. LA function can be assessed by volumetric measurements and includes reservoir, conduit, and pump function which can be expressed as absolute volumes or fractions. Recently speckle tracking echocardiography (STE) has been validated for LA measurements³; LA strain and strain rate can be measured which reflect LA myocardial function without the need for geometrical assumptions.

The clinical value of LA volumetric and myocardial function has not been translated into recommendations to be used in clinical practice. This is in part because solid reference ranges have not been established, neither for volumetric measurements⁴⁻⁶ nor for strain measurements.⁷⁻¹²

Therefore this study aims to provide reference ranges for LA myocardial and volumetric function in healthy adults and investigates the impact of age, sex, and BSA.

2 | METHODS

2.1 | Study design and population

Healthy volunteers were enrolled in 2014–2015 for this prospective cross-sectional study and stratified into 5 age groups: 20–29, 30–39, 40–49, 50–59, 60–72 years ($n \geq 28$ for each group, each 50% female). Details have been published earlier.¹³ Briefly, subjects were recruited via advertisement and underwent a questionnaire regarding medical history and current health status, physical examination, venous blood sampling, 12-lead ECG, and an echocardiogram. Subjects were excluded if one or more of the following criteria were present: (prior) cardiovascular disease, systemic disease, the finding of cardiac abnormalities during the examination (including any valvular abnormalities) or risk factors including hypertension (cutoff values: 140/80 mm Hg), diabetes mellitus, impaired renal function or hypercholesterolemia. In case of elevated blood pressures, follow-up measurements were performed by the general practitioner to confirm this. If follow-up revealed normal blood pressures, the subject was included. Reasons for exclusion due to abnormalities on ECG were conduction disorders: Atrial fibrillation, right or left bundle branch block, pro-

longed PR interval, and prolonged QRS. Professional athletes, people who were morbidly obese (BMI > 40 kg/m²), having breast implants or pregnant were excluded. This study was carried out according to the principles of the Declaration of Helsinki and approved by the local ethics committee. Written informed consent was obtained from every participant.

2.2 | Echocardiographic image acquisition

Echocardiographic studies were performed by one of two experienced sonographers. Two-dimensional grayscale harmonic images were obtained in the left lateral decubitus position using a iE33 or EPIQ7 ultrasound system (Philips Medical Systems, Best, The Netherlands) equipped with a transthoracic broadband X5-1 matrix transducer (composed of 3040 elements with 1–5 MHz). The LA was acquired in dedicated apical four- and two-chamber views with frame rates ≥ 50 frames/s.¹⁴ At least 2 consecutive heartbeats were recorded.

2.3 | Volumetric analysis

In order to assess LA maximum volume, the revised recommendations for cardiac chamber quantification were used.¹ LA minimum volume (measured at mitral valve closure) and pre-a-wave volume (one frame before atrial contraction starts) were measured using the biplane method-of-disk summation technique (Figure 1) and the area-length method. All measurements were performed with Xcelera (Philips Medical Systems). Using the above volumes, LA function can be assessed as follows:

Left atrial reservoir function:

- Left atrial total emptying volume (TEV) = LA maximum volume – LA minimum volume.
- Left atrial total emptying fraction = TEV/LA maximum volume.
- Left atrial expansion index = TEV/LA minimum volume.

Left atrial conduit function:

- Left atrial passive emptying volume (PEV) = LA maximum volume – LA pre-a-wave volume.
- Left atrial passive emptying fraction = PEV/LA maximum volume.

Left atrial pump function:

- Left atrial active emptying volume (AEV) = LA pre-a-wave volume – LA minimum volume.
- Left atrial active emptying fraction = AEV/LA pre-a-wave volume.

All reported volumes are indexed for BSA. Since the Dutch population is the tallest in the world,¹⁵ we indexed for an allometric function of height^{2.7}.¹⁶ LV diastolic function was assessed according to the EAE–ASE recommendations for diastolic function.¹⁷

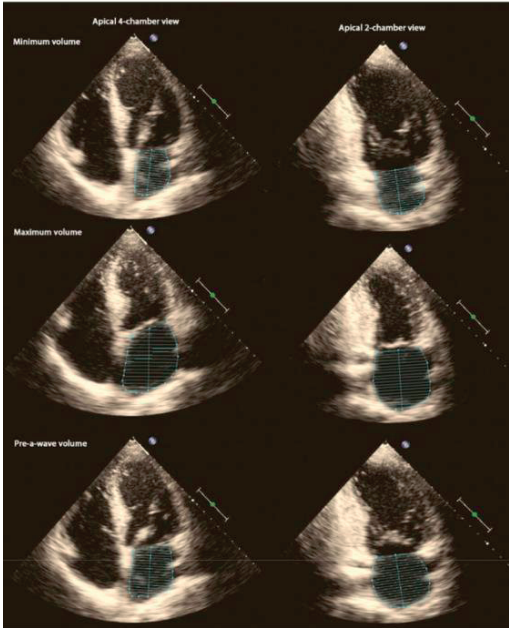


Figure 1. Example of the volumetric measurements using the method-of-disk summation technique in dedicated apical four- and two-chamber views. From top to bottom: the left atrial minimum, maximum, and pre-a-wave volume

2.4 | Speckle tracking analysis

Offline analysis was performed using QLAB10 (Philips Medical Systems). LA myocardial function was assessed according to an earlier published guideline and a recent validation study,^{18,19} using the apical four- and two-chamber views and the R-wave as reference point. LA reservoir function can be expressed as peak strain (LA-strain) and LA conduit and pump function with LA strain rate. The negative peak in early diastole represents LA conduit function (LA-SRe) and the negative peak in late diastole represents LA pump function (LA-SRa) (Figure 2).

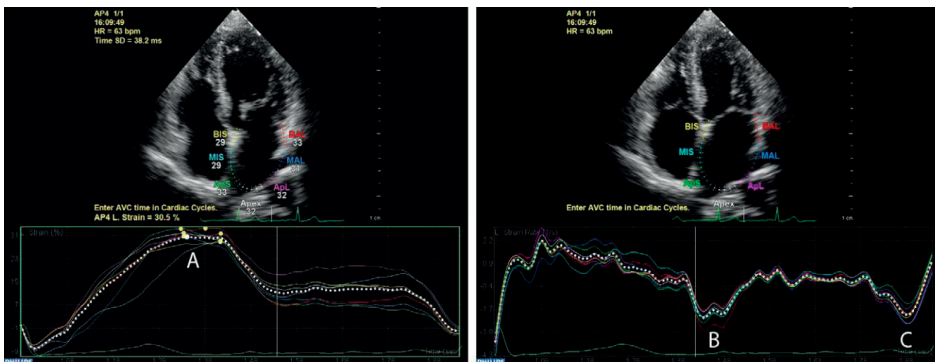


Figure 2. Example of left atrial (LA)-strain measurement in a apical four-chamber view. LA-strain(A) is measured as the maximum strain value during atrial diastole. Conduit (B) and pump (C) function are measured using strain rate

2.5 | Statistical analysis

Normal distribution was checked using histograms and Shapiro–Wilk tests. Depending on data distribution, continuous data are presented as mean \pm standard deviation (SD) or median with first–third quartile. Categorical data are presented as frequencies and percentages. Student’s *t*-test, the Mann–Whitney *U* test, chi–square test or Fisher’s exact test was used when appropriate. Correlations between LA measurements and baseline characteristics were assessed using the Pearson correlation test. When a variable was statistically significant and did not show collinearity with another variable, they were included in a multi-variable linear regression model. In case of collinearity, the one with the strongest correlation was selected. Statistical analysis was done with the Statistical Package for Social Sciences version 21 (IBM DPDD Statistics for Windows, Armonk, NY, USA). A *P*-value of ≤ 0.05 (two–sided) was considered statistically significant.

Interobserver (RG, MS) agreement was assessed for LA volumetric and strain parameters using Bland–Altman plots in a sample of 30 random subjects.²⁰ Measurements were done while being blinded for the other measurement approximately 1 month later. Agreement between two measurements was determined as the mean of the difference ± 1.96 SD.

3 | RESULTS

Out of the 155 eligible subjects, 147 subjects were included (median age 43.8 [32.7–56.2], 50% female) into 5 age groups ($n \geq 28$ per group). In total, 8 subjects were excluded: 2 due to having breast implants, 2 subjects had valvular pathology, 1 had a surgically closed ductus, 1 had hypertension, 1 with morbid obesity, and 1 with a right bundle branch block. Table 1 shows the baseline characteristics of the study population.

3.1 | LA volumetric function

Feasibility for volumetric measurements was good, ranging from 92.5% to 95.9% (Table 2). LA volumes were indexed for BSA (Table 2), and an additional analysis was performed with height indexed parameters (Table 3). Changes in volumes can be seen between the age groups regardless of the indexation method. LA minimum and pre–a–wave volumes increased with each age decade. With regard to function, LA reservoir and conduit function decreased while pump function increased with age (Table 4).

3.2 | LA myocardial function

Left atrial–strain analysis results are shown in Table 4, including the feasibility, which ranged from 78.2% to 80.3%. LA–strain was lowest in the oldest age groups as was LA–

Sre, but LA--Sra increased with age (Figure 3). LA--Sra was significantly more negative in men than women, no sex--dependent differences were found in LA--strain and LA--Sre (Figure 4). The limits of normal (mean \pm 2 SD) were also calculated (Table 5).

3.3 | Correlations

Besides age, LA reservoir function did not correlate with baseline characteristics (Table 6). Conduit function decreased slightly with increasing weight, BMI, and blood pressure, while pump function increased with BMI, heart rate, and blood pressure. Conduit and pump function correlated well with LV diastolic parameters. LA--strain, LA--Sre, and LA--Sra correlated well with their volumetric counterparts, LA expansion index and passive and active emptying fraction (r : 0.471 P : <0.001, r : -0.613 P : <0.001, r : -0.541 P : <0.001).

3.4 | Reproducibility

Interobserver agreement was assessed for volumetric and strain measurements: Mean difference for LA maximum volume was -5.2 ± 12.1 mL. For pre--a--wave and minimum volume, this was -0.9 ± 10.2 and -1.0 ± 8.4 mL, respectively. Regarding strain measurements, mean difference for LA peak strain, early and late strain rate were $1.83 \pm 7.91\%$, -0.04 ± 0.63 , and 0.03 ± 0.67 s⁻¹, respectively.

Table 1. Baseline table

	Total n = 147	Male n = 73	Female n = 74	P-value
Age (years)	44.6 \pm 13.8	44.0 \pm 13.7	45.3 \pm 13.8	ns
Height (cm)	175 \pm 9	181 \pm 7	169 \pm 6	<0.001
Weight (kg)	74.6 \pm 12.8	82.4 \pm 11.2	66.9 \pm 9.0	<0.001
Body mass index (kg/m ²)	24.4 \pm 3.3	25.2 \pm 3.3	23.6 \pm 3.0	0.002
Body surface area (m ²)	1.89 \pm 0.19	2.03 \pm 0.15	1.76 \pm 0.12	<0.001
Systolic blood pressure (mm Hg)	127 \pm 15	131 \pm 16	123 \pm 12	0.001
Diastolic blood pressure (mm Hg)	80 \pm 9	82 \pm 9	77 \pm 9	<0.001
Creatinine (μ mol/L)	78 \pm 12	85 \pm 10	71 \pm 10	<0.001

Bold means statistically significant difference between both groups.

4 | DISCUSSION

This prospective study shows that LA function assessed with volumetric and myocardial methods is feasible in a healthy population and that age and LV diastolic function are important determinants of LA function. This study presents values per age decade for LA volumetric and myocardial function in a healthy population.

Table 2 Left atrial echocardiographic volumes indexed for BSA per age decade

Entire study	20–29 y	30–39 y	40–49 y	50–59 y	60–72y	r
	n = 32	n = 28	n = 28	n = 31	n = 28	
Feasibility (%) n = 147						
Method--of--disk summation technique	827. ± 5.7	128. ± 6.6	029. ± 9.2	429. ± 5.5	030. ± 9.1	ns
8LAmaximumvolume(mL/m ²)						
n=136(92.5%)28. ± 7.2						
1LAminimumvolume(mL/m ²)	78. ± 2.5	49. ± 2.8	810. ± 4.0	410. ± 3.2	911. ± 5.2	2520.4370.
n=141(95.9%)10. ± 3.7						
1LApre--a--wavevolume(mL/m ²)	514. ± 3.8	416. ± 3.9	818 ± 5.9	419. ± 4.0	921. ± 6.9	
n=141(95.9%)18. ± 5.5						
Area-length method	929. ± 6.0	230. ± 6.7	131. ± 9.4	731. ± 6.1	332. ± 9.6	ns
0LAmaximumvolume(mL/m ²)						
n=136(92.5%)31. ± 7.5						
9LAminimumvolume(mL/m ²)	49. ± 2.8	010. ± 3.1	511. ± 4.2	311. ± 3.3	013. ± 5.4	2730.4630.
n=141(95.9%)10. ± 3.9						
4LApre--a--wavevolume(mL/m ²)	815. ± 3.9	517. ± 3.9	919. ± 6.1	021. ± 4.2	723. ± 7.1	
n=141(95.9%)19. ± 5.7						

Correlation with age and corresponding --value are reported. *P* Bold means statistically significant correlation with age as a continuous variable.

The largest body of evidence with regard to LA assessment is on LA maximum volume; this reflects remodeling due to increased LV filling pressures. The upper limit of normal is set at 34 mL/m², regardless of age, though recent studies showed that LA maximum volume increases with age.^{3–5,21} This is especially true in the elderly; no correlation was found in our cohort which included individuals up to 72 years old. We speculated that by using STE, LA dysfunction could be detected earlier, which suggests that LV diastolic dysfunction can be detected before apparent LA dilatation, providing clinicians a possibility to intervene earlier. Our results show that LA peak strain did increase with age, which may implicate that strain is a more sensitive marker for LA remodeling in an earlier stage. A recent study also demonstrated that LA myocardial function was diminished in patients with LV diastolic dysfunction while there was no apparent LA dilatation.¹⁹

4.1 | LA volumetric vs myocardial function

This study demonstrates that LA volumetric and myocardial assessment is highly feasible. We recognize that the BSA--indexed maximum volume in our study was large according to current guidelines. However, with parameters such as LA expansion index, passive and active emptying fraction this is no longer relevant, since these measurements are relative.²² Therefore, the reference values of LA volumetric and myocardial function can be extrapolated to other populations. However, there are certain disadvantages to volumetric assessment, like the assumption of geometrical shapes and relatively low reproducibility of especially smaller volumes. STE can overcome these shortcomings because strain analysis does not rely on geometrical assumptions.

4.2 | Factors influencing LA function

There are a lot of factors that could influence LA volume and consequently function. We have assessed the LA through volumetric function with total emptying fraction, a sort of ejection fraction of the LA. It is well known that this is divided into a passive and active phase and that a portion will flow back into the pulmonary veins. Therefore, we also provided LA expansion index, which better describes reservoir function. Instances that influence LA volumes are age, sex, height, and weight. To address these, LA volumes are often indexed using BSA. In our study, we no longer found differences between men and women after correcting for BSA but we did find relatively high values; a quarter of these volunteers had a LA max volume above the upper limit of normal.¹ This might be explained by the fact that height and weight are not both as important for LA volume. The Dutch are the tallest people in the world¹⁵ which is why an additional analysis was done correcting for height as done previously by Eshoo et al.¹⁶ We found no differences when comparing these results with the BSA corrected volumes. The only exception was that LA maximum volume became significantly but weakly correlated with age ($r: 0.202$, $P: 0.018$).

Table 3. Left atrial echocardiographic volumes indexed for an allometric function of height^{2,7}

	Entire study					<i>r</i>	<i>P</i> -value
	20–29 y	30–39 y	40–49 y	50–59 y	60–72 y		
	<i>n</i> = 147	<i>n</i> = 32	<i>n</i> = 28	<i>n</i> = 28	<i>n</i> = 31	<i>n</i> = 28	
LA maximum volume (mL/m ^{2.7})	12.2 ± 3.4	11.2 ± 2.5	11.7 ± 2.7	12.2 ± 4.4	12.6 ± 2.7	13.1 ± 4.4	0.202 0.018
LA minimum volume (mL/m ^{2.7})	4.3 ± 1.7	3.5 ± 1.0	4.0 ± 1.1	4.5 ± 1.9	4.4 ± 1.3	5.2 ± 2.5	0.307 <0.001
LA pre-a-wave volume (mL/m ^{2.7})	7.7 ± 2.6	5.9 ± 1.6	6.9 ± 1.5	7.9 ± 2.7	8.3 ± 1.9	9.5 ± 3.4	0.474 <0.001

Values are presented per age group and the correlation with age and corresponding *P*-value are reported. Bold means statistically significant correlation with age as a continuous variable.

4.3 | Effects of age and LV diastolic function on LA function

Several studies have looked at possible age-related effects on LA size and function, with mixed results.^{3–6,23} The idea that age influences LA function is not new; Benjamin et al²⁴ stated that E-wave velocity decreases while A-wave velocity increases with advancing age. Our study demonstrates that age influences LA myocardial function. LA-strain and LA-Sre are lowest in older subjects while LA-Sra is higher, which is as expected. This is partly in line with the study of Morris et al,¹⁹ who implicated as much for LA-strain measurements. In our study, LA-Sre and LA-Sra also changed with age, though the values that we found for LA-strain were slightly lower than reported earlier.¹⁹ This may be due to age differences between studies or intervender differences, as a recent study showed that QLAB10 reports slightly lower values for GLS than other software packages.²⁵ The study of Miglioranza et al,²⁶ which looked at influences due to age, showed similar effects, though the actual results cannot be compared as the P-wave was used as onset.

Currently, there is no consensus on how to assess LA phasic function with STE. In this study, we used R-wave as onset because that would allow extrapolation of our data to patients with atrial fibrillation. There are other recent studies that used either the R-wave or the P-wave as onset showing that both these techniques are possible.^{19,26,27} We choose for strain rate to assess LA booster pump function instead of peak strain, as this was found to be superior.^{27,28} Pathan et al²⁹ performed a meta-analysis to formulate normal values for LA function. Reservoir function was 39.4% which corresponds very well with our findings, unfortunately for conduit and pump function, strain instead of strain rate was used, which makes it impossible to compare our findings.

Left ventricular diastolic dysfunction is closely related with LA function, and our results reflect that as well. E- and A-wave velocity correlated well with LA conduit and pump function, regardless of the method used. An increase in LV stiffness leads to a reduction in LA conduit function, which is compensated by an increase in pump function. This can be witnessed by the E/A-ratio, which inverses with age. This was seen for the LA myocardial function parameters.

4.4 | Limitations

This was a single-center study including Dutch Caucasian subjects. Extrapolation to other ethnicities should be done with caution. We used QLAB for the strain analysis, though a recent study found no differences between vendors for LA measurements,²⁹ comparison with other vendors should be done with caution. Also, subjects had no restrictions regarding food intake prior to the echocardiographic examination. This could influence tissue- and pulsed-Doppler measurements.³⁰

4.5 | Clinical implications

The results from this study may add to the foundation to formulate reference values regarding LA functional analysis, in preparation for studies to determine potential diagnostic and prognostic value which may eventually be used to assess patients in a clinical setting. In our experience, LA functional analysis, especially myocardial deformation, is easy and quick to perform. As expected, age plays an important role, which is why we propose age-dependent reference ranges. The fact that LA maximum volume did not correlate with age but LA-strain did indicates that functional assessment is a more sensitive marker.

Future studies should investigate the potential prognostic value of LA function and which technique, myocardial deformation or volumetric assessment, is most valuable.

Table 4. Left atrial function per age decade

	Entire study n = 147	20–29 y n = 32	30–39 y n = 28	40–49 y n = 28	50–59 y n = 31	60–72 y n = 28	r	P-value
Feasibility (%)								
LA volumetric function	n = 136 (92.5%)							
LA reservoir function (%)	18.7 ± 4.8	19.2 ± 4.7	18.7 ± 4.5	18.3 ± 6.3	19.0 ± 4.1	18.1 ± 4.7	ns	ns
Total emptying volume	201.2 ± 71.4	238.5 ± 83.5	206.2 ± 46.2	184.2 ± 70.8	199.4 ± 77.2	169.3 ± 51.8	-0.262	0.002
Expansion index	65.9 ± 7.7	68.8 ± 7.3	66.6 ± 5.0	62.9 ± 8.5	64.8 ± 7.8	61.5 ± 7.4	-0.279	0.001
Total emptying fraction	10.8 ± 4.2	13.3 ± 3.1	11.7 ± 4.0	10.3 ± 4.6	10.0 ± 3.6	8.1 ± 3.9	-0.399	<0.001
LA conduit function (%)	37.1 ± 11.3	47.9 ± 6.9	40.8 ± 9.4	34.7 ± 8.7	33.8 ± 9.4	26.6 ± 9.4	-0.613	<0.001
Passive emptying fraction	8.0 ± 2.9	5.9 ± 2.3	7.0 ± 1.8	8.0 ± 3.0	9.0 ± 2.6	10.0 ± 2.8	0.512	<0.001
LA pump function (%)	44.2 ± 10.0	40.3 ± 10.5	43.1 ± 7.5	43.3 ± 9.8	46.7 ± 10.2	47.1 ± 10.3	0.281	0.001
Active emptying fraction								
LA myocardial deformation analysis								
LA--strain (%)	n = 118 (80.3%)	39.6 ± 6.3	41.7 ± 6.5	40.4 ± 5.3	39.1 ± 5.8	37.1 ± 6.3	-0.227	0.014
LA--Sre (s ⁻¹)	n = 115 (78.2%)	-2.76 ± 0.63	-3.29 ± 0.54	-3.06 ± 0.32	-2.77 ± 0.38	-2.23 ± 0.45	-0.715	<0.001
LA--Sra (s ⁻¹)	n = 118 (80.3%)	-2.57 ± 0.62	-2.33 ± 0.52	-2.35 ± 0.40	-2.65 ± 0.55	-2.83 ± 0.80	0.348	<0.001
LV function								
E--wave (m/s)	0.69 ± 0.16	0.79 ± 0.15	0.75 ± 0.16	0.66 ± 0.15	0.65 ± 0.11	0.59 ± 0.13	-0.457	<0.001
A--wave (m/s)	0.49 ± 0.15	0.38 ± 0.14	0.43 ± 0.09	0.47 ± 0.10	0.57 ± 0.11	0.62 ± 0.17	0.582	<0.001
E/A--ratio	1.6 ± 0.7	2.3 ± 0.8	1.8 ± 0.4	1.4 ± 0.4	1.2 ± 0.3	1.0 ± 0.3	-0.68	<0.001
Deceleration time (ms)	190 ± 41	178 ± 28	181 ± 32	185 ± 29	195 ± 32	216 ± 64	0.313	<0.001
E' (LV septum) (cm/s)	9.5 ± 2.6	12.5 ± 1.8	10.4 ± 1.6	9.2 ± 1.6	8.2 ± 1.8	6.9 ± 1.7	-0.756	<0.001
E/E'--ratio	7.6 ± 1.9	6.5 ± 0.2	7.3 ± 1.5	7.3 ± 1.7	8.1 ± 1.4	9.1 ± 2.4	0.472	<0.001
LV ejection fraction (%)	60 ± 5	60 ± 3.6	61 ± 5	59 ± 5	62 ± 5	59 ± 5	ns	ns

The upper part of the table present volumetric assessment, followed by LA myocardial function. Additionally, LV diastolic and systolic values are presented. Correlations with age and corresponding P-values are given.

Bold means statistically significant correlation with age as a continuous variable.

5 | CONCLUSION

Left atrial volumetric and myocardial function measurement is a viable option, and age--dependent reference ranges for LA phasic function are presented. LA myocardial and volumetric function pa-rameters have proven to be age--but not sex--dependent. Considering the high feasibility and clinical relevance of LA myocardial function mea-surements, these results can help integrate LA STE analysis into clinical practice.

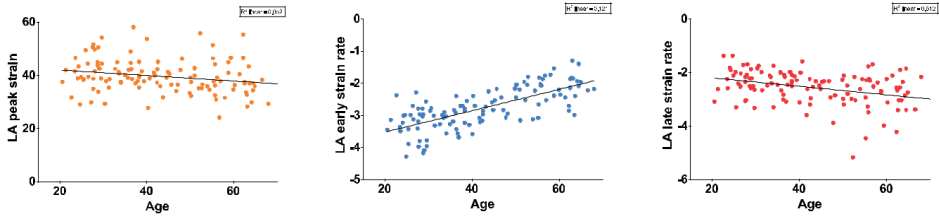


Figure 3. Correlations between left atrial (LA)--strain, LA--Sre and LA--Sra and age. Each dot represents one individual's measurement. The fitted lines and r^2 values are given. All three variables were significantly correlated with age

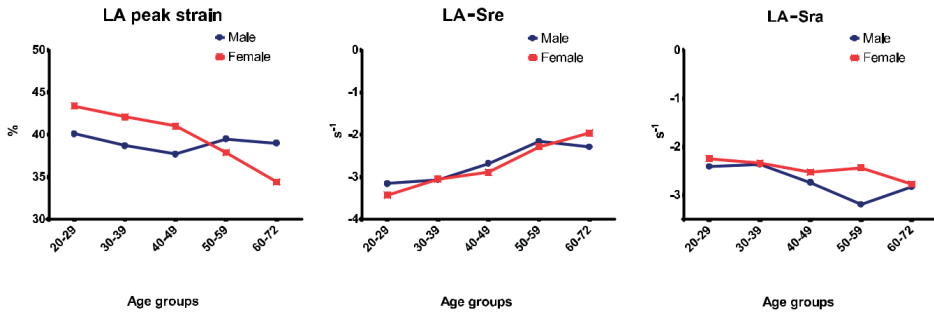


Figure 4. Three graphs showing left atrial myocardial function per sex for each age group

Table 5. Limits of normal for LA function assessed with volumetric and myocardial deformation

	Entire study		20-29 y		30-39 y		40-49 y		50-59 y		60-72 y	
	LLN	ULN	LLN	ULN	LLN	ULN	LLN	ULN	LLN	ULN	LLN	ULN
LA volumetric function												
Total emptying volume (mL/m ²)	9.1	28.3	9.8	28.6	9.7	27.7	5.7	30.9	10.8	27.2	8.7	27.5
Total emptying fraction (%)	50.5	81.3	54.2	83.4	56.6	76.6	45.9	79.9	49.2	80.4	46.7	76.3
Expansion index (%)	58.4	344	71.5	405.5	113.8	298.6	42.6	325.8	45	353.8	65.7	272.9
Passive emptying volume (mL/m ²)	2.4	19.2	7.1	19.5	3.7	19.7	1.1	19.5	2.8	17.2	0.3	15.9
Passive emptying fraction (%)	14.5	59.7	34.1	61.7	22	59.6	17.3	52.1	15	52.6	7.8	45.4
Active emptying volume (mL/m ²)	2.2	13.8	1.3	10.5	3.4	10.6	2	14	3.8	14.2	4.4	15.6
Active emptying fraction (%)	24.2	64.2	19.3	61.3	28.1	58.1	23.7	62.9	26.3	67.1	26.5	67.7
LA myocardial deformation analysis												
LA--strain (%)	27	52.2	28.7	54.7	29.8	51	27.5	50.7	24.9	52.5	-49.7	-24.5
LA--Sre (s ⁻¹)	-4.02	-1.5	-4.37	-2.21	-3.7	-2.42	-3.53	-2.01	-3.13	-1.33	-3.06	-1.26
LA--Sra (s ⁻¹)	-3.81	-1.33	-3.37	-1.29	-3.15	-1.55	-3.75	-1.55	-4.43	-1.23	-4.07	-1.55

LLN = lower limit of normal; ULN = upper limit of normal.

Table 6. Table describing correlations between LA function (volumetric and myocardial) and baseline characteristics

	LA--strain	LA--Sre	LA--Sra
	<i>r</i>	<i>r</i>	<i>r</i>
Age	-0.227[*]	0.715^{**}	-0.348^{**}
Height	-0.045	0.011	-0.012
Weight	-0.068	0.246[*]	-0.153
Body mass index	-0.043	0.307[*]	-0.197[*]
Body surface area	-0.067	0.185[*]	-0.119
Heart rate	-0.052	0.076	-0.254[*]
Systolic blood pressure	-0.081	0.186[*]	-0.275[*]
Diastolic blood pressure	-0.1	0.333[*]	-0.295[*]
E--wave	0.331^{**}	-0.566^{**}	0.182[*]
A-wave	-0.004	0.422^{**}	-0.367^{**}
E'	0.331^{**}	-0.697^{**}	0.268[*]
E/e'	-0.111	0.298[*]	-0.128
Left atrial expansion index	0.468^{**}	-0.381^{**}	-0.257[*]
Left atrial passive emptying fraction	0.354^{**}	-0.590^{**}	0.249[*]
Left atrial active emptying fraction	0.198[*]	0.115	-0.545^{**}
LA--Sra	-0.478^{**}	-	-

Bold mean statistically significant, **P*--value < 0.05, ***P*--value < 0.001

REFERENCES

1. Lang RM, Badano LP, Mor-Avi V, et al. Recommendations for cardiac chamber quantification by echocardiography in adults: an update from the American Society of Echocardiography and the European Association of Cardiovascular Imaging. *Eur Heart J Cardiovasc Imaging*. 2015;16:233–270.
2. Appleton CP, Galloway JM, Gonzalez MS, et al. Estimation of left ventricular filling pressures using two-dimensional and Doppler echocardiography in adult patients with cardiac disease. Additional value of analyzing left atrial size, left atrial ejection fraction and the difference in duration of pulmonary venous and mitral flow velocity at atrial contraction. *J Am Coll Cardiol* 1993;22:1972–1982.
3. Okamoto K, Takeuchi M, Nakai H, et al. Effects of aging on left atrial function assessed by two-dimensional speckle tracking echo-cardiography. *J Am Soc Echocardiogr*. 2009;22:70–75.
4. Nikitin NP, Witte KK, Thackray SD, et al. Effect of age and sex on left atrial morphology and function. *Eur J Echocardiogr*. 2003;4:36–42.
5. Boyd AC, Schiller NB, Leung D, et al. Atrial dilation and altered function are mediated by age and diastolic function but not before the eighth decade. *JACC Cardiovasc Imaging*. 2011;4:234–242.
6. Kou S, Caballero L, Dulgheru R, et al. Echocardiographic reference ranges for normal cardiac chamber size: results from the NORRE study. *Eur Heart J Cardiovasc Imaging*. 2014;15:680–690.
7. Cameli M, Caputo M, Mondillo S, et al. Feasibility and reference values of left atrial longitudinal strain imaging by two-dimensional speckle tracking. *Cardiovasc Ultrasound*. 2009;7:6.
8. Vianna-Pinton R, Moreno CA, Baxter CM, et al. Two-dimensional speckle-tracking echocardiography of the left atrium: feasibility and regional contraction and relaxation differences in normal subjects. *J Am Soc Echocardiogr*. 2009;22:299–305.
9. Kim DG, Lee KJ, Lee S, et al. Feasibility of two-dimensional global longitudinal strain and strain rate imaging for the assessment of left atrial function: a study in subjects with a low probability of cardiovascular disease and normal exercise capacity. *Echocardiography*. 2009;26:1179–1187.
10. Saraiva RM, Demirkol S, Buakhamsri A, et al. Left atrial strain measured by two-dimensional speckle tracking represents a new tool to evaluate left atrial function. *J Am Soc Echocardiogr*. 2010;23:172–180.
11. Sun JP, Yang Y, Guo R, et al. Left atrial regional phasic strain, strain rate and velocity by speckle-tracking echocardiography: normal values and effects of aging in a large group of normal subjects. *Int J Cardiol*. 2013;168:3473–3479.
12. Xia J, Gao Y, Wang Q, et al. Left atrial function examination of healthy individuals with 2D speckle-tracking imaging. *Exp Ther Med*. 2013;5:243–246.
13. Menting ME, McGhie JS, Koopman LP, et al. Normal myocardial strain values using 2D speckle tracking echocardiography in healthy adults aged 20 to 72 years. *Echocardiography*. 2016;33:1665–1675.
14. Rosner A, Barbosa D, Aarsaether E, et al. The influence of frame rate on two-dimensional speckle-tracking strain measurements: a study on silico-simulated models and images recorded in patients. *Eur Heart J Cardiovasc Imaging*. 2015;16:1137–1147.
15. Collaboration NCDRF. A century of trends in adult human height. *Elife*. 2016;5:e13410.

16. Eshoo S, Ross DL, Thomas L. Impact of mild hypertension on left atrial size and function. *Circ Cardiovasc Imaging*. 2009;2:93–99.
17. Nagueh SF, Smiseth OA, Appleton CP, et al. Recommendations for the evaluation of left ventricular diastolic function by echocardiography: an update from the American Society of Echocardiography and the European Association of Cardiovascular Imaging. *Eur Heart J Cardiovasc Imaging*. 2016;17:1321–1360.
18. Mor-Avi V, Lang RM, Badano LP, et al. Current and evolving echo-cardiographic techniques for the quantitative evaluation of cardiac mechanics: ASE/EAE consensus statement on methodology and indications endorsed by the Japanese Society of Echocardiography. *Eur J Echocardiogr*. 2011;12:167–205.
19. Morris DA, Takeuchi M, Krisper M, et al. Normal values and clinical relevance of left atrial myocardial function analysed by speckle-tracking echocardiography: multicentre study. *Eur Heart J Cardiovasc Imaging*. 2015;16:364–372.
20. Bland JM, Altman DG. Statistical methods for assessing agreement between two methods of clinical measurement. *Lancet*. 1986;1:307–310.
21. D’Andrea A, Riegler L, Rucco MA, et al. Left atrial volume index in healthy subjects: clinical and echocardiographic correlates. *Echocardiography*. 2013;30:1001–1007.
22. van Grootel RWJ, Menting ME, McGhie J, et al. Echocardiographic chamber quantification in a healthy Dutch population. *Neth Heart J*. 2017;25(12):682–690.
23. Spencer KT, Mor-Avi V, Gorcsan J 3rd, et al. Effects of aging on left atrial reservoir, conduit, and booster pump function: a multi-institution acoustic quantification study. *Heart*. 2001;85:272–277.
24. Benjamin EJ, Levy D, Anderson KM, et al. Determinants of Doppler indexes of left ventricular diastolic function in normal subjects (the Framingham Heart Study). *Am J Cardiol*. 1992;70:508–515.
25. Farsalinos KE, Daraban AM, Unlu S, et al. Head-to-head comparison of global longitudinal strain measurements among nine different vendors: the EACVI/ASE inter-vendor comparison study. *J Am Soc Echocardiogr*. 2015;28:1171–1181, e1172.
26. Miglioranza MH, Badano LP, Mihaila S, et al. Physiologic determinants of left atrial longitudinal strain: a two-dimensional speckle-tracking and three-dimensional echocardiographic study in healthy volunteers. *J Am Soc Echocardiogr*. 2016;29:1023–1034. e1023.
27. Rimbaz RC, Mihaila S, Vinereanu D. Sources of variation in assessing left atrial functions by 2D speckle-tracking echocardiography. *Heart Vessels*. 2016;31:370–381.
28. Hayashi S, Yamada H, Bando M, et al. Optimal analysis of left atrial strain by speckle tracking echocardiography: P-wave versus R-wave trigger. *Echocardiography*. 2015;32:1241–1249.
29. Pathan F, D’Elia N, Nolan MT, et al. Normal ranges of left atrial strain by speckle-tracking echocardiography: a systematic review and meta-analysis. *J Am Soc Echocardiogr*. 2017;30:59–70. e58.
30. Dencker M, Bjorgell O, Hlebowicz J. Effect of food intake on commonly used pulsed Doppler and tissue Doppler measurements. *Echocardiography*. 2011;28:843–847.

A large, bold, dark grey number '6' is positioned on the right side of the page. It is partially overlaid by a solid grey rectangular shape that extends from the top right corner towards the center.

The mitral annular displacement by two-dimensional speckle tracking – a new tool in evaluating the left atrial function

Based on:

Strachinaru M, Annis C, Catez E, Jousten I, Lutea ML, Pavel O, Morissens M. *The mitral annular displacement by two-dimensional speckle tracking: a new tool in evaluating the left atrial function.*

J Cardiovasc Med (Hagerstown). 2016;17:344-53.

ABSTRACT

Background: The methods used to characterize the volume change and the deformation of the left atrium(LA) are highly dependent on technical factors and difficult to use in a clinical environment. The aim of this study was to demonstrate that mitral annulus displacement(MAD) by speckle tracking can be an alternative method to studying the longitudinal LA function.

Methods: 90 subjects(54% males), with a mean age of 53(\pm 15), underwent a complete echocardiographic examination, comprising 2D, 3D and TDI. They were divided into normal individuals(35) and patients having an abnormal echocardiography(55).

Results: There was a very strong correlation between 3D volumetric function and MAD, both for the reservoir($r=0,78$; $p<0,0001$) and contractile($r=0,76$; $p<0,0001$) functions. The correlation with the longitudinal strain displayed an $r=0,87$, $p>0,0001$ for the reservoir and $r=0,81$, $p<0,0001$ for the contractile function. The systolic speed in pulsed TDI and the systolic displacement had an $r=0,83$, $p<0,0001$. MAD was a very good discriminator for normal vs abnormal subjects(AUC for reservoir= $0,872$ and for contractile= $0,843$; $p<0,0001$), performing less well than 3D(AUC reservoir= $0,892$ and contractile= $0,915$; $p<0,0001$) or deformation(AUC= $0,921$ and $0,903$ respectively; $p<0,0001$), but better than pulsed TDI(AUC= $0,807$; $p<0,0001$). The percentage error was $\pm 15\%$ for inter and $\pm 12\%$ for intra-observer variability. The time taken for displacement analysis was 9 ± 3 sec for an experienced cardiologist and 12 ± 4 sec for a beginner.

Conclusion: MAD by speckle tracking is a reliable and fast method to evaluate LA function. Given the strength of the correlations with strain parameters, it could be used as a surrogate measure of the deformation of LA.

INTRODUCTION

Left atrium global and longitudinal function have been subjects of study for a long time¹⁻⁶. The particular shape of the left atrium makes the volumetric methods employed for the left ventricle difficult to use⁷⁻⁸. Numerous articles describe the role of the 2D and 3D imaging⁹⁻¹², and deformation techniques, using tissue Doppler¹³⁻¹⁸ or 2D speckle tracking¹⁹. The results are globally encouraging, and there is a growing body of evidence concerning the prognostic value of the left atrium function, in particular the deformation parameters related to atrial reservoir, conduit or contractile function²⁰⁻²⁴. However, these methods are not easy to use in everyday clinical practice. They are time consuming and they rely (especially for the 2D methods), on algorithms designed initially for the evaluation of the left ventricle²⁵.

The purpose of this methodological study was to demonstrate that the displacement of the mitral annulus, computed by speckle tracking, can be an easy and fast alternative method to studying the longitudinal function of the left atrium, having the advantages of the 2D speckle tracking and TDI techniques.

METHODS

Subjects referred for cardiac ultrasound examination were divided into two groups. The normal subjects were disease-free individuals above the age of 18, undergoing a routine screening evaluation. The main inclusion criteria for this group were the absence of significant medical history and a strictly normal echocardiographic examination, defined as the absence of any abnormal findings and echocardiographic parameters situated in the defined normal range²⁶. The abnormal subjects group was chosen among general cardiology patients, with significant history of cardiovascular disease, having an enlarged left atrium, with or without other abnormal echocardiographic findings. Patients having prosthetic valves, important annular calcification (more than 2/3 of the posterior annulus²⁷), significant areas of myocardial scar (more than 3 myocardial segments, involving the basal segments), atrial fibrillation/flutter at the time of image acquisition, or more than mild mitral regurgitation were excluded from the study.

The study was approved by the Medical Ethical Committee. The subjects gave their informed consent for the inclusion in this research.

Echocardiography

Two-dimensional and three-dimensional echocardiography was performed at inclusion, using a Philips iE33 system (Philips, Best, The Netherlands), with the patient in the left lateral decubitus position. The examinations were performed by two different experienced cardiologists (MS and MM) and then interpreted separately offline by MS and CA (resident doctor in Cardiology), who were blinded to the status of the subject, using the QLab9 Software (Philips). The results of their evaluations were compared in order to assess the inter and intra observer agreement. 2D images were acquired in standard apical 2, 3 and 4 chambers. Full volume of at least 4 beats, optimized for the visualization of the left atrium (LA), were also obtained in the apical window²⁶.

The indexation for the body surface area was considered unnecessary, since this value was stable for the same patient.

a) 3D full volume semi automated border detection method

The LA maximum volume was considered the largest volume of the LA measured at the end of the left ventricular systole, in the frame just before mitral valve opening. The LA minimum volume is defined as the smallest LA volume, just after the P wave on ECG, at mitral valve closure. The LA pre-systolic volume is measured in the frame before the onset of the P wave on the ECG.

The emptying fraction (EptF) was defined as $EptF = (LA \text{ maximum volume} - LA \text{ minimum volume}) / LA \text{ maximum volume}$. The ejection fraction (EF) was defined as $EF = (LA \text{ pre-systolic volume} - LA \text{ minimum volume}) / LA \text{ pre-systolic volume}$ ²⁶.

The 3D EptF and EF were used as reference for the other methods.

b) Tissue Doppler

Tissue Doppler pulsed-wave acquisitions were obtained in the apical 2 and 4 chambers views, at the level of the 4 mitral annulus points: medial(septal), lateral, anterior and inferior, using a narrow tissue Doppler sector and a parallel alignment for an optimal image.

The value used to characterize left atrium contractile function was the maximum velocity of the a' wave on the tissue Doppler tracing (the late diastolic negative deflection following the P wave on the ECG).

c) *2D speckle tracking*

The left atrial strain and strain rate were estimated using the 2d speckle tracking method, also initially designed for the evaluation of the left ventricle, in 2,3 and 4 chambers apical views. The baseline point was set at the onset of QRS. We retained the global longitudinal strain (GLS= mean maximal atrial strain during atrial diastole) as a marker of the reservoir function of the left atrium and the atrial systolic strain rate²⁸ (SSR= the maximal negative deflection of the mean strain rate curve, after the P wave on the ECG) as a marker of the contractile function (Figure 1).

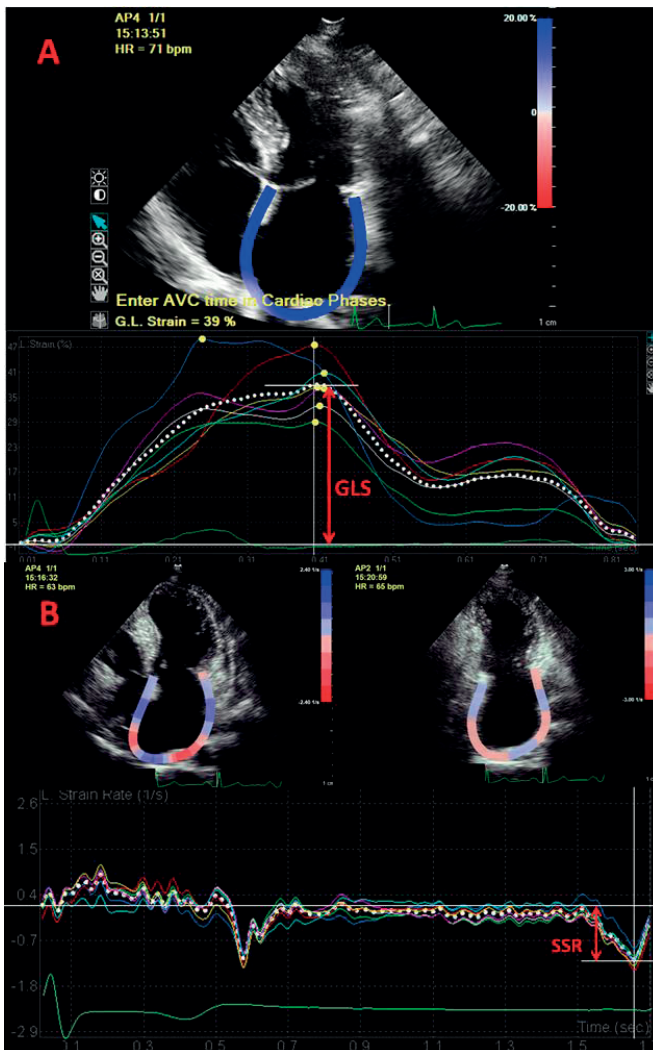


Figure 1. The longitudinal deformation of the left atrial wall by speckle tracking. A: maximal strain (GLS); B: atrial systolic strain rate (SSR).

d) ***Mitral annular displacement***

Mitral annulus displacement by speckle tracking was calculated offline using the QLAB 9 software²⁹ (Philips Healthcare). In order to minimize the errors, the “apical” fixed point was chosen at the bottom of the left atrium, together with the classical four mitral annular points (Figure 2). Using the time-displacement curves the maximum negative and positive displacement points were noted, as well as the position during diastasis. Because the program was developed for the assessment of left ventricular function, the baseline is considered at the onset of QRS. The annular displacement is calculated as the arithmetic sum of the displacement values. The global displacement (D) can be obtained by averaging the four annular points, between the maximal negative and positive positions (Figure 3A). The systolic displacement (S) is defined as the average of the four points movement between diastasis and maximal positive position (Figure 3B).

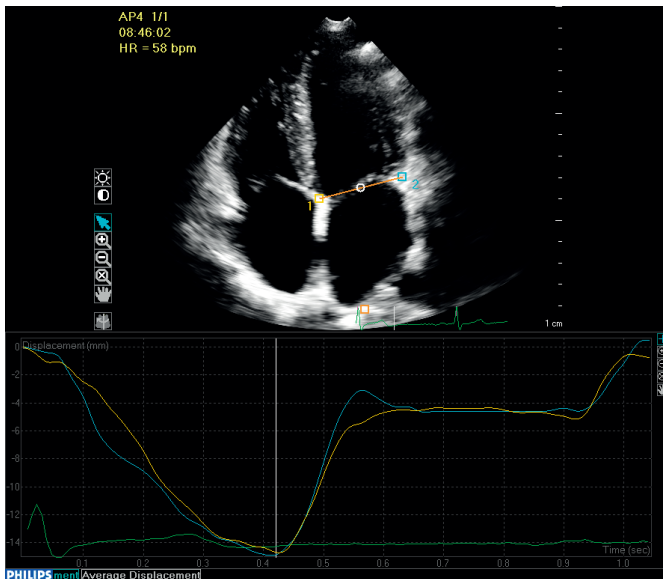


Figure 2. Mitral annular displacement by speckle tracking in apical 4 chambers view. The “apical” fixed point is situated at the bottom of the left atrium.

Statistical analysis

Continuous variables are presented as means (\pm SD). Categorical variables are presented as frequencies and percentages. Differences between proportions were estimated by the chi-square test, between mean values by the unpaired *t* test, and between similar parameters by the paired *t*-test. Correlations were computed using Pearson’s method, and graphically represented with linear regression lines. ROC curve analysis was used to estimate the discriminative power of the different methods. A two-sided *p* value of less than 0.05 was used for declaring statistical significance.

The mitral annular displacement by two-dimensional speckle tracking – a new tool in evaluating the left atrial function

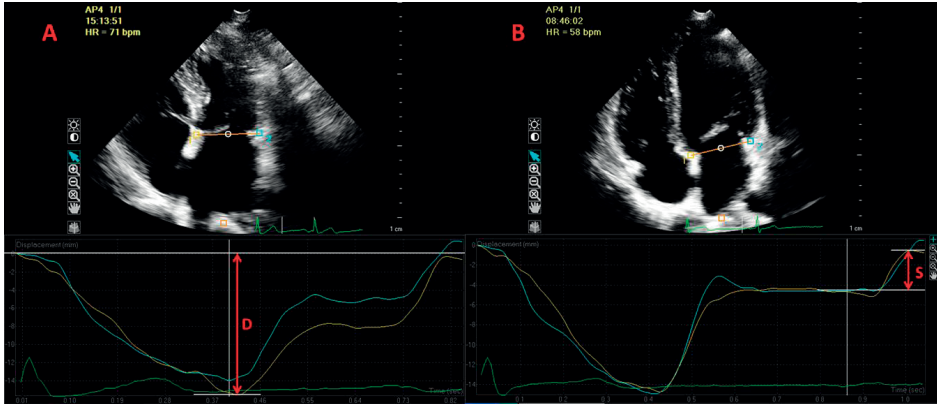


Figure 3. Displacement values calculated from the time-displacement curves, for the medial point. A: D(total displacement value) from maximal negative to the maximal positive position; B: systolic displacement S, between diastasis and maximal positive position.

The inter and intra observer variability were assessed using Bland-Altman plots, and reported as bias, limits of agreement and percentage error. This variability was compared to the variability between subjects as reference for the limits of agreement³⁰.

All statistical analyses were performed with SPSS 21.0 software (SPSS Inc, Chicago, IL, USA).

RESULTS

90 patients (54% males), with a mean age of 53 ± 15 , were included in the study. 35 (39%) of them had a normal echocardiographic examination. 55 patients with abnormal echo examination were also selected. The baseline clinical features are depicted in Table 1.

Table 1. Baseline clinical features of study participants (normal vs abnormal)

Parameter	Normal N=35	Abnormal N=55	p
Age	48±17	56±11	0,008
Male gender	16 (46%)	34(62%)	0,13
Obesity	8(23%)	18(33%)	0,31
Smoking	11(31%)	17(31%)	0,95
Dyslipidemia	16(46%)	36(66%)	0,06
Diabetes	0	11(20%)	
Hypertension	0	28(51%)	
Renal failure	0	4(7%)	
Atrial fibrillation (converted to sinus rhythm)	0	36(66%)	
Coronary artery disease	0	3(6%)	
COPD	0	2(4%)	

Table 2. Echocardiographic variables

<i>Variable</i>	<i>Normal individuals n=35</i>	<i>Abnormal echo n=55</i>	<i>p</i>
LA 3D maximal volume (ml)	47(±8)	68(±19)	<0,0001
LA EptF (%)	67(±8)	49(±16)	<0,0001
LA EF (%)	39(±12)	21(±16)	<0,0001
TDI mean a'	10(±2)	7(±3)	<0,0001
LA GLS (%)	39(±8)	24(±12)	<0,0001
LVEF (%)	65(±4)	59(±10)	0,001
Systolic strain rate (%)	2,8(±0,5)	1,7(±1,1)	<0,0001
Total mean annulus displacement (mm)	14(±1,7)	10(±3,3)	<0,0001
Atrial systolic annulus displacement (mm)	7(±1,7)	4,5(±2,5)	<0,0001

Data are presented as mean ±SD or number (percentage %)

EF= ejection fraction of the LA; EptF= emptying fraction of the LA; GLS=global longitudinal strain of the left atrium; LA=left atrium; LVEF=left ventricle ejection fraction; TDI=tissue Doppler Imaging

The main echocardiographic variables analyzed in this population are shown in Table 2. Significant differences existed for all variables between normal and abnormal echocardiography groups.

Intra and inter observer agreement for the mitral annulus displacement by speckle tracking

24 consecutive patients were analyzed by MS at the time of acquisition of data, on the QLAB 9 postprocessing software available on the echo machine, and reviewed lately in a blinded random manner, together with all the other patients. The same group was evaluated by AC (resident doctor in Cardiology), to estimate for inter observer variability. The results concerning the intra and inter observer variability are shown in Table 3 and the Bland-Altman plots in Figure 4. The limits of agreement were tighter for the intra compared to inter observer variability (a percentage error of -11% to 13% vs -15% to 15%), and the variability between subjects largely greater than inter or intra observer variabilities.

Table 3. Intra and inter observer variability for the measure of global displacement D in millimeters

	<i>Mean D initial</i>	<i>Mean D second</i>	<i>Bias</i>	<i>Lower limit/ percentage error</i>	<i>Upper limit/ percentage error</i>
Intra observer	11,8(±2,9)	11,9(±3,2)	0,12	-1,29 (-11%)	1,53 (13%)
Inter observer	11,8(±2,9)	11,8(±3,3)	-0,03	-1,77 (-15%)	1,74 (15%)

The mitral annular displacement by two-dimensional speckle tracking – a new tool in evaluating the left atrial function

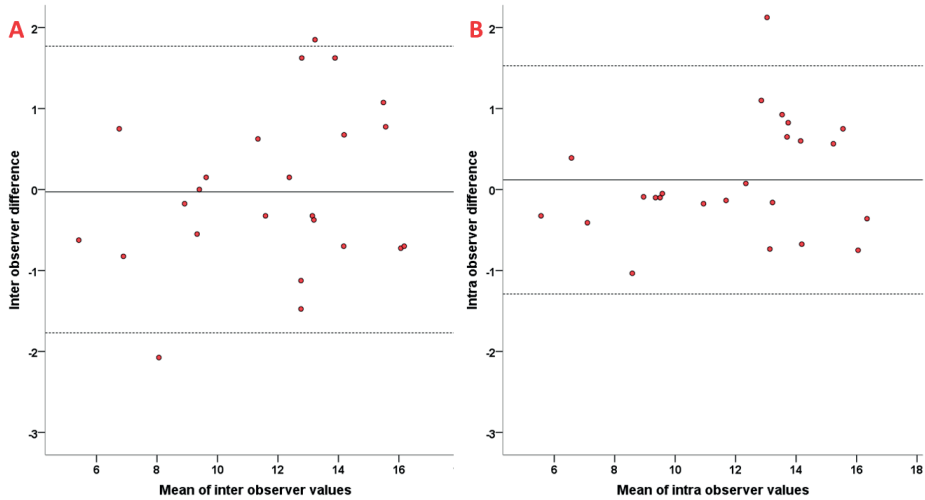


Figure 4. Bland-Altman plots showing the limits of agreement for intra observer (A) and inter observer (B) agreement.

Time requirements

The time taken to obtain the mitral annulus displacement was estimated for an experienced user (MS) and for a beginner (CA). The time taken to obtain a tracking in only apical 4 chambers view was 9 ± 3 sec for MS and 12 ± 4 sec for CA. The time taken to measure the displacement values in this single apical window was 72 ± 14 sec for MS and 106 ± 19 sec for CA. The total time necessary to obtain all the displacement values used in this study was 164 ± 36 sec for MS and 233 ± 49 sec for CA.

Correlations between variables in the overall group

The GLS was strongly correlated to the EptF, $r=0,80$, $R^2=0,65$, $p<0,0001$. The total annular displacement D correlated strongly with the EptF, $r=0,78$, $R^2=0,61$, $p<0,0001$. The global longitudinal strain strongly related to D, $r=0,87$, $R^2=0,75$, $p<0,0001$ (Figure 5).

The mean value of annular velocity in TDI correlated well with the EF, $r=0,66$, $R^2=0,44$, $p=0,0001$. The atrial systolic strain rate (SSR) displayed a strong correlation with the EF, $r=0,76$, $R^2=0,57$, $p<0,0001$. The relation of the systolic annular displacement S with the EF was strong with $r=0,76$, $R^2=0,58$, $p<0,0001$. The correlation of the SSR and S was very good, $r=0,81$, $R^2=0,65$, $p<0,0001$ (Figure 5). The mean TDI speed of the annular teledia-stolic motion correlated very strongly with S, $r=0,83$, $R^2=0,69$, $p<0,0001$.

Correlations of variables in the normal echo group

In the patients' group having a normal echocardiography (n=35, 43% males), the level of correlation of the empty fraction EptF to the GLS was moderate, $r=0,47$, $R^2=0,22$, $p=0,004$. The mean annular displacement D, when compared with EptF, had an $r=0,641$, $R^2=0,41$, $p<0,0001$. The relation between GLS and D was good, $r=0,624$, $R^2=0,39$, $p<0,0001$.

The mean annular systolic speed measured in TDI was not related to the EF, $r=0,311$, $p=0,07$. The SSR correlated moderately to the EF, $r=0,402$, $R^2=0,16$, $p=0,02$. The systolic displacement of the annulus (S) correlated strongly with the ejection fraction, $r=0,67$, $R^2=0,45$, $p<0,0001$, and with the mean value of TDI annular speed $r=0,608$, $R^2=0,37$, $p<0,0001$. The systolic strain rate was also moderately associated with the systolic displacement, $r=0,411$, $R^2=0,17$, $p=0,01$.

Correlations of variables in the abnormal echo group

In the patients with an abnormal echocardiography (n=55, 62% males), the global longitudinal strain was strongly correlated to the EptF, $r=0,77$, $R^2=0,59$, $p<0,0001$. The total mean annular displacement D was also strongly correlated with EptF, $r=0,73$, $R^2=0,53$, $p<0,0001$. The GLS was very strongly correlated with displacement $r=0,89$, $R^2=0,79$, $p<0,0001$.

The mean value of tissue Doppler annular speed correlated well with the EF, $r=0,68$, $R^2=0,46$, $p<0,0001$. The SSR relation with EF had an $r=0,78$, $R^2=0,60$, $p<0,0001$. The systolic displacement of the mitral annulus correlated strongly with the EF, $r=0,75$, $R^2=0,56$, $p<0,0001$. The correlation between SSR and S was very strong, $r=0,84$, $R^2=0,70$, $p<0,0001$. The same level of correlation of S could be found with the mean value of the annular displacement speed in TDI, $r=0,85$, $R^2=0,73$, $p<0,0001$.

Comparison of the parameters of global function, the deformation indices and the local annular displacement

ROC curves were plotted to compare the global longitudinal strain (GLS) and the emptying fraction (EptF), as measurements of the global function of the left atrium with the global and local total displacement of each annular point (medial, lateral, inferior and anterior). The ejection fraction (EF), the A velocity in TDI and the atrial systolic strain rate (SSR) were compared with the systolic displacement globally and point by point.

The results are presented in Table 4 and graphically represented in Figure 6. We have found that the best discriminators of abnormal vs normal patients were the global longitudinal strain, with an area under the curve (AUC)=0,921, the ejection fraction of the left atrium (AUC=0,915), and the SSR (AUC=0,903). They were followed by the empty-

ing fraction of the LA (AUC=0,892), the total displacement D (AUC=0,872), the systolic displacement S (AUC=0,843) and the mean value of A in TDI (AUC=0,807). On the point-by-point analysis, the medial point was a better predictor than the other annular points when considering the total (AUC=0,872) or systolic displacement (AUC=0,846).

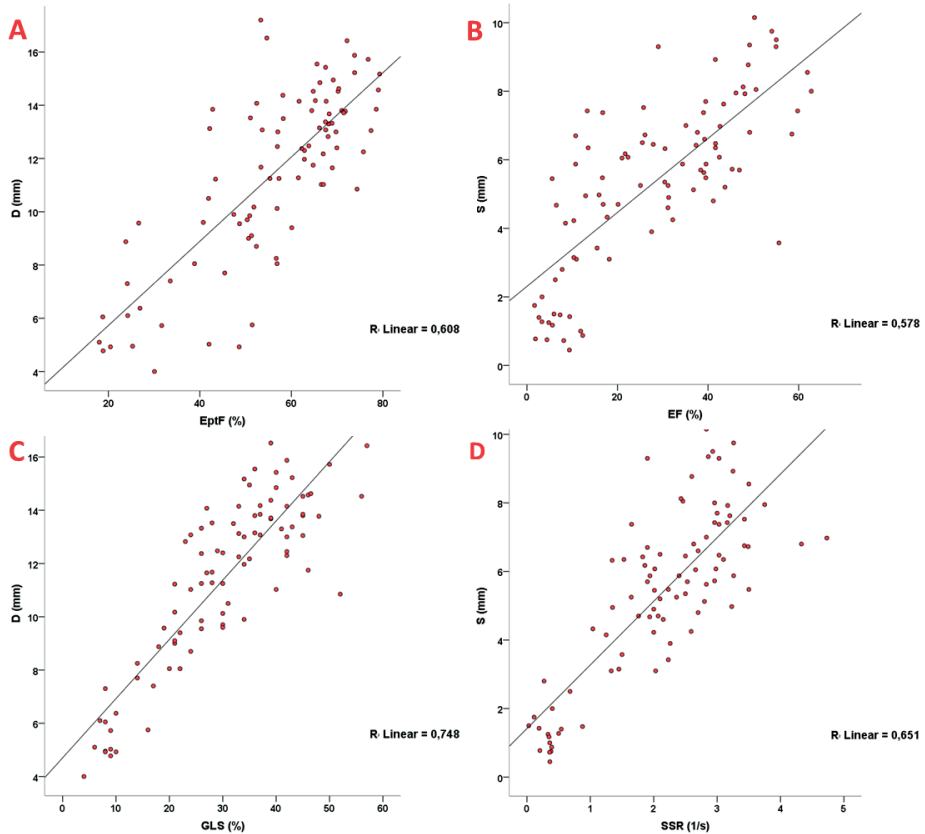


Figure 5. Correlations in the overall group. A: correlation between the global displacement (D) and the emptying fraction (EptF); B: Relation between systolic displacement (S) and the ejection fraction of the left atrium (EF); C: Correlation between the global longitudinal strain (GLS) and D; C: Correlation of the systolic strain rate (SSR) and S.

Table 4. Comparison between volumetric, TDI and deformation parameters and the mitral annulus displacement

Functional parameter	ROC area under the curve			
	Area under the curve (AUC)	95% Confidence interval		p
Lower bound		Upper bound		
GLS (%)	0,921	0,868	0,974	<0,0001
EptF (%)	0,892	0,825	0,958	<0,0001
Lateral D (mm)	0,812	0,723	0,901	<0,0001
Medial D (mm)	0,872	0,797	0,946	<0,0001
Anterior D (mm)	0,838	0,754	0,922	<0,0001
Inferior D (mm)	0,858	0,775	0,941	<0,0001
D (mm)	0,872	0,797	0,947	<0,0001
EF (%)	0,915	0,857	0,972	<0,0001
SSR (s ⁻¹)	0,903	0,836	0,971	<0,0001
TDI mean A (cm/s)	0,807	0,714	0,908	<0,0001
Lateral S (mm)	0,749	0,645	0,852	<0,0001
Medial S (mm)	0,846	0,764	0,928	<0,0001
Anterior S (mm)	0,826	0,736	0,916	<0,0001
Inferior S (mm)	0,798	0,705	0,892	<0,0001
S (mm)	0,843	0,761	0,926	<0,0001

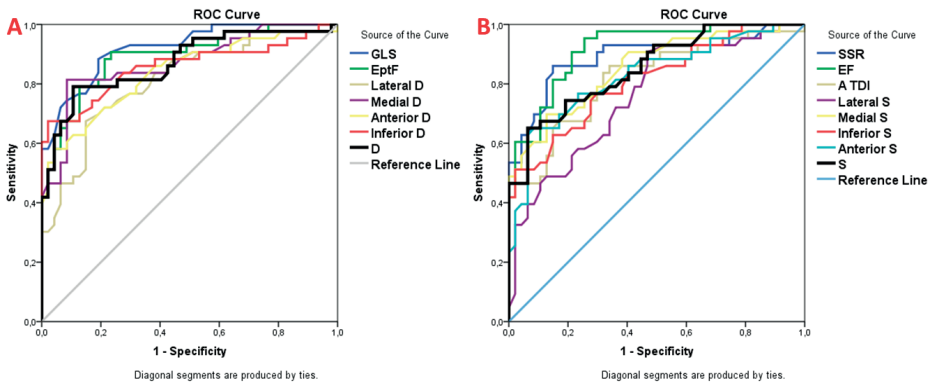


Figure 6. ROC plots for the global and point-by-point displacement of the mitral annulus and the classical functional parameters. A: global function parameters: EptF, GLS and D; B: atrial systolic parameters: EF, TDI A velocity, SSR and S. D and S are represented with black lines.

DISCUSSION

The main findings of this study were: 1) mitral annular displacement by speckle tracking is a reliable and simple method to evaluate the left atrium function; 2) there is a

very strong correlation between the volumetric parameters of left atrial function and deformation indices on one side and the mitral annulus displacement on the other; and 3) the annulus displacement is a very good discriminator between normal and abnormal subjects. It performs less than well the deformation indices (GLS and SSR) or the volumetric fractions (EptF and EF), but better than TDI velocities.

The present guidelines for chamber quantification recommend the use of the biplane Simpson method in the assessment of maximal left atrial volume²⁶, as a powerful index of the overall burden of disease on the left heart, in several pathological states. The prognostic signification of this volume has also been stressed by numerous studies³¹⁻³⁶. The global change in atrial volume during the cardiac cycle is simpler than the one of the left ventricle, having mainly a longitudinal component, mostly due to the motion of the mitral annulus (which in turn is mostly due to LV contraction). But in order to characterize the left atrial function using a volumetric approach, the Simpson method becomes very difficult to use in real clinical practice, because three volumes are needed (the maximal atrial volume, the minimal volume and the pre-A volume), corresponding to the reservoir, conduit and contractile atrial function^{26,28, 37}. The same difficulty is present for area/length methods. The most practical method, proven to be accurate and fast, allowing the extraction of virtually all atrial volumes in a very rapid way, is the use of tridimensional imaging. For 3D techniques, however, it is important to have sufficient image quality in order to have reliable and reproducible results.

During recent years, a great deal of attention has been directed towards the deformation of the left atrium as an index of left atrial function, and to its prognostic importance. These methods are still highly dependent on image quality. For example, an ideal LA strain analysis should have a frame rate of 50-70Hz and a clear visualization of the left atrial wall so as to obtain a good tracking²⁸. This quality is sometimes difficult to obtain at the level of the left atrium, situated in the far field of view, and with thin walls, interrupted by the pulmonary veins and the left atrial appendage. As for TDI, its angle-dependency is well known³⁸, but it has the advantage of being useful even when 2D images are not so good. The problem for deformation studies derived from TDI would be the excess of noise and the signal/noise ratio. The pulsed tissue Doppler of the mitral annulus is very feasible, even for low-quality images, with a good intra and inter-observer agreement, mainly because it follows the movement of a strong acoustic reflector (the mitral annular points), but it remains angle-dependent, and cannot give direct information about wall deformation⁶.

The mitral annular displacement using speckle tracking was studied as a method of evaluation of the left ventricular function, and correlated well with the ejection fraction,

especially when the quality of the image did not allow a good tracing of the endocardial borders, but still a good visualization of the hyperechoic annulus³⁹⁻⁴¹. The mitral annular displacement by speckle tracking can also reflect the left atrial function. Preliminary results of this method were promising⁴².

This method has no angle dependency, as any speckle tracking technique, and theoretically does not need a high quality image, because it is following the same strong reflectors as the pulsed TDI. It is also much simpler than the 2D tracking of the whole atrial wall, because it neglects completely the pulmonary veins or the left atrial appendage. The thickness of the wall also poses no problem.

In this study there was a very strong correlation between the function of the left atrium, estimated by using a tridimensional volumetric method, and the mitral annulus displacement by speckle tracking. This is very significant for the reservoir ($r=0,78$, $p<0,0001$) and contractile ($r=0,76$, $p<0,0001$) functions. The deformation parameters derived from 2D speckle tracking of the atrial wall display an excellent level of correlation with the displacement of the annulus, both for the reservoir ($r=0,87$, $p<0,0001$) and contractile function ($r=0,81$, $p<0,0001$). There was also an excellent correlation between the mean telediastolic (atrial systolic) speed of the annulus in pulsed TDI and the systolic annular displacement ($r=0,83$, $p<0,0001$). The level of correlation with 3D volumetric function was similar between the mitral annular displacement and the usual deformation parameters derived from 2D speckle tracking. The abnormal echo group displayed a clearly lower atrial function, and the difference with the normal group was highly significant. They had stronger correlations with the functional parameters derived from 3D volumes. The relationship with the deformation indices and the pulsed TDI was also stronger in abnormal subjects. We hypothesize that in pathologically enlarged atria, the tracing of the endocardial border by the 3D algorithm and the detection of the left atrial wall by speckle tracking is easier than in normal sized atria. The constant underestimation of left atrial volumes by 3D algorithms is already known, and the degree of error is probably more important for the smaller atrial volumes.

The age difference between groups was statistically significant but biologically irrelevant (mean value 48 vs 56, thus practically belonging to the same age group). It is explained by the difficulty of including elderly disease-free individuals with a normal echocardiography.

The mitral annular displacement was a very good discriminator for normal vs abnormal subjects, performing less well than volumetric or deformation indices, but better than TDI. When analyzing separately the displacement of the classical annular points, the

medial (septal) point in apical 4 chambers view performed best, with an AUC equal to the one of the mean displacement. This could be due to the axial position of the medial point, thus in the best resolution region, and with a strictly longitudinal excursion. According to these results, we could even discuss the use of only the displacement of the medial (septal) point in order to characterize the global longitudinal function of the left atrium.

The intra and inter observer variability were acceptable, the larger inter observer variability probably being explained by the second evaluation being done by an inexperienced user. The time taken for the analysis was relatively short, even for a beginner. The time taken to have an estimation of the displacement (for example only the medial point) was less than 2 minutes.

Comparison with results in the literature

Very recently, a normal values' estimation for the deformation parameters of the left atrium was published²⁸. In our normal population, the GLS of the LA was 39%(±8) and the atrial SSR = 2,8(±0,5)s⁻¹. These values are very close to the mean proposed by Morris *et al*. That was also the case for the GLS of the abnormal echo group, with a GLS mean of 24±12 and a SSR of 1,7±1,1. These comparisons have been made bearing in mind that the study by Morris *et al* was performed using General Electric machines and software, and addressing different pathologies than in our study population.

To our knowledge, this is the first study to look at the use of mitral annular displacement by speckle tracking in the estimation of the left atrial function. However, this tracking is practically the same as the one used for the left ventricular function⁴³. A very good correlation was already noted between the left ventricular global longitudinal strain⁴⁴ and the mitral annular systolic displacement derived from TDI⁴⁵⁻⁴⁶.

Study limitations

The number of patients in this study was limited, but the statistical significance of the results was very high. The patients were selected so as to have a good quality image, in order to allow the use of deformation imaging and 3D. In the absence of an independent reference method, we can only speculate on the feasibility of the mitral annular displacement in low quality echo, by extension of the results already published regarding the left ventricular function. The use of a 3D method for volume estimation has specific limitations that were mentioned above.

The choice of patients' population makes the results only apply to pathologies with a homogenous left ventricle, without important annular calcification or valvular prosthe-

sis. Most likely the results cannot be extrapolated to patients with mitral valve lesions or pericardial disease.

Another issue is the need for vendor-specific software that is not widely available. However, our study proves that the displacement of one single annular point remains a very good discriminator between pathological or normal subjects. Linear displacement by speckle tracking is available on all ultrasound systems.

CONCLUSION

Mitral annulus displacement by speckle tracking proves to be a reliable and simple method to evaluate the left atrial function. Given the strength of the associations found with the deformation parameters derived from 2D strain, it could be used as a surrogate measure of the deformation of the left atrial wall.

REFERENCES

1. Palka P, Lange A, Fleming AD, Sutherland GR, Fenn LN, McDicken WN. Doppler tissue imaging: myocardial wall motion velocities in normal subjects. *J Am Soc Echocardiogr* 1995;8(Pt 1):659–68.
2. D’Hooge J, Heimdal A, Jamal F *et al*. Regional strain and strain rate measurements by cardiac ultrasound: principles, implementation and limitations. *Eur J Echocardiogr* 2000;1:154–70.
3. Kasikcioglu E, Oflaz H, Akhan H, *et al*. Left atrial geometric and functional remodeling in athletes. *Int J Sports Med* 2006;27:267–71.
4. Gottdiener JS, Kitzman DW, Aurigemma GP, Arnold AM, Manolio TA. Left atrial volume, geometry, and function in systolic and diastolic heart failure of persons ≥ 65 years of age (the cardiovascular health study). *Am J Cardiol* 2006;97:83–9.
5. Spencer KT, Mor-Avi V, Gorcsan J III, *et al*. Effects of aging on left atrial reservoir, conduit, and booster pump function: a multi-institution acoustic quantification study. *Heart* 2001;85:272–7.
6. Blume GG, Mcleod CJ, Barnes ME, *et al*, Left atrial function: physiology, assessment, and clinical implications, *European Journal of Echocardiography* (2011) 12, 421–430, doi:10.1093/ejecho-card/jeq175
7. Boyd AC, Thomas L., Left atrial volumes: two-dimensional, three-dimensional, cardiac magnetic resonance and computed tomography measurements, *Curr Opin Cardiol*. 2014 Sep;29(5):408-16. doi: 10.1097/HCO.0000000000000087
8. Perez de Isla L, Feltes G, Moreno J, Martinez W, *et al*, Quantification of left atrial volumes using three-dimensional wall motion tracking echocardiographic technology: comparison with cardiac magnetic resonance, *Eur Heart J Cardiovasc Imaging*. 2014 Jul;15(7):793-9. doi: 10.1093/ehjci/jeu001
9. Abhayaratna WP, Seward JB, Appleton CP, *et al*. Left atrial size: physiologic determinants and clinical applications. *J Am Coll Cardiol*. 2006;47:2357–63. doi: 10.1016/j.jacc.2006.02.048.
10. Jenkins C, Bricknell K, Marwick TH. Use of real-time three-dimensional echocardiography to measure left atrial volume: comparison with other echocardiographic techniques. *J Am Soc Echocardiogr*. 2005;18:991–7. doi: 10.1016/j.echo.2005.03.027.
11. Murata M, Iwanaga S, Tamura Y, *et al*. A real-time three-dimensional echocardiographic quantitative analysis of left atrial function in left ventricular diastolic dysfunction. *Am J Cardiol*. 2008;102:1097–102. doi: 10.1016/j.amjcard.2008.05.067.
12. Artang R, Migrino RQ, Harmann L, Bowers M, Woods TD. Left atrial volume measurement with automated border detection by 3-dimensional echocardiography: comparison with magnetic resonance imaging, *Cardiovasc Ultrasound*. 2009; 7: 16.
13. Hesse B, Schuele SU, Thamilarasan M, Thomas J, Rodriguez L. A rapid method to quantify left atrial contractile function: Doppler tissue imaging of the mitral annulus during atrial systole. *Eur J Echocardiogr* 2004;5:86–92.
14. Telagh R, HuiW, Abd El Rahman M, Berger F, Lange PE, Abdul-Khaliq H. Assessment of regional atrial function in patients with hypertrophic cardiomyopathies using tissue Doppler imaging. *Pediatr Cardiol* 2008;29:301–8.

15. Quintana M, Lindell P, Saha SK, *et al.* Assessment of atrial regional and global electromechanical function by tissue velocity echocardiography: a feasibility study on healthy individuals. *Cardiovasc Ultrasound* 2005;3:4.
16. Yip G, Abraham T, Belohlavek M, Khandheria BK. Clinical applications of strain rate imaging. *J Am Soc Echocardiogr* 2003;16:1334–42.
17. Thomas L. Assessment of atrial function. *Heart Lung Circ* 2007;16:234–42.
18. Sirbu C, Herbots L, D’Hooge J, *et al.* Feasibility of strain and strain rate imaging for the assessment of regional left atrial deformation: a study in normal subjects. *Eur J Echocardiogr* 2006;7:199–208.
19. Vianna-Pinton R, Moreno CA, Baxter CM, Lee KS, Tsang TS, Appleton CP. Twodimensional speckle-tracking echocardiography of the left atrium: feasibility and regional contraction and relaxation differences in normal subjects. *J Am Soc Echocardiogr* 2009;22:299–305.
20. Tsang TS, Barnes ME, Gersh BJ, *et al.* Prediction of risk for first age-related cardiovascular events in an elderly population: the incremental value of echocardiography. *J Am Coll Cardiol*. 2003;42:1199–205. doi: 10.1016/S0735-1097(03)00943-4.
21. Donal E, Raud-Raynier P, Racaud A, Coisne D, Herpin D. Quantitative regional analysis of left atrial function by Doppler tissue imaging-derived parameters discriminates patients with posterior and anterior myocardial infarction. *J Am Soc Echocardiogr* 2005;18:32–8.
22. Choi JI, Park SM, Park JS, *et al.* Changes in left atrial structure and function after catheter ablation and electrical cardioversion for atrial fibrillation. *Circ J* 2008;72:2051–7.
23. Triposkiadis F, Moysakis I, Hadjinikolaou L, *et al.* Left atrial systolic function is depressed in idiopathic and preserved in ischemic dilated cardiomyopathy. *Eur J Clin Invest* 1999;29:905–12.
24. Montserrat S, Gabrielli L, Bijmens B, *et al.* Left atrial deformation predicts success of first and second percutaneous atrial fibrillation ablation, *Heart Rhythm*. 2015 Jan;12(1):11-8. doi: 10.1016/j.hrthm.2014.08.032.
25. Leong DP, Dokainish H, Left atrial volume and function in patients with atrial fibrillation, *Curr Opin Cardiol*. 2014;29(5):437-44. doi: 10.1097/HCO.0000000000000088
26. Lang RM, Badano LP, Mor-Avi V, *et al.* Recommendations for cardiac chamber quantification by echocardiography in adults: an update from the American society of echocardiography and the European association of cardiovascular imaging. *Eur Heart J Cardiovasc Imaging*. 2015 Mar;16(3):233-70. doi: 10.1093/ehjci/jev014
27. Movva R, Murthy K, Romero-Corral A, Seetha Rammohan HR, Fumo P, Pressman GS. Calcification of the mitral valve and annulus: systematic evaluation of effects on valve anatomy and function, *J Am Soc Echocardiogr*. 2013 Oct;26(10):1135-42. doi: 10.1016/j.echo.2013.06.014
28. Morris DA, Takeuchi M, Krisper M, *et al.* Normal values and clinical relevance of left atrial myocardial function analysed by speckle-tracking echocardiography: multicentre study, *Eur Heart J Cardiovasc Imaging*. 2014 . pii: jcu219
29. Eto Y, Yamada H, Shin JH, *et al.* Automated mitral annular tracking: a novel method for evaluating mitral annular motion using two-dimensional echocardiography, *J Am Soc Echocardiogr*. 2005 Apr;18(4):306-12
30. Donner A. A review of inference procedures for the intraclass correlation coefficient in a one-way random effects model. *Int Stat Rev* 1986;54:67–82.

31. Osranek M, Fatema K, Qaddoura F, *et al.* Left atrial volume predicts the risk of atrial fibrillation after cardiac surgery: a prospective study. *J Am Coll Cardiol.* 2006;48:779–86. doi: 10.1016/j.jacc.2006.03.054
32. Modena MG, Muia N, Sgura FA, Molinari R, Castella A, Rossi R. Left atrial size is the major predictor of cardiac death and overall clinical outcome in patients with dilated cardiomyopathy: a long-term follow-up study. *Clin Cardiol.* 1997;20:553–60. doi: 10.1002/clc.4960200609
33. Tsang TS, Barnes ME, Gersh BJ, Bailey KR, Seward JB. Left atrial volume as a morphophysiologic expression of left ventricular diastolic dysfunction and relation to cardiovascular risk burden. *Am J Cardiol.* 2002;90:1284–9. doi: 10.1016/S0002-9149(02)02864-3
34. Le Tourneau T, Messika-Zeitoun D, Russo A, Detaint D, Topolsky Y, Mahoney DW *et al.* Impact of Left Atrial Volume on Clinical Outcome in Organic Mitral Regurgitation. *J Am Coll Cardiol.* 2010;56:570–578.
35. Lonborg JT, Engstrom T, Moller JE, *et al.* Left atrial volume and function in patients following ST elevation myocardial infarction and the association with clinical outcome: a cardiovascular magnetic resonance study. *Eur Heart J Cardiovasc Imaging.* 2013;14:118–126.
36. Ersboll M, Anderson MJ, Valeur N, *et al.* The prognostic value of left atrial peak reservoir strain in acute myocardial infarction is dependent on left ventricular longitudinal function and left atrial size. *Circ Cardiovasc Imaging.* 2013;6:26–33.
37. Nappo R, Degiovanni A, Bolzani V, *et al.* Quantitative assessment of atrial conduit function: a new index of diastolic dysfunction. *Clin Res Cardiol.* 2015. DOI 10.1007/s00392-015-0882-8
38. Castro PL, Greenberg NL, Drinko J, Garcia MJ, Thomas JD. Potential pitfalls of strain rate imaging: angle dependency. *Biomed Sci Instrum* 2000;36:197–202.
39. Buss SJ, Mereles D, Emami M, *et al.* Rapid assessment of longitudinal systolic left ventricular function using speckle tracking of the mitral annulus. *Clin Res Cardiol.* 2012 Apr;101(4):273-80. doi: 10.1007/s00392-011-0389-x
40. Pan C, Hoffmann R, Kuhl H, Severin E, Franke A, Hanrath P. Tissue Tracking Allows Rapid and Accurate Visual Evaluation of Left Ventricular Function, *Eur J Echocardiography* 2001; 2: 197–202
41. DeCara J M, Toledo E, Salgo I S, Lammertin G, Weinert L, Lang R M. Evaluation of Left Ventricular Systolic Function Using Automated Angle-Independent Motion Tracking of Mitral Annular Displacement, *Journal of the American Society of Echocardiography*; 18,(12): 1266–1269
42. Strachinaru M, Catez E, Jousten I, Pavel O, Janssen C, Morissens M. Left atrium longitudinal function in normal subjects, a multiparametric approach, *Eur Heart J Cardiovasc Imaging* 2014;15Suppl 2:ii109-ii136. doi: 10.1093/ehjci/jeu253
43. Black DE, Bryant J, Peebles C, Godfrey KM, Hanson M, Vettukattil JJ. Tissue motion annular displacement of the mitral valve using two-dimensional speckle tracking echocardiography predicts the left ventricular ejection fraction in normal children, *Cardiol Young.* 2014 Aug;24(4):640-8. doi: 10.1017/S1047951113000863
44. Gjesdal O, Vartdal T, Hopp E, *et al.* Left ventricle longitudinal deformation assessment by mitral annulus displacement or global longitudinal strain in chronic ischemic heart disease: are they interchangeable? *J Am Soc Echocardiogr.* 2009 Jul;22(7):823-30. doi: 10.1016/j.echo.2009.04.023

45. Ito K, Noma M, Mohri M, *et al.* Mitral annulus displacement measured by tissue-tracking method with Doppler-tissue images is a useful marker of the severity of heart failure. *J Cardiol.* 2007 Sep;50(3):159-66
46. Roberson DA, Cui W. Tissue Doppler imaging measurement of left ventricular systolic function in children: mitral annular displacement index is superior to peak velocity. *J Am Soc Echocardiogr.* 2009 Apr;22(4):376-82. doi: 10.1016/j.echo.2009.01.008

7

Repeated Echocardiograms do not provide Incremental Prognostic Value to Single Echocardiographic Assessment in Minimally Symptomatic Patients with Chronic Heart Failure: Results of the Bio-SHiFT Study

Based on:

van den Berg VJ, **Strachinaru M**, Akkerhuis KM, Baart S, Brankovic M, Constantinescu AA, Cornel JH, Manintveld OC, Victor Umans VAWM, Rizopoulos D, Geleijnse ML, Boersma E, van Dalen BM, Kardys I. *Repeated Echocardiograms do not provide Incremental Prognostic Value to Single Echocardiographic Assessment in Minimally Symptomatic Patients with Chronic Heart Failure: Results of the Bio-SHiFT Study*. J Am Soc Echocardiogr. 2019; 32(8):1000-1009.

ABSTRACT

Background: We aimed to compare the prognostic value of a single 'baseline' echocardiogram with repeated echocardiography in stable chronic heart failure (CHF) patients. We hypothesized that repeated echocardiograms would contain incremental prognostic information.

Methods: In the prospective Bio-SHIFT study, we performed 332 echocardiograms in 106 patients during a median follow-up of 2.3 years. The endpoint comprised HF hospitalization, left-ventricular assist device implantation, heart transplantation, and cardiovascular death. We compared hazard ratios (HRs; adjusted for NT-proBNP) from Cox models for the first available measurement with HRs from joint models, which model individual trajectories based on the repeated measurements and link these to the time-to-event data.

Results: Mean age was 58.1 years, 78.3% were male, 12.6% had NYHA-class >II, all had reduced ejection fraction (rEF) and most common HF etiologies were cardiomyopathies (51%) and ischemia (40%). The endpoint occurred in 25 patients. Both the single measurements and the temporal trajectories were significantly associated with the endpoint (adjHR Cox model (95%CI) vs adjHR joint model (95%CI)): Left ventricular (LV) ejection fraction: 1.47(0.93-2.31) vs 1.77(1.13-2.93), diastolic LV diameter: 1.64(1.09-2.47) vs 1.68(1.12-2.57), systolic LV diameter: 1.72(1.10-2.69) vs 1.68(1.13-2.63), systolic left atrial diameter: 1.88(1.18-3.00) vs 2.60(1.48-4.97), E/A-ratio 2.73(1.42-5.26) vs 3.87(1.75-10.13), and E/e'-ratio 2.30(1.38-3.84) vs 2.99(1.68-6.19). None of the trajectories from the investigated parameters showed worsening prior to events.

Conclusion: Although single baseline or repeatedly measured echocardiographic parameters were associated with the endpoint, all parameters remained on average stable during the 2.3 years follow-up in this, largely, minimally symptomatic CHF cohort. Thus, regular echocardiographic monitoring of systolic or diastolic LV function within this time-frame does not carry incremental prognostic information over a single baseline measurement.

Abbreviations

CHF	Chronic heart failure
LVEF	Left ventricular ejection fraction
E	Peak early filling velocities
A	Peak late filling velocities
rEF	Reduced ejection fraction
NT-proBNP	N-terminal pro-Brain Natriuretic peptide
Bio-SHiFT	Serial Biomarker Measurements and New Echocardiographic Techniques in Chronic Heart Failure Patients Result in Tailored Prediction of Prognosis
TR	Tricuspid regurgitation
e'	Early diastolic mitral annular velocity
SD	Standard deviation
IQR	Interquartile range
HR	Hazard ratio
CI	Confidence interval

INTRODUCTION

Echocardiography plays a central role in chronic heart failure (CHF) and is used on a daily basis for diagnosis and follow-up.[1] Echocardiography is relatively inexpensive, has a high feasibility and is capable of producing robust and simple measurements, such as left ventricular ejection fraction (LVEF), the dimensions of the left ventricle and atria, and the ratio of peak early (E) and late (A) filling velocities. For many of these measurements, studies have shown that they carry prognostic value in patients with heart failure.[2-6] However, in these studies, single, baseline echocardiographic measurements were related to the clinical endpoints of interest. Single measurements merely provide a snapshot of a patient's condition and fail to identify high-risk periods in individual patients. We hypothesize that repeating echocardiography may provide incremental insights into individual temporal patterns of systolic and diastolic function in CHF patients, and may herewith help identify periods in which an individual is at high risk of an event. If our hypothesis is confirmed and such periods exist, we could use dynamic predictions for updating the current risk of an event after each new echocardiogram, leading to an individual and up-to-date risk assessment which could be helpful for treatment adjustment.[7]

To investigate our hypothesis, we compared the prognostic value of a single 'baseline' echocardiogram with the prognostic value of repeated echocardiograms in clinically stable patients with CHF. In addition, we investigated if the repeatedly measured echocardiographic parameters have incremental prognostic value over repeatedly measured N-terminal pro-Brain Natriuretic peptide (NT-proBNP).

MATERIAL AND METHODS

Details on the design of the *Serial Biomarker Measurements and New Echocardiographic Techniques in Chronic Heart Failure Patients Result in Tailored Prediction of Prognosis (Bio-SHiFT)* study have been published previously.[8] In short, Bio-SHiFT is a prospective, observational cohort of stable patients with CHF, conducted in Erasmus MC, Rotterdam, and Northwest clinics, Alkmaar, The Netherlands. Patients were recruited during their regular outpatient visits while in clinically stable condition (i.e. they had not been hospitalized for HF in the three months prior to inclusion). The main inclusion criterion was a diagnosis of HF according to the guidelines of the European Society of Cardiology three or more months before inclusion.[9] We excluded patients younger than 18 years.

After inclusion, the patients were followed for a maximum duration of 30 months, during which study follow-up visits were scheduled every three months (a window of +/- one month was allowed). At each follow-up visit, a short medical evaluation was performed, blood samples were drawn, and occurrence of adverse cardiovascular events since the previous visit were recorded. During the study, the routine outpatient follow-up by the treating physician continued for all patients, independently of the study visits. The study was approved by the medical ethics committees, conducted in accordance with the Declaration of Helsinki, and registered in ClinicalTrials.gov (NCT01851538). All patients signed informed consent for their participation in the study.

Three hundred ninety-eight patients were included in Bio-SHiFT. In this repeated echo substudy, we aimed to include 100 patients. The substudy was only performed at Erasmus MC, and consisted of repeated echocardiograms performed every six months during follow-up, additional to the tri-monthly blood sampling in Bio-SHiFT.

Echocardiography measurements and evaluation

Two-dimensional grayscale harmonic images were obtained in the left lateral decubitus position using a commercially available ultrasound system (iE33, Philips, Best, The Netherlands), equipped with a broadband (1-5MHz) S5-1 transducer (frequency transmitted 1.7MHz, received 3.4MHz) and stored in the echo core lab of Erasmus MC. Using specialized software (TOMTEC imaging, Unterschleissheim, Germany), the following parameters were measured: left ventricular ejection fraction (LVEF, using triplane), end-diastolic and end-systolic LV diameter, and end-systolic left atrial diameter.[10] The vena cava inferior diameter (including the results of the 'sniff test'), the tricuspid regurgitation (TR) velocity and the function of the aortic, mitral, and tricuspid valve, were also assessed but currently not evaluated in the longitudinal models.

The diastolic parameters were evaluated using Philips Excellera version R4.1 (Philips medical systems, the Netherlands). In order to assess diastolic function, the E/A ratio and the ratio of the E and early diastolic mitral annular velocity (e') were calculated. For the e', we used the average of the lateral and medial e' when available; however, if only one of the two was available, this value was used.

All echocardiographic measurements were performed blinded to biomarker and clinical event data.

NT-proBNP measurement

Blood samples were processed and stored at a temperature of -80C within 2 hours after blood collection. To determine NT-proBNP levels, a batch analysis was performed using

an electrochemiluminescence immunoassay (Elecsys 2010; Roche Diagnostics, Indianapolis, IN). Accordingly, results of the biomarker assays were not available to treating physicians at the time of the outpatient visits and did not interfere with usual care.

Clinical study endpoints

The endpoint comprised the composite of hospitalization for the management of acute or worsened HF, left ventricular assist device implantation, cardiac transplantation, and cardiac death, whichever occurred first in time. All events were adjudicated by a clinical event committee blinded to the echocardiographic assessments and biomarker measurements, after reviewing corresponding hospital records and discharge letters.

Statistical analyses

Distributions of continuous variables were tested for normality using the Shapiro-Wilk test. Normally distributed continuous variables are presented as mean \pm standard deviation (SD), and non-normally distributed variables as median and interquartile range (IQR). Categorical variables are presented as numbers and percentages. Differences in baseline characteristics between patients that experienced the endpoint and those who did not were tested using t-test and Mann-Whitney test respectively for continuous variables, and chi square tests and Fisher's exact tests for categorical variables.

We first evaluated the association between the echo parameters from the first available echocardiogram with the time until the occurrence of the composite endpoint or censoring using a Cox proportional hazard model corrected for baseline NT-proBNP. Hereafter, we assessed the incremental value of repeated echocardiographic measurements. For this purpose, we used the framework of joint models for longitudinal and survival data. In these joint models, a linear mixed-effects (longitudinal) model provided estimates of the individual temporal trajectories for each echo parameter, while accounting for the correlation in the repeated measurements. These estimated trajectories were then combined with a Cox proportional hazards model, to study their association with the risk of the study endpoint. The individual trajectories, resulting from the linear mixed models, were adjusted for all variables (age, sex, renal failure and heart rate) for whom the p-value for the difference between those reaching the endpoint and those remaining endpoint-free was < 0.1 . The associations between the temporal evolutions and the endpoint, resulting from the Cox model, were firstly adjusted for baseline NT-proBNP levels. In a second series of multivariable joint models, we combined the repeatedly performed echocardiograms with repeatedly measured NT-proBNP, in order to investigate the incremental value of repeated echos when repeated biomarker measurements are also available.

In order to compare effect sizes of different variables, all investigated echo parameters and the NT-proBNP measurements were firstly transformed to achieve a normal distribution after which the corresponding Z-score was calculated. This standardization was performed on the entire dataset (containing all repeated measurements). Hereafter, to obtain the HRs entailed by the first echoes only, first echoes were selected and entered into Cox models; whilst to obtain the HRs entailed by the repeatedly measured echoes, joint models were performed on all available echoes. Thus, the results of the regression analyses of the Cox and joint models can be directly compared and are presented as hazard ratios (HR) which represent risk per SD increase/decrease of the standardized variable, along with the corresponding 95% confidence intervals (CI). As interpretation of the unit of these HRs may not be straightforward, we back-transformed the mean and +/- SD of the transformed variables and depicted these values in the tables.

As described above, our aim was to investigate whether repeatedly assessed echocardiographic parameters carry incremental predictive value to repeatedly measured NT-proBNP. We chose to present our results solely as hazard ratios adjusted for NT-proBNP and not combine them with C-statistics. Pepe et al. have demonstrated that testing for improvement in prediction performance is actually redundant if a variable has already been shown to be an independent risk factor, and that standard testing procedures for C-indices are very conservative and thus insensitive to improvements in prediction performance.[11]

Missing values in echo parameters were, except for the A wave, always due to poor image quality and were as such missing completely at random. Accordingly we chose to perform a complete case analysis. Missing values for the A wave were mostly due to atrial fibrillation during the echo or due to mitral valve replacement or clipping. In this specific patient group imputation of missing values is inappropriate, as the A wave can never be measured. Thus, we again chose for a complete case analysis here. The results of this analysis should not be extrapolated to patients excluded from the analysis.

All analyses were performed with R Statistical Software using packages 'nlme'[12] and 'JMbayes'.[13] All tests were two-tailed and p-values <0.05 were considered statistically significant.

RESULTS

Baseline characteristics and clinical endpoints

From 2011 to 2017, 106 patients were included in the echocardiography substudy. All patients had reduced ejection fraction (rEF). Specifically, all patients in whom EF was

measured by the automated software had EF <50%. In 2 patients, EF could not be measured in the first available echo by the automated software due to reduced image quality; based on the available images EF in these patients was classified as poor. A summary of the baseline characteristics is displayed in table 1. The majority of the included patients were men (78.3%), the mean age was 58 ±11 (SD) years and 40% had HF due to ischemic disease.

In total 25 (23.6%) patients reached the combined endpoint; 18 patients were re-hospitalized for acute or worsened heart failure; 2 patients received a left-ventricular assist device implantation, 2 patients received a heart transplantation, and 3 patients died from cardiovascular causes. Patients who later experienced an endpoint had a higher baseline heart rate, NT-proBNP, and were more likely to have renal failure than their counterparts who remained endpoint-free.

Echocardiography

In the 106 HF_rEF patients, a total of 332 echocardiograms were performed with a median (IQR) of 3 (2-4) echocardiograms per patient during a median (IQR) follow-up time of 2.3 (1.7-2.7) years. Missing exams mostly occurred due to logistic circumstances (e.g. the unavailability of an ultrasound technician during the study visit). The median time between the last echo and the moment that the event or censoring occurred was 69 (37-165) days in patients in whom the event occurred and 180 (92-280) days in event-free patients.

Echocardiographic parameters were successfully measured in more than 90% of available echocardiograms except for E/A ratio. Due to atrial fibrillation and severe mitral valve disease, we were only able to determine E/A-ratio from 81.3% of the echos (270 echos, 94 patients, 20 events). At least one measurement of each of the other repeatedly assessed parameters was available in all 106 patients, except for end-systolic left atrial diameter and E/e'-ratio, which were missing completely in one patient.

First available echocardiogram

Table 2 displays the characteristics of the first available echocardiogram for each included patient. Because of logistic reasons, seventy-two percent of these echos were performed during the baseline visit (follow-up time zero), 14.2% during the first follow-up visit (target follow-up time 3 months), 8.5% during the second follow-up visit (target 6 months), and the remaining 5.7% hereafter.

Patients who experienced the endpoint had a lower LV ejection fraction and larger LV and atrial dimensions than patients who remained endpoint-free. In addition, those

Repeated Echocardiograms do not provide Incremental Prognostic Value to Single Echocardiographic Assessment in Minimally Symptomatic Patients with Chronic Heart Failure: Results of the Bio-SHiFT Study

Table 1. Baseline patient characteristics in relation to the occurrence of the composite endpoint

Variable	Total	Composite endpoint reached		P value
		No	Yes	
N	106	81	25	
Demographics				
Age, years (mean (SD))	58.1 (10.7)	57.8 (10.4)	59.3 (11.7)	0.56
Men, n (%)	83 (78.3)	63 (77.8)	20 (80.0)	1.00
Clinical characteristics, (mean (SD))				
BMI, kg/m ² (median (IQR))	26.8 (24.2-30.6)	26.8 (24.1-31.3)	26.5 (24.2-29.2)	0.46
Heart rate, bpm (mean (SD))	65 (9)	64 (9)	66 (9)	0.05
Systolic blood pressure, mmHg (mean (SD))	110 (19)	111 (19)	105 (19)	0.14
Diastolic blood pressure, mmHg (median (IQR))	70 (60-79)	70 (61-79)	65 (60-70)	0.19
Features of heart failure				
NYHA class, n (%)				0.30
NYHA class I	32 (31.1)	27 (34.2)	5 (20.8)	
NYHA class II	58 (56.3)	43 (54.4)	15 (62.5)	
NYHA class III	13 (12.6)	9 (11.4)	4 (16.7)	
LVEF, % (mean (SD))	27 (9)	29 (9)	23 (6)	0.02
NT-proBNP, pmol/L (median (IQR))	124.7 (37.5. 219.3)	86.0 (27.3. 192.5)	235.0 (139.6. 422.0)	<0.01
Etiology of heart failure, n (%)				
Ischemic	40 (39.6)	30 (38.5)	10 (43.5)	0.85
Hypertension	2 (2.1)	2 (2.7)	0 (0.0)	1.00
Secondary to valvular disease	3 (3.1)	1 (1.3)	2 (9.5)	0.23
Cardiomyopathy	51 (52.0)	39 (52.0)	12 (52.2)	1.00
Other	13 (13.5)	11 (14.7)	2 (9.5)	0.80
Unkown	6 (6.8)	5 (7.4)	1 (5.0)	1.00
Medical history, n (%)				
Time since first HF episode, years (median(IQR))	5.7 (2.2-10.2)	5.1 (2.2-9.4)	7.6 (4.3-11.6)	0.20
Prior MI	39 (36.8)	29 (35.8)	10 (40.0)	0.89
Prior PCI	36 (34.3)	27 (33.8)	9 (36.0)	1.00
Prior CABG	8 (7.5)	6 (7.4)	2 (8.0)	1.00
Atrial fibrillation	27 (25.7)	17 (21.2)	10 (40.0)	0.11
Diabetes	26 (24.5)	19 (23.5)	7 (28.0)	0.85
Renal failure	42 (40.0)	26 (32.1)	16 (66.7)	<0.01
COPD	12 (11.4)	10 (12.3)	2 (8.3)	0.86
Medication use, n (%)				
Beta-blocker	102 (97.1)	79 (97.5)	23 (95.8)	1.00
ACE-Inhibitor	77 (74.0)	59 (73.8)	18 (75.0)	1.00
ARB	26 (24.8)	22 (27.2)	4 (16.7)	0.44
Loop diuretics	96 (92.3)	72 (90.0)	24 (100.0)	0.24
Aldosterone antagonist	68 (65.4)	51 (63.7)	17 (70.8)	0.69

n: number; SD: standard deviation; IQR: interquartile range; BMI: body mass index; bpm: beats per minute; mmHg: Millimeter of mercury; NYHA: New York Heart Association; LVEF: left ventricular ejection fraction; NT-proBNP: N-terminal pro brain natriuretic peptide; pmol/L: picomole per liter; HF: heart failure; MI: myocardial infarction; PCI: percutaneous coronary intervention; CABG: coronary artery bypass grafting; COPD: chronic obstructive pulmonary disease; ACE: angiotensin converting enzyme; ARB: Angiotensin receptor blocker

Table 2. Echocardiographic characteristics from first available echo in relation to the occurrence of the composite endpoint

	N of echos in which variable was measured (%)	Total	Composite endpoint reached		P value
			No	Yes	
N		106	81	25	
Systolic parameters					
LVEF (mean (sd))	104 (98.1)	28 (9)	30 (9)	22 (7)	<0.001
DiasLVD (median (IQR))	101 (95.3)	64 (59, 73)	63 (58, 69)	73 (64, 79)	0.001
SysLVD (median (IQR))	99 (93.4)	57 (49, 64)	53 (46, 62)	63 (56, 72)	0.001
SysLAD (mean (sd))	97 (91.5)	43.28 (8.64)	41.38 (7.80)	49.39 (8.52)	<0.001
Diastolic parameters (median (IQR))					
E/A ratio	83 (78.3)	1.10 (0.80, 1.88)	0.99 (0.73, 1.24)	2.38 (1.29, 3.38)	<0.001
E/E' ratio	97 (91.5)	13.2 (9.7, 18.3)	11.0 (9.0, 14.7)	22.9 (17.9, 27.8)	<0.001
TR velocity	70 (66.0)	2.50 (2.24, 2.86)	2.42 (2.14, 2.65)	2.89 (2.44, 3.32)	0.005
Vena Cava					
VCI (median (IQR))	84 (79.2)	16 (12, 19.25)	15 (12, 19)	20 (11, 22)	0.062
Valvular dysfunction (%)					
<i>Mitral valve regurgitation</i>	101 (95.3)				0.002
none		31 (30.7)	29 (37.7)	2 (8.3)	
mild		41 (40.6)	29 (37.7)	12 (50.0)	
moderate		22 (21.8)	17 (22.1)	5 (20.8)	
severe		7 (6.9)	2 (2.6)	5 (20.8)	
<i>Aorta valve regurgitation</i>	101 (95.3)				0.121
none		90 (89.1)	71 (92.2)	19 (79.2)	
mild		8 (7.9)	5 (6.5)	3 (12.5)	
moderate		3 (3.0)	1 (1.3)	2 (8.3)	
<i>Tricuspid valve regurgitation</i>	101 (95.3)				0.004
none		55 (54.5)	46 (59.7)	9 (37.5)	
mild		37 (36.6)	28 (36.4)	9 (37.5)	
moderate		3 (3.0)	2 (2.6)	1 (4.2)	
severe		6 (5.9)	1 (1.3)	5 (20.8)	

P-values were based on T-test or Mann-Whitney test for continuous variables depending on their distribution. To test for differences in the categorical variables, chi-square tests were performed.

N: number; LVEF: left ventricular ejection fraction; sd: standard deviation; IQR: interquartile range; DiasLVD: diastolic left ventricular diameter; SysLVD: systolic left ventricular diameter; SysLAD: systolic left atrial diameter; E: peak early filling velocity; A: peak late filling velocity; e': early diastolic mitral annular velocity; TR: tricuspid regurgitation; VCI: inferior vena cava

who experienced an endpoint had higher E/A-ratios, E/e'-ratios, and TR-velocities and were more likely to have (severe) mitral valve regurgitation and tricuspid valve regurgitation. All echocardiographic parameters except for LVEF, were significantly associated with the study endpoint, independently of the baseline NT-proBNP (table 3). Although the estimate did not reach statistical significance for LVEF, it was substantial (HR(95%CI): 1.47 (0.93-2.31)). The E/A ratio and the E/e' ratio (available in 97 of 106 patients), were the strongest predictors with hazard ratios per SD increase of 2.73 (95%CI 1.42 – 5.26) and 2.30 (95%CI 1.38 – 3.84) respectively.

Table 3. Results from first available echo

Variable	N of patients (N of events)	mean \pm SD	HR (95%CI)	P value
Left ventricular Ejection fraction [*]	104 pt (24)	29 (20, 38)	1.47 (0.93 - 2.31)	0.101
Diastolic left ventricular diameter [†]	101 pt (24)	65 (55, 77)	1.64 (1.09 - 2.47)	0.017
Systolic left ventricular diameter [†]	99 pt (24)	56 (45, 69)	1.72 (1.10 - 2.69)	0.017
Systolic left atrial diameter [†]	97 pt (23)	42 (35, 51)	1.88 (1.18 - 3.00)	0.008
E/A-ratio [‡]	83 pt (20)	1.00 (0.65, 2.00)	2.73 (1.42 - 5.26)	0.003
E/e'-ratio [‡]	97 pt (24)	12.9 (7.4, 22.5)	2.30 (1.38 - 3.84)	0.001

HRs represent change in risk of the endpoint for a 1 standard deviation change in the echo parameter at any point in time during follow-up.

All models are corrected for baseline NTproBNP

* HR per one SD decrease

† HR per one SD increase on the log₂ scale

‡ HR per one SD increase after \wedge .66 transformation

Repeated echocardiograms

The individual trajectories of all of the investigated echo parameters were significantly associated with the clinical endpoint independently of baseline NT-proBNP. The corresponding HRs were comparable, or slightly larger, to those found for the first available measurements (Table 4). In line with the results from the 'single measurement' analysis, E/A-ratio and E/e' ratio showed the greatest HR per SD increase.

Although the repeatedly measured echo parameters were associated with occurrence of the endpoint, we could not identify any increase or decrease of their average temporal patterns as the endpoint approached (Figure 1 & Figure 2). The average trajectories of the echo parameters remained stable as the composite endpoint or the moment of censoring approached.

Repeated echocardiograms and NT-proBNP measurements combined

During follow-up of the 106 patients a total of 819 (median 8 (IQR 7-10) per patient) blood samples were taken for NT-proBNP measurement. The results of the multivariable joint models in which both the repeatedly measured NT-proBNP and the repeat-

Table 4. Results for repeatedly measured parameters

Variable	N of available echos (N of patients, N of events)	mean \pm SD	HR (95%CI)	P value
Left ventricular Ejection fraction*	327 (106 pt, 25 events)	29 (20, 38)	1.77 (1.13 - 2.93)	0.017
Diastolic left ventricular diameter†	325 (106 pt, 25 events)	65 (55, 77)	1.68 (1.12 - 2.57)	0.012
Systolic left ventricular diameter†	320 (106 pt, 25 events)	56 (45, 69)	1.68 (1.13 - 2.63)	0.011
Systolic left atrial diameter†	316 (105 pt, 24 events)	42 (35, 51)	2.60 (1.48 - 4.97)	0.001
E/A-ratio‡	270 (94 pt, 20 events)	1.0 (0.65, 2.0)	3.87 (1.75 - 10.13)	0.001
E/e'-ratio†	311 (105 pt, 25 events)	12.9 (7.4, 22.5)	2.99 (1.68 - 6.19)	<0.001

HRs represent change in risk of the endpoint for a 1 standard deviation change in the echo parameter at any point in time during follow-up.

* HR per one SD decrease

† HR per one SD increase on the log₂ scale

‡ HR per one SD increase after \wedge .66 transformation

The survival part of the models, captured by the Cox-model, were corrected for NTproBNP at baseline. In addition the trajectories of the biomarkers, captured by the linear mixed model, were corrected for age, sex, renal failure, and heart rate.

N: Number; HR: HR ratio; SD: standard deviation; pt: patient; E: peak early filling velocities; A: peak late filling velocities

edly measured echo parameters were entered are shown in table 5. The HRs of all of the echo parameters somewhat decreased compared to the joint model adjusted solely for baseline NT-proBNP. Although repeatedly measured NT-proBNP was a much stronger predictor of the composite endpoint, all repeatedly assessed echo parameters except for LVEF were independently associated with the endpoint, and herewith clearly provided incremental prognostic value. LVEF was not an independent predictor but the corresponding estimate was still substantial (HR (95%CI): 1.52 (0.95-2.45)). Notably, of all investigated echo parameters, the E/A-ratio and the E/e'-ratio again were again the strongest predictors of the composite endpoint.

DISCUSSION

In our study in stable, minimally symptomatic, chronic HFReF patients, repeatedly measured LV dimensions and left atrial dimensions, and E/A and E/e'-ratio were significantly associated with adverse cardiac events during a median follow-up of 2.3 years, independent of both baseline and repeated NT-proBNP measurements. Higher E/A-ratio and E/e'-ratio, both representing diastolic function of the heart, were the strongest predictors. Although repeated echocardiographic measurements were associated with cardiovascular outcome, they remained stable during follow-up and did not worsen as an adverse event approached. Thus, patients with adverse cardiac events had lower LVEF, larger LV dimensions and larger ratios throughout the entire follow-up period, but the temporal trajectories of these parameters did not show diverging slopes in patients with events vs those without events. This stability of the echo parameters was

Repeated Echocardiograms do not provide Incremental Prognostic Value to Single Echocardiographic Assessment in Minimally Symptomatic Patients with Chronic Heart Failure: Results of the Bio-SHIFT Study

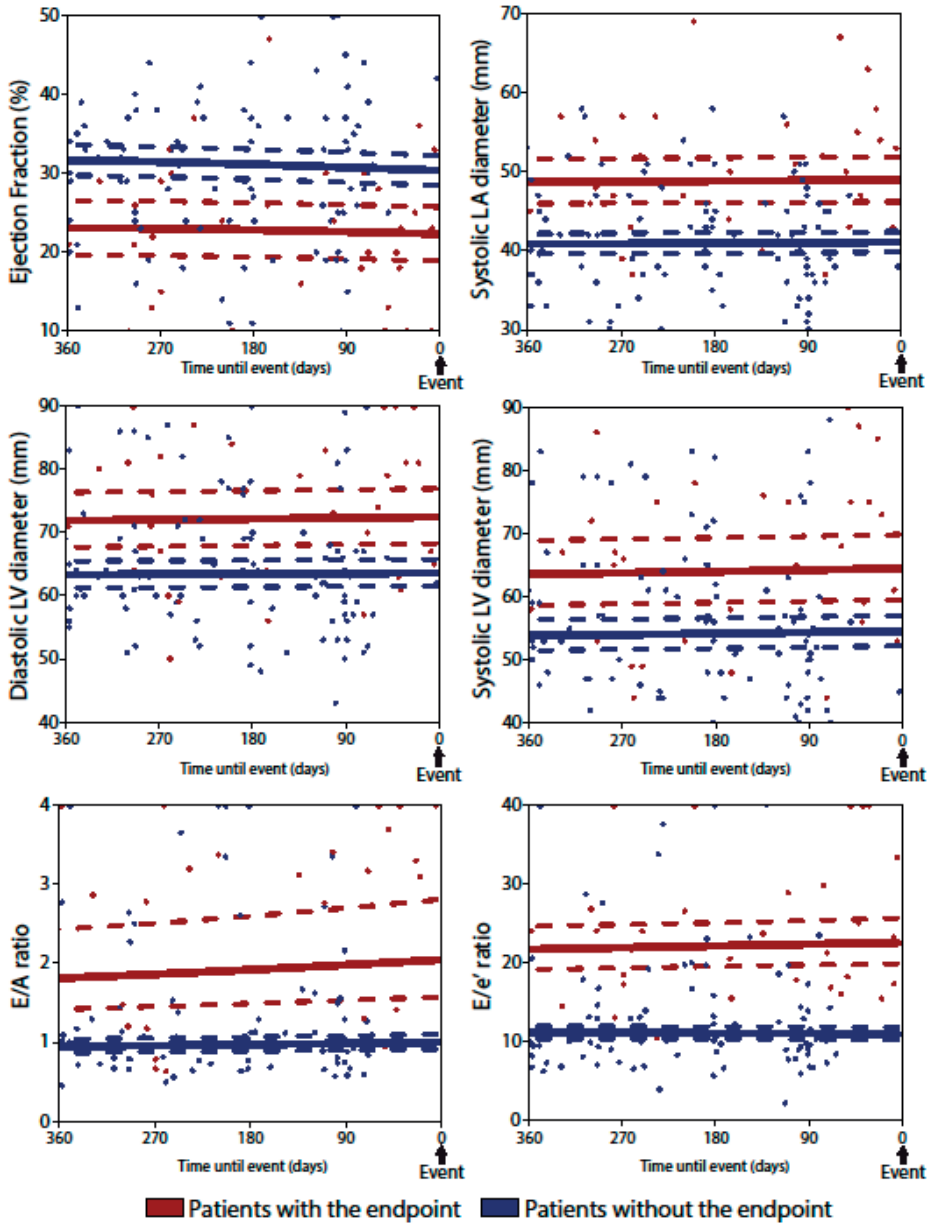


Figure 1. Average levels of echocardiographic parameters at the first and last measurement

The results of each of the investigated echo parameters are depicted in two paired boxplots. In these pairs, the left boxplot shows the average echocardiographic parameter levels in patient with the endpoint; while the right boxplot shows the average biomarker levels in endpoint-free patients. Within each boxplot, the left box represents the average of the last available measurement for each patient. Abbreviations: LV: left ventricular; LA: left atrial; E: peak early filling velocity; A: peak late filling velocity; e': early diastolic mitral annular velocity; mm: millimeter

confirmed by the comparable HRs per SD increase found in the single measurement Cox models and the corresponding repeated measurements joint models, which further underscores the lack of incremental value of repeated echocardiograms compared to single echocardiographic assessment in this category of patients. Finally, we showed that repeated NT-proBNP measurements carry more prognostic information than repeated echo measurements do.

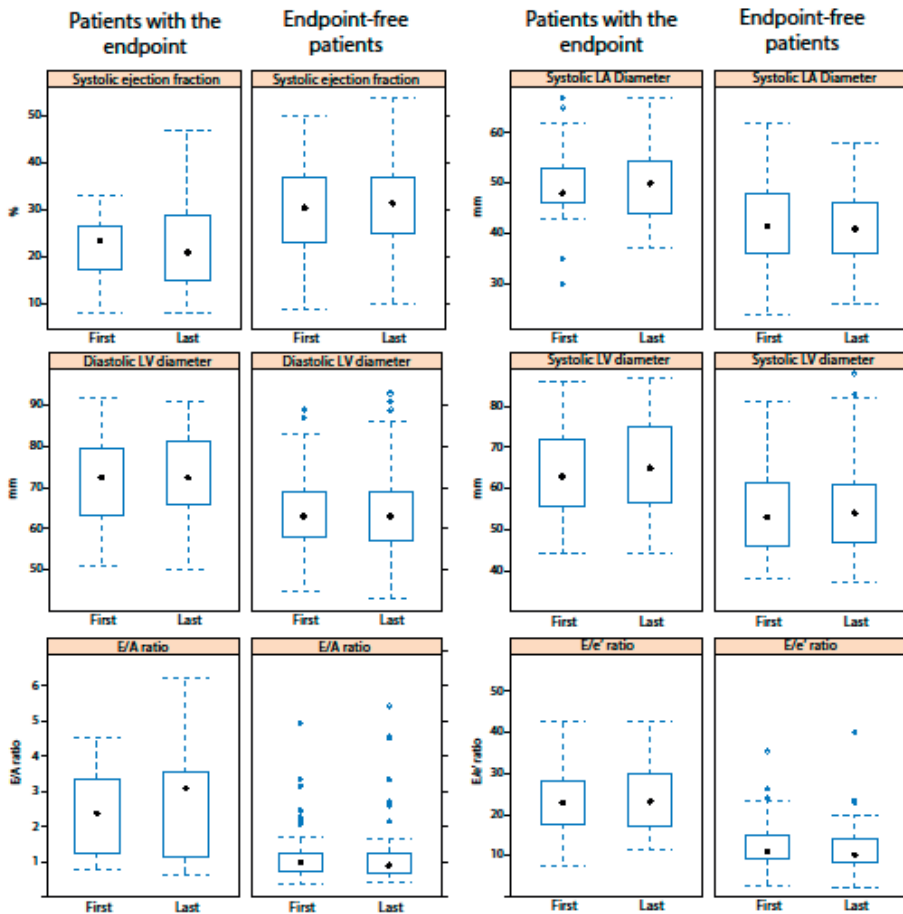


Figure 2. Average levels of echo parameters until time of event

The X-axis represents the time remaining to the primary endpoint (for patients who experienced incident adverse events) or time remaining to censoring (for patients who remained event-free). Of note is that 'time zero' is defined as the occurrence of the endpoint and is depicted on the right side of the x-axis, so that the average echocardiographic parameter can be visualized as the endpoint approaches. The continuous lines represent the average temporal pattern for patients with the endpoint (red) and endpoint-free patients (blue) as extracted from the joint model. The corresponding dotted lines depict the 95% confidence intervals. Finally, each dot represents a single measurement. Abbreviations: LV: left ventricular; LA: left atrial; E: peak early filling velocity; A: peak late filling velocity; e': early diastolic mitral annular velocity; mm: millimeter

Repeated Echocardiograms do not provide Incremental Prognostic Value to Single Echocardiographic Assessment in Minimally Symptomatic Patients with Chronic Heart Failure: Results of the Bio-SHIFT Study

Table 5. Results for repeatedly measured parameters, adjusted for repeatedly measured NT-proBNP

Variable	N of available echos (N of patients, N of events)	mean \pm SD	HR (95%CI)	P value
Left ventricular Ejection fraction*	327 (106 pt, 25 events)	29 (20, 38)	1.52 (0.95 - 2.45)	0.076
NT-proBNP†		84.4 (21.3, 334.2)	6.47 (3.24 - 13.60)	<0.001
Diastolic left ventricular diameter†	325 (106 pt, 25 events)	65 (55, 77)	1.56 (1.04 - 2.38)	0.026
NT-proBNP†		84.4 (21.3, 334.2)	7.53 (3.67 - 15.54)	<0.001
Systolic left ventricular diameter†	320 (106 pt, 25 events)	56 (45, 69)	1.53 (1.05 - 2.41)	0.032
NT-proBNP†		84.4 (21.3, 334.2)	7.39 (3.60 - 15.76)	<0.001
Systolic left atrial diameter†	316 (105 pt, 24 events)	42 (35, 51)	2.02 (1.15 - 3.76)	0.008
NT-proBNP†		84.4 (21.3, 334.2)	6.65 (3.35 - 14.15)	<0.001
E/A-ratio‡	270 (94 pt, 20 events)	1.0 (0.65, 2.0)	2.70 (1.16 - 8.32)	0.026
NT-proBNP†		84.4 (21.3, 334.2)	7.59 (3.16 - 19.82)	<0.001
E/e'-ratio†	311 (105 pt, 25 events)	12.9 (7.4, 22.5)	2.51 (1.22 - 5.68)	0.012
NT-proBNP†		84.4 (21.3, 334.2)	5.00 (2.22 - 11.53)	0.002

HRs represent change in risk of the endpoint for a 1 standard deviation change in the echo parameter at any point in time during follow-up.

* HR per one SD decrease

† HR per one SD increase on the log2 scale

‡ HR per one SD increase after \wedge .66 transformation

The trajectories of both the echo biomarker and NT-proBNP, captured by the linear mixed model, were corrected for age, sex, renal failure and heart rate.

N: Number; HR: HR ratio; SD: standard deviation; pt: patient; E: peak early filling velocities; A: peak late filling velocities; NT-proBNP: N-terminal pro-Brain Natriuretic peptide

The current HF guideline does not recommend periodically repeating echos in otherwise stable HF patients; reassessing myocardial structures and functions is only warranted when patients present with symptoms of worsening HF or experience any important cardiovascular event, prior to device implantations, and during exposure to cardiotoxic therapies.[14] However, this is primarily based on expert opinion. The results of our study are the first to explicitly substantiate that single echocardiographic assessment suffices in the context of prognosis. In our study we performed echocardiography each six months. Increasing the frequency of the echocardiographic assessments might improve the ability of echocardiography to reveal deterioration of myocardial function and structure prior to adverse events. However, the feasibility in clinical practice would be limited as this would significantly increase costs. Furthermore, subtle deterioration may not always be recognized as it cannot easily be distinguished from changes caused by normal inpatient variability and intra and interobserver variability.[15] Finally, prolonging follow-up may also reveal incremental value of repeated echocardiography.

The prognostic value of baseline echo parameters, independent of baseline NT-proBNP, has been reported earlier in HF patients. In a prospective study by Hinderliter et al.

among 211 chronic HFREF patients, baseline LVEF, LV end-diastolic volume and LV volume index were significantly associated with all-cause mortality during a median of 4 years follow-up.[4] Furthermore, a systematic review of risk prediction models in patients with heart failure showed that baseline LVEF was often incorporated in the final models together with (NTpro)BNP levels, indicating LVEF carried additional prognostic value.[16] In our analysis, LVEF went from being not predictive to predictive for single vs repeated measures (the latter being assessed by means of joint modeling). This was most likely caused by the fact that repeated measurements entail higher statistical power. Both analyses show similar point estimates, but in the repeated measurement analysis a much higher number of LVEF measurements were taken into account, leading to narrower 95% CIs and thus a statistically significant finding.

Although it is thus clear that echocardiographic parameters carry prognostic value independent of NT-proBNP, in our study we extend the evidence by comparing effect sizes; by standardizing the variables we demonstrate that the association of NT-proBNP with adverse outcomes in CHF is much stronger than that of echocardiographic parameters. Several prior studies have already established that single baseline measurements of NT-proBNP are strongly associated with adverse outcomes in CHF.[17-19] In addition, an earlier study from our research group that used joint modeling has demonstrated that repeatedly measured NT-proBNP can identify high-risk periods in the Bio-SHiFT patients. [8] In that study, patients in whom the endpoint occurred had on average not only a higher baseline level of NT-proBNP, but also showed a significant rise of NT-proBNP levels as the endpoint approached. Similar results were reported in a study by Miller et al. among 190 NYHA III and IV CHF patients during a follow-up of 2 years, in whom BNP was measured every 3 months.[20] Altogether, previous studies taken together with the current study, suggest that for individualized assessment of CHF status and treatment, repeated NT-proBNP measurements are more useful than repeated echocardiographic assessments.

Limitations

A first limitation is that the treating physicians were not blinded to the echocardiograms. Due to ethical considerations this was not possible. A second limitation is that the number of endpoints in the current investigation is limited, and consequently the number of variables that could be entered in the models. Although residual confounding will surely be present, all our models were corrected for either baseline level or repeated measurements of NT-proBNP, which is a strong predictor of outcomes in chronic heart failure. [21, 22] In addition, the longitudinal trajectories were also corrected for any differences in baseline characteristics between those who reached the endpoint and those who did not. The limited number of endpoints has also precluded us from investigating whether

there would be differences in the results as a function of etiology of heart failure. Thirdly, we did not examine global longitudinal strain nor the grade of diastolic function, although these parameters could potentially predict clinical outcome. However, the use of GLS is limited in clinical practice and it is often not measured by default. As for grade of diastolic function, it is known that in practice classification of diastolic function is not always straightforward. When attempting to perform such a classification using the ASE guidelines [23], we were able to assign the grade in 61.3% of the echocardiograms only. This precluded performing a robust analysis. Finally, compared to previous CHF cohorts and also to the full Bio-SHiFT cohort, the patients in our current echo study were relatively young and the proportion of HF patients in NYHA class I and II was high, which may have obscured an association that would be present in ‘sicker’ patients.

CONCLUSIONS

Although individual trajectories of echocardiographic parameters were associated with cardiovascular outcome independent of NT-proBNP levels, the parameters remained stable during 2.3 years follow-up and did not worsen as an adverse event approached. It thus seems that, in such a timeframe, routine frequent monitoring of systolic or diastolic function with echocardiography does not carry incremental prognostic information over a single measurement in a, largely, minimally symptomatic and relatively young patient group.

REFERENCES

- [1] Ponikowski P, Voors AA, Anker SD, Bueno H, Cleland JGF, Coats AJS, et al. 2016 ESC Guidelines for the diagnosis and treatment of acute and chronic heart failure: The Task Force for the diagnosis and treatment of acute and chronic heart failure of the European Society of Cardiology (ESC) Developed with the special contribution of the Heart Failure Association (HFA) of the ESC. *Eur Heart J*. 2016;37:2129-200.
- [2] Carluccio E, Dini FL, Biagioli P, Lauciello R, Simioniuc A, Zuchi C, et al. The 'Echo Heart Failure Score': an echocardiographic risk prediction score of mortality in systolic heart failure. *Eur J Heart Fail*. 2013;15:868-76.
- [3] Carerj S, La Carrubba S, Antonini-Canterin F, Di Salvo G, Erlicher A, Liguori E, et al. The incremental prognostic value of echocardiography in asymptomatic stage a heart failure. *J Am Soc Echocardiogr*. 2010;23:1025-34.
- [4] Hinderliter AL, Blumenthal JA, O'Conner C, Adams KF, Dupree CS, Waugh RA, et al. Independent prognostic value of echocardiography and N-terminal pro-B-type natriuretic peptide in patients with heart failure. *Am Heart J*. 2008;156:1191-5.
- [5] Grayburn PA, Appleton CP, DeMaria AN, Greenberg B, Lowes B, Oh J, et al. Echocardiographic predictors of morbidity and mortality in patients with advanced heart failure: the Beta-blocker Evaluation of Survival Trial (BEST). *J Am Coll Cardiol*. 2005;45:1064-71.
- [6] Rossi A, Ciccoira M, Zanolla L, Sandrini R, Golia G, Zardini P, et al. Determinants and prognostic value of left atrial volume in patients with dilated cardiomyopathy. *J Am Coll Cardiol*. 2002;40:1425-30.
- [7] Rizopoulos D. Dynamic predictions and prospective accuracy in joint models for longitudinal and time-to-event data. *Biometrics*. 2011;67:819-29.
- [8] van Boven N, Battes LC, Akkerhuis KM, Rizopoulos D, Caliskan K, Anroedh SS, et al. Toward personalized risk assessment in patients with chronic heart failure: Detailed temporal patterns of NT-proBNP, troponin T, and CRP in the Bio-SHiFT study. *Am Heart J*. 2018;196:36-48.
- [9] McMurray JJ, Adamopoulos S, Anker SD, Auricchio A, Bohm M, Dickstein K, et al. ESC guidelines for the diagnosis and treatment of acute and chronic heart failure 2012: The Task Force for the Diagnosis and Treatment of Acute and Chronic Heart Failure 2012 of the European Society of Cardiology. Developed in collaboration with the Heart Failure Association (HFA) of the ESC. *Eur J Heart Fail*. 2012;14:803-69.
- [10] Lang RM, Badano LP, Mor-Avi V, Afilalo J, Armstrong A, Ernande L, et al. Recommendations for cardiac chamber quantification by echocardiography in adults: an update from the American Society of Echocardiography and the European Association of Cardiovascular Imaging. *J Am Soc Echocardiogr*. 2015;28:1-39 e14.
- [11] Pepe MS, Kerr KF, Longton G, Wang Z. Testing for improvement in prediction model performance. *Stat Med*. 2013;32:1467-82.
- [12] Pinheiro J, Bates D, DebRoy S, Sarkar D. R Core Team (2014) nlme: linear and nonlinear mixed effects models. R package version 3.1-117. Available at <http://CRAN.R-project.org/package=nlme>. 2014.
- [13] Rizopoulos D. The R package JMBayes for fitting joint models for longitudinal and time-to-event data using MCMC. arXiv preprint arXiv:14047625. 2014.

Repeated Echocardiograms do not provide Incremental Prognostic Value to Single Echocardiographic Assessment in Minimally Symptomatic Patients with Chronic Heart Failure: Results of the Bio-SHiFT Study

- [14] Yancy CW, Jessup M, Bozkurt B, Butler J, Casey DE, Drazner MH, et al. 2013 ACCF/AHA guideline for the management of heart failure: a report of the American College of Cardiology Foundation/American Heart Association Task Force on Practice Guidelines. *J Am Coll Cardiol.* 2013;62:e147-e239.
- [15] Thavendiranathan P, Grant AD, Negishi T, Plana JC, Popovic ZB, Marwick TH. Reproducibility of echocardiographic techniques for sequential assessment of left ventricular ejection fraction and volumes: application to patients undergoing cancer chemotherapy. *J Am Coll Cardiol.* 2013;61:77-84.
- [16] Rahimi K, Bennett D, Conrad N, Williams TM, Basu J, Dwight J, et al. Risk prediction in patients with heart failure: a systematic review and analysis. *JACC: Heart Failure.* 2014;2:440-6.
- [17] Berger R, Huelsman M, Strecker K, Bojic A, Moser P, Stanek B, et al. B-type natriuretic peptide predicts sudden death in patients with chronic heart failure. *Circulation.* 2002;105:2392-7.
- [18] Koglin J, Pehlivanli S, Schwaiblmair M, Vogeser M, Cremer P. Role of brain natriuretic peptide in risk stratification of patients with congestive heart failure. *J Am Coll Cardiol.* 2001;38:1934-41.
- [19] Tsutamoto T, Wada A, Maeda K, Hisanaga T, Maeda Y, Fukai D, et al. Attenuation of compensation of endogenous cardiac natriuretic peptide system in chronic heart failure: prognostic role of plasma brain natriuretic peptide concentration in patients with chronic symptomatic left ventricular dysfunction. *Circulation.* 1997;96:509-16.
- [20] Miller WL, Hartman KA, Burritt MF, Grill DE, Rodeheffer RJ, Burnett JC, et al. Serial biomarker measurements in ambulatory patients with chronic heart failure: the importance of change over time. *Circulation.* 2007;116:249-57.
- [21] Masson S, Latini R, Anand IS, Barlera S, Angelici L, Vago T, et al. Prognostic value of changes in N-terminal pro-brain natriuretic peptide in Val-HeFT (Valsartan Heart Failure Trial). *J Am Coll Cardiol.* 2008;52:997-1003.
- [22] Savarese G, Musella F, D'Amore C, Vassallo E, Losco T, Gambardella F, et al. Changes of natriuretic peptides predict hospital admissions in patients with chronic heart failure: a meta-analysis. *JACC Heart Fail.* 2014;2:148-58.
- [23] Nagueh SF, Smiseth OA, Appleton CP, Byrd BF, 3rd, Dokainish H, Edvardsen T et al. Recommendations for the Evaluation of Left Ventricular Diastolic Function by Echocardiography: An Update from the American Society of Echocardiography and the European Association of Cardiovascular Imaging. *J Am Soc Echocardiogr* 2016;29:277-314.

Part 2



A large, bold, black number '8' is positioned on the right side of the page. It is partially overlaid by a grey rectangular shape that extends from the top right corner towards the center.

Cardiac shear wave elastography using a clinical ultrasound system

Based on:

Strachinaru M, Bosch JG, van Dalen BM, van Gils L, van der Steen AFW, de Jong N, Geleijnse ML, Vos HJ. *Cardiac Shear Wave Elastography Using a Clinical Ultrasound System*. *Ultrasound Med Biol.* 2017;43(8):1596-1606.

ABSTRACT

The propagation velocity of shear waves relates to tissue stiffness. We prove that a regular clinical cardiac ultrasound system can determine shear wave velocity with a conventional unmodified Tissue Doppler Imaging (TDI) application. The investigation was performed on five tissue phantoms with different stiffness using a research platform (R) capable of inducing and tracking shear waves, and a clinical (C) cardiac system (Philips iE33, achieving frame rates of 400-700Hz in TDI by tuning the normal system settings). We also tested the technique *in vivo* on a normal individual and on typical pathologies modifying the consistency of the left ventricular wall. The R scanner was used as reference. Shear wave velocities measured with TDI on the C system were very close to those measured by the R scanner. The mean difference between the clinical and the research system was 0.18 ± 0.22 m/s, limits of agreement from -0.27 to $+0.63$ m/s. *In vivo*, the velocity of the wave induced by aortic valve closure in the interventricular septum increased in patients with expected increased wall stiffness.

INTRODUCTION

Many fast mechanical phenomena have been described in the heart, such as electromechanical activation, blood flow noise, and shear waves generated in the heart walls by the closure of the valves (Kanai 2005, Cikes et al 2014). The shear waves could potentially be used to estimate non-invasively the stiffness of the myocardium (Brekke et al 2014, Couade et al 2011), with huge potential implications in multiple pathologies characterized by a deterioration of the diastolic properties of the left ventricle. To track these fast mechanical waves, high frame rate (>200 frames per second) imaging is mandatory. The frame rate in conventional ultrasound imaging is limited by the finite velocity of sound in human tissue (around 1540 m/s), the imaging depth (15cm in an apical view), as well as the reconstruction of one image frame from many transmit-receive events. This leads to a conventional recording time of about 30 ms per frame, implying a frame rate of around 30 Hz. Yet, modern clinical scanners achieve frame rates well over 50 Hz in gray-scale 2D imaging by multiline acquisition, in which multiple lines are reconstructed simultaneously from a single transmit-receive event (Tong et al 2012). Recent approaches to even further increase the frame rate include plane wave imaging or diverging waves, as well as high-level multiline transmit beam forming (Cikes et al 2014), or selective field-of-view imaging (Kanai 2005, Brekke et al 2014) thereby reaching frame rates between 500 and 12,000Hz, depending on technology and the depth of the tissue imaged. Moreover, recent advances in full-channel capture systems show that high frame rates can be achieved with relatively high contrast, signal-noise ratio (SNR) and sector size (Papadacci et al 2014), albeit with similar resolution as in conventional or multiline acquisition (MLA) beamforming techniques. However, up to now, none of these technologies have been implemented in a clinical cardiac ultrasound system (Couade et al 2011, Konofagou et al 2011, Lee et al 2012, Song et al 2013). On the other hand, current clinical Tissue Doppler Imaging (TDI) applications use frame rates up to 200 Hz, by multiline acquisition and reduced resolution (Cikes et al 2014, Sutherland et al 1999). The use of a clinical scanner to track waves in the human heart has already been described (Pislaru et al 2014) at frame rates of 350-450 Hz. In this study, we reached higher frame rates in TDI using a clinical cardiac ultrasound system, by carefully tuning the imaging parameters, and hypothesized that this fast TDI modality could allow the detection and quantification of shear waves after valve closure. Similar to any other measurement method, both accuracy and precision of the measurement are important in clinical practice. However, measuring this *in vivo* is very difficult because of absence of any ground truth method for cardiac shear wave tracking, thus preventing estimation of accuracy, and because every heart beat is different, thus preventing estimation of single-shot precision. The core aim of our study therefore is assessing the accuracy and precision of the clinical TDI method to track shear waves. To get a reliable ground truth,

we used a phantom setup where the propagation velocity of shear waves is constant and verified by using a high frame rate research scanner.

METHODS

Shear parameters. The propagation velocity of shear waves in an isotropic, homogeneous, elastic bulk material is related to the shear modulus μ and density ρ (Shiina et al 2015), by

$$V_s = \sqrt{(\mu/\rho)} \quad (1)$$

The simplifying conditions (isotropic, homogeneous, elastic, bulk material) will not be met in cardiac tissue, and therefore we refrain from converting the measured shear wave velocity to shear modulus or Young's modulus E ($E \approx 3 \mu$ in soft biological tissue, Couade et al. 2011) in the *in vivo* pilot data. However, we presume a monotonic relation between shear wave velocity and tissue stiffness. In the phantom experiment described below, the conditions are well met and this relation will be used to convert Young's modulus into an expected shear wave propagation velocity.

Materials. The investigation was carried out on 5 different tissue ultrasound phantoms (CIRS inc., Norfolk, Virginia, USA). The physical properties of these phantoms are presented in Table 1. Baseline calibration was performed on the multi-purpose 40GSE model, and further testing for different tissue stiffness was performed on the Model 039 phantom set.

Table 1. Tissue phantoms properties

<i>Tissue phantom properties</i>	<i>Model 40GSE Calibration phantom</i>	<i>Model 039 Phantom 1</i>	<i>Model 039 Phantom 2</i>	<i>Model 039 Phantom 3</i>	<i>Model 039 Phantom 4</i>
Expected shear wave velocity	2,80m/s	1,01m/s	1,57m/s	2,43m/s	3,56m/s
Young's modulus E	25 kPa	2,7 kPa	11 kPa	20 kPa	48 kPa
Density	1030 kg/m ³				
Poisson ratio	0,5				
Attenuation	0,5 dB/cm/MHz				
Velocity of sound	1540m/s				

We used two ultrasound scanners. The first was a research platform (R) inducing a shear wave through an acoustic radiation force push pulse, and tracking it (as reference). It was a Verasonics Vantage system with extended burst option (Verasonics, Kirkland, WA, USA), equipped with a linear array L7-4 probe (Philips, Bothell, WA 98041-3003 USA). Recorded raw channel RF data and reconstructed ultrasound images were stored for offline

analysis. The second scanner was a normal clinical cardiac ultrasound system (C). This was a Philips iE33 system (Philips Medical, Best, The Netherlands) with an S5-1 probe. A 2-heartbeat TDI movie was recorded and stored in DICOM format for offline analysis. Philips Qlab 9 post-processing software was used for the data analysis.

Setup. In preparation for the measurements, the probes were placed on the upper surface of the phantom, using clinical ultrasound gel as a contact medium. The probes were carefully aligned with their 2D sectors in-line, thus oriented perpendicularly to the direction of propagation of the shear wave. The leads of both an external Cardiometer (CWE CT-1000) and the clinical scanner were attached to one of the researchers (M.S.) for the purpose of synchronisation of the R and C scanners through the ECG signal. The cardiometer produced a trigger signal at the QRS-peak, which initiated the R system to generate an acoustic radiation force push pulse at a depth of 32 mm. In alternating paired recordings, the resulting shear wave was detected either with the R scanner for reference, or with the C scanner for its characterisation. In order to avoid cross-talk between the tracking pulses of the two scanners, the imaging of the shear wave with the R scanner was performed with C in freeze mode. Reciprocally, when investigating the waves with the C system, the R scanner was used to induce the acoustic push only.

The acquisitions were performed on separate days, with intermittent probe repositioning, varied locations of the push pulse, and variation of the acquisition settings. In order to obtain maximum frame rate with the C system, a depth of 6 cm was investigated. The XRes image enhancement modality was turned off, the 2D line density was set to minimum and TDI frame rate to maximum. Smoothing and persistence settings were also minimized. The ultrasound frequency was set to 3.4 MHz, and the velocity range to ± 1.5 cm/s. The frame rate range achieved was between 420 and 645 Hz, depending mainly on the opening of the TDI field of view. At this depth, a 4cm maximal opening (40°) of the TDI sector can provide 470 Hz, a 3 cm opening (30°) 570 Hz and a 2 cm opening (20°) 645 Hz. The maximal frame rate is thus highly dependent on sector opening. Yet, since the shear wave tracking needs both a high temporal resolution and a wide field of view, there may be an optimal setting in which the combination of frame rate and sector width produces the most accurate and precise results. This optimal setting was investigated by analysing three frame rates ranges (400-500 Hz, 500 – 600 Hz, 600 – 700 Hz).

In vivo data. A normal healthy volunteer and two patients were tested using the same setup of the clinical scanner. This research was approved by the local Medical Ethical Committee and informed consent was obtained from all subjects. At 9 cm depth, we obtained over 500 Hz for a window opening of 3 cm (20°) (suitable for parasternal application).

Data processing

Research scanner setup

The characteristics of the acoustic radiation force push pulse and the tracking pulses are displayed in Table 2.

Table 2. Research scanner setup and parameters

Acoustic radiation force pulse	<i>Center frequency</i>	4 MHz
	<i>Duration</i>	1.4 ms (5600 cycles)
	<i>F number</i>	1.5
	<i>Driving voltage</i>	60 V
Tracking	<i>Center frequency</i>	5.2 MHz
	<i>Duration</i>	0.4 μ s (2 cycles)
	<i>Transmit type</i>	Three angled plane waves
	<i>Driving voltage</i>	60 V
	<i>Frame rate</i>	4762 Hz

Data processing for the research scanner

The analytical signal $S(x, z, i)$ in frame i for every pixel at (x, z) was generated by the internal Verasonics image reconstruction algorithm. In the following, the (x, z) coordinates within the brackets are omitted for simplicity of the equations. Local tissue velocity $v(i)$ was obtained with a phase estimator for every pixel based on the cross-correlation of the analytic signal with temporal lag one (Brekke et al 2014),

$$R_1(i) = S(i) \cdot S^*(i-1) \quad (2)$$

$$v(i) = v_N \cdot \angle R_1(i) / \pi \quad (3)$$

$$v_N = c \cdot F / (4 \cdot f_c), \quad (4)$$

in which R_1 is the cross-correlation value per pixel for a time offset of 1 frame, an $*$ denotes the complex conjugate, \angle denotes the angle [rad], v_N is the Nyquist velocity, f_c is the center frequency of the pulse, c is the velocity of sound in the medium and F is the frame rate. The value of the Nyquist velocity was 0.35 m/s, which was high enough to avoid any aliasing effect in the local tissue velocity measurements.

Similar to Brekke et al (2014), we applied a spatial smoothing filter to the cross-correlation frames R_1 (Eq. 2) before calculating the phase (Eq. 3) to remove the influence of speckle. This smoothing consisted of a moving average filter with a size of 1.5 mm in both axial and lateral direction, which is on the same order as the speckle size in the

research system. Since the wavelength of the mechanical waves was around 10 mm, the chosen kernel size did not reduce the signal levels significantly.

The resulting local particle velocity $v(i)$ is a dataset containing subsequent TDI frames at a framerate equal to the original frame rate. Along a horizontal virtual M-mode line located at the depth of the push pulse (32 mm), the forward propagating wave was extracted and gathered in a 2D panel. This panel thus shows the wavelet propagating as function of time and distance along the M-mode line (Fig. 1).

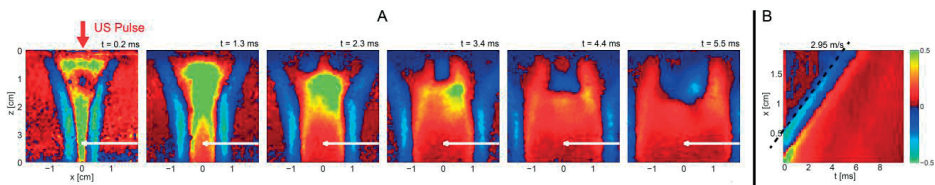


Figure 1. Illustration of shear wave propagation as detected by the research system. A: high-framerate TDI images of travelling shear waves. The shear waves are displacing away from the external acoustic radiation force push focal zone, in a few selected successive frames; time is noted, with $t = 0$ ms at the push. The white arrow represents the virtual M-mode line. B: Virtual M-mode along the line in A. The slope of the wave front is tracked with a Radon transform in a region of interest with the research system, giving a velocity estimate of 2.95 m/s in this recording.

The slope $\Delta x/\Delta t$ with which this wave propagates is the propagation velocity that acts as the ground truth to the wave propagation measured with the clinical scanner. Yet, in the data processing of the clinical scanner, we tracked the wave *front* which is most clearly visible for the observer. In the data processing of the research scanner, we wanted to automate the tracking, for which the Radon transform produces accurate outcome (Rouze et al 2010, Urban and Greenleaf 2012). The Radon transform tracks the wave *peak* path. To match the wave *front* tracking in the clinical scanner with the wave *peak* tracking in the research scanner, we first took a time derivative of the local particle velocity in the research scanner. This effectively yielded a map containing the local particle *acceleration*, with the rationale that the wave front correlates to the first trace of highest magnitude in this acceleration map. Next we extracted the slope of the trace using a Radon transform in the region of interest (Rouze et al 2010, Urban and Greenleaf 2012, Vos et al 2015).

Data processing for the clinical scanner

The DICOM TDI loops (DICOM pixel array of 768 rows and 1024 columns, with a pixel spacing of 0.088/0.088mm) were processed using Qlab 9. A virtual M-mode line was horizontally traced across the TDI sector at the depth of the focal point of the push pulse, which was applied to the left, immediately outside the sector (Figure 2A). Its length and

direction was pre-defined by the user. For consistency, we chose the direction of the M-mode line to always point towards the shear wave source, perpendicular to the wave front. The velocity propagation of the wave front was estimated through

$$V_s = D/T, \quad (5)$$

where D is the (user-defined) length of the M-mode line and T is the time the wave travels along the M-mode line.

The software provides a virtual M-Mode map (Figure 2B), allowing to manually trace the slope of the propagating wave. This map does not display a time axis in QLab. Yet, the propagation time T can be obtained through a work-around. By manually clicking on the base and top of the slope of the wave, the program returned the corresponding active points on the time-velocity curve that is automatically computed by the software (Figure 2C). The time interval T between these points is then displayed automatically (Figure 2D). From this time, and pre-defined M-mode length, the velocity is calculated (Figure 2 and Equation 5).

Statistical analysis. Baseline testing and calibration was performed on the 40GSE phantom. Thirty independent paired measurements were performed on this tissue phantom. The resulting velocities were represented as mean \pm standard deviation (SD). The differences between mean values were estimated by paired-samples T-test. If not normally distributed, the data sets were also compared using the Wilcoxon signed-rank test. The distribution was represented by box plots. Testing for other stiffness values (other shear wave velocities) was performed by additional five to seven paired measurements for each of the five phantoms. Variability was calculated as 1.96 SD of the mean arithmetic difference according to Bland and Altman. Accuracy was defined as the proximity of the mean value to the reference value; precision as the closeness of the agreement between results (represented by the standard deviation). For the calibration study, standard error was also calculated to support the assessment of accuracy. Inter- and intra-observer variability for the clinical scanner was assessed on 10 randomly chosen acquisitions. Intra-observer test-retest variability was evaluated on the initial measurements performed by M.S. with a new measurement set one month later, blinded to the first result. Inter-observer variability was estimated between the result of M.S., and the results obtained by a first-time user, without any prior knowledge of the experiment or the software application (L.G.). SPSS software (version 21, IBM 2012) was used for all analyses, with a p-value of <0.05 considered significant.

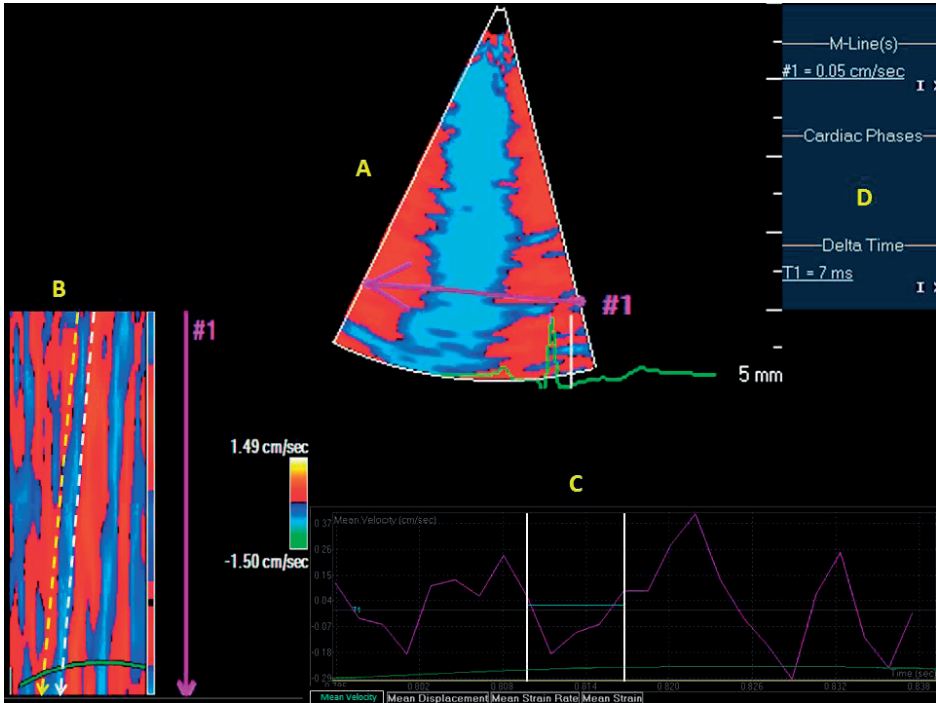


Figure 2. Detailed view (modified to indicate the main elements) of the data obtained in the tissue phantom, using offline processing in Philips Qlab. The ECG signal belongs to one of the researchers (M.S.) and was only used to synchronize the two ultrasound systems. In the spatiotemporal color map, we have highlighted the moving wavefront with dotted arrows for clarity. A: virtual M-mode line (#1) traced across the TDI sector; B: virtual M-mode map of a shear wave demonstrating the wave front (leftmost dotted arrow) and the first velocity zero crossing (rightmost dotted arrow); C: mean velocity curve (averaged over the M-mode line). The time interval in which the wave occurs is marked with the solid white lines; D: results panel, showing the time interval.

RESULTS

Both scanners detected the waves propagating away from the push region in a time span variable according to the phantom's stiffness (Figure 1 and 2, and Movie 1). We measured the propagation velocity of the wave front.

Research scanner. The automated detection algorithm was used to track the wave front, resulting in a velocity of 2.87 ± 0.07 m/s in the calibration phantom and different velocities in the Model 039 phantoms (Table 3).

Table 3. Tissue phantoms shear wave velocities according to the clinical (C) and research (R) scanner

Phantom	Model 40GSE	Model 039 Phantom 1	Model 039 Phantom 2	Model 039 Phantom 3	Model 039 Phantom 4
<i>Expected shear wave velocity</i>	2,80 m/s	1,01 m/s	1,57 m/s	2,43 m/s	3,56 m/s
<i>Clinical scanner velocity</i>	2,85±0,21 m/s (N=7)	1,06±0,05 m/s (N=7)	1,59±0,08 m/s (N=6)	2,76±0,17 m/s (N=5)	3,87±0,21 m/s (N=7)
<i>Research scanner velocity</i>	2,87±0,07 m/s	0,87±0,01 m/s	1,51±0,02 m/s	2,34±0,01 m/s	3,56±0,07 m/s

Clinical scanner.

Frame Rate Calibration

The propagation velocities of the wave front of the shear wave in the calibration phantom at different frame rate ranges of the C scanner are summarized in Table 4. The velocity ranged between 2.77 ± 0.14 m/s and 2.83 ± 0.18 m/s, depending on the frame rate (Figure 3). The velocities recorded at frame rates of 500 - 600 Hz and 600 - 700 Hz were statistically similar to the R scanner results (lowest mean difference of -0.04 ± 0.20 m/s, Wilcoxon $Z=-0.99$; $p=0.318$ for the frame rate range 500 to 600 Hz). The limits of agreement were smaller than ± 0.45 m/s (Table 4).

Table 4. The difference between velocities calculated by the clinical and research scanner, according to the frame rate range of the clinical system, for calibration

Statistical method	Paired-samples T-test			Bland-Altman			Wilcoxon signed-rank test			
	Mean \pm SD C scanner speed (m/s)	Standard error of the mean	95% CI	P (T-test)	Mean difference \pm SD between C and R scanner #	Limits of agreement (± 1.96 SD)	T	Z	P-value	r (effect size)
400-500 Hz	2.77 \pm 0.14	0.028	0.04-0.16	0.002	-0.09 \pm 0.16	-0.39 to 0.22	8	-2.75	0.006	-0.50
500-600 Hz	2.83 \pm 0.18	0.037	-0.04-0.12	0.298	-0.04 \pm 0.20	-0.43 to 0.35	14	-0.99	0.318	-0.18
600-700 Hz	2.80 \pm 0.18	0.037	-0.01-0.14	0.075	-0.06 \pm 0.20	-0.30 to 0.45	13	-1.80	0.072	-0.33

The non-significant p values were highlighted in bold

C=clinical; CI=confidence interval; R=research; SD= standard deviation

R scanner speed was 2.87 ± 0.07 m/s

Velocity measurements using the calibrated settings

A new measurement set was performed on all 5 phantoms, using the best fitted settings from the calibration (frame rate of 513 Hz). The results are displayed in Table 3. Velocities measured with the two scanners were similar and close to the reference values.

Intra and inter-observer variability

For intra-observer test-retest variability (No=10 readings), the first reading displayed a velocity of 2.73 ± 0.13 m/s. At the second reading, the mean value was 2.81 ± 0.08 m/s ($p=0.10$). The mean difference was -0.07 ± 0.13 m/s. The limits of agreement were -0.33 to $+0.18$ m/s.

For inter-observer variability, the mean value of velocity obtained by the second observer (No=10 readings) was 2.92 ± 0.25 m/s ($p=0.08$). The mean difference between observers was -0.19 ± 0.29 m/s. The limits of agreement were -0.76 to $+0.38$ m/s.

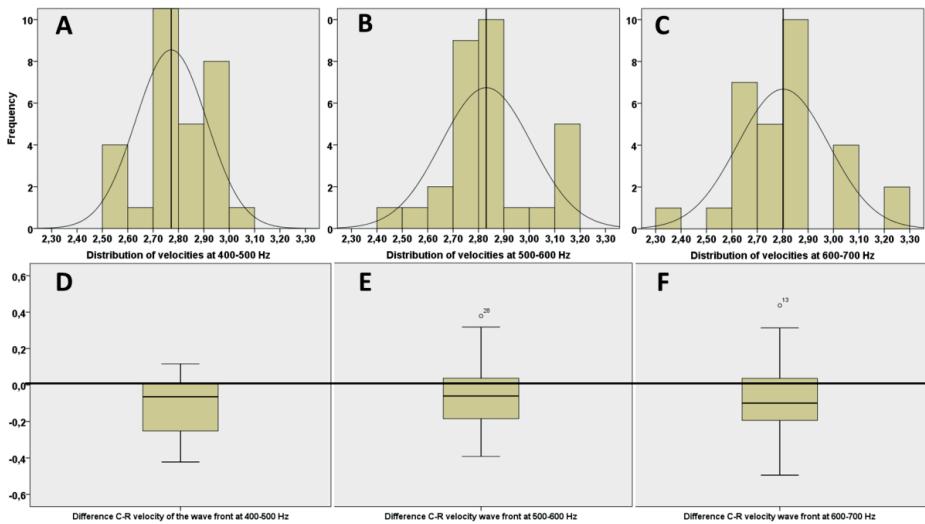


Figure 3. Calibration study. The distribution of velocities (A, B, C) measured at different frame rate ranges and the difference in measured velocity between the clinical and the research system (D,E, F), comparing the results in box plots, demonstrating the bias and the distribution of the differences. A, D: frame rate range=400 to 500 Hz; B, E: frame rate range=500 to 600 Hz; C, F: frame rate range=600 to 700 Hz. The mean velocity is marked with a vertical line in panels A, B, C. The horizontal line in the lower panels marks the zero point (perfect agreement).

Accuracy

Taking the measurements of the R scanner as reference, the difference in the measurements obtained by the clinical scanner was assessed on the last set of 5 to 7 paired measurements performed with each of the 5 phantoms. The correlation between the two scanners (Figure 4A) was excellent ($R^2=0.952$; $p<0.0001$). The mean difference between the clinical and the research system was 0.18 ± 0.22 m/s, limits of agreement from -0.27 to $+0.63$ m/s (Figure 4B).

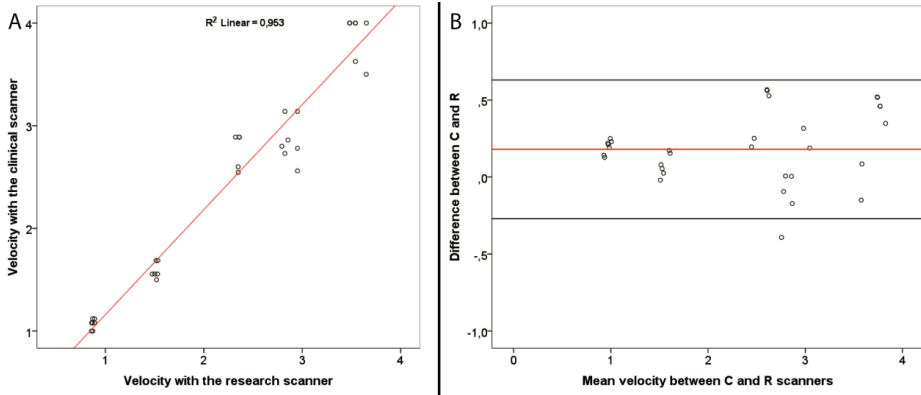


Figure 4. Accuracy study. A: The correlation of the velocities measured with the two systems; B: Bland-Altman analysis of the agreement between the two scanners.

***In vivo* detection of shear waves in patients.** A 28-year-old healthy male underwent a cardiac ultrasound exam, while simultaneously recording the ECG and phonocardiogram. High frame rate TDI (510 Hz at 8 cm depth, velocity scale 3.5 cm/s) signals were acquired from the parasternal window, from the proximal part of the interventricular septum. The velocity of the shear wave travelling into the septal wall after aortic valve closure was 3.0 m/s for an M-mode line traced at mid-wall level (Figure 5A).

In a 43-year-old female patient with a dilated ischemic cardiomyopathy, high frame rate TDI (513 Hz at 8 cm depth, velocity scale of 2.5 cm/s) showed a velocity of 4.4 m/s (Figure 5B and Movie 2). The shear wave is clearly separated from the myocardial displacement occurring in early isovolumetric relaxation.

A 48-year-old male patient having received a heart transplant 9 months before, with signs of rejection, underwent a routine ultrasound examination. Although the image quality was poor, it still allowed visualization of left ventricular walls. A high frame rate TDI acquisition (541 Hz, 9cm depth, velocity scale of 1.5 cm/s) in the parasternal view was added, that showed a fast wave travelling into the septum after the aortic valve closure, similar to the other cases, but at a velocity of 5.4 m/s (Figure 5C).

DISCUSSION

The main findings of this study were: 1) the visualization of shear waves induced by acoustic radiation force into a tissue phantom is possible with a clinical TDI application, at a surprisingly high frame rate (400-645Hz); 2) the waves can be tracked and their velocity quantified in this *in vitro* setting, with sufficient precision and accuracy at a frame

rate range above 500 Hz; 3) *In vivo* tracking is feasible in patients, and the results seem to confirm that the velocity of the waves is increasing where increased wall stiffness is expected based on pathology.

In several studies the detection of fast phenomena in the heart has been described (Brekke et al 2014, Cikes et al 2014, Kanai et al 2000, Kanai 2005, Pernot et al 2011), using experimental systems or modified software. In our study a normal modern clinical scanner achieved surprisingly high TDI frame rates, between 400 and 700 Hz at depths less than 10 cm, by turning off image enhancement modalities and by carefully tuning the relationship between the depth of the image, the 2D line density and aperture and the TDI field of view. We hypothesized that the time resolution of 2ms (500Hz frame rate) could allow the detection and quantification of the very fast phenomena that are naturally occurring in the heart such as shear-like waves caused by the closure of the valves. The present study shows that shear waves in a tissue phantom are accurately detected by the TDI clinical application. As the reference wave velocity could be validated by the research scanner, both the accuracy and precision of the method were investigated.

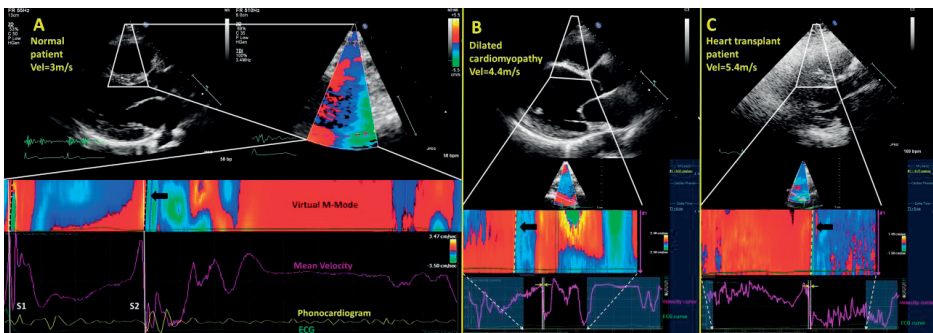


Figure 5. Clinical application of the high frame rate tissue Doppler technique. A: normal male subject. The wave front is synchronous to the onset of the second heart sound (S2) on the phonocardiogram (PCG); the velocity is computed at 3.0m/s; the shear wave after mitral valve closure is also visible synchronous to the first heart sound (S1). The upper panels show the classical echocardiographic image and the focused TDI window over the interventricular septum; In the lower panel one full cardiac cycle was reconstructed off-line; the slope of the aortic shear wave (black arrow), extracted from the virtual M-mode, is marked with a dashed line. B: dilated cardiomyopathy. The velocity of the wave front reaches 4.4m/s. C: heart transplant patient; the velocity of the shear wave is even higher, computed at 5.4m/s. At a velocity scale of 1.5 cm/s a velocity shift (zero crossing) is seen separating the shear wave (black arrow). Time intervals are extracted from the velocity/time curves, and underlined by vertical white lines. The M-mode map displays only a fraction of the cardiac cycle around the closure of the aortic valve (depending on the relation frame rate versus heart rate). This corresponds to the clear window in the velocity/time/ECG panels and is indicated with white dashed arrows.

The precision of the measurement is restricted by the field of view (represented by M-mode length D) and frame rate (F) in the clinical scanner. With reference to Eq. 5, the

standard deviation in the propagation speed δV_s can be caused by variance in both D and T . Standard deviation in D , is caused by limited lateral resolution R (Elegbe and McAleavey 2013) in the sector of the phased array probe (despite the fixed length of the virtual M-mode line). Variance in T is caused by rounding off to integer frame intervals. Applying the generic equations of statistically independent variables to Eq. 5 gives the approximate equation (see Appendix A for details)

$$\delta V_s = V_s/D \sqrt{\{(R/2)^2 + 1/6 \cdot (V_s/F)^2\}}. \quad (6)$$

For example, when taking a width of 3.5 cm of the TDI window, a frame rate of 500 Hz, and a typical speckle size of 5 mm, a wave with 2.8 m/s propagation velocity has an expected standard deviation of 10%, which is similar to the actually observed value (6 %). For a wave travelling with 5 m/s, the expected value increases to 14%, due to the relatively increased influence of frame rate (see also Table 3). The standard deviation can only be improved by taking the average over multiple recordings. On the contrary, the research system has both a higher temporal and spatial resolution, thanks to a larger linear probe, higher imaging frequency, and full channel acquisition. This allows for very precise single measurements.

In the calibration measurements the average propagation velocities yielded by the clinical scanner were statistically similar to the research ones in the frame rate range 500-600Hz (2.83 ± 0.18 m/s, $p=0.298$) and 600-700 Hz (2.80 ± 0.18 m/s, $p=0.075$). In conventional echocardiographic measurement (Chukwu et al 2008, Lang et al 2015), mean percent errors are reported to be around 10-20%, which is similar to the errors in our findings. The precision was increased in the calibration study by averaging 30 measurements, leading to a standard error of around 0.04 m/s (1% relative error). These settings were used for the accuracy study, which demonstrated tight limits of agreement, comparable with the measurement variability. The inter-observer variability was of the same magnitude as the difference between individual measures. Based on these values, the accuracy and precision can be considered acceptable for research purposes. The clinical relevance of this variability remains to be established, being dependent on the physiological or pathological range of velocities.

Clinical application

In the past years we have developed a high frame rate ultrasound imaging modality which determined the propagation velocity of Lamb waves (which are shear wave-like) in the septal wall (Vos et al 2016) that are naturally caused by the aortic and mitral valve closure. The recorded velocities are in close agreement with those reported with an alternative method that uses externally induced shear waves, which however is either

insensitive (Song et al 2013) or invasive (Hollender et al 2012). Other teams have been working on clinical TDI with modified software in order to achieve the very high frame rate needed to image these phenomena (Brekke 2014). Our *in vivo* data shows that shear waves can be measured with a clinical system in cardiac mode, which could, in one step, make the translation from lab research to clinical research or even everyday clinical practice, without major investments in new equipment or software.

Since Doppler is most sensitive for axial motion, it has the highest detection sensitivity for shear waves propagating laterally in the field of view, at a TDI velocity scale adapted to match the particle velocity. Please note that although the angle between the propagation direction and the ultrasound beam may influence the apparent amplitude of the shear wave, it has no influence on the apparent propagation velocity, the latter being the property of interest in the current study. Translating these properties into clinical echocardiography, a TDI system would be most sensitive for shear waves traveling through the interventricular septal wall in a *parasternal* view, rather than in an *apical* view. We have tested the technique (using the same clinical scanner, probe and TDI settings as the experimental results) on a normal individual and several typical pathologies modifying the consistency of the left ventricular wall. The velocity scale allowing for clear visualization of the shear wave matches the particle displacement velocity observed in previous studies (1.5 - 3 cm/s) (Brekke et al 2014, Vos et al 2015). The velocity of the wave induced in the interventricular septum seems to increase in the cases where the stiffness of the wall is expected to increase, as compared to the normal individual. Although no definitive conclusion can be drawn from this limited data, it shows that the detection and quantification of these naturally-occurring shear-like waves is feasible in patients, and could represent a direct measurement of wall stiffness, with potential implications in multiple pathologies characterized by a deterioration of the left ventricular function.

In the present *in vivo* study we focused on the aortic valve closure. However, the waves after mitral valve closure were also detectable in our study subjects, as can be noticed on the M-mode map in Figure 5A and Movie 2 (online; leftmost at the beginning of the movie). Thus, the detection method is able to record the stiffness during two moments in the cardiac cycle, when the muscle is dilated, and when it is compact. Specific relations of the two points (ratio, difference) may have an additional clinical relevance next to their individual values because of cancellation of possible confounding factors such as pre-load, afterload, and wall thickness, although such relevance needs to be thoroughly tested in a larger study population. During the short isovolumetric periods in which the waves propagate there is only minor motion of the myocardial walls, making shear wave quantification presumably easier and more reliable. On the other hand, the intrinsic myocardial stiffness may vary over the short period in which the waves propagate (order

10 – 20 ms), thus changing the instantaneous shear wave speed. Although Kanai showed a time dependency of the wave propagation velocity after aortic valve closure (Kanai 2005), we have not observed such a phenomenon in our data. Yet, to further elucidate this phenomenon, the dynamic components of stiffness may be studied, for example, in a more experimental setup involving accurately-timed acoustic-radiation force shear wave elastography.

Strain, strain-rate and data derived from TDI velocities are recent applications that assess myocardial deformation and, indirectly, elasticity. A down-side of these methods is a large dependence on hydrodynamic parameters (preload, afterload), as the strain is a ratio of pressure and myocardial stiffness. Although a dependency may also exist in the shear wave method, it is expected to be weaker since hydrodynamic pressure is not found in the principal relation between shear wave propagation velocity and stiffness. A comparison with the high frame-rate TDI derived shear wave velocity may be further studied based on data that is recorded with the same clinical scanner.

The myocardial wall exhibits a complex fiber structure, so shear wave propagation might be inhomogeneous across the width of the septum. For simplicity, in our *in vivo* data, we have chosen the mid-wall position, having presumably the highest consistency in placement. Further clinical studies are warranted in order to detect and characterize this phenomenon.

The propagation velocity in our healthy subject is lower than that found in a group of 10 human subjects by Brekke et al (2014) (5.41 ± 1.28 m/s) specifically, and more generally found in human and animal studies (Hollender et al 2012). We speculate that this difference is originating from the different probe positioning: parasternal in our study, and apical in Brekke et al (2014) and Kanai et al (2000).

The longitudinal myocardial stretch during late diastole as described by Pislaru et al (2014), was also visible in our human subjects. The expected velocity of these phenomena is between 1 and 2 m/s, which can be easier to track with lower frame rates than the faster waves after aortic valve closure.

Unfortunately, the exact TDI beamforming technique and settings are not disclosed on the clinical system, although it is known that the Philips iE33 implements an MLA technique. Yet, we could make a general estimation based on the work by Tong et al. (2012) who compared various fundamental-frequency MLA beamforming techniques. The speckle size in our color TDI movies was 4-5 mm in lateral direction. Tong et al. calculated lateral beamwidths in the order of 2-3 mm up to 50 mm depth, and 3-5 mm for imaging depth

> 50 mm. Although significant differences exist between the specific implementations of MLA, the differences are relatively small, and the values are very similar to our measurements. This implies a reasonably good resolution in our current TDI measurements. As discussed by Papadacci et al, more recent full-channel capture systems -which enable an extremely high degree of MLA and compounding- do not improve on resolution but they will simultaneously improve on contrast, SNR, imaging sector size and framerate. Of these aspects, SNR proved to be sufficient in our measurements, but a larger image sector and slightly higher frame rate (order 1000 frames/second) would reduce the variance in the measurements, according to Eq. 6. The effect of a higher image contrast has yet to be studied in a more realistic phantom with higher tissue contrast. Therefore, although measurement precision may be improved with recent full-channel capture systems, the performance of the currently used clinical scanner is reasonably good.

Study limitations and future directions

A limitation of the study may be the limited velocity range of the phantom set (1 – 4 m/s), although the results show neither signs nor trends of bias for these velocities. Further confirmation of the strength of the method should come from clinical studies with a large pathology spectrum. The present work shows that shear waves can be measured with good consistency with a regular clinical scanner, thus opening the way to more *in vitro* and *in vivo* studies.

As demonstrated above, a TDI frame rate of 500 Hz could be insufficient when it comes to higher velocities, because such waves would quickly travel through the limited field of view. We hope that the advancement in technology, with even higher frame rates becoming available, and/or the changes in data processing would allow for the use of wider fields of view.

Manual tracking as allowed by the manufacturer-designed software is time consuming and prone to errors. Therefore, future research should focus on a robust method of automated velocity tracking from the DICOM frames. A possible candidate for such robust analysis is the Radon transform as illustrated in this study for the research scanner data.

CONCLUSION

A regular clinical cardiac TDI application can visualize and quantify shear waves induced by acoustic radiation force in a tissue phantom at sufficiently high frame rates (order 500 Hz). *In vivo* tracking is feasible in patients, and the results seem to confirm that the velocity of the waves is increasing where increased wall stiffness is expected based on pathology.

APPENDIX A

In this appendix we derive the standard deviation of the measured propagation velocity, based on both the temporal and spatial uncertainties in values by which the propagation velocity is calculated.

The wave propagation velocity in the measurements is calculated by

$$V_s = D/T. \quad (\text{A.1})$$

Conventionally, the standard deviation δV_s in the propagation velocity is derived from the respective standard deviation of the statistically independent D and T :

$$\delta V_s = \sqrt{\{ (\partial V_s / \partial D \delta D)^2 + (\partial V_s / \partial T \delta T)^2 \}}, \quad (\text{A.2})$$

with ∂/∂ denoting the partial difference.

Inserting Eq. A1 in Eq. A2 yields the equation for relative standard deviation

$$\delta V_s / V_s = \sqrt{\{ (\delta D / D)^2 + (\delta T / T)^2 \}}. \quad (\text{A.3})$$

The value of δD can be estimated by first approach from the speckle size as speckle prevents exact localisation of the wave (Elegbe and McAleavey 2013). With R defined as the typical (lateral) speckle size, the value of δD is approximated by $R/2$.

The value of δT can be estimated from the frame rate F . The travel time T is determined from the time interval between the frames where the waves enter and exit the field of view. In both cases, the times are rounded off to discrete values of $T (=n/F, n \text{ integer})$ in our manual tracking. From conventional theory, each rounding gives a standard deviation of $1/\sqrt{12} \cdot 1/F$, and the independently combined standard deviation for the time interval between entering and exiting is $\delta T = 1/\sqrt{6} \cdot 1/F$. The value of T is derived from V_s , $T = D / V_s$. Inserting these values in (A.3) yields

$$\delta V_s / V_s = \sqrt{\{ (R / (2 \cdot D))^2 + 1/6 \cdot (V_s / (F \cdot D))^2 \}}, \quad (\text{A.4})$$

or

$$\delta V_s = V_s / D \sqrt{\{ (R/2)^2 + 1/6 \cdot (V_s / F)^2 \}}. \quad (\text{A.5})$$

Figure A1 shows the resulting absolute and relative standard deviation for given propagation velocities in the typical range of 1 – 10 m/s. Typical values of $F = 500$ Hz, $D = 3.5$ cm, and $R = 5$ mm are used to obtain this graph.

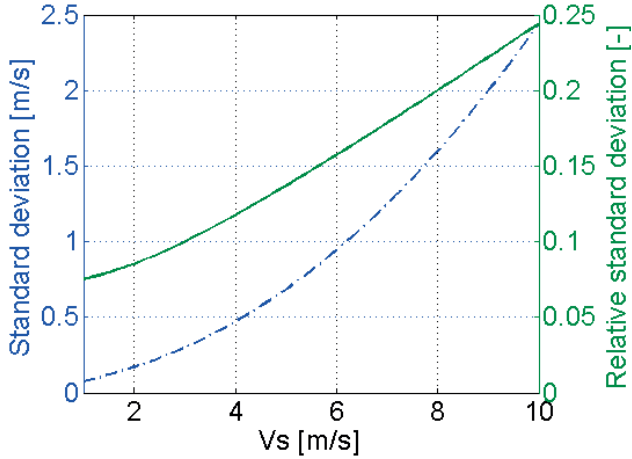


Figure A.1. Estimated theoretical standard deviation of V_s , and its relative value, based on the variance in both the temporal and spatial measurement.

REFERENCES

- Brekke B, Nilsen LC, Lund J, Torp H, Bjastad T, Amundsen BH, Stoylen A, Aase SA. Ultra-high frame rate tissue Doppler imaging, *Ultrasound Med Biol*. 2014;40:222-31.
- Cikes M, Tong L, Sutherland GR, D'hooge J. Ultrafast cardiac ultrasound imaging: technical principles, applications, and clinical benefits, *JACC Cardiovasc Imaging*. 2014;7:812-23.
- Chukwu EO, Barasch E, Mihalatos DG, Katz A, Lachmann J, Han J, Reichek N, Gopal AS. Relative importance of errors in left ventricular quantitation by two-dimensional echocardiography: insights from three-dimensional echocardiography and cardiac magnetic resonance imaging. *J Am Soc Echocardiogr*. 2008;21:990-7.
- Couade M, Pernot M, Messas E, Ba M, Hagege A, Fink M, Tanter M. In vivo quantitative mapping of myocardium stiffening and transmural anisotropy during the cardiac cycle, *IEEE Trans Med Imaging*, 30 (2011), pp. 295-305
- Elegbe EC, McAleavey SA. Single tracking location methods suppress speckle noise in shear wave velocity estimation. *Ultrasonic imaging* 35, no. 2 (2013): 109-125.
- Hollender PJ, Wolf PD, Goswami R, Trahey GE. Intracardiac echocardiography measurement of dynamic myocardial stiffness with shear wave velocimetry. *Ultrasound Med Biol*, vol. 38, pp. 1271-1283, 2012.
- Kanai H, Yonechi S, Susukida I, Koiwa Y, Kamada H, Tanaka M. Onset of pulsatile waves in the heart walls at end-systole, *Ultrasonics*. 2000;38:405-11.
- Kanai H. Propagation of spontaneously actuated pulsive vibration in human heart wall and in vivo viscoelasticity estimation, *IEEE Trans Ultrason Ferroelectr Freq Control*, 52 (2005), pp. 1931-1942
- Konofagou E, Lee WN, Luo J, Provost J, Vappou J. Physiologic cardiovascular strain and intrinsic wave imaging, *Annu Rev Biomed Eng*. 2011;13:477-505.
- Lang RM, Badano LP, Mor-Avi V, Afilalo J, Armstrong A, Ernande L, Flachskampf FA, Foster E, Goldstein SA, Kuznetsova T, Lancellotti P, Muraru D, Picard MH, Rietzschel ER, Rudski L, Spencer KT, Tsang W, Voigt JU. Recommendations for cardiac chamber quantification by echocardiography in adults: an update from the American Society of Echocardiography and the European Association of Cardiovascular Imaging. *J Am Soc Echocardiogr*. 2015 Jan;28(1):1-39.e14.
- Lee W, Pernot M, Couade M, Messas E, Bruneval P, Bel A, Hagège AA, Fink M, Tanter M. Mapping myocardial fiber orientation using echocardiography-based shear wave imaging, *IEEE Trans Med Imaging*, 31 (2012), pp. 554-562
- Papadacci C, Pernot M, Couade M, Fink M, Tanter M. High-contrast ultrafast imaging of the heart. *IEEE Trans Ultrason Ferroelectr Freq Control*. 2014;61(2):288-301.
- Pernot M, Couade M, Mateo P, Crozatier B, Fischmeister R, Tanter M. Real-time assessment of myocardial contractility using shear wave imaging, *J Am Coll Cardiol*. 2011;58:65-72.
- Pislaru C, Pellikka PA, Pislaru SV. Wave propagation of myocardial stretch: correlation with myocardial stiffness. *Basic Res Cardiol*. 2014;109(6):438.
- Rouze NC, Wang MH, Palmeri ML, Nightingale KR. Robust estimation of time-of-flight shear wave speed using a radon sum transformation. *IEEE Trans Ultrason Ferroelectr Freq Control*. 2010;57:2662-70.
- Shiina T, Nightingale KR, Palmeri ML, Hall TJ, Bamber JC, Barr RG, Castera L, Choi BI, Chou YH, Cosgrove D, Dietrich CF, Ding H, Amy D, Farrokh A, Ferraioli G, Filice C, Friedrich-Rust M, Nakashima K, Scha-

- fer F, Sporea I, Suzuki S, Wilson S, Kudo M. WFUMB guidelines and recommendations for clinical use of ultrasound elastography: Part 1: basic principles and terminology, *Ultrasound Med Biol.* 2015;41:1126-47.
- Song P, Zhao H, Urban M, Manduca A, Pislaru S, Kinnick R, Pislaru C, Greenleaf J, Chen S. Improved shear wave motion detection using pulse-inversion harmonic imaging with a phased array transducer, *IEEE Trans Med Imaging*, 32 (2013), pp. 2299–2310
- Sutherland GR, Bijmens B, McDicken WN. Tissue Doppler Echocardiography: Historical Perspective and Technological Considerations, *Echocardiography.* 1999;16:445-453.
- Tong L, Gao H, Choi HF, D'hooge J. Comparison of conventional parallel beamforming with plane wave and diverging wave imaging for cardiac applications: a simulation study. *IEEE Trans Ultrason Ferroelectr Freq Control.* 2012;59(8):1654-63.
- Urban MW, Greenleaf JF, Use of the radon transform for estimation of shear wave speed. *J Acoust Soc Am*, vol. 132, pp. 1982-1982, 2012
- Vos HJ, van Dalen BM, Bosch JG, van der Steen AFW, de Jong N, “Myocardial passive shear wave detection”, in: *IEEE Internat. Ultras Symp, Taipei, Taiwan*, 2015.
- Vos HJ, van Dalen BM, Heinonen I, Bosch JG, Sorop O, Duncker DJ, van der Steen AF, de Jong N, Cardiac Shear Wave Velocity Detection in the Porcine Heart. *Ultrasound Med Biol.* 2017 Jan 5. pii: S0301-5629(16)30412-4.

9

Reproducibility of Natural Shear Wave Elastography Measurements

Based on:

Keijzer LBH, **Strachinaru M**, Bowen DJ, Geleijnse ML, van der Steen AFW, Bosch JG, de Jong N, Vos HJ. *Reproducibility of Natural Shear Wave Elastography Measurements*. Ultrasound

Med Biol. 2019

ABSTRACT

For the quantification of myocardial function, myocardial stiffness can potentially be measured non-invasively using shear wave elastography. Clinical diagnosis requires high precision. In ten healthy volunteers, we studied the reproducibility of the measurement of propagation speeds of shear waves induced by aortic and mitral valve closure (AVC, MVC). Inter-scan was slightly higher but in similar ranges as intra-scan variability (AVC: 0.67m/s (IQR: 0.40 – 0.86m/s) versus 0.38m/s (IQR: 0.26 – 0.68m/s); MVC: 0.61m/s (IQR: 0.26 – 0.94m/s) versus 0.26m/s (IQR: 0.15 – 0.46m/s)). For AVC, the propagation speeds obtained on different days were not statistically different ($p=0.13$). We found different propagation speeds between two systems (AVC: 3.23 – 4.25m/s (Zonare ZS3) versus 1.82 – 4.76m/s (Philips iE33), $p=0.04$). No statistical difference was found between observers (AVC: $p=0.35$). Our results suggest that measurement inaccuracies dominate the variabilities measured among healthy volunteers. Therefore, measurement precision can be improved by averaging over multiple heartbeats.

INTRODUCTION

In developed countries, about 1-2% of the adult population has heart failure. The prevalence is even rising to >10% among people older than 70 years (Ponikowski et al. 2016). Currently, geometrical volumes and non-invasive Doppler measurements of tissue and blood are used for the echocardiographic evaluation of cardiac myocardial function (Lang et al. 2015; Nagueh et al. 2016). Nonetheless, these parameters mainly measure effects of myocardial function are load dependent (Voigt 2019). No accurate method currently exists for non-invasive cardiac stiffness measurements. Measuring the stiffness of the myocardium likely gives more direct insights in the condition of the myocardium (Voigt 2019), as recently shown by Villemain et al. (2018) in a group of volunteers and hypertrophic cardiomyopathy patients using shear wave elastography measurements (SWE). To distinguish different types of diastolic and systolic dysfunctions and to accommodate more personalized treatments, noninvasive stiffness measurements could be a valuable tool.

Several studies have shown the potential of shear waves (SWs) to be used for measuring the stiffness of the myocardium non-invasively (Arani et al. 2017a; Petrescu et al. 2019; Santos et al. 2019; Strachinaru et al. 2019; Villemain et al. 2019; Wassenaar et al. 2016). The propagation speed of these SWs is expected to be linked to Young's modulus of the myocardium.

Magnetic resonance and ultrasound imaging have been used in different animal and human studies to perform SWE measurements. The advantage of using magnetic resonance imaging is that the 3-D displacement field of the SWs in the complex cardiac geometry can be measured (Arani et al. 2017b). However, MRI is expensive, uncomfortable and slow; moreover, it cannot be used for patients with arrhythmia because of cardiac gating. For SWE using ultrasound imaging, several studies have used external sources such as mechanical shakers (Pislaru et al. 2014b; Tzschätzsch et al. 2012; Urban et al. 2013) or acoustic radiation forces (ARF) (Bouchard et al. 2009; Couade et al. 2011; Hollender et al. 2012; Pernot et al. 2011; Pernot et al. 2016; Song et al. 2016; Villemain et al. 2019) to induce SWs. The SWs naturally occurring due to aortic valve closure (AVC) or mitral valve closure (MVC) have been investigated as well (Brekke et al. 2014; Kanai 2005; Pernot et al. 2007; Pislaru et al. 2014a; Santos et al. 2019; Strachinaru et al. 2019; Vos et al. 2017). An advantage of exploiting the SWs induced by valve closure is that these SWs were found to have larger tissue velocity amplitudes (~40 mm/s) (Vos et al. 2017) than the SWs induced by an external acoustical force (~10 mm/s) (Couade et al. 2011), likely leading to higher signal to noise ratios. However, the low frequency content of natural SWs (Kanai 2005; Santos et al. 2019; Vos et al. 2017) compared to external sources

(Couade et al. 2011; Hollender et al. 2012; Pislaru et al. 2014b) and thus the inherently larger wavelengths form a disadvantage of natural shear wave speed (SWS) measurements. Since the SWs can only be tracked over the limited length of a few centimeters of the interventricular septum (IVS), smaller fractions of the wavelength can be tracked for SWs with low frequencies, causing measurement inaccuracy. Additionally, for 2D natural SWS measurements, the source of the SWs is not assured to be in plane with the field of view, as is the case for ARF-based measurements, and therefore out-of-plane propagation could also induce measurement inaccuracy (Vos et al. 2017). These measurement inaccuracies should be minimized for clinical diagnosis where high precision of the SWS measurements is needed.

Besides measurement inaccuracies, SWS measurements are expected to be affected by various phenomena. First of all, the myocardial stiffness measured depends on the intrinsic viscoelastic material characteristics of the myocardium independent of loading-conditions. Significant different propagation speeds have been measured after AVC and MVC for pathological stiff myocardium as in hypertrophic cardiomyopathy (Strachinaru et al. 2019) and amyloidosis patients (Petrescu et al. 2019) compared to healthy volunteers. Second, the moment in the cardiac cycle will determine to what extent passive myocardial stiffness and additional myocardial contractility are measured. This is opposite to the alternative method of using ARF to induce SWs, as the ARF push can be timed throughout the cardiac cycle and hence is able to capture the myocardium in a relaxed state. The variations in myocardial stiffness during the cardiac cycle have been measured in several studies (Couade et al. 2011; Hollender et al. 2017). However, SWs induced by valve closure only occur at two stages of the cardiac cycle, during which the heart is not completely relaxed. Therefore, natural SWS measurements probably measure a combination of passive myocardial stiffness and contractility, potentially giving information about diastolic and systolic function, albeit that the disentangling is a challenge. Third, due to the non-linear stress-strain relation of biological materials (Mirsky and Parmley 1973), the filling state of the ventricle is still expected to influence SWS measurements, even when measured at end-diastole (Voigt 2018). Furthermore, contractility is also known to be affected by pre-load via the Frank-Starling mechanism. Therefore, besides measurement inaccuracies, hemodynamic variations are also expected to affect reproducibility.

For the application of clinical diagnosis, knowledge on measurement reproducibility is needed in order to distinguish normal and pathological myocardial function. This study tests the reproducibility of determining the propagation speed of natural SWs induced in the IVS by AVC and MVC in healthy volunteers. Previous studies have shown that propagation speeds after AVC can be determined in-vivo by using a clinical ultrasound

system using conventional or adapted Tissue Doppler Imaging (TDI) (Brekke et al. 2014; Kanai 2005; Strachinaru et al. 2017). Other studies have demonstrated the feasibility of measuring the SWs induced by AVC and MVC in a single recording using diverging waves (Petrescu et al. 2019; Santos et al. 2019; Vos et al. 2017). Slope-estimator, intra-observer, inter-observer and test-retest variabilities have been recently tested for natural SWs in healthy volunteers (Santos et al. 2019). However, we previously found that anatomical M-line location on the IVS, along which the SWs are tracked, affects the measured propagation speed in pigs, causing intra-scan variability (Keijzer et al. 2018). Furthermore, besides test-retest variabilities between measurements performed on different days, variabilities between subsequently performed measurements could have been present. In addition, Santos et al. (2018) performed SWS measurements with only one (non-clinical) echographic scanning system, while inter-system variability should be limited for clinical diagnosis. Also, hemodynamic variations could have caused variabilities in SWS measurements. When patients undergo an echocardiographic exam, they may experience different levels of psychological and/or physiological stress, potentially changing loading conditions and thus affecting SWS measurements.

To the best of our knowledge, our study is the first to simultaneously report on inter-system, test-retest, inter-scan, intra-scan and inter-observer variabilities of natural SWS measurements after AVC and MVC in healthy volunteers and to report on the effect of stress causing hemodynamic variations. To test inter-system variability, we directly compared the results obtained by using a clinical system in a conventional Tissue-Doppler-Imaging (TDI) mode (Philips) with a second clinical system with a customized high frame rate mode using a diverging-wave pulse-inversion transmission scheme (Zonare).

MATERIALS AND METHODS

Study population

The study included 10 volunteers aged 24 to 45 years, existing of 5 males and 5 females. Table 1 gives an overview of the demographic characteristics of the volunteers. The study was approved by the local medical ethics committee (Erasmus MC MEC-2014-611) and all volunteers gave informed consent. The following exclusion criteria were used; a history of cardiovascular disease, cardiovascular risk factors including hypertension (cutoff value of 140/90 mmHg), being pregnant or being morbidly obese (BMI > 40 kg/m²).

Table 1. Overview of the demographics of the study population. The characteristics are averaged over all volunteers during both scanning sessions.

Characteristic	Mean \pm standard deviation	Range
Age [years]	29.8 \pm 6.2	24 - 45
Weight [kg]	67 \pm 9.5	55 - 90
Body length [m]	1.75 \pm 0.06	1.65 - 1.83
BMI (Weight/Body length ²) [kg/m ²]	21.9 \pm 2.3	19.4 - 27.5
Heart rate in rest [bpm]	62 \pm 7	50 - 73
Systolic blood pressure in rest [mmHg]	106 \pm 13	90 - 138
Diastolic blood pressure in rest [mmHg]	62 \pm 9	50 - 81
Heart rate during handgrip test [bpm]	67 \pm 8	51 - 81
Systolic blood pressure during handgrip test [mmHg]	110 \pm 10	94 - 138
Diastolic blood pressure during handgrip test [mmHg]	67 \pm 9	52 - 85

Data acquisition

An overview of the study design and the tested variabilities are shown in Figure 1. Measurements were performed with two echographic scanning systems. First, a clinical system programmed by the manufacturer to have a high frame rate imaging mode (Zonare ZS3, P4-1C probe, Mindray Innovation Center, San Jose, California) was used. Live B-mode images with a low frame rate (LFR) were used to position the probe. Then a smaller box (approximately 5 x 7 cm) was selected within these LFR images for the high frame rate (HFR) acquisition. During these recordings the LFR images were frozen on the screen of the system and no live feedback was present. A diverging-wave pulse-inversion transmission sequence was used for the HFR acquisition, and beamformed in-phase and quadrature components (IQ-based data) with a frame rate of 1000 frames/second during 1.2 seconds were saved for offline processing. In this way, at least a full cardiac cycle was measured for a minimum heart rate of 50 bpm. The acquisitions with this machine were carried out by a sonographer (D.J.B.). Second, acquisitions were performed by a cardiologist (M.S.) with a clinical echographic scanner in conventional TDI mode (Philips iE33, S5-1 probe, Philips, Bothell, WA, USA). To obtain maximum frame rates, a balance between opening angle and depth of TDI field was searched for, as described by Strachinaru et al. (2017). In this way frame rates from 490 – 570 frames/second were realized. Simultaneously a phonocardiogram (PCG) (Fukuda Denshi MA-300HDS(V), Fukuda Denshi Co., Tokyo, Japan) was recorded and the electrocardiographic (ECG) signal was used as trigger. All data during 2 cardiac cycles were saved in DICOM format for offline processing.

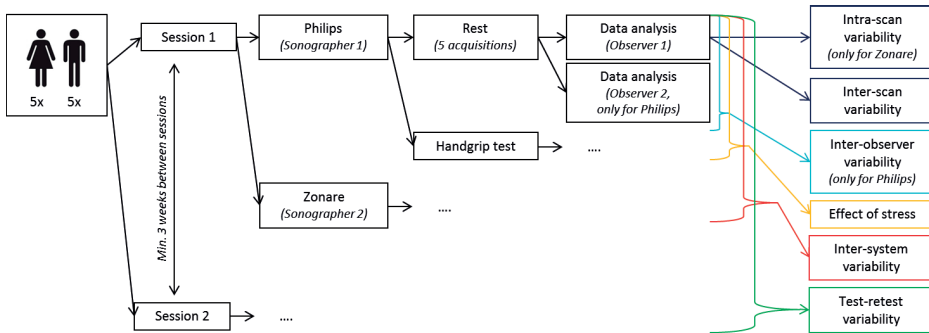


Figure 1 Schematic overview of the study design. The same measurements were performed during Session 1 and Session 2. Rest and handgrip test measurements were performed with the Zonare and the Philips system. Inter-observer variability was tested for the Philips system only, while intra-scan variability was only tested for the Zonare system.

For every volunteer, first 5 long-axis parasternal view measurements, with intermittent probe repositioning, were performed with the Zonare system. It was ascertained that both aortic and mitral valves were in the image plane. Directly after the measurements with the Zonare system, measurements were repeated with the Philips system. Subsequently, the effect of physiological stress causing hemodynamic variations on the SWS measurements was tested by performing handgrip tests. During the handgrip measurements, the volunteers were asked to keep a stress ball continuously squeezed with their left hand. While volunteers kept on squeezing, measurements were repeated with both machines. All measurements were performed within 30 minutes per volunteer. Furthermore, to investigate test-retest variability, all measurements were repeated per volunteer during a second scanning session on a separate day. The time period between the first and second session for the volunteers varied between 21 and 93 days.

Shear wave propagation speed analysis

The propagation speeds of the SWS induced by the AVC and MVC were determined by using different methods for the Zonare and Philips system. Although one method applicable to the data of both systems could be searched for, we choose to use different methods that were more suitable for the data format of the individual systems.

Clinical system with custom HFR mode

Offline IQ-based data stored from the Zonare system were analyzed in Matlab R2017a (The Mathworks, Natick, MA, USA). To remove high frequency TDI information mainly corresponding to blood and noise, a 6th order lowpass Butterworth filter with a cutoff frequency of 250 Hz was applied to the IQ data in slowtime. Axial tissue velocities were obtained by using a one-lag autocorrelation technique (Brekke et al. 2014). To reduce

the effect of speckle and noise, a Gaussian spatial smoothing filter with a size of 4 mm by 6.7° was applied to the autocorrelation frames before calculating the phase (Brekke et al. 2014; Strachinaru et al. 2017; Vos et al. 2017). The moments of AVC and MVC were visible in the B-mode images. However, since the HFR box was relatively small, the aortic valves were not visible in all recordings, while they were visible in the LFR overview images captured in the seconds before and after the HFR recordings. Therefore, the moments of valve closure in the HFR acquisitions were determined based on the movement of the mitral valves, on the overall motion of the heart and on the derived TDI movies. For each recording, an anatomical M-line was manually drawn on the basal-mid part of the IVS at the moment of valve closure, see Figure 2 A and D. Depending on the position of the IVS in the field of view and on the visible propagation length of the SWs, the length of the M-line varied between 1.9 - 4.1 cm (AVC) and 2.1 - 5.7 cm (MVC). Then, the axial particle velocities over the M-line were assembled in a motion-panel (M-panel) for a period of 75 ms around the moment of valve closure. The SWs induced by the AVC and MVC are depicted as wave patterns propagating over slowtime along the M-lines in the M-panels, see Figure 2 B and E. The slope of these patterns represents the propagation speed of these SWs. The AVC and MVC occur during the isovolumetric relaxation and isovolumetric contraction phase respectively and therefore no gross motion was assumed nor seen to be present. Nonetheless, a 6th order bandpass Butterworth filter between 15 and 100 Hz was applied to the axial tissue velocities in slowtime, since the SWs were found to be in this frequency range. Therefore, also any offset due to gross motion was removed. To obtain the propagation speeds of the SWs induced by the different valve closures, the slope of the patterns shown in the M-panels was determined by using a Radon transform (Rouze et al. 2010; Song et al. 2013; Vos et al. 2017), see Figure 2 C and F. Before applying the Radon transform, the M-panels were first resampled to have an equal number of pixels in space and time and then tapered in both directions. Furthermore, the Radon domain was normalized, as described by Vos et al. (2017). The minimum intensity, corresponding to the particle motion away from the transducer, was selected in the Radon domain to determine the propagation speed. As also reported in pig data (Keijzer et al. 2018), the location of the manually drawn M-line was found to affect the results. Therefore to test intra-scan variability, for every recording the M-lines were drawn 10 times. The location of these M-lines was chosen based on the visibility of the SW propagation. When the SW propagation was found to be less reliable on the right and left ventricle sides of the IVS, M-lines were drawn more to the middle. Data analysis of the Zonare data was done by the researcher who wrote the Matlab analysis script (L.B.H.K.). Except from determining the moments of valves closure and drawing the M-lines, the data analysis process was fully automated. Since 10 M-lines were already drawn for every recording, inter-observer variability testing was not considered meaningful for the Zonare system.

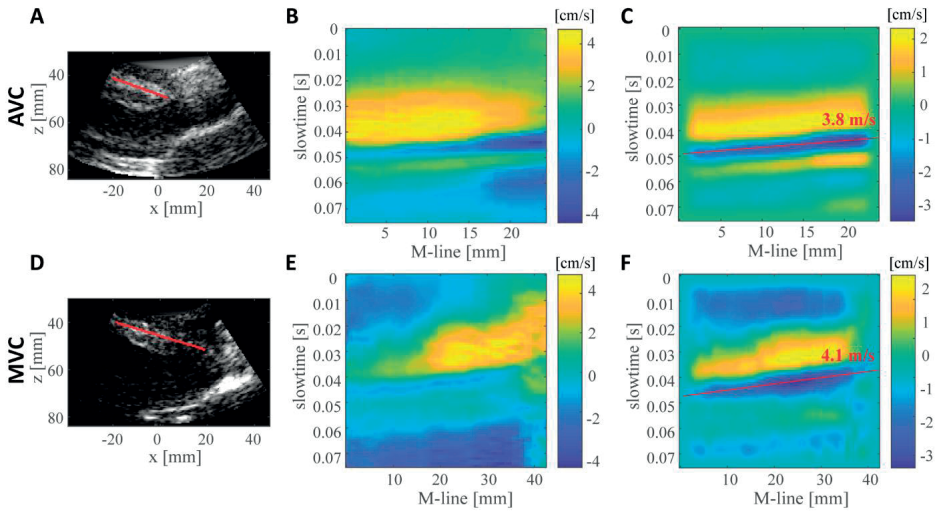


Figure 2. Zonare: Example of an M-line drawn at AVC (A) and MVC (D). The corresponding M-panels are shown in (B) and (E) respectively. After applying a BPF, a Radon transform was applied to obtain the propagation velocities as shown in (C) and (F).

For every volunteer 7 measurements were performed per session leading to 140 measurements in total. SWs after AVC and MVC were tracked in 122/140 (87%) and 92/140 (66%) measurements respectively. Main reasons to exclude recordings from the measurements were a poor B-mode quality (approx. 5% of measurements after AVC and/or MVC), or the IVS moving out of the field of view (approx. 5%). Furthermore, acquisitions with no visible propagating SWs or with propagation over only short distances (<1.8 cm) (approx. 20%) were excluded. In one of the volunteers (volunteer 8), propagating SWs after MVC could not be seen in any recording.

Clinical system with clinical HFR mode

The Philips QLab8 software program (Philips, Bothell, WA, USA) was used for post-processing of the Philips DICOM data as described before (Strachinaru et al. 2017). The method is repeated here in brief. Since the depth and width of the TDI was minimized to obtain high frame rates, valves were not visible in the measurements. Therefore, the moments of valve closure were determined based on the PCG signals (onset of S1 and S2) and the appearance of SWs in TDI, see Figure 3. Although the moment of valve closure could not visually be determined in the B-mode images, the onset of heart sounds are well known to correspond to valve closure. Furthermore, natural SWS induced by valve closure propagate from the aortic root to the apex (Strachinaru et al. 2019; Vos et al. 2017), unlike electromechanical waves starting at midlevel of the IVS and propagating towards base and apex (Provost et al. 2011). Anatomical M-lines were manually drawn

over the IVS and the length of these M-lines was defined based on the width of the TDI field of view. This length ranged between 2 and 3 cm. Subsequently, an M-panel and a mean tissue velocity curve were provided by the software, see Figure 3. By visually checking the pattern shown on the M-panel (B), the tissue velocity curve (C) and the TDI movie (A) itself, the time period needed for the SW to propagate over the M-line was determined. Since data analysis was not automated and the TDI data of the entire septum could be used as a reference by visually checking the TDI movies, the effect of M-line location was minimal. Therefore, only 1 M-line was drawn per recording. The transition from positive to negative TDI values of the SWs were tracked, since these were most visible to the observer. Since the SWs were tracked visually, inter-observer variability was considered as an important factor. Data analysis of the Philips data was done by the same researcher who analyzed the Zonare data (L.B.H.K). To test inter-observer variability, data analysis of the Philips measurements was repeated by a cardiologist experienced with the post-processing software (M.S.) blinded to earlier values.

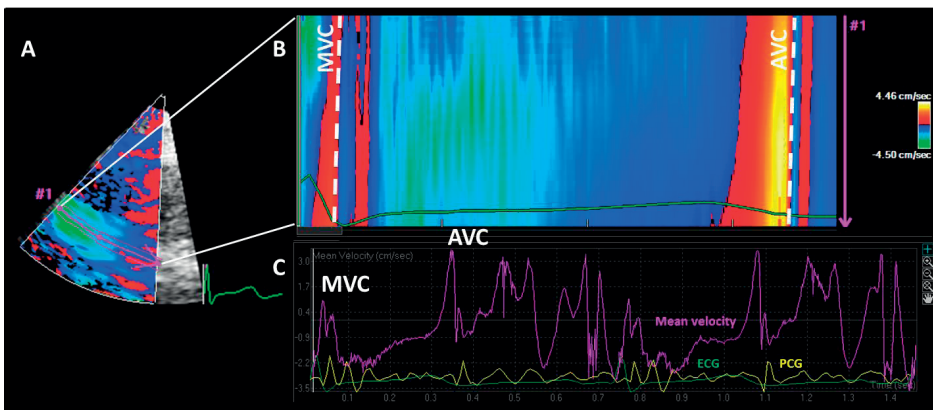


Figure 3 Philips: Example of a measurement where SWs were tracked after AVC and MVC. The Philips QLab8 software program shows the TDI movie (A), the M-panel (B) and the mean velocity curve (C).

For the Philips system, SWs could be tracked after AVC in 365/474 (77%) and after MVC in 71/474 (15%) recorded cardiac cycles. In this study we measured the SWs after AVC and MVC in single recordings. TDI limits were chosen for the visualization of the SWs after AVC, as these had our focus for the measurements. Lower TDI limits might have been chosen when focusing on the SWs induced by MVC, as these have lower magnitudes. Therefore, the transition from positive to negative TDI values after MVC was not visible in many DICOM images and we obtained a low feasibility for the MVC measurements compared to MVC data with this method (Strachinaru et al. 2019). Furthermore, values above 10 m/s were removed since they were assumed to be non-physical, as was done by Vos et al. (2017).

Statistics

Statistical analysis was done by using a statistical toolbox in Matlab R2017a (The Mathworks, Natick, MA, USA). Kolmogorov-Smirnov tests were used to test for normal distributions. Propagation speeds are presented as median values and inter-quartile ranges (IQR). To compare our results with literature values, also mean and standard deviations were reported. We noticed that some volunteers were nervous when entering the scanning room. To test whether all measurements in rest could be grouped, the first and last of five rest measurements were compared. A Wilcoxon signed-rank test was applied to the median values per recording for the Zonare data and to the individual values per heart cycle for the Philips data. Also a Bland-Altman analysis was used to depict differences (mean differences, limits of agreement (LOA) and range). A similar analysis was done to test the effect of the handgrip test and the test-retest and inter-system variability. For the Zonare data, intra-scan variability was investigated by computing the median of all IQRs of the values obtained per measurement for the 10 M-lines of all rest and stress measurements. The median value of the IQRs of the median recording values was used to measure inter-scan variability.

RESULTS

Hemodynamic characteristics

Average blood pressures of 106 ± 13 mmHg (systolic) and 62 ± 9 mmHg (diastolic) were measured in rest, while average pressures of 110 ± 10 mmHg and 67 ± 9 mmHg were measured during the handgrip test. The diastolic blood pressure was statistically significantly different during the handgrip test ($p=0.0088$) while the systolic blood pressure was not ($p=0.077$). Also the heart rate, measured with the ECG connected to the Philips system, was found to increase significantly ($p<0.01$) from 62 ± 7 bpm to 67 ± 8 bpm.

Clinical system with custom HFR mode

Figure 4 shows the results obtained for the 10 volunteers for the AVC and MVC respectively. The median values in rest ranged from 3.23 to 4.25 m/s for AVC and from 2.06 to 4.72 m/s for MVC. These median values were not normally distribution. Furthermore, we cannot assume that all volunteers have the same SW propagation speeds. Nevertheless, for comparison with other studies, the mean and standard deviations of these median values were computed to be 3.8 ± 0.4 m/s (AVC) and 3.4 ± 1.0 m/s (MVC). Table 2 gives an overview of the statistical characteristics of all measurements. For every measurement, 10 M-lines were drawn over the IVS. The IQRs per measurement shown in Figure 4 thus represent the intra-scan variabilities. For the AVC measurements in rest, a median value of 0.38 m/s (IQR: 0.26 – 0.68 m/s) was found for all IQRs, for the MVC measurements

in rest this was found to be 0.26 m/s (IQR: 0.15 – 0.46 m/s). The variations in median values per recording per volunteer were used as measure for the inter-scan variability. The median IQRs of median values in rest per volunteer per session were found to be 0.67 m/s (IQR: 0.40 – 0.86 m/s) for the AVC and 0.61 m/s (IQR: 0.26 – 0.94 m/s) for the MVC. To test whether all rest measurements could be grouped despite a possible time-dependency during the period of the exam, the medians obtained for the first and last rest measurement per volunteer for both sessions were compared (Figure 5 A and D).

Table 2 Overview of the statistical characteristics of the Zonare and Philips data. P-values denoted with an asterisk(*) correspond to a statistically significant difference ($p < 0.05$). LOA: limits of agreement Bland-Altman analysis (± 1.96 SD).

Type of variability	Performed test	Zonare		Philips
		AVC	MVC	AVC
Intra-scan	Median of all IQRs of the values obtained per measurement for the 10 M-lines	0.38 m/s, n=136 (IQR: 0.26 – 0.68m/s)	0.26 m/s, n=99 (IQR: 0.15 – 0.46 m/s)	-
Inter-scan	Wilcoxon signed-rank test on medians of first and last rest measurement per volunteer per session	p=0.90, n=19	p=0.53, n=16	p=0.15, n=20
	Bland-Altman: medians of first – medians of last rest measurement per volunteer per session	Mean: -0.0017 m/s, n=19 (LOA: -1.22 – 1.23 m/s) (Range: -1.06 – 0.96 m/s)	Mean: -0.10 m/s, n=16 (LOA: -1.85 – 1.64 m/s) (Range: -1.56 – 2.36 m/s)	Mean: -0.36 m/s, n= 20 (LOA: -2.29 – 1.58 m/s) (Range: -2.63 – 1.06 m/s)
Inter-scan	Median of all IQRs of (median) rest values per volunteer per session	0.67 m/s, n=19 (IQR: 0.40 – 0.86 m/s)	0.61 m/s, n=16, (IQR: 0.26 – 0.94 m/s)	0.71 m/s, n=19 (IQR: 0.33 – 1.07 m/s)
Test-retest	Wilcoxon signed-rank test on medians of all rest measurements per volunteer for Session 1 and Session 2	p=0.13, n=10	p=0.047*, n=7	p=0.28, n=10
	Bland-Altman: medians of all rest measurements per volunteer for Session 1- for Session 2	Mean: -0.51 m/s, n=10 (LOA: -2.05 – 1.02 m/s) (Range: -1.81 – 0.45 m/s)	Mean: 0.37 m/s, n=7 (LOA: -0.35 – 1.08 m/s) (Range: -0.034 – 1.04 m/s)	Mean: -0.19 m/s, n=10 (LOA: -1.59 – 1.21 m/s) (Range: -1.44 – 1.19 m/s)
Inter-volunteer	Range of median rest values per volunteer	3.23 – 4.25 m/s, n=10	2.06 – 4.72 m/s, n=9	1.82 – 4.76 m/s, n=10
Handgrip test	Wilcoxon signed-rank test on medians of all rest and all handgrip test measurements per volunteer per session	p=0.073 , n=20	p=0.56, n=15	p=0.079, n=19

Table 2 Overview of the statistical characteristics of the Zonare and Philips data. P-values denoted with an asterisk(*) correspond to a statistically significant difference ($p < 0.05$). LOA: limits of agreement Bland-Altman analysis (± 1.96 SD). (continued)

Type of variability	Performed test	Zonare		Philips
		AVC	MVC	AVC
	Bland-Altman: medians of all rest – medians of all handgrip test measurements per volunteer per session	Mean: -0.33 m/s, n=20 (LOA: -1.94 – 1.27 m/s) (Range: -3.07 – 0.74 m/s)	Mean: -0.0723m/s, n=15 (LOA: -1.82 – 1.68 m/s) (Range: -2.22 – 0.93 m/s)	Mean: -0.39 m/s, n=19 (LOA: -2.22 – 1.44 m/s) (Range: -2.38 – 1.49 m/s)
Inter-observer	Wilcoxon signed-rank test on medians of rest measurement per volunteer per session analyzed by Observer 1 and Observer 2	-	-	p=0.35, n= 20
	Bland-Altman: medians of all rest measurements per volunteer per session for Observer 1 – for Observer 2	-	-	Mean: 0.11 m/s, n=20 (LOA: -1.42 – 1.65 m/s) (Range: -1.55 – 1.21 m/s)
Inter-system	Wilcoxon signed-rank test on median rest values per volunteer per echographic scanner			p=0.044*, n=20
	Bland-Altman on median rest values per volunteer per echographic scanner bias + limits of agreement			Mean -0.43 m/s, n=20 (LOA: -2.23 – 1.37 m/s) (Range: -1.95 – 1.08 m/s)
AVC vs MVC	Median ratio of median rest values per volunteer per session for AVC and MVC			Zonare 1.20, n=16 (IQR: 1.00 – 1.58)
	Median difference of median rest values per volunteer per session for AVC and MVC			0.64 m/s, n=16 (IQR: -0.019 – 1.50 m/s)

Average differences of -0.0017 m/s (LOA: -1.22 – 1.03 m/s) (AVC) and -0.10 m/s (LOA: -1.85 – 1.64 m/s) (MVC) were found with a Bland-Altman analysis. No statistically significant differences were found ($p=0.90$ for AVC and $p=0.53$ for MVC). Therefore, we grouped all rest measurement per volunteer per session to compute the test-retest variability, see Figure 5. Mean differences of -0.51 m/s (LOA: -2.05 – 1.02 m/s) (AVC) and 0.37 m/s (LOA: -0.35 – 1.08 m/s) (MVC) were found for the test-retest variability of all measurements, (Figure 5 B and E).

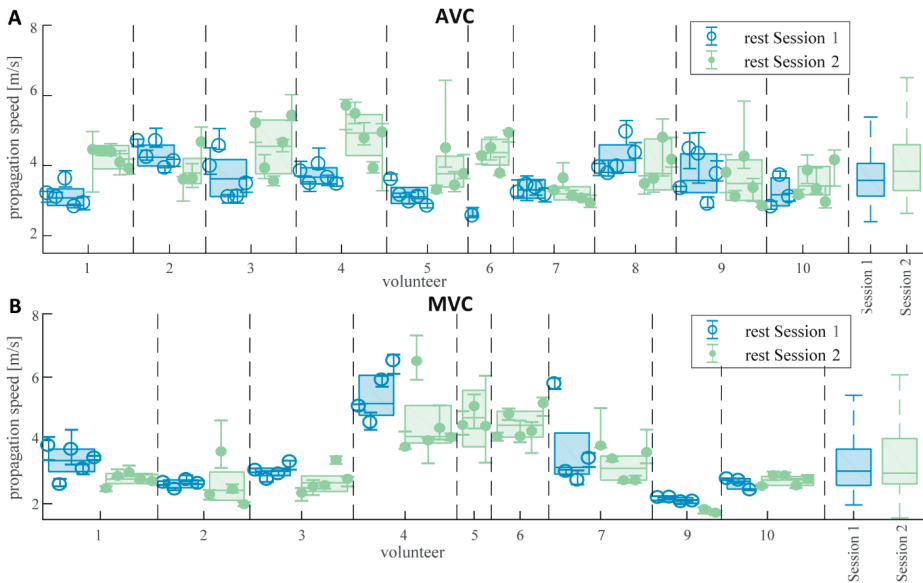


Figure 4 Zonare: Median values and IQRs of the measurements in rest performed for the AVC (A) and the MVC (B). For every recording, 10 M-lines were drawn over the IVS. The IQRs depict the intra-scan variabilities. Inter-scan variabilities (median values and IQRs) per volunteer for every session are depicted in box-plots. Inter-scan variabilities were found to be slightly higher than, but in similar ranges as, intra-scan variabilities.

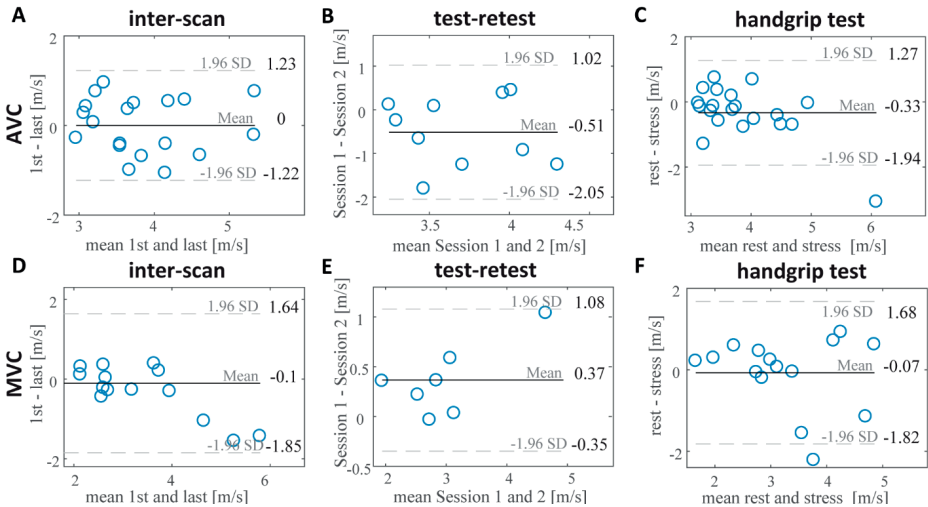


Figure 5 Zonare: Bland-Altman analysis of the inter-scan variability, the test-retest variability and the effect of the handgrip test for the AVC (A, B and C) and MVC (D, E and F). No significant differences were found between the first and last rest measurement per volunteer per session. Test-retest differences were found to be just significant for the MVC, but not for the AVC. No significant effect was found for the handgrip test.

These differences were found to be just significant for the MVC ($p=0.047$) but not for the AVC ($p=0.13$). We grouped both sessions before computing the inter-volunteer variability. The median values of the rest measurements per volunteer were found to be in the ranges of 3.23 - 4.25 m/s and 2.06 - 4.72 m/s for the AVC and MVC respectively. Subsequently, rest and handgrip measurements are compared (Figure 5 C and F). Average differences of -0.33 m/s (LOA: -1.94 - 1.27 m/s) for the AVC measurements and -0.072 m/s (LOA: -1.82 - 1.68 m/s) for the MVC measurements were found. These differences were not found to be significant ($p=0.073$ for AVC and $p=0.56$ for MVC), see Figure 6.

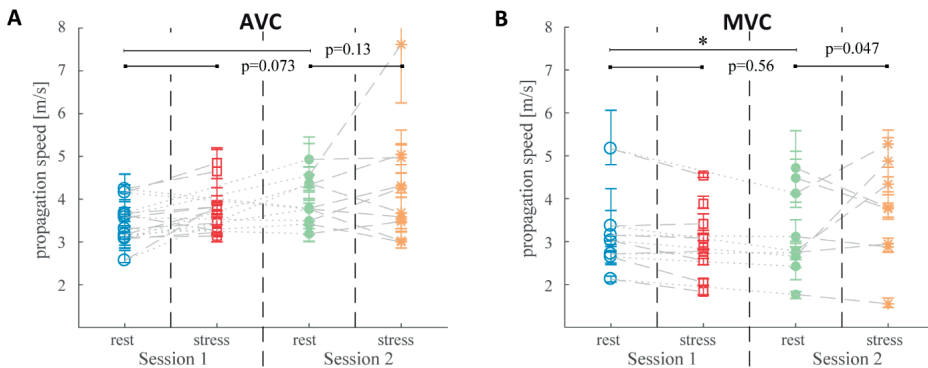


Figure 6 Zonare: Comparison of the median values and IQRs of the rest and stress measurements of Session 1 and Session 2 per volunteer for AVC (A) and MVC (B). Test-retest differences were found to be just significant for the MVC, but not for the AVC. No significant effect was found for the handgrip test (rest vs stress).

Clinical system with clinical HFR mode

The propagation speeds obtained from the Philips data are shown in Figure 7. Since the feasibility of the MVC measurements was low, no statistical tests were performed on these few MVC measurements. Therefore only the statistics of the AVC measurements are described in this paragraph. The median values in rest ranged from 1.82 to 4.76 m/s, see Table 2. As done for the Zonare, mean and standard deviation was computed for illustrative purposes (3.2 ± 0.9 m/s). A median value of the IQRs of the propagation speed values in rest per session per volunteer of 0.71 m/s (IQR: 0.33 - 1.07 m/s) was found, representing the inter-scan variability. It should be noted that these values seem to be higher than the inter-scan variability values of the Zonare data, where first median values over the 10 M-lines per scan were obtained before computing inter-scan variability. As for the Zonare data, no statistically significant difference was found between the first and last rest measurement per volunteer per session ($p=0.15$).

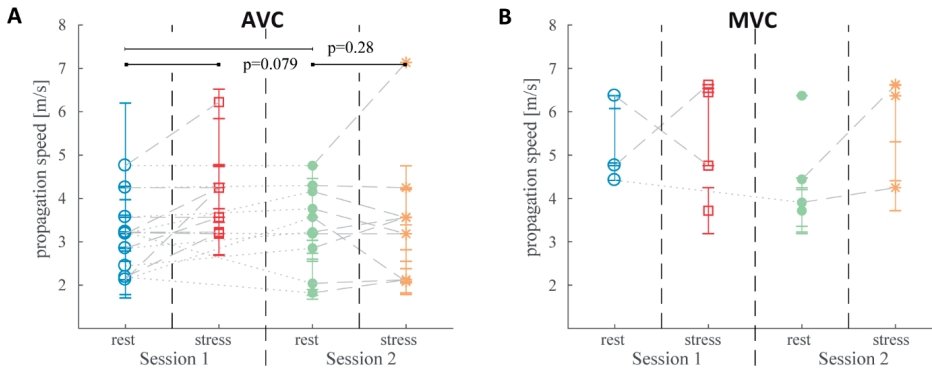


Figure 7 Philips: Comparison of the median values and IQRs of the rest and stress measurements of Session 1 and Session 2 per volunteer for AVC (A) and MVC (B). No statistical tests were performed on the MVC measurements because of a low feasibility. For the AVC measurements, no significant effects were found for test-retest and the handgrip test.

A Bland-Altman analysis showed a mean difference between the first and last rest measurement of -0.36 m/s (LOA: $-2.29 - 1.58$ m/s) (Figure 8 A). Therefore, all rest measurements were grouped for measuring the test-retest variability. A mean difference of -0.19 m/s (LOA of $-1.59 - 1.21$ m/s) was found, which was not statistically significant ($p=0.28$) (Figure 8 B). Therefore, as for the Zonare data, the measurements in Session 1 and Session 2 were grouped to obtain inter-volunteer variability ranges. The median rest values per volunteer were found to be in the range of $1.82 - 4.76$ m/s. Also similar to the Zonare data, the difference between rest and stress measurements was not found to be significant ($p=0.079$). A mean differences of -0.39 m/s (LOA: $-2.22 - 1.44$ m/s) was found.

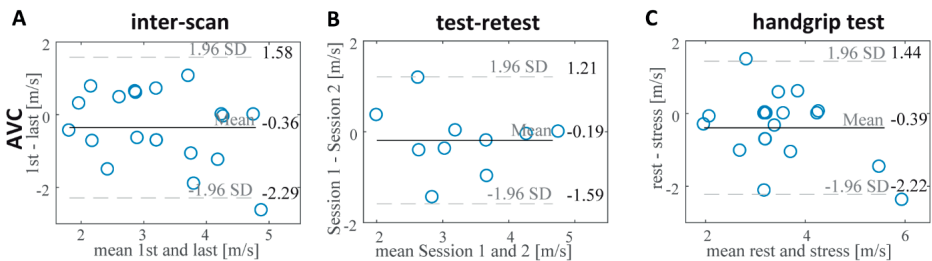


Figure 8 Philips: Bland-Altman analysis of the inter-scan variability (A), the test-retest variability (B) and the effect of the handgrip test (C) of the AVC measurements. No statistical tests were performed on the MVC measurements because of a low feasibility. For the AVC measurements, the first and last rest measurement per volunteer per session were not found to be statistically significantly different. Also no significant effect was found for the handgrip test.

Intra-scan variability was not tested for the Philips data, since only 1 M-line curve and thus 1 propagation speed value was obtained per heart cycle with the Philips system.

Instead of intra-scan variability, inter-observer variability was measured for the Philips data. The second observer computed propagation speeds per volunteer per session averaged over 3 heart cycles. These propagation speeds were compared with the median rest values obtained by the first observer. An average difference of 0.11 m/s (LOA: -1.42 – 1.65 m/s) was found (Figure 9), which was not found to be significant ($p=0.35$). The feasibility of the MVC measurements was higher for the second than for the first observer. While the first observer obtained propagation speeds in 7 sessions, the second observer obtained values for 14 sessions. Nonetheless, for consistency, also no statistical tests were performed on the MVC measurements analyzed by the second observer.

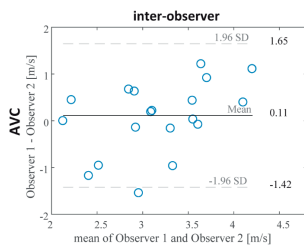


Figure 9 Philips: Bland-Altman analysis of the inter-observer variability for the AVC measurements per session. No statistically significant effect was found.

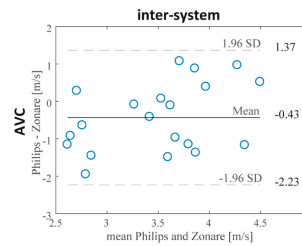


Figure 10 Zonare and Philips: Bland-Altman analysis of the inter-system variability for the AVC measurements per session. Statistically different propagation speeds were obtained with the different systems.

Comparison of the systems

Due to the low feasibility of the MVC measurements with the current settings on the Philips system, only the AVC measurements of the Zonare and the Philips system were compared. The difference in results obtained with the Zonare and the Philips system was found to be statistically significant ($p=0.044$). The Bland-Altman analysis shows a median bias of -0.43 m/s (LOA: -2.23 – 1.37 m/s), indicating that we consistently measured a lower propagation speed with the Philips system (Figure 10).

As suggested by others (Santos et al. 2019; Vos et al. 2017), the difference and ratio of the propagation speeds obtained for the AVC and MVC might be of clinical relevance due to hemodynamics. Due to the low feasibility of the MVC measurements with the Philips system, these ratios and differences were only computed for the Zonare system (Figure 11). The median ratio and difference were found to be 1.20 (IQR: 1.00 – 1.58) and 0.64 m/s (IQR: -0.019 – 1.50 m/s) respectively.

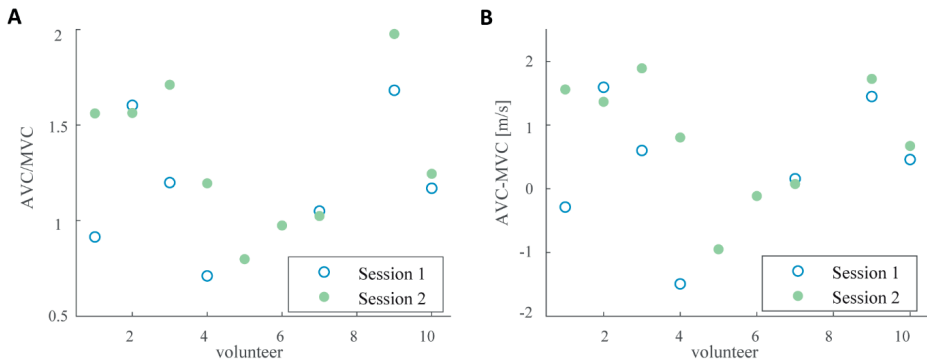


Figure 11 Zonare: Ratio (A) and difference (B) between propagation speeds obtained after AVC and after MVC for all volunteers. Due to the low feasibility of the MVC measurements with the Philips system, only the ratio's and differences for the Zonare system are shown.

DISCUSSION

In this study, we tested the reproducibility of the propagation speeds of natural SWs induced by the aortic valve closure (AVC) and mitral valve closure (MVC) in 10 healthy volunteers. For the AVC measurements, no statistically different propagation speeds were obtained on different days. Our results suggest that the variabilities of natural shear wave speed (SWS) measurements are dominated by measurement inaccuracies rather than mild hemodynamic variations. Statistically, different propagation speeds after AVC were obtained for two different systems.

Measurement variations can have physiological causes or can arise due to measurement inaccuracies. Intra-scan variability is measured within individual recordings, and, therefore, physiological causes are assumed to be non-existing. Inter-scan variabilities can also occur because of physiological variations, and these variations are expected to be even larger when comparing different sessions. We found inter-scan variabilities (Zonare: 0.67 m/s (IQR: 0.40 – 0.86 m/s) for AVC and 0.61 m/s (IQR: 0.26 – 0.94 m/s) for MVC) to be slightly higher than, but in similar ranges as, intra-scan variabilities (Zonare: 0.38 m/s (IQR: 0.26 – 0.68 m/s) for AVC and 0.26 m/s (IQR: 0.15 – 0.46 m/s) for MVC). Moreover, test-retest variabilities were found to also be in similar ranges as inter-scan variabilities (Figure 5 and 8). Therefore, our results suggest that the measurement variations were dominated by several measurement inaccuracies, which are expected to have different causes. First of all, we found qualitatively that contrast in the B-mode images affected the results. For recordings with a low visible contrast between tissue and blood, we experienced that positioning the M-lines on the IVS was more challenging. This was especially important for the Zonare system, where a diverging-wave transmission

scheme was used and therefore B-mode contrast was sometimes limited due to clutter. Furthermore, clutter could have affected the determination of tissue velocities. Second, the SWs could only be tracked over the limited visible length of about 3 cm of the IVS. A SW with a center frequency of, for example, 50 Hz (Santos et al. 2019) and a propagation speed of 3.5 m/s, has a wavelength of 7.0 cm. This means that only a fraction of this wavelength can be tracked, which causes measurement inaccuracy, increasing with propagation speed.

In a uniform shear wave phantom with ARF-push induced shear waves, Strachinaru et al. (2017a) obtained similar propagation speeds with a research scanner as with the clinical Philips system. However, for the AVC measurements, we obtained statistically different propagation speeds with the Philips system compared to the Zonare system. As the measurements with the different systems were performed within half an hour per session, the differences are expected to be mainly due to the differences in data processing for the different systems. First of all, for the Zonare measurements, a Radon transform was used to track the maximum negative particle velocities, while for the Philips measurements, the onset of the wave, as visible from positive to negative tissue velocities, was tracked. This means that slightly different aspects of the SW pattern were tracked. We previously found in measurements in an animal model different propagation speeds as well when tracking different rims of the SWs (Keijzer et al. 2018). Second, while a frame rate of 1000 Hz was used for the Zonare, frame rates varied between 490 – 570 Hz for the Philips system and therefore the time resolution differed by a factor of two. This is expected to induce more uncertainties and thus more variability (Strachinaru et al. 2017), as observed in our study, see Figure 5 and Figure 6. Third, the SWs were tracked automatically with the Radon transform for the Zonare system, while for the Philips system visual feedback obtained from the M-panel, the tissue velocity curve and the TDI movie was used to determine the propagation speeds. Therefore, when comparing different studies, these methodological aspects described should also be taken into account. Furthermore, the effect of using different systems and methods should be studied also for pathological hearts in more detail.

Advantage of using the Radon transform for the Zonare system is that data analysis can be more automated. To minimize the effect of noise, as described in the method section, we applied a lowpass filter to the IQ data in slowtime. Furthermore, a Gaussian spatial smoothing filter was applied to the autocorrelation frames. In addition, for every measurement 10 M-lines were drawn over the IVS. Moreover, we interpolated the M-panels to a panel with an equal number of pixels in space and time. We also normalized the Radon domain by dividing by the Radon transform of a panel with an equal number of pixels with only unit values, to avoid an apparent bias (Vos et al. 2017). To further reduce

the effect of noise, the performance of using a least-square or high resolution Radon transform (Thorson and Claerbout 1985) could be investigated in the future.

The potential hemodynamic variation due to psychological stress related to the examination was estimated by comparing the first and last rest measurement within a session. No significant differences were found. This indicates that when patients are nervous at the beginning of a scanning session, this does not strongly affect these measurements, which is beneficial for the application of clinical diagnosis. Nonetheless, it should be noted that the number of measurements in this study was limited and thus not enough statistical power might be present to detect small differences. Therefore to investigate the effect of larger variations in hemodynamics, a handgrip test was performed during the SWS measurements. This test is not only relevant for the different levels of physiological stress patients may experience, but also since diastolic dysfunction patients might show normal hemodynamic characteristics in rest, but have abnormal LV diastolic pressures during exercise (Nagueh et al. 2016). Although heartrate did increase significantly during the handgrip test, the propagation speeds obtained during rest and the handgrip test were not found to be statistically different. It should be noted that for AVC we found p-values only slightly above $p=0.05$ ($p=0.073$ and $p=0.079$ for Zonare and Philips respectively). Possibly, the statistical power could be too limited to measure significant differences. For the AVC, we did find a mean increase in propagation speed during stress of 0.33 m/s and 0.39 m/s with the Zonare and Philips system respectively (Figure 5 and 8). Nonetheless, the differences between the measurements in rest and during the handgrip test are in the same range as the inter-scan variabilities (Figure 5 and 8). This suggests that no extra variabilities are induced because of the handgrip test. However, only low levels of stress causing small hemodynamic changes are induced by handgrip tests. While higher levels of stress could be induced by using an exercise test, performing HFR acquisitions would be more challenging. Whether the measurement of the natural SWS induced by AVC and MVC is completely independent of loading conditions should be further investigated in a study with higher statistical power.

Several studies have reported on the propagation speed of SWS in healthy volunteers, as summarized in Table 3. Some studies used a long-axis parasternal view, while Brekke et al. (2014) used a 4-chamber apical view. However, the exact effect of the imaging view on the measured propagation speed is currently unclear. The propagation speeds obtained in this study for the SWS after AVC are in the same range as the values measured in other human studies. Some studies used ARF to induce SWS during diastole in healthy volunteers. However, these values cannot be directly compared with the values obtained after closure of the valves, since the timing of the measurements is different. MVC and AVC occur around the onset of contraction and relaxation respectively (Remme et al. 2008).

Previous studies showed stiffness variation over the cardiac cycle in animals (Couade et al. 2011; Pernot et al. 2011; Vejdani-jahromi et al. 2015) and human (Hollender et al. 2017; Tzschätzsch et al. 2012). Couade et al. (2011) reported on an increase in shear modulus from about 5 kPa to 15 kPa in the first 50 ms after the R peak in sheep, which corresponds to an increase in propagation speed of about 70%. With the Zonare system, we found in general higher values after MVC than ARF-based studies at diastole.

Table 3 Overview of human shear wave elastography measurements described in literature. The following abbreviations are used in the table: HCM: hypertrophic cardiomyopathy, PLAX: parasternal long-axis view, PSAX: parasternal short-axis view, AP4C: apical 4-chamber view, LVFW: left ventricular free wall, IVS: inter-ventricular septum.

<i>Natural SWS</i>				
Study	View	Subject	MVC	AVC
Kanai, (2005)	PLAX, IVS	Healthy volunteer	-	1 – 7 m/s (10-90 Hz)
Brekke et al., (2014)	AP4C, IVS	Healthy volunteers	-	5.41 ± 1.28 m/s
Santos et al., (2018)	PLAX, IVS	Healthy volunteers	3.2 ± 0.6 m/s (2.1 – 4.4 m/s)	3.5 ± 0.6 m/s (2.2 – 4.5 m/s)
Petrescu et al., (2019)	PLAX, IVS	Healthy volunteers	3.54 ± 0.93 m/s	3.75 ± 0.76 m/s
		Cardiac amyloidosis	6.33 ± 1.63 m/s	5.63 ± 1/13 m/s
Strachinaru et al., (2019)	PLAX, IVS	Healthy volunteers	4.65 ± 0.77 m/s (3.25 – 6.50 m/s)	3.61 ± 0.46 m/s (3.10 – 4.66 m/s)
		HCM patients	6.88 ± 1.22 m/s (5.45 – 8.91 m/s)	5.13 ± 0.68 m/s (3.75 – 6.94 m/s)
Keijzer et al., current study	PLAX, IVS	Healthy volunteers	Zonare 3.4 ± 1.0 m/s (2.06 – 4.72 m/s) -	Zonare 3.8 ± 0.4 m/s (3.23 – 4.25 m/s) Philips 3.2 ± 0.9 (1.82 – 4.76 m/s)
<i>ARF based SWS</i>				
Study	View	Subject	End-diastole	End-systole
Song et al.,(2016)	LAPV and PSAX, LVFW and IVS	Healthy volunteers	1.29 – 1.96 m/s	-
Villemain et al., (2018)	PLAX and PSAX, IVS	Healthy volunteers	2.1 ± 1.30* m/s	-
		HCM Patients	3.56 ± 1.71* m/s	-

* Speed values c obtained by converting elasticity values E , using $E = \rho c^2$ with a tissue density ρ of 1000 kg/m³.

Several authors suggested that the difference and ratio of the propagation speeds obtained after AVC and MVC are potentially more clinically relevant due to hemodynamics (Santos et al. 2019; Vos et al. 2017). We found a median difference of 0.60 m/s (IQR: -0.31 – 1.25 m/s) and a mean ratio of 1.21 (IQR: 0.93 – 1.46) with the Zonare system. However, these values have relatively high variability, likely caused by the combined variability of both the AVC and MVC measurements, which may reduce relevance for clinical diagnosis. Nonetheless, Santos et al. (2018) found a mean difference of 0.4 ± 0.6 m/s and mean ratio

of 1.1 ± 0.2 , which is close to the values we obtained. Also Petrescu et al. (2019) found higher mean propagation speeds for AVC than for MVC (3.48 ± 0.70 m/s vs 3.07 ± 0.51 m/s) for healthy volunteers aged 20-39 years. However, for older age groups, no statistical difference was found between the propagation speeds after AVC and MVC (Petrescu et al. 2019). In contrast, Strachinaru et al. (2019) found higher propagation speeds for MVC than for AVC (4.68 ± 0.66 m/s vs 3.51 ± 0.38 m/s) in healthy volunteers. What exact clinically relevant information can be obtained from natural SWS measurements should be further investigated.

Both systems have their own advantages and disadvantages to be used for clinical diagnosis with SWS. Translation of using the clinical Philips system and its clinical data analysis package to daily clinical practice takes less time, which is a major advantage. However, the Zonare system saves IQ data instead of DICOM data, giving the possibility to apply different tracking and filter methods and to automate data analysis. Furthermore, with the Zonare system a two times higher frame rate is obtained, theoretically corresponding to lower measurement variabilities. The higher feasibility of measuring the SWs after MVC and AVC for the Zonare system is another important advantage. In addition, the inter-volunteer range was found to be smaller or similar, depending on the observer, for the Zonare compared to the Philips system. However, ECG and PCG could not yet be measured with the Zonare system in HFR mode. This practically means that the moment of valve closure had to be determined visually and that measurements could not be linked to a heartrate, as only one heartbeat was recorded per movie. However, we expect that ECG and PCG could be implemented in the HFR mode of the Zonare system in the future. Image quality was higher with the Philips system, and TDI data was directly shown on the Philips system. This made it easier to perform a direct quality check of the recording than with the Zonare system. However, when performing the measurements with the Philips system, separate recordings should be made for the AVC and MVC measurements as the TDI velocity scale needs optimization for either measurement. Strachinaru et al. (2019) showed much higher feasibilities for the MVC measurements (89% of 45 healthy volunteers) by using the same system but by performing separate recordings for measuring the SWs after AVC and MVC. For the Zonare system, AVC and MVC measurements can be performed simultaneously. As such, in this stage of developments, both systems can be used as a research bridge to further clinical translation of the technique.

For clinical diagnostic application, it is important to be able to show significant differences between healthy volunteers and a patient at risk with a certain confidence. Our study suggests that measurement variabilities are dominated by measurement inaccuracies. Therefore, by averaging over multiple heartbeats, the standard error is expected

to be minimized. The variabilities presented in this study can be used to estimate the minimum amount of measurements needed for clinical diagnosis, once the minimal difference in propagation speed between a patient at risk and a healthy subject are suitably investigated. Considering that data processing is done offline and that measurements can be performed subsequently, we estimate that recording up to 10 heart beats for averaging is feasible with respect to time and effort.

The ultimate goal is to measure the increased stiffness of the myocardium. However, in this study, we only reported on linear propagation speeds. Since the typical wavelength of the SWs measured (about 7 cm) is large compared to the thickness of the IVS (about 1 cm), guided waves instead of bulk shear waves are expected. Guided waves show dispersion even for purely elastic media, and, thus, measured propagation speeds cannot be directly converted to shear moduli. However, the resolution in 2-D Fourier domain was restricted due to the limited visible propagation length of the SWs, to measure dispersive effects. Xu et al. (2018) proposed a dispersive Radon transform. However, prior knowledge on the theoretical dispersion curves of the induced modes is needed. Since the IVS is a complex structure with respect to geometry and fiber orientation, we expect that the dispersion curves of Lamb waves in plate structures are too simplistic. As such, the relation between geometry of the myocardium, propagation speed and early diagnosis of cardiac dysfunction should be further investigated.

CONCLUSIONS

This study investigated the reproducibility of the measurement of propagation speeds of shear waves naturally induced by aortic and mitral valve closure (AVC and MVC) in healthy volunteers. Propagation speeds of 3.23 – 4.25 m/s (AVC) and 2.06 – 4.72 m/s (MVC) were obtained. Inter-scan variabilities were slightly higher than intra-scan variabilities. For the AVC measurements, no different propagation speeds were obtained after test-retest ($p=0.13$). However, significantly different values were obtained with a second clinical system (1.82 – 4.76 m/s for AVC), potentially caused by differences in measurement methods. For this second system, inter-observer variability was tested and no statistical differences were found. Based on the results of this study, measurement inaccuracies are expected to dominate measurement variations among healthy volunteers. Thus, by averaging over multiple heartbeats precision for the application of clinical diagnosis can potentially be improved.

REFERENCES

- Arani A, Arunachalam SP, Chang ICY, Baffour F, Rossman PJ, Glaser KJ, Trzasko JD, Mcgee KP, Manduca A, Grogan M, Dispenzieri A, Ehman RL, Araoz PA. Cardiac MR Elastography for Quantitative Assessment of Elevated Myocardial Stiffness in Cardiac Amyloidosis. *J Magn Reson Imaging* 2017a;46:1361–1367.
- Arani A, Glaser KL, Arunachalam SP, Rossman PJ, Lake DS, Trzasko JD, Manduca A, McGee KP, Ehman RL, Araoz PA. In Vivo, High-Frequency Three-Dimensional Cardiac MR Elastography: Feasibility in Normal Volunteers. *Magn Reson Med* 2017b;77:351–360.
- Bouchard RR, Hsu SJ, Wolf PD, Trahey GE. In Vivo Cardiac, Acoustic-Radiation-Force-Driven, Shear Wave Velocimetry. *Ultrason Imaging* 2009;31:201–213.
- Brekke B, Nilsen LCL, Lund J, Torp H, Bjastad T, Amundsen BH, Stoylen A, Aase SA. Ultra-High Frame Rate Tissue Doppler Imaging. *Ultrasound Med Biol* 2014;40:222–231.
- Couade M, Pernot M, Messas E, Bel A, Ba M, Hagege A, Fink M, Tanter M. In Vivo Quantitative Mapping of Myocardial Stiffening and Transmural Anisotropy During the Cardiac Cycle. *IEEE Trans Med Imaging* 2011;30:295–305.
- Hollender P, Kakkad V, Trahey G. Calibration of ARFI displacements using diastolic shear wave speeds for estimating systolic elasticity. *IEEE Int Ultrason Symp* 2017.
- Hollender PJ, Wolf PD, Goswami R, Trahey GE. Intracardiac Echocardiography Measurement of Dynamic Myocardial Stiffness with Shear Wave Velocimetry. *Ultrasound Med Biol* 2012;38:1271–1283.
- Kanai H. Propagation of Spontaneously Actuated Pulsive Vibration in Human Heart Wall and In Vivo Viscoelasticity Estimation. *IEEE Trans Ultrason Ferroelectr Freq Control* 2005;52:1931–1942.
- Keijzer LBH, Bosch JG, Verweij MD, de Jong N, Vos HJ. Intra-Scan Variability of Natural Shear Wave Measurements. *IEEE Int Ultrason Symp* 2018.
- Lang RM, Badano LP, Victor MA, Afilalo J, Armstrong A, Ernande L, Flachskampf FA, Foster E, Goldstein SA, Kuznetsova T, Lancellotti P, Muraru D, Picard MH, Retzschel ER, Rudski L, Spencer KT, Tsang W, Voigt JU. Recommendations for cardiac chamber quantification by echocardiography in adults: An update from the American Society of Echocardiography and the European Association of Cardiovascular Imaging. *Eur Hear J - Cardiovasc Imaging* 2015;16:233–371.
- Nagueh SF, Smiseth OA, Appleton CP, Byrd BF, Dokainish H, Edvardsen T, Flachskampf FA, Gillebert TC, Klein AL, Lancellotti P, Marino P, Oh JK, Popescu BA, Waggoner AD. Recommendations for the Evaluation of Left Ventricular Diastolic Function by Echocardiography: An Update from the American Society of Echocardiography and the European Association of Cardiovascular Imaging. *J Am Soc Echocardiogr Elsevier Inc*, 2016;29:277–314.
- Pernot M, Couade M, Mateo P, Crozatier B, Fischmeister R, Tanter M. Real-Time Assessment of Myocardial Contractility Using Shear Wave Imaging. *J Am Coll Cardiol* 2011;58:65–72.
- Pernot M, Fujikura K, Fung-Kee-Fung SD, Konofagou EE. ECG-gated, Mechanical and Electromechanical Wave Imaging of Cardiovascular Tissues In Vivo. *Ultrasound Med Biol* 2007;33:1075–1085.
- Pernot M, Lee WN, Bel A, Mateo P, Couade M, Tanter M, Crozatier B, Messas E. Shear Wave Imaging of Passive Diastolic Myocardial Stiffness: Stunned Versus Infarcted Myocardium. *JACC Cardiovasc Imaging* 2016;9:1023–1030.

- Petrescu A, Santos P, Orłowska M, Pedrosa J, Bézy S, Chakraborty B, Cvijic M, Dobrovie M, Delforge M, D'hooge J, Voigt J-U. Velocities of Naturally Occurring Myocardial Shear Waves Increase With Age and in Cardiac Amyloidosis. *JACC Cardiovasc Imaging* 2019;in press.
- Pislaru C, Pellikka PA, Pislaru S V. Wave propagation of myocardial stretch: correlation with myocardial stiffness. *Basic Res Cardiol* 2014a;109.
- Pislaru C, Urban MW, Pislaru S V., Kinnick RR, Greenleaf JF. Viscoelastic properties of normal and infarcted myocardium measured by a multifrequency shear wave method: comparison with pressure-segment length method. *Ultrasound Med Biol* 2014b;40:1785–1795.
- Ponikowski P, Voors AA, Anker SD, Bueno H, Cleland JGF, Coats AJS, Falk V, González-Juanatey JR, Harjola V-P, Jankowska EA, Jessup M, Linde C, Nihoyannopoulos P, Parissis JT, Pieske B, Riley JP, Rosano GMC, Ruilope LM, Ruschitzka F, Rutten FH, van der Meer P. 2016 ESC Guidelines for the diagnosis and treatment of acute and chronic heart failure. *Eur Heart J* 2016;2129–2200.
- Provost J, Lee W-N, Fujikura K, Konofagou EE. Imaging the electromechanical activity of the heart in vivo. *Proc Natl Acad Sci* 2011;108:8565–8570.
- Remme EW, Lyseggen E, Helle-Valle T, Opdahl A, Pettersen E, Vartdal T, Ragnarsson A, Ljosland M, Ihlen H, Edvardsen T, Smiseth OA. Mechanisms of preejection and postejection velocity spikes in left ventricular myocardium: interaction between wall deformation and valve events. *Circulation* 2008;118:373–380.
- Rouze NC, Wang MH, Palmeri ML, Nightingale KR. Robust Estimation of Time-of-Flight Shear Wave Speed Using a Radon Sum Transformation. *IEEE Trans Ultrason Freq Control* 2010;57:21–24.
- Santos P, Petrescu A, Pedrosa J, Orłowska M, Komini V, Voigt J-U, D'hooge J. Natural shear wave imaging in the human heart: normal values, feasibility and reproducibility. *IEEE Trans Ultrason Ferroelectr Freq Control* 2019;66:442–452.
- Song P, Bi X, Mellema DC, Manduca A, Urban MW, Greenleaf JF, Chen S. Quantitative Assessment of Left Ventricular Diastolic Stiffness Using Cardiac Shear Wave Elastography. *J Ultrasound Med* 2016;35:1419–1427.
- Song P, Zhao H, Urban MW, Manduca A, Pislaru S V, Kinnick RR, Pislaru C, Greenleaf JF, Chen S. Improved Shear Wave Motion Detection Using Pulse-Inversion Harmonic Imaging With a Phased Array Transducer. *IEEE Trans Med Imaging* 2013;32:2299–2310.
- Strachinaru M, Bosch JG, van Dalen BM, van Gils L, van der Steen AFW, de Jong N, Geleijnse ML, Vos HJ. Cardiac Shear Wave Elastography Using a Clinical Ultrasound System. *Ultrasound Med Biol* 2017;43:1596–1606.
- Strachinaru M, Bosch JG, van Gils L, van Dalen BM, Schinkel AFL, van der Steen AFW, de Jong N, Michels M, Vos HJ, Geleijnse ML. Naturally Occurring Shear Waves in Healthy Volunteers and Hypertrophic Cardiomyopathy Patients. *Ultrasound Med Biol* 2019;45:1977–1986.
- Thorson JR, Claerbout JF. Velocity-stack and slant-stack stochastic inversion. *Geophysics* 1985;50:2727–2741.
- Tzschätzsch H, Elgeti T, Rettig K, Kargel C, Klaua R, Schultz M, Braun J, Sack I. In vivo time harmonic elastography of the human heart. *Ultrasound Med Biol* 2012;38:214–222.
- Urban MW, Pislaru C, Nenadic IZ, Kinnick RR, James F. Measurement of viscoelastic properties of in vivo swine myocardium using Lamb Wave Dispersion Ultrasound Vibrometry (LDUV). *IEEE Trans Med Imaging* 2013;32:247–261.

- Vejdani-jahromi M, Nagle M, Trahey GE, Wolf PD. Ultrasound Shear Wave Elasticity Imaging Quantifies Coronary Perfusion Pressure Effect on Cardiac Compliance. *IEEE Trans Med Imaging* 2015;34:465–473.
- Villemain O, Correia M, Mousseaux E, Baranger J, Zarka S, Podetti I, Soulat G, Damy T, Hagège A, Tanter M, Pernot M, Messas E. Myocardial Stiffness Evaluation Using Noninvasive Shear Wave Imaging in Healthy and Hypertrophic Cardiomyopathic Adults. *JACC Cardiovasc Imaging* 2019;12:1135–1145.
- Voigt JU. Direct Stiffness Measurements by Echocardiography. Does the Search for the Holy Grail Come to an End? *JACC Cardiovasc Imaging* 2019;12:1146–1148.
- Vos HJ, van Dalen BM, Heinonen I, Bosch JG, Sorop O, Duncker DJ, van der Steen AFW, de Jong N. Cardiac Shear Wave Velocity Detection in the Porcine Heart. *Ultrasound Med Biol* 2017;43:753–764.
- Wassenaar PA, Eleswarpu CN, Schroeder SA, Mo X, Raterman BD, White RD, Kolipaka A. Measuring Age-Dependent Myocardial Stiffness across the Cardiac Cycle using MR Elastography: A Reproducibility Study. *Magn Reson Med* 2016;75:1586–1593.
- Xu K, Laugier P, Minonzio J-G. Dispersive Radon transform. *J Acoust Soc Am* 2018;143:2729–2743.

10

Naturally occurring shear waves in healthy volunteers and hypertrophic cardiomyopathy patients

Based on:

Strachinaru M, Bosch JG, van Gils L, van Dalen BM, Schinkel AFL, van der Steen AFW, de Jong N, Michels M, Vos HJ, Geleijnse ML. *Naturally occurring shear waves in healthy volunteers and hypertrophic cardiomyopathy patients*. *Ultrasound Med Biol*. 2019.

ABSTRACT

We apply a high frame rate (over 500 Hz) tissue Doppler method to measure the propagation velocity of naturally-occurring shear waves (SW) generated by aortic and mitral valves closure. The aim of this work is to demonstrate clinical relevance. We included 45 healthy volunteers, and 43 patients with hypertrophic cardiomyopathy (HCM). The mitral SW (4.68 ± 0.66 m/s) was consistently faster than the aortic (3.51 ± 0.38 m/s) in all volunteers ($p < 0.0001$). In HCM patients SW velocity correlated with E/e' ratio ($r = 0.346$, $p = 0.04$ for aortic SW and $r = 0.667$, $p = 0.04$ for mitral). A subgroup of 20 volunteers were matched for age and gender to 20 HCM patients. In HCM the mean velocity of 5.1 ± 0.7 m/s for the aortic SW (3.61 ± 0.46 m/s in matched volunteers, $p < 0.0001$) and 6.88 ± 1.12 m/s for the mitral SW (4.65 ± 0.77 m/s in matched volunteers, $p < 0.0001$). A threshold of 4 m/s for the aortic SW correctly classified pathological myocardium with a sensitivity of 95% and specificity of 90%. Naturally occurring SW can be used to assess differences between normal and pathological myocardium.

INTRODUCTION

The prevalence of heart failure is approximately 1–2% of the adult population in developed countries, rising to $\geq 10\%$ among people >70 years of age (Ponikowski *et al* 2016). Heart failure with preserved ejection fraction represents around 50%, but its diagnosis remains challenging. Demonstration of cardiac functional and structural alterations is key to the diagnosis. However, no validated non-invasive gold standard exists for measuring the precise degree of myocardial stiffness (Nagueh *et al* 2016).

Stiffness can be estimated *in vivo* by measuring the propagation velocity of externally induced shear waves travelling through a tissue (Shiina *et al* 2015), the general principle being that shear waves travel faster in stiffer materials. This *shear wave elastography* can be performed by magnetic resonance or ultrasound imaging. The main present-day applications are liver fibrosis and breast, thyroid, prostate, kidney and lymph node imaging (Shiina *et al* 2015; Parker *et al* 2011). Several research groups have used external sources to induce shear waves in the myocardium (Bouchard *et al* 2009; Pernot *et al* 2011; Hollender *et al* 2012; Song *et al* 2013; Urban *et al* 2013; Vejdani-Jahromi *et al* 2016), demonstrating that diastolic myocardial stiffness can be determined using ultrasonic shear wave imaging (Villemain *et al* 2017, 2018). It has been found that shear-like waves also naturally occur in the myocardium after valve closure (Kanai 2009; Brekke *et al* 2014), caused by the impulse of the snapping valve on the mitral and aortic annuli which propagates within the cardiac wall. We have recently shown that these waves can be measured with an ultrasound system in regular clinical mode by using high-frame-rate Tissue Doppler Imaging (TDI) (Strachinaru *et al* 2017).

In this work, we study naturally-occurring shear waves in normal volunteers and hypertrophic cardiomyopathy (HCM) patients, as a pathological model of increased muscle stiffness and diastolic dysfunction (Villemain *et al* 2017, 2018; Elliott *et al* 2014; Lu *et al* 2018; Finocchiaro *et al* 2018). The aim was to demonstrate the feasibility in a clinical setting and investigate the potential application of the method for discriminating normal from pathological myocardium.

METHODS

Study population

This prospective study was conducted in 2016–2017 according to the principles of the Declaration of Helsinki and approved by the Institutional Medical Ethical Committee (MEC-2014-611, MEC-2017-209). Written informed consent was obtained from every participant.

-*Healthy volunteers* aged 18 to 62 years. Subjects were excluded if one or more of the following criteria were present: a history of cardiovascular disease, systemic disease, the finding of cardiac abnormalities during the examination (including QRS duration over 100ms), cardiovascular risk factors including hypertension (cutoff value 140/90 mmHg), diabetes mellitus or hypercholesterolemia, having breast implants or being pregnant. Professional athletes or morbidly obese ($BMI >40\text{kg/m}^2$) were excluded.

-*Hypertrophic cardiomyopathy patients* recruited from the HCM outpatient clinic. Subjects were included if they had a definitive diagnosis of hypertrophic cardiomyopathy (Elliott *et al* 2014), regardless of the localization of the most hypertrophic segments (for example, apical forms were not excluded). Exclusion criteria were: associated known coronary artery disease, more than mild valve disease (systolic anterior movement of the mitral valve was not considered as exclusion criterion), prior septal reduction (either surgical or interventional).

Echocardiography

All echocardiographic studies were performed by one experienced sonographer (MS). Normal complete echocardiographic studies were performed, including 2D, Doppler and pulsed-wave TDI of the mitral annulus. The peak velocity of the early diastolic mitral inflow was measured (E wave), as well as the peak early diastolic tissue velocity of the medial mitral annulus in apical four-chambers view (e' wave). Their ratio (E/e') was then calculated as an index of the early diastolic properties of the left ventricle. Tissue velocities of the LV myocardium were sampled in Color Tissue Doppler (color TDI) in standard parasternal long axis view (PLAX) using a Philips iE33 system (Philips Medical, Best, The Netherlands) equipped with a S5-1 transducer. As previously described (Strachinaru *et al* 2017), we used a clinical color TDI application with a frame rate over 500 Hz, acquiring five separate recordings for each subject, timed to the ECG in order to obtain two heart beats per recording. The probe was lifted off the chest between recordings and repositioned in order to optimize the image. Typically, the TDI sector had an opening angle of 40° , which at a depth of 6 cm leads to a 4 cm sector width. The 2-D line density was set to minimum, leading to TDI frame rates over 500 Hz (range 500 to 590 Hz). The TDI movies were stored in DICOM format for offline analysis.

The DICOM TDI loops were processed using Qlab 9 (Philips Medical, Best, The Netherlands), see Figure 1 and Movie 1. A shear wave in the color TDI data is detected on the septal wall as a rapid up-and-down tissue displacement, visible in the form of a color shift (red to blue or blue to red depending on the direction). This pattern initiates at the exact visible moment of valve closure which also corresponds to the onset of the heart

sounds in the phonocardiography signal, and then propagates over the septal wall away from the valve towards the apex.

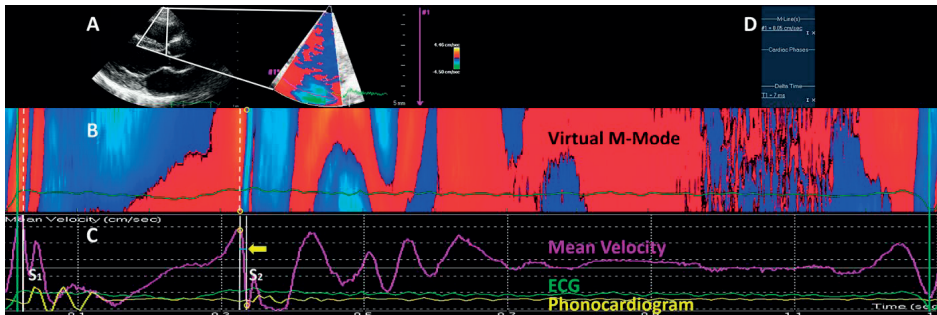


Figure 1. Detailed view (modified to indicate the main elements) of the data obtained in the study subjects by using offline processing in Philips Qlab. A: classical parasternal long axis and the focused TDI window over the interventricular septum. The M-Mode line is traced mid-wall, pointing towards the shear wave source; B: virtual M-mode map of a full heart cycle (reconstructed offline), at 513Hz, demonstrating the shear waves after mitral and aortic valve closure. The onset of the waves is marked with dotted lines; C: mean tissue velocity curve as a function of time (averaged over the M-mode line, this velocity should not be mistaken with the shear wave propagation velocity), synchronous to the ECG (green) and PCG (yellow). The onset of both shear waves is synchronous to the onset of the respective heart sounds (S1, S2). By clicking on the base and the top of the wave front's slope in the color M-mode map (small circles), the program highlights the corresponding points on the mean velocity time curve. The time interval in which the wave occurs is marked with the solid white lines (arrow); D: results panel, showing the time interval.

A curved virtual M-mode line was traced along the center of the LV wall (Figure 1A). Its length and direction were pre-defined by the user. No axial range gate was used. The shear wave source is expected to be at the valvular annulus, as demonstrated in Movie 2. Previous literature also mentions that the waves start at the annulus and progresses to the apex (Kanai 2009; Brekke et al 2014). For consistency, the arrow of the M-mode line always pointed towards the shear wave source, perpendicular to the wave front. The software provides a virtual M-Mode map (Figure 1B), allowing us to manually trace the leading slope of the propagating wave, as previously described (Strachinaru *et al* 2017).

The propagation velocity of the wave front was estimated through

$$V_s = D/T, \quad (1)$$

where D is the (user-defined) length of the M-mode line and T is the time the wave travels along the M-mode line. The propagation velocity was averaged over 3 heartbeats for every subject. The 3 cycles were freely selected by each observer from the 10 available cycles per subject per exam as the heartbeats where the best visualization of the shear waves could be obtained.

The very short isovolumic times are complex to analyze (Goetz *et al* 2005; Golde and Burstin 1970). In order to identify the exact times of valve closure and discriminate shear waves from other events, the acquisitions included a synchronous phonocardiography signal (PCG), by using a Fukuda Denshi MA-300HDS(V) phonocardiography microphone. Also, the timing of valve closure from the underlying 2D data was confirmed by direct visual correlation and anatomic M-mode, using a general post-processing platform (Tomtec Imaging System 4.6, Unterschleissheim, Germany).

Statistical analysis

Distribution of data was checked by using histograms and Shapiro-Wilk tests. Continuous variables were represented as mean±standard deviation (SD). Categorical data are presented as absolute number and percentages. For comparison of normally distributed continuous variables we used the dependent or independent means t-test when appropriate. In case of a skewed distribution of continuous variables, the Mann-Whitney-U test was applied. For comparison of frequencies the Chi-square test or Fisher's exact test was used. Correlations were computed using Pearson's method. Matching of the patients and control groups was done after inclusion, using a propensity score method, with 1:1 nearest neighbor matching according to age and gender.

The relationship between individual variables was estimated using univariate linear regression. Parameters found to be significant or considered relevant based on theoretical assumptions were entered into a multivariate model. Receiver operating characteristic (ROC) analysis was applied in order to evaluate the discriminating power of the method.

Intra-observer variability was evaluated on 11 randomly-chosen subjects, on the initial recordings with a new measurement set performed by M.S. two months later, blinded to the first result. Inter-observer variability was estimated on the same recordings, between the result of M.S. and the results obtained by a first-time user, with limited prior knowledge of the software application (L.G.), also in a blinded manner. Inter-acquisition variability was evaluated on a different randomly-chosen group of 13 study subjects, between the initial recordings and a new ultrasound recording set three months later, blinded to the first result. In all variability measurements the velocity was averaged over 3 heartbeats for every subject, the reader being allowed to select the best heart cycle from a recording for each measurement. Variability was estimated by using the Bland-Altman method (Bland and Altman 1986).

Every statistical analysis was performed using the Statistical Package for Social Sciences version 21 (IBM SPSS Statistics for Windows, Armonk, New York, USA). Testing was done two-sided and considered significant if the p value was smaller than 0.05.

RESULTS

Shear wave behaviour in healthy volunteers

Forty-five healthy volunteers, 64% males, mean age 34 ± 13 underwent a high frame rate ultrasound study (mean TDI frame rate= 516 ± 13 Hz, range 500 to 590 Hz). Shear waves were visible and quantifiable in the interventricular septum in parasternal long axis (PLAX) view (Figure 1, Movie 1) after mitral valve closure in 40 volunteers (89%) and after aortic valve closure in 42 (93%). These waves were synchronous to onset of the heart sounds on the PCG and could clearly be linked to the valvular events (Movie 2, Movie 3).

In PLAX the mean velocity of the mitral valve shear wave was 4.68 ± 0.66 m/s, range 3.25 to 6.50 m/s, with a maximal horizontal length of the TDI region of interest of 3 to 3.5 cm. The mean aortic shear wave velocity was 3.51 ± 0.38 m/s, range 3.00 to 4.66 m/s. The mitral shear wave was consistently faster than the aortic in all individual subjects ($p<0.0001$).

Male and female volunteers had mitral shear wave velocity values of 4.65 ± 0.62 m/s and 4.72 ± 0.76 m/s ($p=0.73$) respectively. The aortic shear wave velocity was 3.43 ± 0.32 m/s in males and 3.67 ± 0.45 m/s ($p=0.05$) in females. There was no correlation between the age of the subjects and the aortic shear wave velocity ($R^2=0.005$, $p=0.67$) or the mitral shear wave ($R^2=0.006$, $p=0.64$). Also, no correlation existed with systolic blood pressure ($R^2=0.002$, $p=0.93$ for the mitral shear wave and $R^2=0.008$, $p=0.59$ for the aortic shear wave velocity), diastolic blood pressure ($R^2=0.002$, $p=0.79$ for the mitral shear wave and $R^2=0.02$, $p=0.41$ for the aortic), e' ($R^2=0.11$, $p=0.27$ for the aortic shear wave and $R^2=0.04$, $p=0.51$ for the mitral) and E/e' ratio ($R^2=0.14$, $p=0.21$ for the aortic and $R^2=0.01$, $p=0.9$ for the mitral).

Hypertrophic cardiomyopathy patients

Forty-three HCM patients were also screened and investigated with high frame rate TDI (frame rate of 519 ± 18 Hz, range 500 to 558 Hz). Their mean age was 51 ± 12 , 70% males. Shear waves were visible and quantifiable in the interventricular septum in parasternal long axis (PLAX) view (Figure 2) after mitral valve closure in 24 patients (56%) and after aortic valve closure in 38 (88%).

The mitral shear wave had a mean velocity of 6.7 ± 1.3 m/s. No correlation was found between the mitral shear wave velocity and age ($R^2=0.04$, $p=0.53$), systolic blood pressure ($R^2=0.04$, $p=0.57$), diastolic blood pressure ($R^2=0.01$, $p=0.89$) and e' ($R^2=0.09$, $p=0.37$). The aortic shear wave mean velocity was 5.2 ± 0.8 m/s. No correlation was found for the aortic shear wave with age ($R^2=0.02$, $p=0.45$), systolic blood pressure ($R^2=0.03$, $p=0.32$), diastolic blood pressure ($R^2=0.01$, $p=0.48$) and e' ($R^2=0.07$, $p=0.12$).

The E/e' ratio was significantly correlated with the aortic shear wave velocity ($r=0.346$, $R^2=0.119$, $p=0.04$) and mitral shear wave velocity ($r=0.667$, $R^2=0.444$, $p=0.04$).

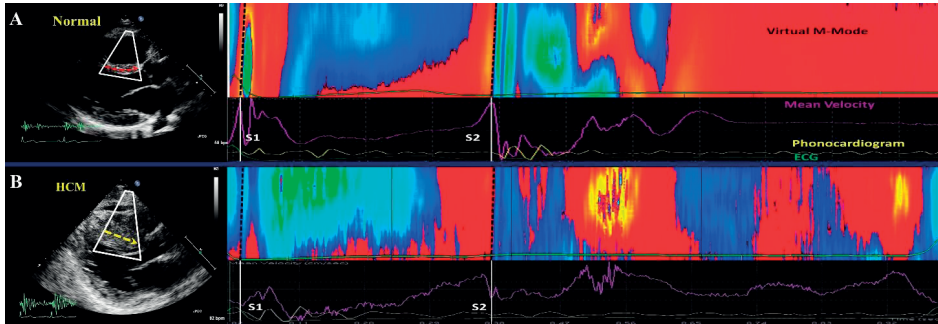


Figure 2. Shear wave comparison in a normal volunteer and a HCM patient. A: A M-mode line was traced in the middle of the IVS, resulting in a color M-mode map. Heart sounds are marked with S1 and S2. The slope of the mitral shear wave (synchronous to S1) and of the aortic shear wave (synchronous to S2) are marked with dotted lines. B: the same diagram, in the case of a HCM patient. In order to compare the slopes of the respective shear waves, the width of the two M-mode maps was adjusted until the respective heart sounds were perfectly aligned (as if the two subjects had the same heart rate).

Factors influencing the shear wave velocity in the two study groups (unmatched)

Given the very good feasibility of the aortic shear wave detection in both groups, the clinical and echocardiographic parameters were compared to the aortic shear wave velocity by univariate and multivariate regression in each separate group. In normal volunteers (Table 1) male gender was the only significant parameter influencing the aortic shear wave velocity, both in univariate and multivariate regression.

In HCM patients, male gender and E/e' ratio were found to significantly influence the aortic shear wave velocity in univariate analysis. In the multivariate model, the only parameter significantly influencing the aortic shear wave velocity was the E/e' ratio.

Matching for comparative analysis

Matching the two groups for age and gender resulted in a group of 20 normal volunteers and 20 HCM patients. The matched subjects' baseline characteristics and echocardiographic results are shown in Table 2.

There were significant differences in BMI, diastolic blood pressure, septal thickness, e' and E/e' ratio between the baseline features of these groups. The velocity of the aortic shear wave (Figure 2, Figure 3) was significantly higher in the HCM group (mean value= 5.13 ± 0.68 m/s, range 3.75 to 6.94 m/s) as compared to the normal (3.61 ± 0.45

m/s, range 3.10 to 4.66 m/s, $p<0.0001$). Mitral shear wave velocity was also significantly higher in HCM (6.88 ± 1.12 m/s, range 5.45 to 8.91 m/s) than in the normal group (Figure 2, Figure 3), (4.65 ± 0.77 , range 3.25 to 6.50 m/s, $p<0.0001$).

Table 1. Parameters influencing the aortic shear wave velocity in normal volunteers and HCM patients, in univariate and multivariate regression analysis

	Normal Volunteers n=45				HCM patients n=43			
	Univariate		Multivariate		Univariate		Multivariate	
	B	P	B	P	B	P	B	P
Male gender	-0.240	0.05	-0.524	0.01	0.538	0.05	0.509	0.06
Age	0.002	0.67			0.008	0.45		
BMI	-0.026	0.16			-0.023	0.38		
Systolic blood pressure	0.003	0.59			-0.007	0.32		
Diastolic blood pressure	0.008	0.41			-0.008	0.48		
Septal thickness	0.012	0.77	0.110	0.12	0.05	0.08	0.026	0.4
e'	-0.044	0.27			-0.108	0.12		
E/e'	0.075	0.21	0.009	0.87	0.42	0.04	0.039	0.045

Significant p values (<0.05) are highlighted in bold

BMI=Body mass index; HCM: Hypertrophic cardiomyopathy

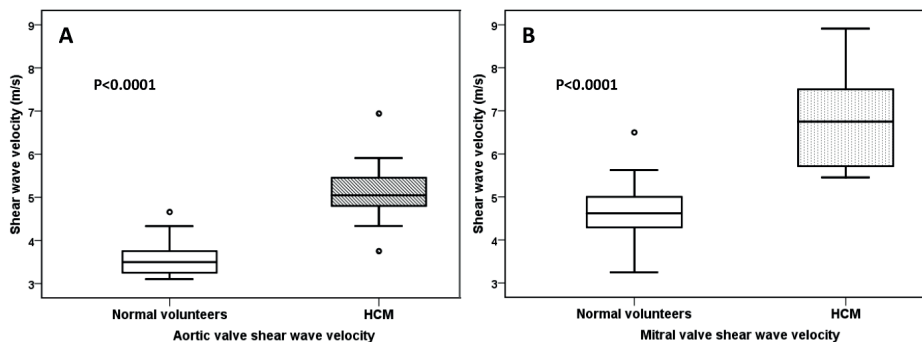


Figure 3. Velocity values for the aortic shear wave (A) and mitral shear wave (B) in normal volunteers and HCM patients. The shear waves are significantly faster in HCM, with no significant overlap of the velocity ranges.

ROC analysis for detecting the pathological myocardium (HCM) by the aortic shear wave velocity showed an area under the curve of 0.98, with a sensitivity of 95% and specificity of 90% for a cut-off value of 4 m/s (Figure 4). The septal thickness used as reference had an area under the curve of 0.95. Figure 4 illustrates subjects' classification according to the two thresholds (septal thickness >15 mm and aortic shear wave velocity >4 m/s). Note that two patients had normal septal thickness and apical hypertrophy, and two others were diagnosed through family screening (in which maximum wall thickness threshold=13mm for diagnosis of HCM)¹⁵.

Table 2. Comparison between matched normal individuals and HCM patients, ordered into demographics, echocardiographic parameters, and study results, respectively.

Parameter	Normal volunteers N=20	HCM patients N=20	P
Age (yrs)	45±13	48±13	0.47
Male gender (%)	60	70	0.51
Height (m)	176±10	176±9	0.96
Weight (kg)	76±15	84±16	0.09
BMI	24±4	27±4	0.04
Systolic blood pressure (mmHg)	119±15	131±24	0.06
Diastolic blood pressure (mmHg)	71±8	80±11	0.01
Septal thickness (mm)	9±1	17±5	<0.0001
Septal e' (cm/s)	8.3±1	5.5±2	<0.0001
Septal E/e'	8±1	17±9	<0.0001
Frame rate parasternal (s ⁻¹)	511±27	511±20	0.98
Aortic shear wave velocity parasternal (m/s)	3.61±0.45	5.13±0.68	<0.0001
Mitral shear wave velocity parasternal (m/s)	4.65±0.77	6.88±1.12	<0.0001

Significant p values (<0.05) are highlighted in bold

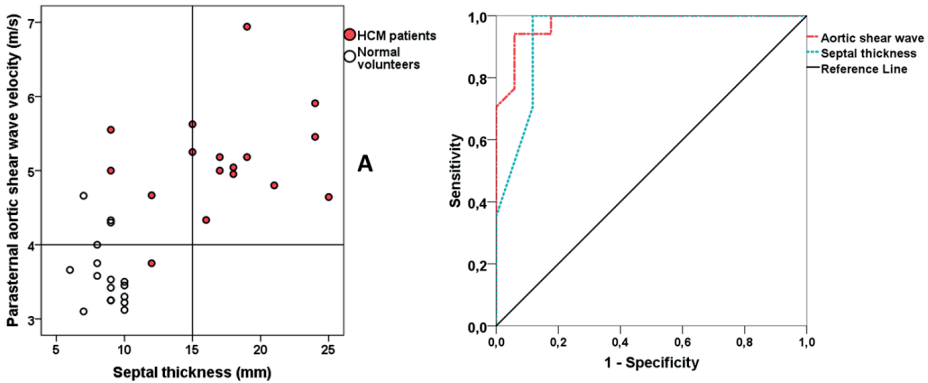


Figure 4. A: Study subjects classified according to the septal thickness (X axis, vertical line at the 15mm threshold) and aortic shear wave velocity (Y axis, horizontal line at the threshold value of 4 m/s determined by ROC analysis). Note that HCM patients with normal or intermediate septal thickness were correctly classified by the 4 m/s threshold; B: Receiver operating characteristic (ROC) curves for detecting normal versus abnormal myocardium by the septal thickness versus the aortic shear wave velocity.

Variability

For intra-observer variability (No=11 readings of parasternal aortic valve shear wave), the first reading displayed a mean velocity of 3.74 ± 0.59 m/s. At the second reading, the mean value was 3.72 ± 1.04 m/s (p=0.86). The mean difference was 0.03 ± 0.52 m/s. The limits of agreement(LOA) were -0.99 to +1.05 m/s (Figure 5A).

For the inter-observer variability (Figure 5B), the mean value of the shear wave velocity obtained by the second observer was 3.51 ± 1.21 m/s ($p=0.29$). The mean difference between observers was -0.23 ± 0.69 m/s (LOA= -1.12 to $+1.59$ m/s).

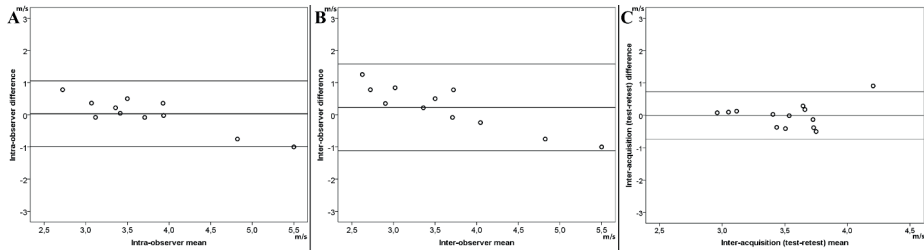


Figure 5. Variability of the shear wave velocity measurement, illustrated by Bland-Altman plots. The central horizontal line represents the mean difference, external lines the limits of agreement. A: intra-observer variability; B: inter-observer variability; C: test-retest (inter-acquisition) variability.

Test-retest (inter-acquisition) variability was estimated on a group of 13 volunteers (Figure 5C). The velocity of the parasternal aortic valve shear wave velocity was 3.51 ± 0.42 on the first recording, and the second imaging recording taken three months later had a velocity of 3.52 ± 0.35 ($p=0.95$). The mean difference was -0.006 ± 0.37 m/s (LOA= -0.74 to $+0.73$ m/s).

DISCUSSION

This prospective study shows that 1) assessment of naturally occurring shear wave velocities is feasible in both normal volunteers and patients, using a high frame rate TDI application available on a clinical echocardiography scanner in regular clinical mode; 2) The velocity of these shear waves is significantly higher in pathological myocardium (HCM patients); 3) the velocity of these waves correlates with the E/e' ratio in HCM patients.

In several studies the detection of these fast phenomena in the heart has been described (Pernot *et al* 2011; Hollender *et al* 2012; Song *et al* 2013; Urban *et al* 2013; Vejdani-Jahromi *et al* 2017; Villemain *et al* 2017, 2018; Brekke *et al* 2014; Kanai *et al* 2000; Kanai 2005, 2009; Couade *et al* 2011; Pislaru *et al* 2017), using experimental systems or modified software. We have already demonstrated that by tuning the relationship between the depth of the image, the 2D line density, sector width and the TDI field of view sufficient time resolution can be achieved, allowing visualization of the shear waves with a conventional clinical scanner (Strachinaru *et al* 2017).

The LV isovolumetric periods are very short (30 to 100ms). However, several mechanical, electrical and hemodynamic events take place during this time (Goetz *et al* 2005; Golde and Burstin 1970; Konofagou and Provost 2012; Costet *et al* 2014). In subjects with normal atrio-ventricular and intraventricular conduction the first component of the two heart sounds is the valvular component: mitral (for the first heart sound) and aortic (for the second heart sound) respectively (Leatham 1954), and thus synchronous with the onset of the fast shear waves generated by the closure of the same valves (Remme 2008). Propagation delay for the PCG tracings is negligible due to the difference in velocity (1540 m/s for sound waves *versus* 1 to 10 m/s for shear waves). In order to clearly delineate the shear waves from other phenomena, the TDI recordings were timed on the PCG. For both aortic and mitral shear waves, the origin and propagation could be documented and linked to the valvular events by using synchronized TDI, 2D, M-mode and PCG tracings (Movies 2-3).

The shear wave is associated with particle vibration with a main component perpendicular to the direction of propagation. In the parasternal position, this main component is parallel to the direction of the ultrasound beam. Therefore, as already demonstrated (Strachinaru *et al* 2017), a TDI system would be most sensitive for shear waves traveling through the interventricular septal wall in a *parasternal* view, rather than in an *apical* view. A slight angulation in the parasternal position between the particle vibration and the ultrasound beam will reduce the apparent amplitude of the shear wave. However, unlike conventional TDI where the magnitude of the axial TDI velocity is measured, it will not affect the apparent lateral propagation velocity of the wave pattern, which is the primary outcome of our measurement.

On the other hand, a misalignment between the 2D imaging plane and the source of the waves can lead to overestimation in the propagation velocity estimation. A classical PLAX lies strictly perpendicular to the mitral annulus and cuts through the middle of the aortic annulus, reducing this risk of misalignment. Also, an angulation of the M-mode line with respect to the true central line of the septum might induce an intra-scan variability estimated to 5-10% (Keijzer *et al* 2018).

The effects of myocardial fiber structure on the wave velocity can be quite significant, which may result in anisotropic shear wave propagation as observed with radiation force-induced shear wave elastography (Villemain *et al* 2017, 2018; Urban *et al* 2016). Yet, the relatively low oscillation frequency (order 50 - 100 Hz) of the waves might reduce the effect of the fiber structure (Song *et al* 2016, Urban *et al* 2016). Furthermore, viscous loss will introduce dispersion (Bercoff *et al* 2004), and the finite wall thickness may lead to dispersive Lamb waves (Kanai 2005), although a previous animal study has shown

only a mild dispersion of the waves after aortic valve closure (Vos *et al* 2017). For simplicity, we have chosen the mid-wall position, presumably having the highest consistency in placement. Further clinical studies are warranted in order to detect and characterize the possible variation in velocity along and across the LV wall.

Moreover, the stiffness itself, hence the shear modulus, varies in time throughout the cardiac cycle (Kanai 2005; Couade *et al* 2011), thus changing the instantaneous shear wave speed. Yet, we track the leading edge of the wave which propagates over relatively short distances and very short intervals ($T < 12$ ms), as imposed by the limited opening of the TDI field of view. Therefore, this variation could be neglected and the propagation assumed to be linear.

The precision of the measurement is restricted by the field of view (represented by M-mode length D) and frame rate. Variance in T is caused by rounding off to integer frame intervals. The precision can be improved by averaging multiple recordings. Also a larger image sector and higher frame rate (order 1000 frames/second) would reduce the variance in the measurements (Strachinaru *et al* 2017). We found a larger variance for the mitral (range of 3.25 m/s) than for the aortic shear wave velocity (range of 1.66 m/s) in healthy volunteers. Several arguments could be evoked: 1) the higher velocity of the wave inherently produces higher variability (Strachinaru *et al* 2017); 2) the lower transvalvular gradient over the mitral valve leads to lower wave amplitudes, 3) the very complex mechanical and electrical events in early systole (Konofagou and Provost 2012) may lead to errors in shear wave quantification during this time instance; and 4) the relative position of the shear wave source (mitral annulus) to the anteroseptal wall in parasternal position may result in overestimation, as the source of the wave is not strictly inside the measurement plane, as mentioned before.

The propagation velocity of the aortic valve closure wave in our healthy subjects is lower than that found in a group of 10 human subjects by Brekke *et al* (2014) (5.41 ± 1.28 m/s), or in animal studies (Hollender *et al* 2012; Vos *et al* 2016). We speculate that the difference is originating from the different detection method and probe positioning: parasternal in our study in agreement with Kanai (2005) as opposed to apical in the study by Brekke *et al*. Interestingly, the propagation velocity of the aortic shear waves may be influenced by gender as demonstrated in our healthy volunteers group. The difference, although statistically significant, seems minor in terms of absolute numbers (3.43 ± 0.32 m/s in males and 3.67 ± 0.45 m/s, $p=0.05$ in females). Full characterization of the behavior of naturally occurring shear waves in the heart remains to be investigated in future studies.

In animal model studies, the propagation of the mitral valve shear wave has been found to be lower than the aortic (Vos *et al* 2017). The opposite finding in the human heart cannot be explained by differences in electromechanical activation (Konofagou and Provost 2012; Costet *et al* 2014). It is however noteworthy that the animal studies were performed under sedation, which has a notable impact on the loading conditions of the left ventricle.

The physiology of the isovolumetric periods remains challenging. The instantaneous LV wall stiffness has several components: an active component due to muscle contraction, a parietal tension derived from Laplace's law and an inert elasticity of the fully relaxed wall (Pernot *et al* 2011; Remme *et al* 2008). The instantaneous value of stiffness is the sum of these dynamic and static components. Our detection method is able to record naturally occurring shear waves during two moments in the cardiac cycle: one in early systole (mitral valve shear wave) and the other in early diastole (aortic valve shear wave). Although none of these moments corresponds to a truly diastolic state (full relaxation of the LV myocardium), the significant difference found in our study between normal and non-compliant myocardium (as demonstrated by the highly significant difference in e'), as well as the positive correlation with the E/e' ratio suggests that the naturally occurring shear waves could be clinically relevant in estimating myocardial stiffness. However, future studies are needed to elucidate the relation between the shear wave propagation velocities measured during the isovolumetric periods and the actual compliance of the left ventricle.

A positive correlation was found in HCM patients between the velocities of the naturally-occurring shear waves (both mitral and aortic) and the E/e' ratio. This observation is consistent with the hypothesis that naturally-occurring shear wave velocity is correlated to the degree of diastolic dysfunction as defined by the E/e' ratio.

Clinical application and future directions

Pediatric and adult HCM patients have already been tested by using shear wave imaging (Villemain *et al* 2017, 2018). These investigations were performed with ultrafast special equipment and externally induced shear waves, and demonstrated a significantly higher shear wave velocity (difference of 1.5 m/s) in HCM patients with proven decreased LV compliance and higher degree of fibrosis. In our study there was also a very significant and similar difference (1.5 m/s for aortic shear wave and 2.1 m/s for the mitral) between shear wave velocities in normal and pathological myocardium, with minimal overlap and an excellent discriminating power. Subjects with normal septal thickness but apical hypertrophy were also correctly classified by using a 4 m/s threshold (Figure 4), as well as subjects with septal thickness ranging from 13 to 15 mm diagnosed through screening.

This suggests that the method could be used to discriminate pathological myocardium regardless of the septal thickness. However, the ROC analysis was performed on limited numbers and only on one extreme pathology. Therefore we refrain from computing and reporting general limits for the normal myocardium. Also, we noticed a lower feasibility for the mitral shear wave in HCM patients than in healthy volunteers, and therefore the same analysis for mitral shear wave velocity was considered less meaningful.

A diagnostic index that uses both waves would theoretically be interesting, but requires a systematic detection of both shear waves in the same heart cycle. This was not always possible in our subjects, for three reasons: first that shear waves velocities were calculated by choosing the heart cycles where the visualization of the respective wave was optimal, but not necessarily the cycle where both shear waves were visualized; second that in some subjects only one of the shear waves was quantifiable; and third, in color TDI the velocity scale for optimally detecting the mitral shear wave was generally different (lower) than the one needed to detect the aortic shear wave. Also, because of the abnormal distribution of variables in the total group (two extremes: normal individuals with low shear wave velocities and HCM patients with much higher shear wave velocities), a linear correlation analysis between the two shear waves could not be performed. Such a correlation should be investigated over a continuum of normality and pathology.

This technique provides a possible quantitative assessment of myocardial stiffness during the isovolumic periods. The potential clinical benefit is major: from early detection of diastolic abnormalities and improved characterization of heart failure with preserved ejection fraction to a possible new endpoint in future studies of pharmacological innovations (Cikes *et al* 2014; Voigt 2018). Further studies with a longitudinal design are needed in order to demonstrate the prognostic implications.

Study limitations

This is a monocentric study on a small population, so the results cannot be directly extrapolated to the general population. Another important limitation is the lack of ground truth. Invasive stiffness measurement in volunteers remains difficult (because of practical and ethical reasons), and no validated non-invasive imaging modality is available for the study of cardiac stiffness *in vivo* (Lancelotti *et al* 2017). Prior clinical studies have however linked the significant difference in shear wave velocities between HCM patients and normal volunteers to a difference in LV compliance and stiffness (Villemain *et al* 2017, 2018). Other confounding factors could also influence this correlation (blood pressure, filling conditions). Before a direct quantification of stiffness can be done, these confounding factors need to be investigated. The added value of the naturally-occurring

shear waves' velocity as an independent diagnostic parameter remains to be shown in a larger population and a wider array of pathology.

A wave with a velocity of 5 m/s travels over 3.5 cm in 7 ms. At 500 Hz the time resolution is 2 ms, so such a fast wave would be captured in 3 to 5 separate frames. This time resolution can be insufficient when trying to quantify velocities over 5 m/s over very short distances. However, the inter- and intra-observer agreement were good, with differences of the same magnitude as the inter-measures variability, as reflected by the standard deviation. This variability is also significantly lower than the difference found between normal and pathological LV. We foresee that the advancement in technology, with even higher frame rates becoming available, and/or changes in data processing will allow a reduction in measurement error.

Manual tracking as allowed by the manufacturer-designed software is time consuming and prone to errors, demonstrated by the larger inter-observer variability. Therefore, new research should focus on a robust method of automated velocity tracking from the DICOM frames.

The lack of correlation with age, blood pressure and E/e' in normal volunteers should be interpreted with caution. The absence of age extremes (under 18 and over 65), and the overall normal blood pressure lead to a tight distribution of data around a normal value, limiting the yield of such analyses.

CONCLUSION

Naturally occurring shear waves in the *in vivo* human heart can be imaged using a standard clinical TDI application. The study demonstrates that quantification of these shear waves is feasible and can be used to assess differences between normal and pathological myocardium, opening the way to a new method of estimating myocardial stiffness.

REFERENCES

- Bercoff J, Tanter M, Muller M, Fink M. The role of viscosity in the impulse diffraction field of elastic waves induced by the acoustic radiation force. *IEEE Trans Ultrason Ferroelectr Freq Control*. 2004;51(11):1523-36.
- Bland JM, Altman DG. Statistical methods for assessing agreement between two methods of clinical measurement. *Lancet*. 1986 ;1(8476):307-10.
- Bouchard RR, Hsu SJ, Wolf PD, Trahey GE. In vivo cardiac, acoustic-radiation-force-driven, shear wave velocimetry. *Ultrason Imaging*. 2009;31(3):201-13.
- Brekke B, Nilsen LC, Lund J, Torp H, Bjastad T, Amundsen BH, Stoylen A, Aase SA. Ultra-high frame rate tissue Doppler imaging, *Ultrasound Med Biol*. 2014;40:222-31. doi: 10.1016/j.ultrasmed-bio.2013.09.012.
- Cikes M, Tong L, Sutherland GR, D'hooge J. Ultrafast cardiac ultrasound imaging: technical principles, applications, and clinical benefits, *JACC Cardiovasc Imaging*. 2014;7:812-23. doi: 10.1016/j.jcmg.2014.06.004.
- Costet A, Provost J, Gambhir A, Bobkov Y, Danilo P Jr, Boink GJ, Rosen MR, Konofagou EE. Electromechanical wave imaging of biologically and electrically paced canine hearts in vivo. *Ultrasound Med Biol*. 2014;40(1):177-87. doi: 10.1016/j.ultrasmedbio.2013.08.019
- Couade M, Pernot M, Messas E, Bel A, Ba M, Hagege A, Fink M, Tanter M. In vivo quantitative mapping of myocardium stiffening and transmural anisotropy during the cardiac cycle, *IEEE Trans Med Imaging*, 2011;30:295–305
- Elliott PM, Anastasakis A, Borger MA, Borggrefe M, Cecchi F, Charron P, Hagege AA, Lafont A, Limongelli G, Mahrholdt H, McKenna WJ, Mogensen J, Nihoyannopoulos P, Nistri S, Pieper PG, Pieske B, Rapezzi C, Rutten FH, Tillmanns C, Watkins H. 2014 ESC Guidelines on diagnosis and management of hypertrophic cardiomyopathy: the Task Force for the Diagnosis and Management of Hypertrophic Cardiomyopathy of the European Society of Cardiology (ESC). *Eur Heart J*. 2014;35(39):2733-79. doi: 10.1093/eurheartj/ehu284
- Finocchiaro G, Dhutia H, D'Silva A, Malhotra A, Sheikh N, Narain R, Ensam B, Papatheodorou S, Tome M, Sharma R, Papadakis M, Sharma S. Role of Doppler Diastolic Parameters in Differentiating Physiological Left Ventricular Hypertrophy from Hypertrophic Cardiomyopathy. *J Am Soc Echocardiogr*. 2018. pii: S0894-7317(17)30856-8. doi: 10.1016/j.echo.2017.11.022
- Goetz WA, Lansac E, Lim HS, Weber PA, Duran CM. Left ventricular endocardial longitudinal and transverse changes during isovolumic contraction and relaxation: a challenge. *Am J Physiol Heart Circ Physiol*. 2005;289(1):H196-201.
- Golde D, Burstin L. Systolic phases of the cardiac cycle in children. *Circulation*. 1970;42(6):1029-36.
- Hollender PJ, Wolf PD, Goswami R, Trahey GE. Intracardiac echocardiography measurement of dynamic myocardial stiffness with shear wave velocimetry. *Ultrasound Med Biol*, vol. 38, pp. 1271-1283, 2012.
- Kanai H, Yonechi S, Susukida I, Koiwa Y, Kamada H, Tanaka M. Onset of pulsatile waves in the heart walls at end-systole, *Ultrasonics*. 2000;38:405-11.
- Kanai H. Propagation of spontaneously actuated pulsive vibration in human heart wall and in vivo viscoelasticity estimation. *IEEE Trans Ultrason Ferroelectr Freq Control*, 52 2005:52:1931–1942.

- Kanai H. Propagation of vibration caused by electrical excitation in the normal human heart. *Ultrasound Med Biol*. 2009;35(6):936-48. doi: 10.1016/j.ultrasmedbio.2008.12.013.
- Keijzer L, Bosch JG, Verweij M, de Jong N, Vos HJ. Intra-Scan Variability of Natural Shear Wave Measurements. *IEEE IUS* 2018. 10.1109/ULTSYM.2018.8580159.
- Konofagou EE, Provost J. Electromechanical wave imaging for noninvasive mapping of the 3D electrical activation sequence in canines and humans in vivo. *J Biomech*. 2012;45(5):856-64. doi: 10.1016/j.jbiomech.2011.11.027.
- Lancellotti P, Galderisi M, Edvardsen T, Donal E, Goliassch G, Cardim N, Magne J, Laginha S, Hagendorff A, Haland TF, Aaberge L, Martinez C, Rapacciuolo A, Santoro C, Iardi F, Postolache A, Dulgheru R, Mateescu AD, Beladan CC, Deleanu D, Marchetta S, Auffret V, Schwammenthal E, Habib G, Popescu BA. Echo-Doppler estimation of left ventricular filling pressure: results of the multicentre EACVI Euro-Filling study. *Eur Heart J Cardiovasc Imaging*. 2017;18(9):961-968. doi: 10.1093/ehjci/jex067.
- Leatham A. Splitting of the first and second heart sounds. *Lancet*. 1954;267(6839):607.
- Lu DY, Hailelessie B, Ventoulis I, Liu HY, Liang HY, Pozios I, Canepa M, Phillip S, Abraham MR, Abraham T. E/e' ratio and outcome prediction in hypertrophic cardiomyopathy: the influence of outflow tract obstruction. *Eur Heart J Cardiovasc Imaging*. 2018;19(1):101-107. doi: 10.1093/ehjci/jex134.
- Nagueh SF, Smiseth OA, Appleton CP, Byrd BF 3rd, Dokainish H, Edvardsen T, Flachskampf FA, Gillebert TC, Klein AL, Lancellotti P, Marino P, Oh JK, Popescu BA, Waggoner AD. Recommendations for the Evaluation of Left Ventricular Diastolic Function by Echocardiography: An Update from the American Society of Echocardiography and the European Association of Cardiovascular Imaging. *J Am Soc Echocardiogr*. 2016;29(4):277-314. doi: 10.1016/j.echo.2016.01.011.
- Parker KJ, Doyley MM, Rubens DJ. Imaging the elastic properties of tissue: the 20 year perspective. *Phys Med Biol*. 2011;56(1):R1-R29. doi: 10.1088/0031-9155/56/1/R01.
- Pernot M, Couade M, Mateo P, Crozatier B, Fischmeister R, Tanter M. Real-time assessment of myocardial contractility using shear wave imaging. *J Am Coll Cardiol*. 2011;58(1):65-72. doi: 10.1016/j.jacc.2011.02.042.
- Pislaru C, Alashry MM, Thaden JJ, Pellikka PA, Enriquez-Sarano M, Pislaru SV. Intrinsic Wave Propagation of Myocardial Stretch, A New Tool to Evaluate Myocardial Stiffness: A Pilot Study in Patients with Aortic Stenosis and Mitral Regurgitation. *J Am Soc Echocardiogr*. 2017 Nov;30(11):1070-1080. doi: 10.1016/j.echo.2017.06.023.
- Ponikowski P, Voors AA, Anker SD, Bueno H, Cleland JGF, Coats AJS, Falk V, González-Juanatey JR, Harjola VP, Jankowska EA, Jessup M, Linde C, Nihoyannopoulos P, Parissis JT, Pieske B, Riley JP, Rosano GMC, Ruilope LM, Ruschitzka F, Rutten FH, van der Meer P. 2016 ESC Guidelines for the diagnosis and treatment of acute and chronic heart failure: The Task Force for the diagnosis and treatment of acute and chronic heart failure of the European Society of Cardiology (ESC). *Eur Heart J*. 2016;37(27):2129-200. doi: 10.1093/eurheartj/ehw128.
- Remme EW, Lyseggen E, Helle-Valle T, Opdahl A, Pettersen E, Vartdal T, Ragnarsson A, Ljosland M, Ihlen H, Edvardsen T, Smiseth OA. Mechanisms of preejection and postejecion velocity spikes in left ventricular myocardium: interaction between wall deformation and valve events. *Circulation*. 2008;118(4):373-80. doi: 10.1161/CIRCULATIONAHA.107.748491
- Shiina T, Nightingale KR, Palmeri ML, Hall TJ, Bamber JC, Barr RG, Castera L, Choi BI, Chou YH, Cosgrove D, Dietrich CF, Ding H, Amy D, Farrokh A, Ferraioli G, Filice C, Friedrich-Rust M, Nakashima K, Schafer F, Sporea I, Suzuki S, Wilson S, Kudo M. WFUMB guidelines and recommendations for

- clinical use of ultrasound elastography: Part 1: basic principles and terminology, *Ultrasound Med Biol.* 2015;41:1126-47. doi: 10.1016/j.ultrasmedbio.2015.03.009
- Song P, Zhao H, Urban MW, Manduca A, Pislaru SV, Kinnick RR, Pislaru C, Greenleaf JF, Chen S. Improved shear wave motion detection using pulse-inversion harmonic imaging with a phased array transducer, *IEEE Trans Med Imaging*, 2013;32:2299–2310
- Song P, Bi X, Mellema DC, Manduca A, Urban MW, Greenleaf JF, Chen S. Quantitative assessment of left ventricular diastolic stiffness using cardiac shear wave elastography: a pilot study. *J Ultrasound Med.* 2016; 35:1419-1427.
- Strachinaru M, Bosch JG, van Dalen BM, van Gils L, van der Steen AFW, de Jong N, Geleijnse ML, Vos HJ. Cardiac Shear Wave Elastography Using a Clinical Ultrasound System. *Ultrasound Med Biol.* 2017. pii: S0301-5629(17)30177-1. doi: 10.1016/j.ultrasmedbio.2017.04.012.
- Urban MW, Pislaru C, Nenadic IZ, Kinnick RR, Greenleaf JF. Measurement of viscoelastic properties of in vivo swine myocardium using lamb wave dispersion ultrasound vibrometry (LDUV). *IEEE Trans Med Imaging.* 2013;32(2):247-61. doi: 10.1109/TMI.2012.2222656.
- Urban MW, Qiang B, Song P, Nenadic IZ, Chen S, Greenleaf JF. Investigation of the effects of myocardial anisotropy for shear wave elastography using impulsive force and harmonic vibration. *Phys Med Biol.* 2016;61(1):365-82. doi: 10.1088/0031-9155/61/1/365.
- Vejdani-Jahromi M, Freedman J, Nagle M, Kim YJ, Trahey GE, Wolf PD. Quantifying Myocardial Contractility Changes Using Ultrasound-Based Shear Wave Elastography. *J Am Soc Echocardiogr.* 2017;30(1):90-96. doi: 10.1016/j.echo.2016.10.004.
- Villemain O, Correia M, Khraiche D, Podetti I, Meot M, Legendre A, Tanter M, Bonnet D, Pernot M. Myocardial Stiffness Assessment Using Shear Wave Imaging in Pediatric Hypertrophic Cardiomyopathy. *JACC Cardiovasc Imaging.* 2017. pii: S1936-878X(17)30888-4. doi: 10.1016/j.jcmg.2017.08.018.
- Villemain O, Correia M, Mousseaux E, Baranger J, Zarka S, Podetti I, Soulat G, Damy T, Haggège A, Tanter M, Pernot M, Messas E. Myocardial Stiffness Evaluation Using Noninvasive Shear Wave Imaging in Healthy and Hypertrophic Cardiomyopathic Adults. *JACC Cardiovasc Imaging.* 2018. pii: S1936-878X(18)30140-2. doi: 10.1016/j.jcmg.2018.02.002
- Voigt JU. Direct Stiffness Measurements by Echocardiography: Does the Search for the Holy Grail Come to an End? *JACC Cardiovasc Imaging.* 2018 Mar 9. pii: S1936-878X(18)30185-2. doi: 10.1016/j.jcmg.2018.02.004.
- Vos HJ, van Dalen BM, Heinonen I, Bosch JG, Sorop O, Duncker DJ, van der Steen AF, de Jong N. Cardiac Shear Wave Velocity Detection in the Porcine Heart. *Ultrasound Med Biol.* 2017. pii: S0301-5629(16)30412-4. doi: 10.1016/j.ultrasmedbio.2016.11.015.



Local myocardial stiffness variations identified by high frame rate shear wave echocardiography

Based on:

Strachinaru M, Bosch JG, Schinkel AFL, Michels M, Feyz L, de Jong N, Geleijnse ML, Vos HJ. *Local myocardial stiffness variations identified by high frame rate shear wave echocardiography*. Revision submitted to *Ultrasound Med Biol*.

ABSTRACT

Background: Shear waves in the heart are initiated by closure of the valves and can be measured with colour tissue Doppler imaging(TDI). Their propagation velocity can be used to estimate the stiffness of the myocardium. A local variation in stiffness is hypothesized to appear as a variation in the propagation velocity. In this study we aim to demonstrate that in vivo myocardial shear wave imaging(SWI) can detect a localized variation in tissue properties.

Methods: Ten healthy volunteers(group 1), ten hypertrophic cardiomyopathy(HCM) patients without any cardiac intervention(group 2), and ten HCM patients(group 3) with prior(>1 year before) surgical myectomy(n=8) or alcohol septal ablation(n=2) underwent high frame rate TDI studies. The shear wave in the interventricular septum after the closure of the aortic valve was mapped along two virtual M-mode lines, one in the inner layer and one in the outer layer layer. These maps were interpreted to detect a local variation in the propagation velocity. Simultaneous variation in both layers was interpreted as transmural scar. We compared SWI to detection with conventional 2D, 3D echocardiography and deformation imaging(strain).

Results: In group 1 and group 2 no change in velocity was detected. In group 3 8/10 showed a variation in shear wave velocity. For comparison, scar was detected in 6/10 with 2D, in 9/10 with 3D and in 10/10 by 2D strain. SWI accurately detected all three patients having a transmural scar.

Conclusion: Naturally occurring shear waves can be used to detect local variations in myocardial properties through a variation in propagation velocity.

INTRODUCTION

Stiffness can be estimated *in vivo* by measuring the propagation velocity of externally induced shear waves travelling through a tissue [1], the general principle being that shear waves travel faster in stiffer materials. Shear wave elastography is an emerging diagnostic tool in radiology, capable of detecting relatively subtle changes in tissue elasticity [1]. However, in cardiology, the dynamic stiffness of the myocardium over the heart cycle, as well as the limited acoustic access to the organ, present technical challenges to the implementation of cardiac elastography that are only addressed recently [7-15]. One technique relies on generating shear waves in the myocardium with an external source and detecting their propagation. This method was used to demonstrate that myocardial stiffness can be determined using ultrasonic shear wave imaging (SWI) [7-9]. This approach is limited by the need for special equipment in order to induce and track these waves. Another technique, exploited in the current study, detects naturally-occurring shear waves generated by the closing of the valves [10-15]. We have already shown that measuring naturally-occurring shear waves with high frame rate ultrasound tissue Doppler imaging (TDI) in healthy volunteers and hypertrophic cardiomyopathy (HCM) patients is feasible, proving a significant difference in global velocity between normal and pathological myocardium [13]. The studies referred to above focused on diffuse diseases of the myocardium, comparing shear wave velocity in pathological versus normal myocardium. However, no data exists for a structurally inhomogeneous heart wall, where a localized variation in tissue stiffness should result in a local variation in the propagation velocity of such a wave. Myocardial ischemia, initially beginning in the inner layer layer [16], local inflammatory [17] or tumoral infiltrates [18] would all initially present as normal B-mode images in the echo, despite local stiffness variations. In echocardiography, an alternative would be strain imaging [17,19-21], that is able to detect segmental variations in tissue deformability, without being able to precisely quantify stiffness.

In this study we aim to demonstrate that shear wave imaging can detect a localized variation in velocity of naturally occurring shear waves. As a model, we use myocardial tissue remodeling resulting from septal reduction therapy in a group of HCM patients, whereby the presence of tissue remodeling or scar is confirmed by B-mode 2D and 3D analysis and 2D strain echocardiography.

METHODS:

Background

Naturally-occurring shear waves are generated during the isovolumic periods [22-25], so an estimation of the myocardial stiffness may not be applicable for other phases of the cardiac cycle. The instantaneous stiffness (the one related to the propagation velocity of the shear wave that we are able to measure) is the result of several intrinsic and dynamic components: the baseline viscoelastic tissue stiffness, the contractility of the myocardium, the timing of valve closure with respect to the transient relaxation, and a hemodynamic component derived from the Laplace law [3,13,25]. Given the dynamic nature of the last components, the precise quantitative relation between the naturally occurring shear waves' velocity and the first intrinsic component –which would be of primary interest for stiffness quantification– is difficult to establish directly. We therefore aim only at identifying a localized variation in naturally-occurring shear waves velocities, assuming a monotonic relationship with the tissue stiffness [1, 12]; actual stiffness quantification is outside of the scope of the current study.

Shear waves propagate faster through stiffer tissue, as previously demonstrated [1,13,15]. Fibrotic tissue resulting from septal reduction therapy is stiffer than the adjacent myocardium and should induce a local variation in the propagation velocity of the shear waves. This will impact the full thickness of the septum for patients having a transmural scar but only the inner layer for non-transmural scar [26].

Study population

This proof-of-concept pilot study was conducted prospectively in 2017-2018 according to the principles of the Declaration of Helsinki and approved by the Institutional Medical Ethical Committee (MEC-2014-611, MEC-2017-209). Written informed consent was obtained from every participant.

-Group 1: Healthy volunteers (N=10) aged 18 to 62 years. Subjects were excluded if one or more of the following criteria were present: a history of cardiovascular disease, systemic disease, the finding of cardiac abnormalities during the examination (including QRS duration over 100ms), cardiovascular risk factors including hypertension (cutoff value 140/90 mmHg), diabetes mellitus or hypercholesterolemia, having breast implants or being pregnant. Professional athletes or morbidly obese (body mass index (BMI) >40kg/m²), were excluded.

-Group 2: Hypertrophic cardiomyopathy patients (N=10) were recruited from the HCM outpatient clinic. Subjects were included if they had a definitive diagnosis of hypertro-

phic cardiomyopathy [27] with basal septal involvement. Exclusion criteria were: prior septal reduction therapy, associated known coronary artery disease, more than mild valve disease. Systolic anterior motion of the mitral valve was not considered as exclusion criterion.

-Group 3: Hypertrophic cardiomyopathy patients (N=10) recruited from the HCM outpatient clinic, as defined above, but having undergone prior (more than 1 year before) septal reduction therapy, either surgical or interventional.

Echocardiography

All echocardiographic studies were performed by one experienced sonographer (MS) using a Philips iE33 system (Philips Medical, Best, The Netherlands). Normal complete echocardiographic studies were performed, including 2D and 3D grey scale imaging. 2D imaging included the three standard apical views (four, two and three chamber) and parasternal long axis (PLAX). 3D volumes (four-beat full volume LV) were acquired using an X5-1 transducer from the apical window and analyzed using Qlab 9 postprocessing software (Philips Medical, Best, The Netherlands).

The presence of myocardial scarring was verified by 2D, 3D echocardiography and deformation imaging. The 3D volumes were cropped using multislice views in the longitudinal and transversal plane, in order to detect myocardial scarring in the basal septum post septal reduction therapy. Scar was defined in grayscale 2D and 3D imaging as an area of localized myocardial thinning, with hyperechoic appearance, and the presence of localized wall motion abnormalities (Movie 1).

Myocardial deformation was analyzed by global and segmental longitudinal strain (Movie 2), by using a general independent post-processing platform (Tomtec Imaging System 4.6, Unterschleissheim Germany). Global longitudinal strain (GLS) and segmental longitudinal strain were computed in the apical view, according to current recommendations [28]. The results were represented in "bull's eye" diagrams. The longitudinal segmental strain (LSS) in the basal and mid-wall septal segments was averaged and compared in the 4 and 3 chambers views (the views where septal segments are visible). For maximal specificity, transmural scar was defined as the presence of a myocardial segment with $LSS > -5\%$ [20,21,29-31]. Based on the same validation studies, an area with $LSS > -10\%$, but not $> -5\%$ was considered as possible scar without transmural. Data from 2D, 3D and deformation imaging were correlated and compared to the results from high frame rate echocardiography (see statistics section below for details).

In the high frame rate echocardiography, tissue velocities of the LV myocardium were sampled in Color Tissue Doppler (color TDI) in standard parasternal long axis view (PLAX) using the same Philips iE33 system, with an S5-1 transducer. As previously described [12-13], TDI frame rates over 500 Hz were achieved by carefully tuning the imaging parameters. These frame rates were sufficient to resolve the shear waves after aortic valve closure. Similar to the aortic valve closure, also the mitral valve closure generates a wave pattern that might appear in the TDI map. Although generally visible in our study subjects, mitral valve closure was not used in this analysis because of the large number (8/10) of surgical reduction patients who also received mitral valve reconstruction. The consequences of mitral repair on the shear waves induced by valve closure are yet unknown. Shear waves after mitral valve closure were therefore not considered.

The TDI movies were stored in DICOM format for offline analysis. In order to discriminate shear waves from other events, the acquisitions were timed to the synchronous recording of both the electrocardiogram (ECG) and phonocardiography signal (PCG), the latter by using a Fukuda Denshi MA-300HDS(V) phonocardiography microphone.

The DICOM TDI loops were processed using Qlab 9 (Philips Medical). A shear wave in the color TDI data is detected on the septal wall as a rapid up-and-down tissue displacement, visible in the form of a color shift from red to blue or blue to red, depending on the direction (Figure 1). This pattern initiates at the exact visible moment of valve closure which also corresponds to the onset of the heart sounds in the PCG, and then propagates over the septal wall away from the valve towards the apex.

A curved virtual M-mode line can be traced along the LV wall (Figure 1). For consistency, the arrow of the M-mode line always pointed towards the shear wave source, perpendicular to the wave front. The software provides a virtual M-Mode map, allowing to manually trace the leading slope of the propagating wave. As was previously described [12-13], the slope can be quantified to obtain the propagation velocity of the wave. This velocity was computed mid-wall in our previous studies (Figure 1). However, in the current study, we are interested in the existence of local variations of the propagation velocity of the wave, visible by changes in the slope of the wave front. Therefore we qualitatively assess the slope of the wave front in the virtual M-Mode map, in the basal septal segments.

In this study the shear wave front propagating in the basal interventricular septum after the closure of the AoV was mapped along two virtual M-mode lines, one in the inner (subendocardial) layer, the possible location of septal reduction scar, and one in the outer layer (Figure 2A), over a length of 3 cm.

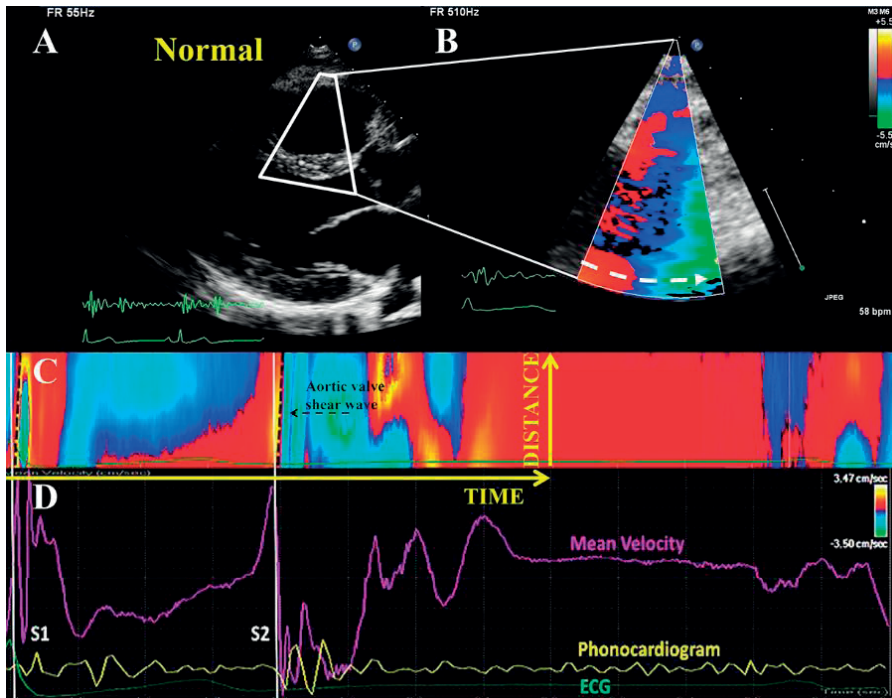


Figure 1. High frame rate color TDI shear wave tracking and analysis in the postprocessing software. A: classical parasternal long axis view and the focused TDI window over the interventricular septum. B: An M-Mode line is put in the septal wall, pointing towards the shear wave source. C: virtual M-mode map of a full heart cycle (reconstructed offline), at 510Hz frame rate, demonstrating the shear waves after mitral and aortic valve closure (dotted slopes). The onset of the waves is marked with solid lines. The shear wave after aortic valve closure is pointed to by the dotted arrow; space and time directions are also indicated. D: mean tissue velocity curve as a function of time (averaged over the M-mode line, this velocity should not be mistaken with the shear wave propagation velocity), synchronous to the ECG (green) and PCG (yellow). The onset of both shear waves is synchronous to the onset of the respective heart sounds (S1, S2).

As previously described [13] we marked the entrance and exit points of the shear wave along the M-mode line (Figure 2), and in the same time interval traced the front of the wave with two different lines, starting from the upper and respectively the lower end of the wave front in the M-mode map. If the upper and lower front lines are parallel, we score this segment of tissue as having uniform velocity of the shear wave along the virtual M-Mode line (Figure 3A). If the upper and lower slopes intersected, forming an angle with an opening of more than one time-frame (2 ms at 500 Hz) over the 3 cm line (Figure 3B), the propagation velocity was considered to vary significantly within the detection capability of our TDI method along the length of the M-mode line. The angle threshold was derived by using the segment length (3 cm) and the time resolution of 2 ms at 500 Hz. For a wave travelling with around 5 m/s over 3 cm the detectable velocity variation is 1.5-2 m/s. In the presence of such a velocity variation we assessed the underlying tissue

as having a variation in its mechanical properties (Figure 3D). If a variation was present in both layers, the scarring was considered transmural.

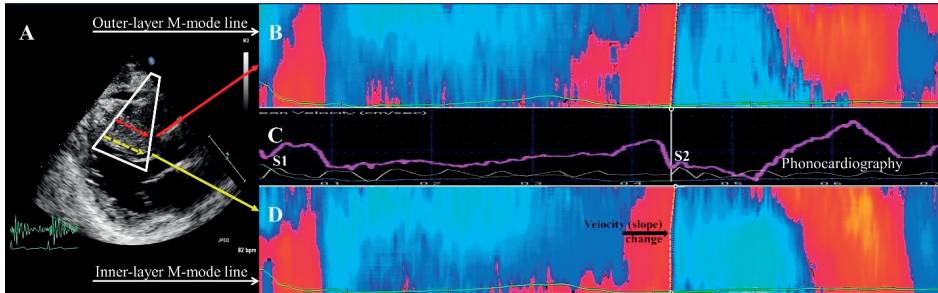


Figure 2. The figure explains the multi-layer TDI method used in this study, in one HCM patient having an inner layer scar. A: parasternal long axis and the focused TDI window over the interventricular septum; two M-Mode lines are traced, one in the outer layer and one in the inner layer, pointing towards the shear wave source. C: The mid panel depicts synchronous ECG signal (green) and phonocardiogram (white). Heart sounds are marked with S1 and S2. The onset of the second heart sound (S2) is marked with a white line. B, D: local tissue velocity along the virtual M-mode lines traced in the outer layer (B) and inner layer (D). The entry and exit points of the shear wave along the two M-mode lines are marked with empty circles, connected by a white dashed straight line as reference. The aortic shear wave front slope is traced with yellow dashed lines. In panel B the wave front line is superposed on the reference line, but in panel D (inner layer) there is a visible shift in the slope, demonstrated by a deviation from the reference line. This indicates a variation in the tissue properties.

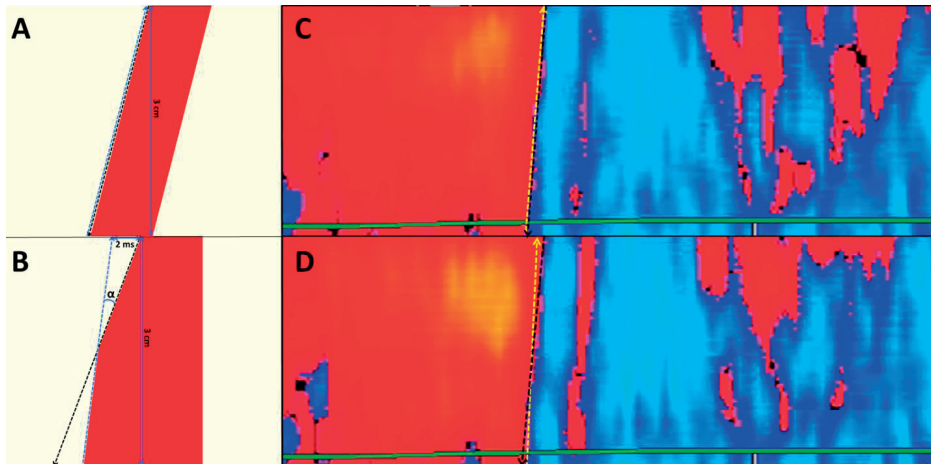


Figure 3. Shear wave velocity variation demonstrated in a M-mode panel, theoretical model (A,B) and patient demonstration (C, D). A: uniform propagation of a wave (theoretical model). By tracing the wave front from the upper (black arrow) and respectively lower (blue arrow) point we obtain two parallel lines; B: velocity variation along the 3 cm M-mode line (theoretical model). The upper point wave front (black arrow line) forms an angle (α) with the lower point arrow line (blue line). This angle is resolved if the opening on either side is at least 2 ms (one time-frame at 500 Hz). It demonstrates a change in propagation velocity; C: outer layer tracing in a HCM patient. The wave front of the aortic shear wave is linear, the upper (black) and lower (yellow) point arrow lines are parallel; D: inner layer tracing in the same patient. There is a visible shift in slope, and the two lines intersect and form an angle. We deduce the presence of a local subendocardial variation in tissue properties.

RESULTS

Baseline characteristics of the three study groups are presented in Table 1. One-way ANOVA determined significant differences between groups regarding age ($F=11.9$, $p<0.0001$), BMI ($F=7.8$, $p=0.002$), septal thickness ($F=25.2$, $p<0.0001$), ejection fraction ($F=5.8$, $p=0.008$) and shear wave velocity in the non-ablated segments ($F=15.5$, $p<0.0001$). A Tukey post hoc test revealed that the age, BMI and septal thickness were significantly different in the HCM groups (2 and 3) as compared to group 1 (normal volunteers), but statistically similar between groups 2 and 3 (Table 1). Ejection fraction was significantly lower ($53\pm 14\%$, $p=0.01$) in group 3 (septal reduction group) as compared to group 1 ($67\pm 5\%$), and also when compared with group 2 (HCM without septal reduction, $65\pm 9\%$, $p=0.03$).

Table 1. baseline characteristics of the three study groups.

Category	1=Normal volunteers N=10	2=HCM patients without septal reduction N=10	ANOVA		ANOVA p 2 vs 3	
			p 1 vs 2	p 1 vs 3		
Age	37±14	51±11	0.002	54±10	0.0001	0.75
Male gender	50%	90%	0.09	60%	0.8	0.3
BMI	22±2	28±5	0.002	27±5	0.02	0.7
Systolic blood pressure [mmHg]	118±16	136±12	0.06	130±22	0.2	0.7
Diastolic blood pressure [mmHg]	70±9	80±12	0.4	76±11	0.5	0.9
Septal thickness [mm]	8±1	19±5	<0.0001	17±4	<0.0001	0.8
Ejection fraction [%]	67±5	65±9	0.9	53±14	0.01	0.03
Color TDI frame rate [Hz]	528±22	530±25	0.9	514±17	0.4	0.3

BMI: Body Mass Index; HCM: hypertrophic cardiomyopathy; TDI: Tissue Doppler Imaging

2D and 3D echocardiography

Three patients (2 alcohol ablations and one surgical) had a transmural scar in the basal septum, six patients had only inner layer scar as detected with 3D. Note that in 1/10 patients no scar was detected with 3D echocardiography. Transmural scarring was visible in all three patients in 2D imaging but isolated inner layer scars only in 3/6 (Table 2). The patient with no visible scar in 3D imaging also had no visible scar in 2D.

Table 2. results from conventional 2D and 3D echocardiography, deformation imaging and shear wave imaging in subjects group 3 (HCM post septal reduction), N=10

	No scar detected	Inner layer scar	Transmural scar
Longitudinal strain	0	10	3
3D echocardiography	1	6	3
2D echocardiography (PLAX+3 apical views)	4	3	3
Shear wave imaging	2	5	3

HCM: hypertrophic cardiomyopathy; PLAX: parasternal long axis view.

By deformation imaging (Table 3) one-way ANOVA noted significant differences between groups in global longitudinal strain ($F=9.6$, $p=0.001$), average septal LSS in 4-chamber view ($F=21.7$, $p<0.0001$) and average septal LSS in 3-chamber view ($F=16.9$, $p<0.0001$). Post-hoc Tukey test showed that global longitudinal strain (GLS) was significantly lower only in group 3 ($-14\pm 5\%$), as compared to group 1 ($-20\pm 2\%$, $p=0.001$) and group 2 ($-19\pm 4\%$, $p=0.004$). Average GLS was not significantly lower in group 2 ($-19\pm 4\%$, $p=0.9$) as compared to group 1. However, average septal LSS in 4 and 3 chamber views were significantly lower in the two HCM groups (Figure 4, Table 3) when compared to normal volunteers (group 1). A significant difference existed between the average septal LSS between group 2 and 3 in apical 3 chamber view ($-16\pm 4\%$ vs $-10\pm 4\%$ respectively, $p=0.01$), but not in 4 chamber view ($-16\pm 4\%$ vs $-13\pm 4\%$ respectively, $p=0.2$).

Furthermore, only in group 3 septal segments with LSS $> -10\%$ were present in every subject. The three patients having transmural scars detected by 2D and 3D imaging had a LSS $> -5\%$ in the scarred segments.

Table 3. 2D longitudinal strain analysis in the study group

<i>Parameter</i>	<i>Group 1</i> <i>Normal</i> <i>volunteers</i>	<i>Group 2</i> <i>HCM patients without</i> <i>septal reduction</i>	<i>ANOVA</i> <i>p</i> <i>1 vs 2</i>	<i>Group 3</i> <i>HCM patients post</i> <i>septal reduction</i>	<i>ANOVA</i> <i>p</i> <i>1 vs 3</i>	<i>ANOVA</i> <i>p</i> <i>2 vs 3</i>
GLS (%)	-20±2	-19±4	0.9	-14±5	0.001	0.004
Average septal[*] LSS 4 chambers (%)	-23±3	-16±4	<0.0001	-13±4	<0.0001	0.2
Average septal[*] LSS 3 chambers (%)	-20±4	-16±4	0.04	-10±4	<0.0001	0.01
Any[*] septal LSS > -10% (number)	0	0	-	10 subjects	-	-
Any[*] septal LSS > -5% (number)	0	0	-	3 subjects	-	-

*: the septal basal and mid-wall segments were considered, in the 4 chambers and 3 chambers views. GLS: Global Longitudinal Strain; LSS: longitudinal segmental strain

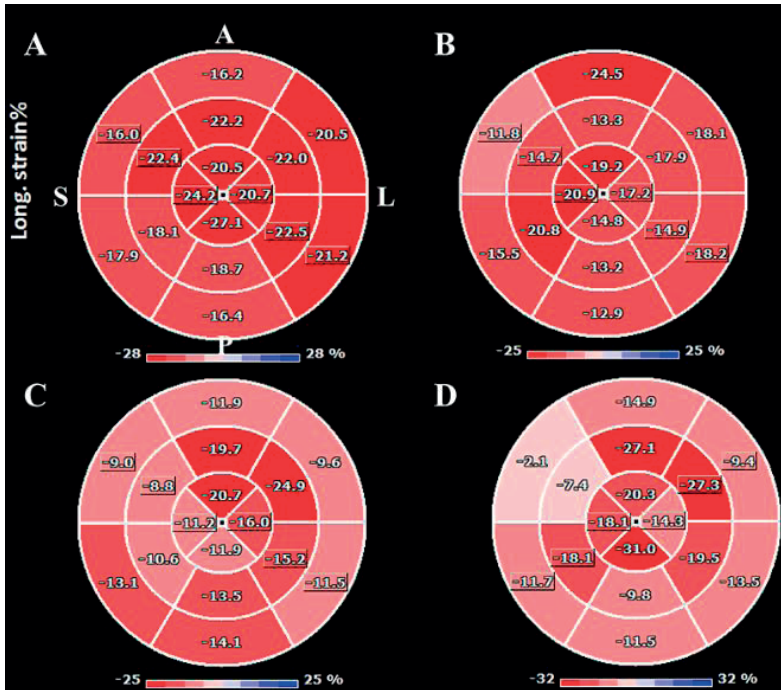


Figure 4. Strain results, represented as bull's eye diagrams, by using a 16-segments model. A: normal volunteer. Local segmental strain (LSS) is homogeneous and normal in all the segments; B: HCM patient without septal reduction. LLS is globally lower than in the normal individual, with even lower values in the anterosseptal and inferior segments; C: HCM patient post septal reduction, having an inner layer scar visible on 2D and 3D echo. Anterosseptal segments have local strain values of $>-10\%$; D: HCM patient with transmural scar: anterosseptal segments have LSS values $>-5\%$.

Shear wave imaging

In high frame rate TDI, shear waves were visible in all 30 subjects after the closure of the AoV in the interventricular septum, synchronous to the onset of the second heart sound. In group 1 (normal) and group 2 (HCM without reduction) the slope of the wave front as traced from the upper and respectively lower point were parallel, no variations in shear wave velocity were detected. In group 3 (HCM post septal reduction), 8/10 patients showed a significant change in the front wave of the shear wave velocity, demonstrated by the intersection of the upper and lower slope trace. The three patients having transmural scarring, as detected by 3D, 2D and deformation imaging, also demonstrated shear wave velocity changes in both the inner and outer layers. The results of the high frame rate study against conventional 2D and 3D echocardiography are presented in Table 2. In the one post-surgical patient where no scar was seen in 3D and 2D, SWI was also negative. In this patient however significant changes (LSS $>-10\%$) were detected by deformation imaging in the septal segments. In the other post-surgical patient in whom

SWI was not diagnostic, discrete inner layer scarring was detected by 3D echocardiography and deformation imaging, but not in 2D.

Variability

The kappa coefficient of agreement between the two readers for the ten HCM subjects was 1, implying that no disagreement existed in the qualitative interpretation of the front waves in the inner and outer layers.

DISCUSSION

The main findings of this study are: 1) Shear wave imaging can detect a local variation in tissue stiffness (in our pathology model induced by septal reduction); 2) Transmural scar was accurately detected by SWI in 3 of 3 cases; 3) SWI was more sensitive than 2D B-mode imaging and equally specific to 3D in detecting isolated inner layer stiffness variation.

This pilot study is based on the hypothesis that instantaneous shear wave velocity, if used qualitatively, can provide important information about the nature of the tissue in which the shear wave propagates, and can detect a local variation in stiffness by a variation in the propagation velocity.

The relationship between shear wave velocity and tissue stiffness is from a physical point of view monotonic [1]. Naturally-occurring shear waves in the heart are produced during periods of variation in muscle tension (contractility or relaxation and intracavitary pressure) [10-15], meaning that the shear wave velocity reding represents a mix of diastolic and contractile properties of the wall. Villemain *et al*, using externally induced shear waves during the diastolic phase, measured an average velocity of 3.5 m/s for HCM patients [9]. We have already reported parasternal aortic shear wave velocity values over 5 m/s in HCM patients, using the same high frame rate TDI methodology [13]. The difference in velocity probably accounts for the role of myocardial contractility and parietal tension during the isovolumetric periods as compared to the diastasis. However, during the very short periods of time when shear waves are detected in the basal septum, this dynamic component is less important, meaning that a change in the propagation velocity should represent a variation in local tissue properties.

Given the method of detecting these waves [12-13] (Figure 1), a variation in velocity is visible by a variation in the slope of the shear wave in the M-mode panel. A slope variation present in only one myocardial layer was interpreted as local (inner or

outer layer) variation in tissue stiffness (tissue stiffening secondary to septal reduction therapy). Simultaneous presence of a velocity variation in the inner and outer layers was interpreted as transmural scar. For confirmation of the presence of local myocardial abnormalities in the investigated segments we used three different ultrasound-derived imaging modalities (2D imaging, 3D and deformation imaging), that have been validated in previous studies [20,29-31].

There were significant differences in age, BMI and cardiac morphology between the normal volunteers and the patient groups, but in this small qualitative study matching was considered unnecessary. Also, in the two patient groups the general features were similar, except for gender distribution and ejection fraction, which was statistically lower in the septal reduction group ($53\pm 14\%$ versus $65\pm 9\%$, $p=0.03$, Table 1), as expected in the presence of a septal motion abnormality. Therefore, we deduce that the variation in shear wave propagation present only in the septal reduction group is indicative of a local variation in tissue stiffness by local remodeling, rather than any other phenomenon that would be typical for HCM such as the thick septal wall or diffusely fibrotic tissue, as these are expected to be equally present in groups 2 and 3.

We noticed a clear velocity variation in the inner layer in 8/10 HCM patients after septal reduction therapy, having a steeper slope in the part of the septum where tissue abnormalities were detected by standard imaging. This is in line with the expectation that these segments would be stiffer than the rest of the myocardium. The velocity variation was not visible in the HCM patients who have not had such an intervention, and it was also not visible in normal healthy volunteers, thus showing a good specificity of the technique. Three patients had a velocity change in both layers, interpreted as transmural scar. In these 3 patients, 2D and 3D echocardiography confirmed the presence of a transmural basal septal scar, demonstrating the accuracy of our diagnostic algorithm in this limited group of patients.

The DICOM TDI loops were set in a pixel array of 768 rows and 1024 columns, with a pixel spacing of 0.088/0.088mm. The speckle size in color TDI in the axial direction was 1-3mm and in the lateral 3-5mm. This spatial resolution was considered sufficient in order to distinguish a propagation velocity difference in different layers of the IVS (smallest width of 8 ± 1 mm in normal volunteers, where this width was interrogated with the axial resolution in the parasternal long axis view).

A wave with a velocity of 3.5-5 m/s travels over 3.5 cm in 7-10 ms while the duration of the isovolumetric relaxation time is about 100 ms, which is significantly longer. At 500 Hz the time resolution is 2 ms, so such a fast wave would be captured in 3 to 5 separate

frames. This time resolution can be insufficient when trying to quantify high velocity waves over very short distances. For this reason, we refrained from precisely calculating the two different velocities along the upper and lower direction of the front wave in the M-mode panel, when the two front wave lines were non-parallel. As already shown in Methods, our qualitative method provides sensitivity for a velocity variation of at least 1.5 m/s.

Limitations and future directions

This prospective proof-of-concept study enrolled only a limited number of patients, so we cannot draw statistically-founded conclusions. To further show the sensitivity and specificity of the technique, other pathologies such as non-transmural myocardial ischemia or inflammation need to be investigated and compared to reference methods (MRI, pathology).

High frame rate color TDI represents a tradeoff between spatial and temporal resolution and frame rate, as demonstrated above. The time resolution used in the current study (< 2 ms) may prove insufficient for very precise quantification of shear wave velocity variation in patients with very stiff ventricles (very high expected shear wave velocity).

Manual tracking as allowed by the manufacturer-designed software is time consuming and prone to errors. In order to reduce the variability in estimating the shear wave slope, we used two straight lines traced between the entry and respectively the exit points of the wave into the M-mode map, along the shear wave slope. This resulted in a very good interobserver agreement. New research should focus on a robust method of automated velocity tracking from the DICOM frames, ideally at a higher frame rate.

Tissue remodeling or scars resulting from the different septal reduction techniques are not similar. Previous MRI studies demonstrated that by using the modern myectomy techniques myocardial scarring may be discrete and limited to a thin endocardial fibrous layer [26], probably smaller than the resolution of some of the imaging methods compared here (3D echocardiography and SWI). Functional imaging by deformation (longitudinal strain) is more sensitive to the local deformation abnormality induced by scarring, giving diagnostic information in these cases.

Scar detection *per se* is not the purpose of this method, since it is better done by other imaging modalities. Being able to detect localized variations in tissue stiffness inside the myocardium however would potentially allow a quantitative mapping of the myocardial stiffness [33], that could for example be rendered in color-coded stiffness maps, in a similar manner to that presently used in parenchymatous organs [1]. We do not antici-

pate this goal to be achievable with the current clinical TDI application used in this work. Its ease of use makes it readily available for research, allowing to demonstrate that shear wave imaging is possible and clinically relevant. With advancement in technology even higher frame rates become available [14-15]. Also, changes in data processing will allow an increase in the velocity range that can be accurately measured.

CONCLUSION

Local variations in stiffness, with myocardial remodeling post septal reduction therapy as model, can be detected by a local variation in the propagation velocity of naturally occurring shear waves.

REFERENCES

1. Shiina T, Nightingale KR, Palmeri ML, Hall TJ, Bamber JC, Barr RG *et al.* WFUMB guidelines and recommendations for clinical use of ultrasound elastography: Part 1: basic principles and terminology. *Ultrasound Med Biol.* 2015;41(5):1126-47. doi: 10.1016/j.ultrasmedbio.2015.03.009.
2. Bouchard RR, Hsu SJ, Wolf PD, Trahey GE. In vivo cardiac, acoustic-radiation-force-driven, shear wave velocimetry. *Ultrason Imaging.* 2009;31(3):201-13.
3. Pernot M, Couade M, Mateo P, Crozatier B, Fischmeister R, Tanter M. Real-time assessment of myocardial contractility using shear wave imaging. *J Am Coll Cardiol.* 2011;58(1):65-72. doi: 10.1016/j.jacc.2011.02.042.
4. Hollender PJ, Wolf PD, Goswami R, Trahey GE. Intracardiac echocardiography measurement of dynamic myocardial stiffness with shear wave velocimetry. *Ultrasound Med Biol.* 2012;38(7):1271-83. doi: 10.1016/j.ultrasmedbio.2012.02.028.
5. Song P, Heng Zhao, Urban MW, Manduca A, Pislaru SV, Kinnick RR *et al.* Improved shear wave motion detection using pulse-inversion harmonic imaging with a phased array transducer, *IEEE Trans Med Imaging.* 2013;32(12):2299-310. doi: 10.1109/TMI.2013.2280903.
6. Urban MW, Pislaru C, Nenadic IZ, Kinnick RR, Greenleaf JF. Measurement of viscoelastic properties of in vivo swine myocardium using lamb wave dispersion ultrasound vibrometry (LDUV). *IEEE Trans Med Imaging.* 2013;32(2):247-61. doi: 10.1109/TMI.2012.2222656.
7. Vejdani-Jahromi M, Freedman J, Nagle M, Kim YJ, Trahey GE, Wolf PD. Quantifying Myocardial Contractility Changes Using Ultrasound-Based Shear Wave Elastography. *J Am Soc Echocardiogr.* 2017;30(1):90-96. doi: 10.1016/j.echo.2016.10.004.
8. Villemain O, Correia M, Khraiche D, Podetti I, Meot M, Legendre A *et al.* Myocardial Stiffness Assessment Using Shear Wave Imaging in Pediatric Hypertrophic Cardiomyopathy. *JACC Cardiovasc Imaging.* 2017. pii: S1936-878X(17)30888-4. doi: 10.1016/j.jcmg.2017.08.018.
9. Villemain O, Correia M, Mousseaux E, Baranger J, Zarka S, Podetti I *et al.* Myocardial Stiffness Evaluation Using Noninvasive Shear Wave Imaging in Healthy and Hypertrophic Cardiomyopathic Adults. *JACC Cardiovasc Imaging.* 2018. pii: S1936-878X(18)30140-2. doi: 10.1016/j.jcmg.2018.02.002
10. Kanai H. Propagation of vibration caused by electrical excitation in the normal human heart. *Ultrasound Med Biol.* 2009;35(6):936-48. doi: 10.1016/j.ultrasmedbio.2008.12.013.
11. Brekke B, Nilsen LC, Lund J, Torp H, Bjastad T, Amundsen BH *et al.* Ultra-high frame rate tissue Doppler imaging, *Ultrasound Med Biol.* 2014;40:222-31. doi: 10.1016/j.ultrasmedbio.2013.09.012.
12. Strachinaru M, Bosch JG, van Dalen BM, van Gils L, van der Steen AFW, de Jong N *et al.* Cardiac Shear Wave Elastography Using a Clinical Ultrasound System. *Ultrasound Med Biol.* 2017. pii: S0301-5629(17)30177-1. doi: 10.1016/j.ultrasmedbio.2017.04.012.
13. Strachinaru M, Bosch JG, van Gils L, van Dalen BM, Schinkel AFL, van der Steen AFW *et al.* Naturally occurring shear waves in healthy volunteers and hypertrophic cardiomyopathy patients. *Ultrasound Med Biol.* 2019. pii: S0301-5629(19)30141-3. doi: 10.1016/j.ultrasmedbio.2019.04.004.
14. Santos P, Petrescu A, Pedrosa J, Orlowska M, Komini V, Voigt JU *et al.* Natural shear wave imaging in the human heart: normal values, feasibility and reproducibility. *IEEE Trans Ultrason Ferroelectr Freq Control.* 2018. doi: 10.1109/TUFFC.2018.2881493.

15. Petrescu A, Santos P, Orłowska M, Pedrosa J, Bézy S, Chakraborty B *et al.* Velocities of Naturally Occurring Myocardial Shear Waves Increase With Age and in Cardiac Amyloidosis. *JACC Cardiovasc Imaging*. 2019. pii: S1936-878X(19)30057-9. doi: 10.1016/j.jcmg.2018.11.029.
16. Detry JM. The pathophysiology of myocardial ischaemia. *Eur Heart J*. 1996;17 Suppl G:48-52.
17. Leitman M, Vered Z, Tyomkin V, Macogon B, Moravsky G, Peleg E *et al.* Speckle tracking imaging in inflammatory heart diseases. *Int J Cardiovasc Imaging*. 2018;34(5):787-792. doi: 10.1007/s10554-017-1284-y.
18. Rathi VK, Czajka AT, Thompson DV, Doyle M, Tewatia T, Yamrozik J *et al.* Can cardiovascular MRI be used to more definitively characterize cardiac masses initially identified using echocardiography?. *Echocardiography*. 2018;35(5):735-742. doi: 10.1111/echo.14017.
19. Ganame J, D'hooge J, Mertens L. Different deformation patterns in intracardiac tumors. *Eur J Echocardiogr*. 2005;6(6):461-4.
20. Cimino S, Canali E, Petronilli V, Cicogna F, De Luca L, Francone M *et al.* Global and regional longitudinal strain assessed by two-dimensional speckle tracking echocardiography identifies early myocardial dysfunction and transmural extent of myocardial scar in patients with acute ST elevation myocardial infarction and relatively preserved LV function. *Eur Heart J Cardiovasc Imaging*. 2013;14(8):805-11. doi: 10.1093/ehjci/jes295.
21. Ünlü S, Mirea O, Pagourelas ED, Duchenne J, Bézy S, Bogaert J *et al.* Layer-Specific Segmental Longitudinal Strain Measurements: Capability of Detecting Myocardial Scar and Differences in Feasibility, Accuracy, and Reproducibility, Among Four Vendors A Report From the EACVI-ASE Strain Standardization Task Force. *J Am Soc Echocardiogr*. 2019;32(5):624-632.e11. doi: 10.1016/j.echo.2019.01.010.
22. Golde D, Burstin L. Systolic phases of the cardiac cycle in children. *Circulation*. 1970;42(6):1029-36.
23. Goetz WA, Lansac E, Lim HS, Weber PA, Duran CM. Left ventricular endocardial longitudinal and transverse changes during isovolumic contraction and relaxation: a challenge. *Am J Physiol Heart Circ Physiol*. 2005;289(1):H196-201.
24. Konofagou EE, Provost J. Electromechanical wave imaging for noninvasive mapping of the 3D electrical activation sequence in canines and humans in vivo. *J Biomech*. 2012;45(5):856-64. doi: 10.1016/j.jbiomech.2011.11.027.
25. Remme EW, Lyseggen E, Helle-Valle T, Opdahl A, Pettersen E, Vartdal T *et al.* Mechanisms of preejection and postejection velocity spikes in left ventricular myocardium: interaction between wall deformation and valve events. *Circulation*. 2008;118(4):373-80. doi: 10.1161/CIRCULATIONAHA.107.748491.
26. Valeti US, Nishimura RA, Holmes DR, Araoz PA, Glockner JF, Breen JF *et al.* Comparison of surgical septal myectomy and alcohol septal ablation with cardiac magnetic resonance imaging in patients with hypertrophic obstructive cardiomyopathy. *J Am Coll Cardiol*. 2007;49(3):350-7.
27. Elliott PM, Anastasakis A, Borger MA, Borggrefe M, Cecchi F, Charron P *et al.* 2014 ESC Guidelines on diagnosis and management of hypertrophic cardiomyopathy: the Task Force for the Diagnosis and Management of Hypertrophic Cardiomyopathy of the European Society of Cardiology (ESC). *Eur Heart J*. 2014;35(39):2733-79. doi: 10.1093/eurheartj/ehu284.

28. Lang RM, Badano LP, Mor-Avi V, Afilalo J, Armstrong A, Ernande L *et al.* Recommendations for cardiac chamber quantification by echocardiography in adults: an update from the American Society of Echocardiography and the European Association of Cardiovascular Imaging. *Eur Heart J Cardiovasc Imaging*. 2015;16(3):233-70. doi: 10.1093/ehjci/jev014.
29. Roes SD, Mollema SA, Lamb HJ, van der Wall EE, de Roos A, Bax JJ. Validation of echocardiographic two-dimensional speckle tracking longitudinal strain imaging for viability assessment in patients with chronic ischemic left ventricular dysfunction and comparison with contrast-enhanced magnetic resonance imaging. *Am J Cardiol*. 2009;104(3):312-7. doi: 10.1016/j.amjcard.2009.03.040.
30. Gorcsan J 3rd, Tanaka H. Echocardiographic assessment of myocardial strain. *Am Coll Cardiol*. 2011;58(14):1401-13. doi: 10.1016/j.jacc.2011.06.038.
31. Bansal M, Jeffriess L, Leano R, Mundy J, Marwick TH. Assessment of myocardial viability at dobutamine echocardiography by deformation analysis using tissue velocity and speckle-tracking. *JACC Cardiovasc Imaging*. 2010;3(2):121-31. doi: 10.1016/j.jcmg.2009.09.025.
32. Cohen J . A coefficient of agreement for nominal scales. *Educational and Psychological Measurement*. 1960; 20(1): 37-46. doi:10.1177/001316446002000104.
33. Voigt JU. Direct Stiffness Measurements by Echocardiography: Does the Search for the Holy Grail Come to an End?. *JACC Cardiovasc Imaging*. 2018 Mar 9. pii: S1936-878X(18)30185-2. doi: 10.1016/j.jcmg.2018.02.004.

12

Myocardial stretch post atrial contraction in healthy volunteers and hypertrophic cardiomyopathy patients

Based on:

Strachinaru M, Geleijnse ML, de Jong N, van den Bosch AE, Michels M, Schinkel AFL, van der Steen AFW, Bosch JG, Vos HJ. *Myocardial stretch post atrial contraction in healthy volunteers and hypertrophic cardiomyopathy patients*. *Ultrasound Med Biol*. 2019.

ABSTRACT

In cardiac high-frame-rate color tissue Doppler imaging (TDI), a wave-like pattern travels over the interventricular septum (IVS) after atrial contraction. The propagation velocity of this myocardial stretch postatrial contraction (MSPa) was proposed as a measure of left ventricular stiffness. The aim of our study was to investigate the MSPa in patients with hypertrophic cardiomyopathy (HCM) compared with healthy volunteers. Forty-two healthy volunteers and 33 HCM patients underwent high-frame-rate (>500 Hz) TDI apical echocardiography. MSPa was visible in TDI, M-mode and speckle tracking. When assuming a wave propagating with constant velocity, MSPa in healthy volunteers (1.6 ± 0.3 m/s) did not differ from that in HCM patients (1.8 ± 0.8 m/s, $p = 0.14$). Yet, in 42% of patients with HCM, the MSPa had a non-constant velocity over the wall: in the basal IVS, the velocity was lower (1.4 ± 0.5 m/s), and in the mid-IVS, much higher (6.1 ± 3.4 m/s, $p < 0.0001$), and this effect was related to the septal thickness. The reason is hypothesized to be the reaching of maximal longitudinal myocardial distension in HCM patients.

INTRODUCTION

The possibility to image the heart at very high frame rates has opened a new window for our understanding of the cardiac physiology and pathology (Cikes *et al* 2014, Voigt *et al* 2018). High frame rate imaging allows minute tracking of many wave-like phenomena that are either naturally present during the cardiac cycle due to valve closure (Brekke *et al* 2014, Kanai 2009, Strachinaru *et al* 2017, Vos *et al* 2017), atrial contraction (Voigt *et al* 2002, Pislaru *et al* 2014, Pislaru *et al* 2017), or induced by external sources (Pernot *et al* 2011, Song *et al* 2016, Vejdani-Jahromi *et al* 2017, Villemain *et al* 2017). The naturally-occurring shear waves secondary to the closure of the valves (Brekke *et al* 2014, Strachinaru *et al* 2017) appear during the time intervals in which the muscle is in the process of contraction (mitral valve closure) or relaxation (aortic valve closure), challenging the physiological interpretation of the data. Such complexity is absent in late diastole, where the left ventricle (LV) is supposed to be in a quasi-relaxed state, allowing estimation of the true intrinsic elasticity of the wall (Voigt *et al* 2002, Pislaru *et al* 2014, Pislaru *et al* 2017). A strain rate wave-like pattern visible in the LV myocardium after atrial contraction was reported by Voigt *et al* (2002) who estimated its propagation velocity between 2 and 4.6 m/s in the interventricular septum (IVS) of normal individuals at a frame rate of 178 Hz. They demonstrated the value to be preload-dependent. Later, Pislaru *et al* investigated the same Tissue Doppler Imaging (TDI) velocity and strain rate pattern with higher frame rates (350-460 Hz) and computed the values at 1.4 ± 0.2 m/s in normal individuals and 2.2 ± 0.7 m/s in severe aortic stenosis patients (Pislaru *et al* 2014, Pislaru *et al* 2017). Yet, the exact nature and behavior of this tissue velocity-based pattern remain unclear. These earlier studies hypothesized that the fast traction on the mitral annulus by the atrial contraction generates a wave into the left ventricle, which travels from base to apex with a constant velocity which is related to the underlying tissue stiffness. It is also possible that this wave has a radial component (Pislaru *et al* 2017).

The aim of this study was to investigate the nature of the wave-like pattern following atrial contraction by integrating multiple high frame rate ultrasound modalities. In order to further test the above hypothesis we studied both normal and hypertrophic hearts, the latter being supposedly stiffer than normal hearts (Elliott *et al* 2014, Mirsky and Parmley 1973, Villemain *et al* 2017, 2018).

METHODS

In apical TDI videos of the interventricular septal wall, wave patterns after atrial contraction are visible, as further described in the next subsection. The pattern has a propaga-

tion velocity on the order of several meters per second (Pislaru et al. 2014, 2017; Voigt et al. 2002), and general theory predicts that waves travel faster in stiffer material (Giorgi 1993). We denote this pattern as myocardial stretch propagation post-atrial contraction (MSPa), in line with a similar definition by Pislaru et al. We started this study with the hypothesis of a wave propagating with constant velocity over the first 4 to 5 cm of the interventricular septum, as previously described in normal and pathologic hearts after atrial contraction (Pislaru et al. 2014, 2017; Voigt et al. 2002).

Study population

This prospective study was conducted in 2016-2017 according to the principles of the Declaration of Helsinki and approved by the Institutional Medical Ethical Committee (MEC-2014-611, MEC-2017-209). Written informed consent was obtained from every participant. The same patient pool was used for selecting the study population in a different work investigating naturally occurring shear waves after valve closure (Strachinaru et al. 2019).

Healthy volunteers aged 18-62 y (N = 42). Patients were excluded if they had a history of cardiovascular disease or systemic disease, a finding of cardiac abnormalities during the examination (including QRS duration >100 ms), cardiovascular risk factors including hypertension (cutoff value: 140/90 mm Hg), diabetes mellitus or hypercholesterolemia, breast implants or were pregnant. Professional athletes or morbidly obese individuals (body mass index >40 kg/m²) were also excluded.

Hypertrophic cardiomyopathy (HCM) patients aged 20 to 73 y, recruited from the HCM outpatient clinic (N = 33). Patients were included if they had a definitive diagnosis of hypertrophic cardiomyopathy (Elliott et al. 2014), with pathologic septal hypertrophy (end-diastolic thickness >15 mm or >13 mm if diagnosed through family screening) and normal systolic function (ejection fraction >55%). Exclusion criteria were associated coronary artery disease, more than mild valve disease (systolic anterior movement was not considered an exclusion criterion), prior septal reduction (either surgical or interventional) and atrial fibrillation.

Echocardiography

All echocardiographic studies were performed by one experienced sonographer (M.S.). Normal complete echocardiographic studies were performed, including 2-D, Doppler and pulsed-wave TDI of the mitral annulus. The peak velocity of the early diastolic mitral inflow was measured (E wave), as was the peak early diastolic tissue velocity of the medial mitral annulus in the apical four-chamber view (e' wave). Their ratio (E/e') was then calculated as an index of the early diastolic properties of the LV. We also quantified

the motion of the atrioventricular annulus with atrial contraction by measuring peak TDI velocity (a' wave) and a' acceleration in pulsed wave tissue Doppler images of the medial mitral annulus in the apical four-chamber view. As a' acceleration is not a standard clinical measurement, we detailed it in Figure 1.

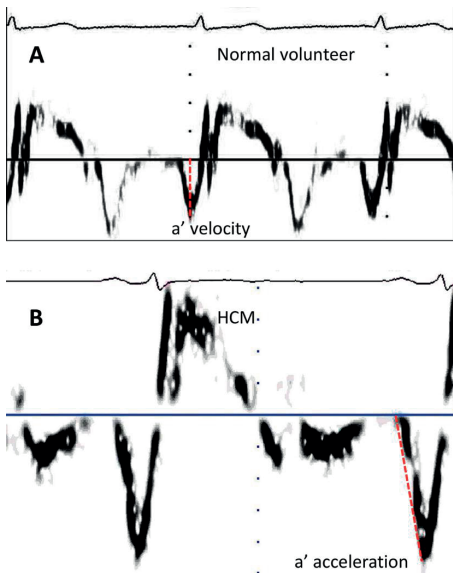


Figure 1. Clinical pulse-wave tissue Doppler imaging recordings of the medial mitral annulus in the apical four-chamber view, with demonstration of the a' velocity and acceleration slope calculation. (a) Normal healthy volunteer. (b) Patient with hypertrophic cardiomyopathy. Note that the velocity scales for the two recordings differ.

Normal complete echocardiographic studies were performed as a reference. Grayscale loops were also acquired at the highest frame rate achievable (frame rates of 200-250 Hz) from the IVS in the parasternal and apical four-chamber views.

Tissue velocities of the LV myocardium were sampled in color TDI in standard parasternal and apical four-chamber views using a Philips iE33 system (Philips Medical, Best, The Netherlands) equipped with an S5-1 transducer (three separate recordings for each view, two heartbeats per clip). As previously described (Strachinaru et al. 2017), by carefully tuning the relationship between the depth of the image, the 2-D line density and the TDI field of view, frame rates >500 Hz were achieved in regular clinical TDI mode. The color tissue velocity scale was set up for optimal visualization of the stretch, leading to scale limits between 1.5 and 3.5 cm/s, corresponding to the amplitude of the wave pattern in TDI, which is not to be confused with its propagation velocity, which is orders of magnitude higher.

Figure 2 illustrates the alignment of the probe with respect to the propagation of the wave on the septal wall in the apical four-chamber view. TDI is extremely sensitive to tissue motion in the axial direction of the probe, indicated by the yellow arrows, but not sensitive to lateral motion. We use this directional sensitivity to determine the dominant tissue motion by TDI. Additionally, we analyze grayscale clips with a speckle tracking algorithm. Speckle tracking detects motion in all directions, albeit with generally lower frame rate, sensitivity and accuracy than TDI.

By combining the information from all modalities, we illustrate the predominant tissue motion after atrial contraction.

The Digital Imaging and Communications in Medicine TDI loops were processed using Qlab 9 (Philips Medical, Best, The Netherlands). As illustrated in Figure 3a and b, the software is used to trace an anatomic M-mode line in the TDI clips. The M-mode line was traced midwall, starting apically and ending at the beginning of the muscular septum, pointing toward the possible wave source (the atrioventricular annulus). The software generates a map of color-coded TDI velocities over time and space, that is, along the M-mode line (Fig. 3c). After atrial contraction, a pattern can be seen, of which the slope of the initial front determines the velocity of the MSPa. The slope is computed by manually fitting a line (Fig. 3c, white dotted line) to the isovelocity front of the wave. To reduce the variability resulting from manual tracking, as previously described for naturally occurring shear waves (Strachinaru et al. 2017, 2019), we compared this slope with the line between the entrance and exit points (frames) of the wave into the M-mode map (Fig. 3c, black dotted line). The entrance and exit points were also adjusted by frame-to-frame analysis. The velocity V of the MSPa is calculated, from the time T , which is the interval between the time stamps of the entrance and exit frames in the map, and the pre-defined M-mode length L , as $V = L/T$ in units of meters per second.

The length L ranged from 4 to 6 cm (4.9 ± 0.4 cm), starting from the onset of the muscular IVS (Fig. 3b). Propagation velocity was averaged over at least 3 heartbeats for every subject, randomly chosen from the three recorded clips.

Speckle tracking of the high-frame-rate 2-D data, represented as velocity vector imaging, was used in Qlab 9 to qualitatively determine the direction and propagation of local motion/deformation of the IVS after the atrial contraction. Anatomic M-mode tracings were also obtained from the same grayscale data along the IVS using a general post-processing platform (Tomtec Imaging System 4.6, Unterschleissheim, Germany). They were also employed for qualitative comparison with the data from the TDI recordings.

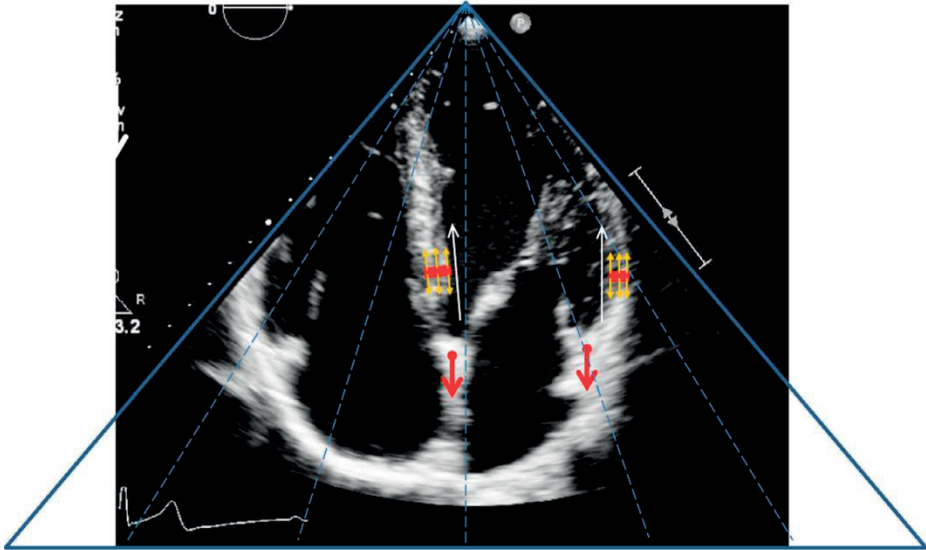


Figure 2. Tissue motion as visible in the left ventricular walls after the atrial contraction, in the apical four-chamber view. Atrial contraction pulls on the mitral annulus (red arrows); this induces a local stretch (small yellow arrows) which propagates along the walls (white arrows) in the form of a tissue Doppler imaging pattern (red line). Note that the direction of the ultrasound in the apical view (blue lines) is in line with both the stretch and the direction of propagation.

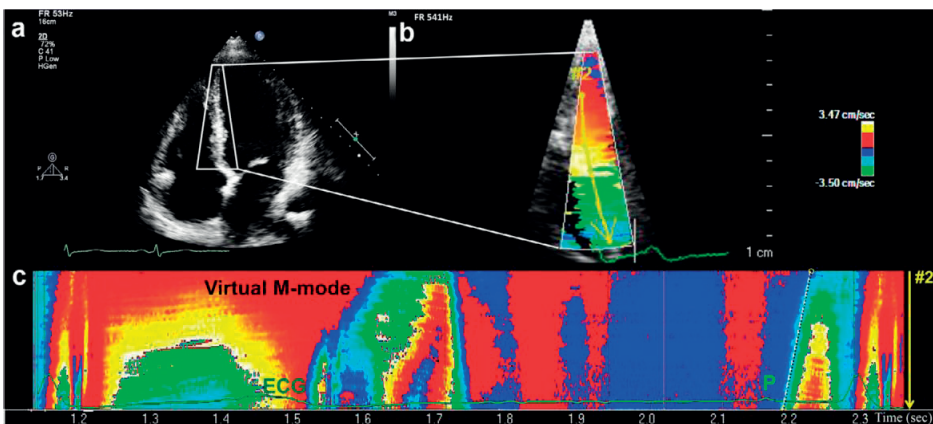


Figure 3. Data obtained in the study patients using offline processing (modified to include one entire heartbeat). (a) Classical echocardiographic apical image and the focus region for high-frame-rate imaging. (b) High-frame-rate tissue Doppler imaging window over the interventricular septum. The M-mode line is traced midwall, ending at the beginning of the muscular septum, pointing toward the possible wave source. (c) Tissue Doppler imaging spacetime map at 541 Hz, collected over the M-mode line of (b), of a full heart cycle (reconstructed offline). This map illustrates the wave-like velocity pattern after atrial contraction (P wave on the echocardiogram). The slope of the MSPa is traced along the isovelocity front (white dotted line) and compared with the line between the entrance and exit points (yellow circles, black dotted line) of the MSPa along the M-mode line. ECG = echocardiogram; MSPa = myocardial stretch post-atrial contraction.

Statistical analysis

Distribution of data was checked by using histograms and ShapiroWilk tests. Continuous variables were represented as the mean \pm standard deviation. Categorical data are presented as absolute number and percentage. For comparison of normally distributed continuous variables, we used the dependent or independent means t-test when appropriate. In case of a skewed distribution of continuous variables, the MannWhitney U-test was applied. For comparison of frequencies, the χ^2 -test or Fisher's exact test was used. Correlations were estimated using Pearson's correlation coefficient. The relationship between variables was investigated using univariate and multivariate regression models.

Each statistical analysis was performed using the Statistical Package for Social Sciences, Version 21 (IBM SPSS Statistics for Windows, Armonk, NY, USA). Testing was done two-sided and considered significant if the p value was <0.05 .

RESULTS

High-frame-rate tissue Doppler

The group characteristics and results are outlined in Table 1. There were significant differences in age, systolic blood pressure, septal thickness, e' , a' , a' acceleration and E/e' .

In the apical view, wave-like tissue velocity patterns were visible in all patients upon atrial contraction. In the parasternal longitudinal view of the LV, the grayscale traction movement of the IVS with atrial contraction was visible in all patients (Supplementary Video S1, online only), but high-frame-rate TDI could not visualize a wave phenomenon. This indicates that the dominant direction of tissue motion was along the septum, in line with the traction of the atria on the LV wall through the atrioventricular annulus.

In normal individuals and some HCM patients (Fig. 4a) the straight line corresponding to the entry/exit points of the MSPa into the M-mode line was superimposed on the first isovelocity trace (as described under Methods), revealing a globally constant propagation velocity. The same constant velocity is visible on the high-frame-rate virtual M-mode of the underlying 2D data (Fig. 4b). Yet, we noticed in a substantial group of HCM patients ($n = 14$) that the MSPa isovelocity front had a non-constant propagation as evidenced by a deviation of more than two frames' time (34 ms) at any point along the first isovelocity tracing from the straight entry-exit line used for reference (Fig. 5): a first mild slope in the basal IVS, followed by a very steep slope in the mid-IVS (Fig. 5a). By use of M-mode tracings from the underlying 2-D data, the same behavior was confirmed (Figs. 5b and 7).

In the case of such non-constant propagation velocity, quantification was done in two ways. The average slope was quantified by computing the slope of the entry/exit points line as described under Methods (see Fig. 5a for an example), thus ignoring the deviation of the slope from a straight line. Alternatively, we manually traced the slowest and fastest first isoveLOCITY slopes visible in the TDI panels (Fig. 5a, 1 and 2), and separately reported the slowest and highest apparent propagation velocities.

When analyzing the measured slope under the assumption of a linear propagation velocity (Fig. 6), the average velocity of the MSPa did not differ between normal volunteers (1.6 ± 0.3 m/s, range = 1.1-2.1 m/s) and the HCM patients (1.8 ± 0.8 , range = 0.9-3.8 m/s, $p = 0.14$). However, the maximum slope in the HCM patients presenting the non-constant TDI slope was 6.1 ± 3.4 m/s (range 2.3-12.5 m/s), which was significantly different from that of the normal volunteers ($p < 0.0001$). The slow slope in these patients was 1.4 ± 0.5 m/s (range = 0.8-2.5 m/s, $p = 0.2$) versus normal volunteers.

Subgroup analysis (Table 1, Fig. 6) among the patients with or without constant propagation velocity of the MSPa revealed a significant difference in septal thickness between the two groups (19 ± 4 mm in the non-constant propagation group and 16 ± 3 mm in the linear group, $p = 0.02$). Also, the linearized MSPa velocity in the non-constant velocity group was significantly higher than that in normal volunteers (2.6 ± 0.8 m/s vs. 1.6 ± 0.3 m/s, $p < 0.0001$).

The only parameter predicting the presence of a non-constant propagation velocity (Table 2) in a univariate and multivariate logistic regression analysis was the septal thickness ($p = 0.03$ univariate and $p = 0.001$ multivariate).

In the total group of 33 HCM patients, the linearized MSPa velocity did not correlate with age ($p = 0.24$), systolic or diastolic blood pressure ($p = 0.75$ and 0.96 , respectively), septal thickness ($p = 0.11$), e' ($p = 0.39$) or E/e' ($p = 0.47$).

The a' velocity and acceleration were significantly higher in the normal volunteers, suggesting either a stronger atrial traction on the mitral annulus or a stiffer IVS.

2-D tissue tracking and M-mode

The grayscale clips were analyzed with speckle tracking and anatomic M-mode, and for normal volunteers, local velocity vectors revealed a traction movement on the mitral annulus, followed by a local downward-only stretch, progressing from base to apex, later followed by a global outward movement of the whole IVS (atrial “volume kick”). As exemplified in Supplementary Video S2 (online only) and Figure 7a, in HCM patients with

a constant velocity of the initial front, the same progressive base-to-apex downward stretch could be seen. In patients having a non-constant velocity, we noticed after the mitral annulus traction an initial basal-only slow downward stretch, followed by a global rigid downward motion of the entire IVS and later a short outward movement (Supplementary Videos S3 and S4). This is consistent with the behavior of the MSPa in TDI and M-mode panels (Fig. 7b).

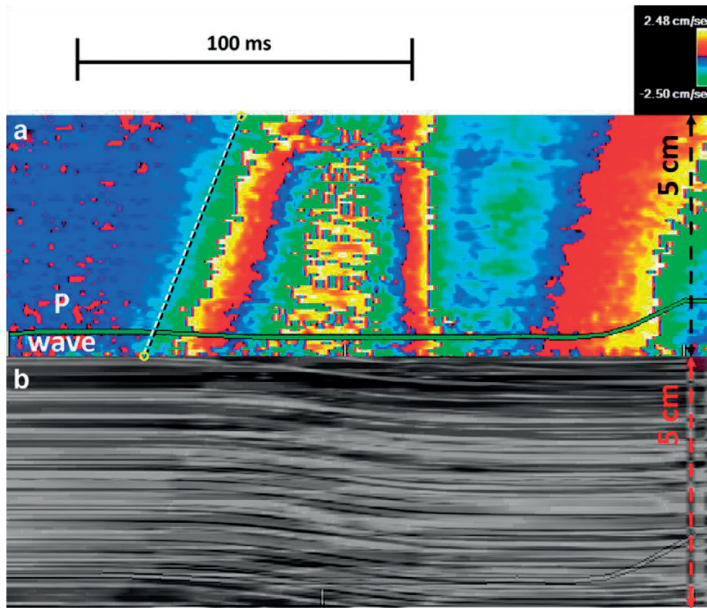


Figure 4. Zoomed-in view of the end-diastolic phase after atrial contraction (P wave). (a) Tissue Doppler imaging velocity pattern starting from the basal interventricular septum. In normal volunteers and some hypertrophic cardiomyopathy patients, the isovelocity front line (white dotted line) was superimposed on the black dotted line traced between the entry and exit points of the myocardial stretch post-atrial contraction (yellow circles) into the M-mode map, revealing a constant slope. (b) Synchronous anatomic M-mode of the underlying 2-D information along the same M-mode line. A progressive base-to-apex downward line shift is visible, following the same contour.

DISCUSSION

The main findings of this prospective study are as follows: (i) No significant difference could be found in the linearized propagation velocity of the wave-like pattern occurring in TDI post-atrial contraction between normal volunteers and HCM patients. (ii) Clinical and classic echocardiographic parameters did not correlate with the linearized propagation velocity of this pattern. (iii) In about half of the HCM patients, the wave front seemed to propagate with non-constant velocity, and this effect was related to disease severity as reflected by the end-diastolic septal thickness.

Table 1. General characteristics and results in the study population, comparisons between groups and subgroups.

Parameter [units]	Normal volunteer N=42		HCM patients total		HCM patients with non-constant MSPa (A)		HCM patients with linear MSPa (B)		P A vs B
	N=33	P vs Normal	N=14	P vs Normal	N=14	P vs Normal	N=19	P vs Normal	
Age[yr]	35±14	0.0001	46±14	0.01	50±12	0.0002	0.4		
Male gender	29(69%)	0.7	12(85%)	0.3	12(63%)	0.8	0.2		
BMI	24±3	0.002	28±5	0.0007	26±5	0.06	0.3		
Systolic blood pressure [mmHg]	117±12	<0.0001	135±14	<0.0001	127±17	0.01	0.2		
Diastolic blood pressure [mmHg]	72±7	0.06	78±10	0.028	75±11	0.2	0.4		
Septal thickness [mm]	8±1	<0.0001	19±4	<0.0001	16±3	<0.0001	0.02		
Frame rate pulsed wave TDI [Hz]	167±17	0.005	197±65	0.02	196±57	0.004	0.9		
e' [cm/s]	8.3±1.3	<0.0001	5.5±1.9	<0.0001	5.4±2.1	<0.0001	0.8		
E/e'	8±1	<0.0001	16±5	<0.0001	16±8	<0.0001	1		
a' [cm/s]	8.6±1.9	0.02	7.7±2.2	0.15	7.5±1.3	0.03	0.7		
a' acceleration [cm/s ²]	0.14±0.04	0.0001	0.10±0.04	0.004	0.10±0.04	0.0006	1		
Frame rate color TDI [Hz]	542±30	0.052	522±22	0.03	536±16	0.4	0.04		
Linearized MSPa [m/s] (range)	1.6±0.3 (1.1-2.1)	0.14	2.6±0.8 (1.3-3.8)	<0.0001	1.4±0.4 (0.9-2.2)	0.03	<0.0001		
First slope MSPa [m/s] (range)	-	-	1.4±0.5 (0.8-2.5)	-	-	-	-		
Second slope MSPa [m/s] (range)	-	-	6.1±3.4 (2.3-12.5)	-	-	-	-		

BMI: body mass index; HCM: hypertrophic cardiomyopathy; MSPa: Myocardial Stretch Propagation post Atrial contraction;

Variables are presented as mean ± standard deviation

Significant p values are highlighted in bold.

Previous studies have described the wave-like phenomena appearing in color TDI after atrial contraction (Pislaru et al. 2014, 2017; Voigt et al. 2002). By using a multimodality (speckle tracking, M-mode, TDI) approach, we found that the dominant direction of local tissue motion within the wave pattern was longitudinal to the wave propagation direction, as illustrated by the absence of the wave pattern in a parasternal TDI recording. When this study was compared with Voigt et al. (2002), there was a significant difference in the reported propagation velocity range, which could be due to errors in manually measuring very fast phenomena with relatively low time resolution in that study. In our study, the velocity range in normal individuals was similar to those found in earlier studies that used similarly high frame rates (Pislaru et al. 2014, 2017) but we could not find a statistically significant difference in linearized velocities between normal and pathologic myocardium, despite the numerous differences (age, body mass index and echocardiographic parameters) between the two study groups. This was an unexpected finding as HCM ventricles were considered a pathologic model of increased muscle stiffness and diastolic dysfunction (Elliott et al. 2014; Mirsky and Parmley 1973; Villemain et al. 2018a, b). Also, the linearized propagation velocity of this wave-like pattern was not correlated with differences in blood pressure, septal thickness or echographic signs of diastolic dysfunction.

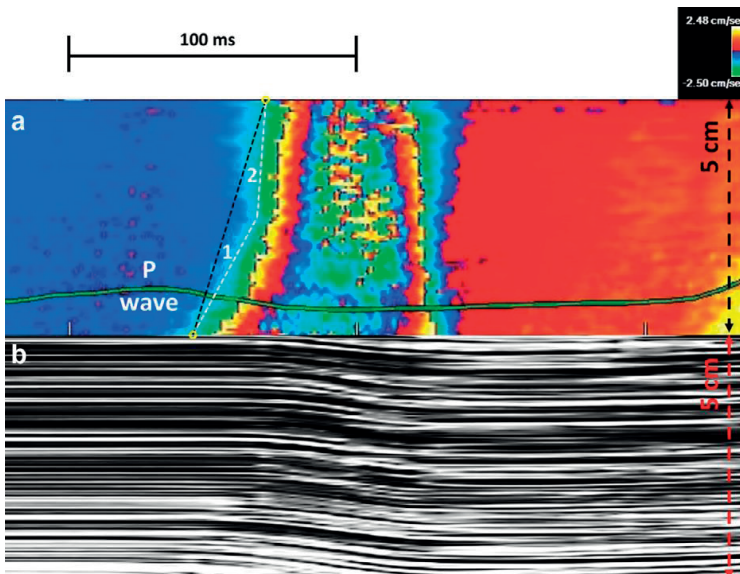


Figure 5. In more than 40% of the patients with hypertrophic cardiomyopathy, a non-constant shape of the initial front could be seen. (a) Tissue Doppler imaging velocity pattern. The straight line between the entry and exit points of the MSPa into the M-mode map (black dotted line) emphasizes the deviation of the first isovelocity front (white lines) from a constant propagation velocity. The first milder slope is marked '1' and the second steeper slope is marked '2'. (b) Anatomic M-mode of the underlying 2-D information along the same M-mode line, revealing the same variation in propagation velocity.

These findings differ from the results of previous studies (Pislaru et al. 2014, 2017). This triggered the in-depth analysis of TDI and 2-D data in search of an explanation.

We noticed the non-constant propagation of the front of the IVS deformation pattern post-atrial contraction, present in 42% of the HCM group, and this finding was statistically related to the septal thickness. Its appearance in the TDI map consists of a first mild slope (1.4 ± 0.5 m/s) in the basal part of the IVS followed by a very steep or almost vertical slope (Figs. 5 and 7) toward the apex, with an average velocity of 6.1 ± 3.4 m/s, which is much higher than the velocities measured in the group of healthy volunteers. Strikingly, the linearized MSPa velocity did not significantly differ between the two groups. On the other hand, it was significantly different when comparing only the non-constant velocity subgroup and normal volunteers (2.6 ± 0.8 m/s vs. 1.6 ± 0.3 m/s, $p < 0.0001$). This would suggest that only those patients with non-constant velocity propagation of the MSPa had higher myocardial stiffness than normal individuals. However, the two HCM groups were statistically similar, except for the septal thickness (19 ± 4 vs. 16 ± 3 mm, $p = 0.02$).

With respect to this very steep slope, although HCM is associated with higher myocardial stiffness, such high propagation velocities have not been measured with an alternative stiffness measurement that uses induced shear waves by (Villemain et al. 2018a,b). They measured an average velocity of 3.5 m/s in the diastolic phase for HCM patients, which is a factor of 2 less than our average values in the steep slope. One explanation might be related to the physics of such traveling waves. The pulling action of the atria on the ventricle induces a wave in which the particle motion is mainly in the direction of its propagation (i.e., along the wall), as also observed by the absence of a TDI wave pattern in the parasternal view. Such waves might behave as symmetric Lamb waves, as opposed to asymmetric Lamb waves or bulk shear waves which are generated with the technique applied by (Villemain et al. 2018a,b). The symmetric zero-order Lamb waves have a higher propagation velocity than bulk shear waves, up to a factor between 1.7 and 2 for a frequency range of nearly 040 Hz, as estimated by a wall thickness of 1 cm and propagation speed of 2 m/s (Brum 2019). Hence, the MSPa, purely because of its dominant longitudinal tissue motion direction, would expectedly lead to propagation velocities higher than those found by Villemain et al., but it is very unlikely that they would reach well over 10 m/s.

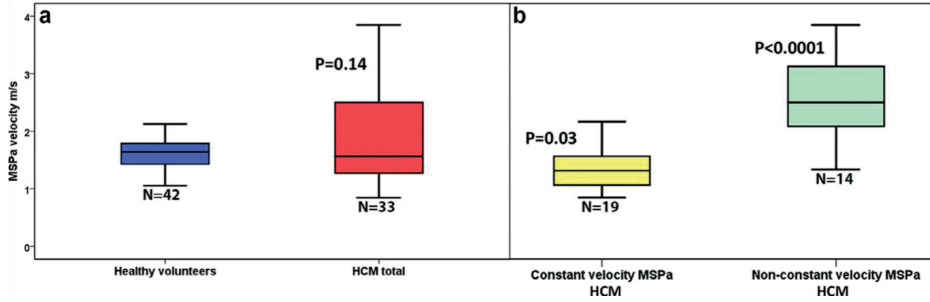


Figure 6. Linearized propagation velocity of the MSPa in the study population of normal volunteers and HCM patients. (a) Comparison between normal volunteers and the whole HCM group. Although the velocity range is larger in HCM, the difference remains statistically non-significant. (b) By splitting the HCM according to the constant or non-constant velocity of the MSPa, we obtain two subgroups. The subgroup with constant-velocity MSPa has a slightly lower linearized MSPa than normal volunteers (1.4 ± 0.4 m/s, $p = 0.03$), whereas the non-constant velocity group has a significantly higher linearized propagation velocity (2.6 ± 0.8 m/s, $p < 0.0001$). HCM = hypertrophic cardiomyopathy; MSPa = myocardial stretch post-atrial contraction.

Table 2. Logistic regression analysis of the parameters predicting an non-constant propagation of the MSPa in HCM patients (N=33).

Parameter	Univariate analysis		Multivariate analysis	
	95% CI	p	95% CI	P
Age	0.93-1.03	0.41	0.88-1.03	0.22
Gender	0.05-1.66	0.16	0.20-11.39	0.68
BMI	0.94-1.24	0.31		
Systolic blood pressure	0.98-1.08	0.21	1.01-1.20	0.02
Septal thickness	1.03-1.61	0.03	1.19-2.01	0.001
e'	0.73-1.48	0.84		
E/e'	0.91-1.11	0.97		

BMI: body mass index; CI: confidence intervals
Significant p values are highlighted in bold.

(Villemain et al. 2018a,b) mentioned that the stiffness was measured in diastole, but it is unclear whether the measurement was timed before, during or after the atrial contraction. This timing may be critical, as experimental studies of the ex vivo myocardium have found an exponential relation between stress and strain (Holzapfel and Ogden 2009; Mirsky and Parmley 1973; Villari et al. 1993; Weber 1989). Atrial contraction in end-diastole leads to a rapid increase in LV strain, which might thus result in a rapid increase in momentary stiffness in the case of HCM, especially when the myocardium is close to its maximum distensibility. On slow-motion 2-D videos (Supplementary Videos S1S4 at 220250 Hz), the progression of the local tissue stretch after atrial contraction can be directly seen, as can its relation to the global displacement of the left ventricular wall. In normal volunteers (Fig. 3), the LV wall never reaches the maximal possible tissue

distension permitted by the stiffer collagen network (Elliott et al. 2014; Weber 1989), allowing a progressive linear tissue stretch from base to apex. In the HCM patients in whom the slope was linear, some tissue distensibility may be preserved, and the LV stretch behaves similarly to that of normal individuals (Figs. 4 and 7a; Supplementary Video S2). In the more severe HCM patients, as the IVS becomes thicker and more rigid, the atrial contraction could induce a limited slow basal stretch, followed by a very steep movement of the entire LV wall as the hypertrophic ventricle reaches maximal longitudinal distension allowed by the collagen network (Figs. 5 and 7b; Supplementary Videos S3 and S4). In other words, the non-constant propagation would be caused by the shift from the myocardial stiffness to the stiffness of the limiting and more rigid collagen network surrounding the myocardial fibers. Depending on the degree of tissue distension existing before the atrial contraction, this shift may occur sooner or later, explaining the pattern in Figures 5 and 6, as well as the rigid wall motion seen in Supplementary Videos S3 and S4. Loading conditions will affect the strain of the myocardium and thus could drastically alter the propagation velocity of the MSPa (Voigt et al. 2002).

With respect to the initial mild slope, we discuss two possible explanations. First, the local stiffness of the basal septum could be lower than that of other parts of the septum, and similar to healthy tissue. Yet, this is less likely in HCM, where muscle stiffening is expected to be diffuse. Second, if the tissue is indeed reaching a maximum distension during the atrial kick, then it would still be in an elastic state at the onset of the atrial kick, with its associated baseline stiffness values. Table 1 outlines a non-significant difference in the linearized propagation velocity of MSPa in the entire HCM group compared with healthy volunteers.

On the other hand, if the HCM group is split on the presence of the nonconstant propagation velocity, the difference between the two HCM subgroups is significant (2.6 ± 0.8 m/s vs. 1.4 ± 0.4 m/s, $p < 0.0001$), as is that between the nonconstant propagation and the healthy volunteer group (2.6 ± 0.8 m/s vs. 1.6 ± 0.3 m/s, $p < 0.0001$). We also noted that HCM patients had a significantly lower a_0 velocity in pulsed TDI, as well as a lower a_0 acceleration slope. This finding could be interpreted as a lower and slower traction on the basal septum, potentially resulting in a slower basal stretch through viscous effects. This slower basal stretch remains directly visible in grayscale motion (Supplementary Video S4).

As for the possible transversal component, we expected this to be visible in the parasternal window in TDI (particle vibration in line with the Doppler), as already found for naturally occurring shear waves (Strachinaru et al. 2017). But in our patients, no wavelike

pattern could be seen in parasternal TDI after atrial contraction. From this observation we conclude that the dominant motion is a longitudinal stretch along the septal wall.

In 2-D imaging, the longitudinal stretch (MSPa) is shortly followed by an outward displacement of the whole LV wall, explained by the pressure rise in the ventricle after atrial contraction, which is called the volume stretch (atrial “volume kick”) and visualized by velocity vector imaging (Supplementary Videos S2 and S3). As it occurs later in time, that phenomenon is separate from the MSPa, which we consider in this study, and therefore out of the scope of the present study.

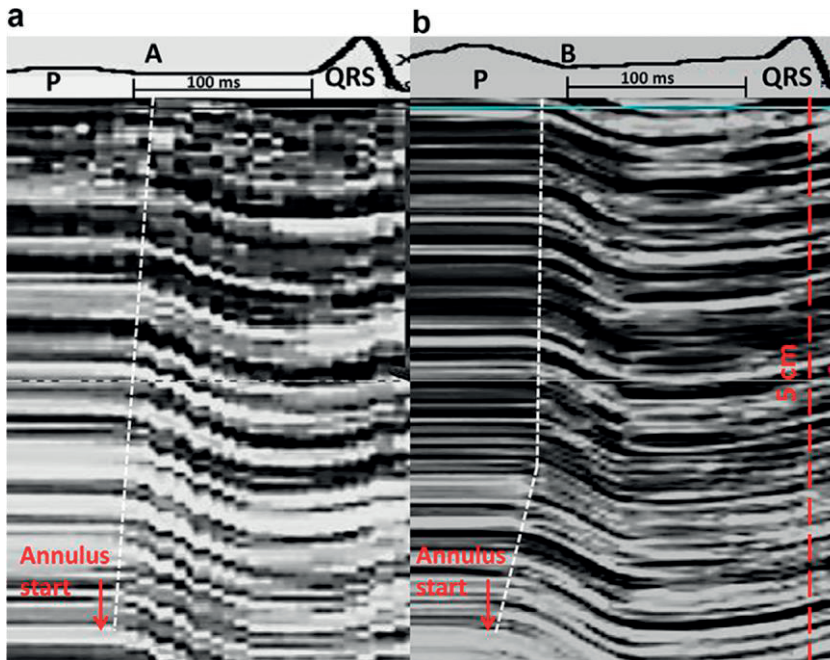


Figure 7. Magnified zoomed-in view of anatomic M-mode tracings along the interventricular septum, at 250 Hz, over 5 cm, just after the start of the echocardiogram P wave and before the onset of the next QRS complex. The annulus is marked with a red arrow. (a) HCM patient with a linear MSPa velocity slope. The downward tissue shift as seen propagating along the M-mode line also follows a straight line (dotted line). (b) HCM patient exhibiting non-constant velocity of the MSPa. The first tissue downward motion has an initial milder slope, followed by a very steep one along the M-mode line. HCM = hypertrophic cardiomyopathy; MSPa = myocardial stretch post-atrial contraction.

Limitations

High-frame-rate imaging represents a compromise between spatial and temporal resolution. The error in velocity estimation for very fast phenomena is larger with higher propagation velocity, lower frame rate and shorter traveling distance. A wave traveling

at 2 m/s needs 25 ms to travel over a 5-cm length. At 5 m/s this time is reduced to 10 ms, and at 10 m/s, to 5 ms. At a frame rate of 540 Hz, the time resolution is a little less than 2 ms, which is sufficient to detect the general behavior of the MSPa in normal individuals, but the error may be significant for velocities >10 m/s (see error analysis in Strachinaru et al. 2017, Appendix 1). Higher frame rates and averaging over multiple measurements would increase the accuracy of the propagation velocity measurements, which may be needed for actual clinical application.

The significance of our findings is limited by the number of patients. However, the non-constant propagation velocity was present in about half the patients even in this small group of HCM patients. Age matching was initially proposed for checking group variances, but was no longer considered, given the absence of statistically significant difference for the linearized MSPa between the study groups, despite their heterogeneity.

Tissue Doppler imaging velocities are known to be subject to angle dependency and cannot differentiate local deformation from global displacement (Dandel et al. 2009). Angle dependency was a minor issue in the TDI signal of the IVS in apical view because the motion was parallel to the ultrasound beam (Fig. 2). The absence of differentiation between local and global displacement was overcome by also studying tissue motion over the anatomic M-mode and by 2-D image analysis. Those measurements confirmed the findings from the TDI analysis.

As in previous studies, tracking of the MSPa was performed manually, which may increase the variability in velocity estimation, but to reduce this variability we traced a straight reference line between the entry and exit points of the MSPa into the M-mode map in all patients and adjusted it by frame-to-frame analysis as described under Methods. This line acted also as reference for the possible deviation of the MSPa from linearity.

Clinical implications and future directions

Analyzing the MSPa provides deeper insight into the diastolic function of the LV, as our findings suggest that the LV wall of HCM patients in diastole rapidly reaches a point where further longitudinal straining is constricted by the stiffer collagen network.

Because the MSPa does not exhibit the typical properties of an oscillatory shear wave, direct calculation of elasticity stiffness from its propagation velocity should be done with caution. Most likely, the propagation of the isovelocity front depends on the stress-strain relationship of the tissue, the actual strain during the atrial contraction, additional stresses caused by the LV loading conditions, and wall thickness, structure and geometry (Holzapfel and Ogden 2009; Villari et al. 1993; Voigt et al. 2002; Weber 1989).

Therefore, calculating stiffness values from TDI measurements assuming a linear propagation velocity, as has been done in earlier studies, may be an oversimplification and may miss clinically relevant deviations from this assumption. However, the presence of a non-linear MSPa seems to indicate more advanced disease in HCM, with a significantly thicker septum and presumably more fibrosis. Further research may be directed to using this as a qualitative sign of disease severity without the need to directly compute stiffness values.

CONCLUSIONS

The onset of the left ventricular end-diastolic myocardial stretch after atrial contraction exhibits a constant and quantifiable propagation velocity in normal individuals, but a non-constant velocity in about half of the HCM patients in the study. This deviation of the TDI velocity pattern can be explained by a non-linear relation between strain and stress and the inhomogeneous structure of the LV wall, even more apparent in thickened hypertrophic myocardium. This would imply clinical relevance, but actual quantification of tissue elasticity should be performed with care.

REFERENCES

- Brekke B, Nilsen LC, Lund J, Torp H, Bjastad T, Amundsen BH, Stoylen A, Aase SA. Ultra-high frame rate tissue Doppler imaging. *Ultrasound Med Biol* 2014;40:222–231.
- Brum J. Transverse Wave Propagation in Bounded Media. In: Nenadic I, Urban M, Greenleaf J, Gennisson JL, Bernal M, Tanter M, (eds). *Ultrasound elastography for biomedical applications and medicine*. Hoboken, NJ: Wiley; 2019. p. 93–96.
- Cikes M, Tong L, Sutherland GR, D'hooge J. Ultrafast cardiac ultrasound imaging: Technical principles, applications, and clinical benefits. *JACC Cardiovasc Imaging* 2014;7:812–823.
- Dandel M, Lehmkuhl H, Knosalla C, Suramelashvili N, Hetzer R. Strain and strain rate imaging by echocardiography—Basic concepts and clinical applicability. *Curr Cardiol Rev* 2009;5:133–148.
- Elliott PM, Anastasakis A, Borger MA, Borggrefe M, Cecchi F, Charron P, Hagege AA, Lafont A, Limongelli G, Mahrholdt H, McKenna WJ, Mogensen J, Nihoyannopoulos P, Nistri S, Pieper PG, Pieske B, Rapezzi C, Rutten FH, Tillmanns C, Watkins H. 2014 ESC Guidelines on diagnosis and management of hypertrophic cardiomyopathy: The Task Force for the Diagnosis and Management of Hypertrophic Cardiomyopathy of the European Society of Cardiology (ESC). *Eur Heart J* 2014;35:2733–2779.
- Giorgi H. *The physics of waves*. 171197 Englewood Cliffs, NJ: Prentice Hall; 1993. p. 282–284.
- Holzapfel GA, Ogden RW. Constitutive modelling of passive myocardium: A structurally based framework for material characterization. *Philos Trans A Math Phys Eng Sci* 2009;367:3445–3475.
- Kanai H. Propagation of vibration caused by electrical excitation in the normal human heart. *Ultrasound Med Biol* 2009;35:936–948.
- Mirsky I, Parmley WW. Assessment of passive elastic stiffness for isolated heart muscle and the intact heart. *Circ Res* 1973;33:233–243.
- Pernot M, Couade M, Mateo P, Crozatier B, Fischmeister R, Tanter M. Real-time assessment of myocardial contractility using shear wave imaging. *J Am Coll Cardiol* 2011;58:65–72.
- Pislaru C, Pellikka PA, Pislaru SV. Wave propagation of myocardial stretch: Correlation with myocardial stiffness. *Basic Res Cardiol* 2014;109:438.
- Pislaru C, Alashry MM, Thaden JJ, Pellikka PA, Enriquez-Sarano M, Pislaru SV. Intrinsic wave propagation of myocardial stretch, a new tool to evaluate myocardial stiffness: A pilot study in patients with aortic stenosis and mitral regurgitation. *J Am Soc Echocardiogr* 2017;30:1070–1080.
- Song P, Bi X, Mellema DC, Manduca A, Urban MW, Greenleaf JF, Chen S. Quantitative assessment of left ventricular diastolic stiffness using cardiac shear wave elastography: A pilot study. *J Ultrasound Med* 2016;35:1419–1427.
- Strachinaru M, Bosch JG, van Dalen BM, van Gils L, van der Steen AFW, de Jong N, Geleijnse ML, Vos HJ. Cardiac shear wave elastography using a clinical ultrasound system. *Ultrasound Med Biol* 2017;43:1596–1606.
- Strachinaru M, Bosch JG, van Gils L, van Dalen BM, Schinkel AFL, van der Steen AFW, de Jong N, Michels M, Vos HJ, Geleijnse ML. Naturally occurring shear waves in healthy volunteers and hypertrophic cardiomyopathy patients [e-pub ahead of print]. *Ultrasound Med Biol*. doi: <https://doi.org/10.1016/j.ultrasmedbio.2019.04.004>, Accessed May 10, 2019.

- Vejdani-Jahromi M, Freedman J, Nagle M, Kim YJ, Trahey GE, Wolf PD. Quantifying myocardial contractility changes using ultrasound-based shear wave elastography. *J Am Soc Echocardiogr* 2017;30:90–96.
- Villari B, Campbell SE, Hess OM, Mall G, Vassalli G, Weber KT, Krayenbuehl HP. Influence of collagen network on left ventricular systolic and diastolic function in aortic valve disease. *J Am Coll Cardiol* 1993;22:1477–1484.
- Villemain O, Correia M, Khraiche D, Podetti I, Meot M, Legendre A, Tanter M, Bonnet D, Pernot M. Myocardial stiffness assessment using shear wave imaging in pediatric hypertrophic cardiomyopathy. *JACC Cardiovasc Imaging* 2018a;11:779–781.
- Villemain O, Correia M, Mousseaux E, Baranger J, Zarka S, Podetti I, Soulat G, Damy T, Hagege A, Tanter M, Pernot M, Messas E. Myocardial stiffness evaluation using noninvasive shear wave imaging in healthy and hypertrophic cardiomyopathic adults [e-pub ahead of print]. *JACC Cardiovasc Imaging* 2018b; doi: 10.1016/j.jcmg.2018.02.002. Accessed November 23, 2018.
- Voigt JU. Direct stiffness measurements by echocardiography: Does the search for the holy grail come to an end? [e-pub ahead of print] *JACC Cardiovasc Imaging*. doi: <https://doi.org/10.1016/j.jcmg.2018.02.004>, Accessed 9 March 2018.
- Voigt JU, Lindenmeier G, Werner D, Flachskampf FA, Nixdorff U, Hatle L, Sutherland GR, Daniel WG. Strain rate imaging for the assessment of preload-dependent changes in regional left ventricular diastolic longitudinal function. *J Am Soc Echocardiogr* 2002;15:13–19.
- Vos HJ, van Dalen BM, Heinonen I, Bosch JG, Sorop O, Duncker DJ, van der Steen AF, de Jong N. Cardiac shear wave velocity detection in the porcine heart. *Ultrasound Med Biol* 2017;43:753–764.
- Weber KT. Cardiac interstitium in health and disease: The fibrillar collagen network. *J Am Coll Cardiol* 1989;13:1637–1652.

13

High Frame Rate echoPIV can estimate the high velocity diastolic flow patterns in 2D

Based on:

Vorneveld J, Keijzer LBH, **Strachinaru M**, Bowen DJ, Goei JSL, Ten Cate F, van der Steen AFW, de Jong N, Vos HJ, van den Bosch AE, Bosch JG. *High Frame Rate echoPIV can Measure the High Velocity Diastolic Flow Patterns*. *Circ Cardiovasc Imaging*. 2019;12(4):e008856.

Left ventricular (LV) flow patterns have been studied as potential early stage markers of cardiac dysfunction (1). A relatively new method of measuring LV flow patterns, named echo-particle image velocimetry (echoPIV), tracks the motion of ultrasound contrast agent (UCA) microbubbles in the blood using echocardiography. However, the low frame rates (50-70 Hz) permitted by the current generation of clinical ultrasound scanners causes velocity magnitudes during filling and ejection to be severely underestimated. This is due to the relatively large displacement of the bubbles between frames. The recent feasibility of high frame rate (HFR) echocardiography, using diverging-wave transmission schemes, has allowed for frame rates of up to 100 times faster than conventional imaging methods (2). The image quality improvements when using HFR contrast enhanced ultrasound (CEUS) over standard CEUS have recently been described in (3). Still, measurement of the high energy and high velocity trans-mitral jet has yet to be demonstrated in humans. We have shown previously, in an *in vitro* LV phantom study, that HFR echoPIV can accurately measure the high energy diastolic flow patterns (4). In this work we demonstrate that this holds true in a patient with heart failure.

A patient with dilated cardiomyopathy, admitted for right decompensation cordis (forming part of a study approved by the medical ethics committee of the Erasmus Medical Center), was scanned using both a clinical scanner (EPIQ 7, Philips Healthcare, Best, the Netherlands), and an open research scanner (Verasonics Vantage 256, Verasonics, Kirkland, WA) with a P4-1 probe (ATL). Pulsed-wave (PW) Doppler measurements were obtained, using the clinical scanner, in the region of the mitral valve. UCA (SonoVue®, Bracco Imaging SpA, Milan, Italy) was then continuously infused at 0.6 ml/min (VueJect BR-INF 100, Bracco Imaging) and arrival in the LV verified with the clinical scanner. The research scanner was then used to obtain HFR CEUS acquisitions using a 2-angle (-7°, 7°) diverging wave sequence with pulse inversion at a pulse repetition frequency of 4900 Hz, resulting in an imaging frame rate of 1225 Hz. EchoPIV analysis was performed in the polar domain, using custom PIV software that used correlation compounding on ensembles of 5 frames for each angled acquisition separately (total of 10 frames of averaging \approx 4 ms) (4). The final vector-grid resolution was 1.25° by 1.25 mm. HFR echoPIV magnitudes were validated by comparing the mean temporal velocity profile to the PW Doppler spectrum captured in the same locations.

The velocities measured with HFR echoPIV agreed well with the PW Doppler spectrum (Figure 1.a), with peak velocities up to 80 cm/s accurately measured in this patient. This is the first demonstration of echoPIV estimating the high velocity trans-mitral jet; where previously the use of conventional echocardiography resulted in severe underestimation of the velocity magnitude. The high temporal resolution also permits study of the flow patterns in greater detail. Such as the large, central clockwise vortex that could be

observed developing off of the trans-mitral jet before migrating apically (Figure 1: b-d: *). Smaller, more transient vortices could also be observed, for example the counter-clockwise vortex between the jet and the free-wall (Figure 1b: #).

HFR echoPIV has been demonstrated in a heart failure patient and we have shown that it is feasible to measure the high velocity diastolic flow patterns in 2D, previously unobtainable through conventional ultrasound imaging.

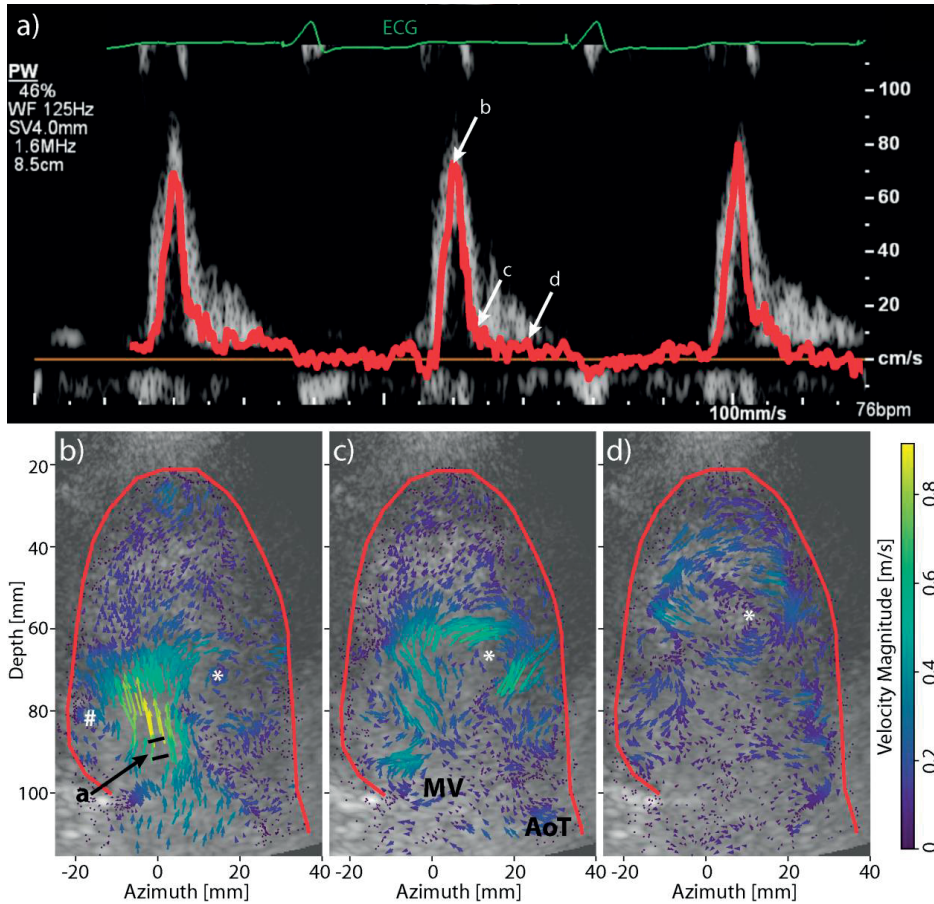


Figure 1. a) Mean echoPIV velocity (red) overlaid on Pulsed-wave Doppler spectrogram obtained in mitral valve region. b-d) Velocity map visualisations during diastolic filling (temporal locations marked in a), showing the high velocity trans-mitral jet entering the ventricle (b) and central clockwise vortex that starts basally and migrates apically (c-d). See Supplementary Media for video of sequence. MV = Mitral valve, AoT = Aortic outflow tract. *Large, persistent clockwise vortex that pinches-off the jet and migrates apically. # Small, transient counter-clockwise vortex constrained by free-wall.

REFERENCES

1. Sengupta PP, Pedrizzetti G., Kilner PJ., et al. Emerging trends in CV flow visualization. *JACC Cardiovasc Imaging* 2012;5(3):305–16. Doi: 10.1016/j.jcmg.2012.01.003.
2. Tanter M., Fink M. Ultrafast imaging in biomedical ultrasound. *IEEE Trans Ultrason Ferroelectr Freq Control* 2014;61(1):102–19. Doi: 10.1109/TUFFC.2014.6689779.
3. Toulemonde MEG., Corbett R., Papadopoulou V., et al. High Frame-Rate Contrast Echocardiography: In-Human Demonstration. *JACC Cardiovasc Imaging* 2018;11(6):923–4. Doi: 10.1016/j.jcmg.2017.09.011.
4. Voorneveld J., Muralidharan A., Hope T., et al. High Frame Rate Ultrasound Particle Image Velocimetry for Estimating High Velocity Flow Patterns in the Left Ventricle. *IEEE Trans Ultrason Ferroelectr Freq Control* 2017:1–1. Doi: 10.1109/TUFFC.2017.2786340.



14

Discussion

Echocardiography has been searching for a long time for a reliable, simple and direct way to characterize the myocardial function and the diastolic properties of the heart¹⁻³. But without being able to "look" inside the muscle, everything was based on shape change, global and local deformation, blood flow, and indirect estimation of pressure gradients.

1. CLASSICAL APPROACHES

The *first part of this thesis* explores the limitations of the classical approach to diastology.

The American Society of Echocardiography and European Association of Echocardiography (ASE/EAE) have published algorithms for the grading of diastolic function by echocardiography². In an effort to increase the yield of clinical diastolic function assessment, we directly compared the feasibility and results of two slightly different diagnostic algorithms for diastolic function based on classical echocardiographic parameters. The ASE/EAE and Thorax Centrum (TXC) algorithms could not precisely classify 48 % of patients and 10 % respectively³. The authors of the multi-center Euro-Filling study found only 17% of undetermined cases by the latest recommended algorithm of the ASE/EAE⁴. Although the TXC algorithm performed better in our patient group, a clinical validation study including outcome and ideally reference gold standard (invasive measurement of left ventricular (LV) pressures) is still necessary. This means that in daily clinical practice it may be difficult to grade diastolic dysfunction with any scheme based on classical echocardiographic parameters, and many relevant patients may fall into the grey area of uncertainty.

One objective parameter of increased LV filling pressures is the echocardiographic ratio of the transmitral E-wave velocity and early diastolic velocity of the myocardium, the so-called E/e' ratio. In the Euro-Filling study only modest correlations were seen between E/e' and invasive pressure measurements⁴. It is not clear whether this poor correlation would also be translated into a poor correlation with other signs, symptoms or biomarkers of heart failure.

In a group of elderly patients with severe symptomatic aortic stenosis we studied the possible relationship between the E/e' ratio and biomarkers of elevated intracardiac pressure. We found a significant but moderate correlation between the E/e' ratio and NT-proBNP⁵. The correlation was best for the septal point E/e' ($r=0.584$, $r^2=0.34$, $P<0.0001$); the lateral ($r=0.377$, $r^2=0.14$, $P<0.0001$) and the average E/e' ($r=0.487$, $r^2=0.24$, $P<0.0001$) having slightly lower levels of correlation. This level of correlation with NT-

proBNP is slightly better than found in the Euro-Filling study against invasive pressure measurements⁴. It is noteworthy that both in our study and the Eurofilling study a slight superiority in measuring the septal point as compared to the lateral or even the average E/e' was seen.

In the same group of elderly patients with severe aortic stenosis, the independent predictors for baseline pulmonary artery pressure (PAP) were the body mass index ($\beta=0.21$, $p=0.006$), COPD GOLD class ($\beta=0.20$; $p=0.009$), the E/e' ratio ($\beta=0.20$; $p=0.02$) and the degree of aortic regurgitation ($\beta=0.20$; $p=0.01$). After receiving a TAVI prosthesis, there was significantly less (51% vs 29%, $p<0.0001$) pulmonary hypertension, defined as a tricuspid regurgitation velocity ≥ 2.8 m/s. The baseline variables related to an improvement in PAP were the tricuspid regurgitation velocity ($p=0.0001$) and the E/e' ($p=0.005$). From the parameters potentially modified with TAVI, the only independent predictor of PAP variation was the change in the E/e' ratio ($\beta=0.23$; $p=0.005$). This suggests that PAP evaluation by echocardiography needs to be a part of the prognostic estimation of potential TAVI candidates, along with the filling pressures of the left ventricle, the two elements being interconnected. E/e' remains the most important echocardiographic parameter to be considered.

Another precise parameter used as a cornerstone in the ASE/EAE algorithm is left atrial (LA) size which reflects the severity and chronicity of LV dysfunction^{2,6}. The clinical value of LA function has not yet been translated into recommendations, in part because of lack of reference ranges for normal condition⁶. In a monocentric prospective study on a healthy population with ages ranging between 20 to 72 years, we show that LA function assessed with volumetric and myocardial deformation methods is influenced by age and LV diastolic function⁷.

The global change in atrial volume during the cardiac cycle is simpler than that of the left ventricle, having mainly a longitudinal component, mostly due to the motion of the mitral annulus (which in turn is mostly due to left ventricular contraction and relaxation)⁸. When looking at the mitral annulus motion from the left atrial perspective, in end-diastole the left atrium contraction induces a supplementary volume inflow⁷ but also a rapid traction motion on the atrioventricular annulus⁸, that induces a supplementary increase in LV global longitudinal strain, contributing to filling and to the LV parietal tension in end diastole.

Classical echocardiographic parameters of systolic and diastolic function have a good sensitivity in symptomatic heart failure patients^{2,6}. However, diagnosing patients in the clinically symptomatic stage may be too late for any intervention aiming to a

complete recovery of function. These parameters should also provide sufficient sensitivity for relevant changes in stable patients or in the early stages of disease^{2,4,6}. In the prospective Bio-SHiFT study, we analyzed 332 echocardiograms in 106 patients during a median follow-up of 2.3 years. The endpoint comprised HF hospitalization, LV assist device implantation, heart transplantation, and cardiovascular-related death. Although individual temporal variations of echocardiographic parameters were associated with cardiovascular outcome independent of NT-proBNP levels, the average of these parameters remained stable during the 2.3 years follow-up and did not worsen as an adverse event approached. It thus seems that, in such a timeframe, routine frequent monitoring of systolic or diastolic function with classical echocardiography parameters does not carry incremental prognostic information over a single measurement in a minimally symptomatic and relatively young patient group⁹, suggesting that their sensitivity may be insufficient for early detection of a variation in the heart function.

The conclusion arising from the clinical investigations in the first part of this thesis is that the present-day echocardiographic evaluation of the LV diastolic function requires multiple parameters and complex algorithms that unfortunately lack sensitivity for detecting subtle changes in the LV function. There is an obvious need for a change in paradigm, with the search for new parameters and new ways of looking at the heart with ultrasound¹⁰.

2. HIGH FRAME RATE ECHOGRAPHY

The **second part of this thesis** proposes a new way of investigating the LV properties, based on passive shear wave imaging and high frame rate tissue Doppler imaging. Shear wave imaging offers a potential way of remotely "touching" the myocardium, thus being able to quantify its stiffness¹⁰. This thesis focuses at the shear waves that naturally occur on the interventricular wall after closure of the aortic and mitral valves. The shear waves consist of minute vibrations of the wall, and are detected through Tissue Doppler imaging. For the first time, we show that a clinical system in regular clinical mode is able to trace these naturally-occurring phenomena, which clearly simplifies the "bench to bedside" step. However, the frame rates provided by present day clinical tissue Doppler¹¹ echocardiography were observed to be on the lower side of obtaining sufficient accuracy to quantify shear waves. Moreover, related to the method itself, the properties of the waves had not yet been related to disease states of the heart. Thus, the second part of the thesis aimed at a clinical translation of the passive shear wave elastography method to the investigation of diseased states of the heart. Given the substance of the new results, we discuss the topics separately.

2.1 Shear wave elastography

We showed that passive shear wave imaging of the heart with a clinical high frame rate tissue Doppler application is feasible *in vivo* and can be used as a research tool. Based on physics, these shear waves propagate with a velocity that is presumed to be monotonically increasing with the stiffness of the tissue¹².

We observed that regular unmodified clinical systems can be set up by using only the normal system controls, in order to obtain color TDI frame rates above 500 Hz (500 to 710 Hz, depending on depth, line density and opening of the field of view). In Chapter 8 we showed that with a clinical tissue Doppler imaging (TDI) application we can accurately quantify the propagation velocity of shear waves induced *in vitro* in tissue phantoms by acoustic radiation force. We also show that we can detect and quantify the naturally-occurring shear waves in the heart with such clinical system¹³. This was the basis of the subsequent chapters.

Clinical cardiac TDI is set up to detect low velocity but high intensity signal, with a velocity scale in the order of cm/s¹¹. What TDI “sees” from a shear wave is the local particle vibration induced by the wave (Figure 11), with a velocity range (1 to 7 cm/s)^{13,14} that falls into the detection range of the TDI. The wave itself propagates with velocities in the range of 1 to 10 m/s in soft biological tissue such as the myocardium.

Because the TDI application detects the local tissue velocity (the velocity amplitude of the wave, see Introduction Section 7 and 10), these shear waves can best be detected by TDI in the parasternal views of the left ventricle rather than the apical views, and this relates, as shown in the Section 7 of the Introduction, to the properties of the wave and the technical particularities of tissue Doppler imaging.

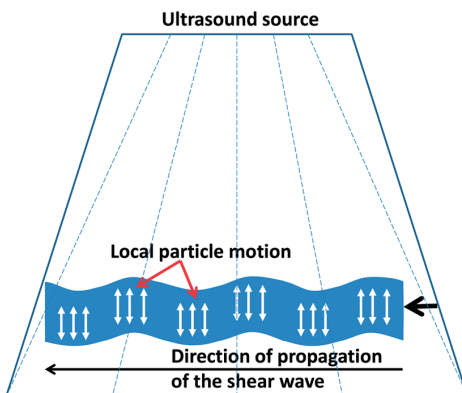


Figure 11. Conceptual drawing (Source: personal collection) of a shear wave propagating in a thin plate (the interventricular septum in parasternal longitudinal view of the left ventricle), with the shear wave source to the right (block arrow), corresponding to the atrioventricular and aortic annulus *in vivo*. Although the direction of propagation is perpendicular to the ultrasound scan lines (dotted lines), the tissue displacement within the wave is in line, and this local displacement is what the TDI system actually detects.

In the parasternal position, there are at least two possible probe rotations in which to investigate shear wave propagation: the long and the short axis views of the LV. We opted for the long axis view, where the propagation direction of the shear wave generated at the mitral or aortic annulus is in the imaging plane, with minimal angulation⁶, as demonstrated in Figure 12. The risk of error due to misalignment is minimized by using the classical anatomical landmarks defining the parasternal longitudinal view of the left ventricle, which place the shear wave sources into the field of view: the aortic valve and aortic annulus and the mid-portion of the mitral valve and mitral annulus.

Other research groups that investigated myocardial stiffness by externally-induced shear waves¹⁵⁻¹⁷ demonstrated an anisotropic propagation of the shear waves in the long versus the short axis. This may be due to geometric reasons (propagation of a wave in a straight versus a curved plate-like material), but also anatomical (tissue anisotropy due to fiber orientation). However, due to the same limitations imposed by the physical properties of the waves and the angle dependency of the clinical TDI application, the passive detection of shear waves in short axis was not feasible with our method.

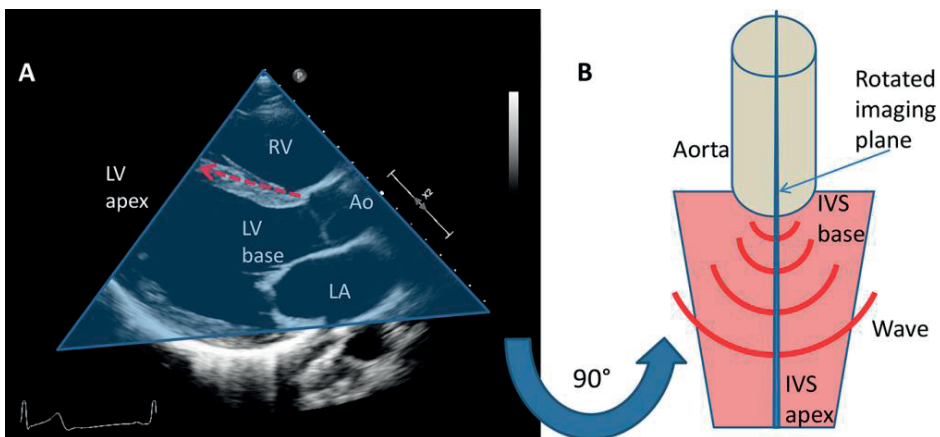


Figure 12. Relation between the shear wave propagation and the imaging plane in the parasternal long axis view (Source: personal collection). A: actual echocardiographic image. The shear waves appear at the valvular annulus and course along the interventricular septum (IVS) to the apex (arrow). B: the imaging plane represented by the transparent triangle in panel A is rotated 90° counterclockwise, with the LV apex towards the viewer. Shear waves generated at the atrioventricular or aortic annulus are perpendicular to the imaging plane (represented by the central blue line).

Other research groups analyzing the naturally-occurring shear waves in the heart with experimental high frame rate TDI have either opted for a parasternal longitudinal view^{18,19} or an apical view²⁰. With respect to the apical position, still being able to see the wave with TDI may be puzzling, given the fact that the particle vibration is perpendicular

to the Doppler interrogation lines. However, if the interventricular septum does not perfectly align in the middle of the image, which is rarely the case in the apical longitudinal view of the left ventricle, some angulation might exist allowing visualization of the shear waves (visualizing the local velocity vector that is parallel to the Doppler interrogation lines).

The shear wave after aortic valve closure in healthy volunteers was evaluated by all the TDI studies^{13,14,18-21}. The feasibility was very good, reported to 92%¹⁸ and 93%¹⁴ respectively, and the results were similar (Chapter 7). The only study describing aortic shear wave velocities in the apical approach reports much higher values (5.41 ± 1.28 m/s) in a group of only 10 healthy subjects²⁰. The reason for this difference is unclear, and may have to do with measurement errors as reflected by the large standard deviation, insufficient statistical power due to low numbers, or on a phenomenological level, the presence of a longitudinal component of the wave displacing with much higher velocity²². Such waves might behave as symmetric Lamb waves, as opposed to asymmetric Lamb waves or bulk shear waves which are measured in the parasternal position²³. The symmetric zero-order Lamb waves have a higher propagation velocity than bulk shear waves, up to a factor of 1.7 for lower frequencies²⁴. This implies that multiple types of waves could be simultaneously induced by valve closure, which would require either caution when translating propagation speeds into tissue stiffness, or standardization of parasternal versus apical measurements. Until such standardization is achieved, this point limits the reproducibility of the method in patients. Current efforts of our research group are directed to further understanding the correlation between parasternal and apical recordings.

For the shear wave after mitral valve closure a lower feasibility was observed^{14,21} possibly explaining the difference in results between the studies (4.65 ± 0.77 m/s in Strachinaru *et al* 2019¹⁴ vs 3.54 ± 0.93 m/s in Petrescu *et al* 2019¹⁹). One of the reasons for this lower feasibility may be the lower transvalvular gradient over the mitral valve leading to lower wave amplitudes. Moreover, Petrescu *et al* (2019) used tissue acceleration values to trace the shear waves, rather than tissue velocity values like we did. These points merit further investigation, since the two studies find a different relation between the aortic and mitral shear wave velocities.

In this thesis we show that we can identify, visualize, and isolate shear waves from other events and measure their velocity. In order to be clinically relevant, shear wave imaging needs to provide new and significant information, that cannot be obtained through present day clinical imaging. As already presented in the Introduction, there is a theoretical relation between shear wave velocity and the stiffness of a material¹².

Other research teams investigating externally-induced shear waves in the myocardium have even computed stiffness values based on this assumption¹⁵⁻¹⁷. Yet, as discussed in Chapter 10, 11 and 12, we believe that the dynamic nature of the instantaneous stiffness, as well as the inhomogeneous wall structure and the already known anisotropy^{15,25,26} in the longitudinal and radial direction make direct estimation of tissue stiffness more complicated than in theoretical homogeneous models. For the naturally-occurring shear waves the dynamic component of muscle contraction or relaxation is even more important because of the location of these events in the isovolumetric periods where the stiffness varies rapidly. Despite all these potential limitations, we demonstrate in Chapter 10 that naturally-occurring (passive) shear waves have very different propagation velocities in hypertrophic versus normal myocardium, which is a significant finding. The magnitude of this difference is around 2 m/s for the mitral valve shear wave and 1.5 m/s for the aortic shear wave (difference of the mean values found in healthy volunteers and hypertrophic cardiomyopathy patients)¹⁴. Similar very significant differences were observed by other research groups when comparing healthy volunteers with amyloidosis patients (2.8 m/s difference in mitral valve shear wave and 1.9 m/s in aortic shear wave)¹⁹. We do not know however how the shear wave velocities evolve over time in an individual patient as the heart progresses from normal to the extreme pathologic as used here for comparison. In other words, future studies should demonstrate that shear wave velocities not only differ drastically in extremely ill patients as compared to normal individuals, but also follow a continuum of velocity values as the myocardium gets progressively sicker and stiffer.

In Chapter 11 we show that passive shear waves can even help differentiate intratissular variations in the elastic properties. The ability to detect two different levels of pathological stiffness in the same patient (the abnormally stiff hypertrophic cardiomyopathy myocardium and the scar tissue post septal reduction therapy) partially gives a positive answer to the question of progression of disease mentioned above. Being able to detect localized variations in tissue stiffness inside the myocardium would potentially allow a quantitative mapping of the myocardial stiffness, that could for example be rendered in color-coded stiffness maps, in a similar manner to that presently used in parenchymatous organs¹². These maps could be obtained by multiple determinations of shear wave velocities across the left ventricular wall, provided that the spatial resolution of this method is smaller than at least the half of the minimum width of the LV wall (allowing at least 2 lines to be traced and separately resolved). Again, the sensitivity threshold should also be sufficient in order to detect significant local variations in velocity.

2.2 The myocardial stretch post atrial contraction

Atrial contraction exerts a mechanical traction motion on the atrioventricular annulus²⁷ (Chapter 6). After atrial contraction a strain rate wave-like pattern visible in the LV myocardium was reported by Voigt *et al*²⁸ who estimated its propagation velocity between 2 and 4.6 m/s in the interventricular septum (IVS) of normal individuals at a frame rate of 178 Hz. They demonstrated the value to be preload dependent. Later, Pislaru *et al* investigated the same Tissue Doppler Imaging (TDI) velocity and strain rate pattern with higher frame rates (250-465 Hz) and computed the values at 1.4 ± 0.2 m/s in normal individuals, 2.2 ± 0.7 m/s in severe aortic stenosis patients^{29,30} and 3.2 ± 1.0 m/s in amyloidosis³¹. Yet, the exact nature and behavior of this tissue velocity-based pattern remain unclear. These earlier studies hypothesized that the fast traction on the mitral annulus by the atrial contraction generates a wave in the left ventricular wall, which travels from base to apex with a constant velocity which is related to the underlying tissue stiffness. It was also hypothesized that this wave had a radial component³⁰.

We show in Chapter 12 that the myocardial stretch in late diastole induced by the atrial contraction (MSPa) does not display a linear behavior in pathological myocardium, making it more difficult to use in directly calculating tissue stiffness from its propagation velocity. As mentioned earlier, this wave-like event showed initially a lot of promise, being ideally situated in late diastole, precisely after a relatively long period of equilibrium (diastasis), when the LV myocardium should be in its most relaxed state. We started our study with the intention of further understanding the behavior of this TDI pattern and further expanding the very interesting results obtained by previous researchers. The results described in Chapter 12 raise concerns regarding the very nature of this event (rather a progressive myocardial stretch than a wave) and its direct relation to the myocardial stiffness (non-linear behavior in pathological myocardium). It is interesting to mention that previous studies found only linear propagation, with the highest velocity in severe aortic stenosis patients³⁰ (2.2 ± 0.7 m/sec) and in amyloidosis (3.2 ± 1.0 m/s)³¹. In our group of hypertrophic cardiomyopathy patients, we found linear and non-linear propagation, the latter appearing in the more diseased ventricles (significantly thicker septum). It is possible that MSPa behaves linearly up to a certain degree of disease (in our study a certain degree of tissue distensibility), and non-linearly beyond. This obviously elicits for more research, in a larger array of pathologies, and in progressive degrees of disease. If the velocity of linear propagation of the MSPa cannot be reliably used for tissue stiffness calculation, the appearance of the non-linear propagation might be used as a qualitative sign of extreme tissue stiffness³² (lack of distensibility in end-diastole).

2.3 Intracardiac flow patterns

High frame rate imaging shows promising results in tracking and quantifying intracardiac diastolic flow patterns. A significant part of the parietal tension of the LV is given by the filling state, currently represented by preload and afterload^{13,32}. There is a dynamic relation between parietal tension induced by filling and filling itself. This has until now been exploited to indirectly estimate the diastolic properties of the LV². As already mentioned in Chapters 10, 11 and 12, *in vivo* tissue stiffness measured by shear wave imaging is expected to be influenced also by preload and afterload. Measured stiffness may need to be corrected for these parameters³². In Chapter 13 we estimated the intracardiac flow with high frame rate imaging, by using an experimental system being able to reach very high frame rates (1000+ FPS) with full sector opening. We propose a new application of high frame rate imaging, the *in vivo* analysis of diastolic blood flow into the left ventricle. Echo-particle image velocimetry (echoPIV) is already used with regular clinical systems³³. However, the relatively low frame rates (50-70 Hz) permitted by the current generation of clinical ultrasound scanners causes velocity magnitudes during filling and ejection to be severely underestimated. Our algorithm (Chapter 13) tracks the motion of ultrasound contrast agent microbubbles in the blood using very high frame rates, allowing to detect diastolic velocities with similar accuracy as the pulsed-wave Doppler³⁴ at least up to about 1 m/s. Future high frame rate systems could incorporate blood flow tracking and shear wave imaging in the same analysis, allowing for combined and corrected indices (shear wave velocity, corrected by volume and inflow velocity variation derived from high frame rate imaging).

3. PHYSIOLOGICAL INTERPRETATION

We show in this thesis that we can quantify markers of instantaneous tissue stiffness, at several points during the cardiac cycle. How can we expand this data to the diastolic function of the left ventricle?

Naturally-occurring shear waves are present during the isovolumetric periods. The instantaneous LV wall stiffness has several components: an active component due to muscle contraction, a parietal tension derived from Laplace's law and an inert elasticity of the fully relaxed wall. The instantaneous value of stiffness is the result of these dynamic and static components^{14,21}. Our detection method is able to record naturally occurring shear waves during these two moments in the cardiac cycle: one in early systole (induced by mitral valve closure) and the other in early diastole (induced by aortic valve closure). Although none of these moments corresponds to a truly diastolic state (full relaxation of the LV myocardium), the significant difference found in this thesis

between normal and non-compliant myocardium suggests that the naturally occurring shear waves could be clinically relevant in estimating myocardial stiffness (Chapter 10). The stiffness and hence, the shear modulus, varies in time throughout the cardiac cycle^{15,23,25,26,35}, thus changing the instantaneous shear wave velocity.

When expanding to the whole duration of the diastole, as already known from pressure-volume loops, LV compliance also varies with each heart cycle, and with the preload and afterload of the ventricles, and may further be influenced by the interventricular interdependence induced by the closed pericardial space^{36,37}. In these conditions, a very punctual measurement may not be completely representative of the diastolic function.

In order to make the step from instantaneous stiffness using just information derived from naturally-occurring shear waves to a more comprehensive evaluation of the diastolic function, we could study an echocardiographic index based on the relation of the shear wave velocities measured during the two isovolumetric periods (difference, average, ratio)^{18,32} (Chapter 9). However, looking at the data obtained so far (Chapter 9 and 10), we note that the feasibility for the mitral valve shear wave is lower than for the aortic shear wave, both with the clinical TDI application (89% in healthy volunteers and 56% in HCM patients)¹⁴ and the modified high frame rate clinical system we used for comparison (66% in healthy volunteers)²¹. That means that in around 50% of the patients such a derived index will not be feasible with the present method. Possible solutions would be using only one of the two time points which has better feasibility (the shear wave after aortic valve closure, with a feasibility of 93% in healthy volunteers and 88% in HCM), or finding a technical solution to optimize the detection of the mitral closing shear wave. In Chapter 10 we opted for the second approach, lowering the TDI velocity scale in separate acquisitions in order to selectively optimize the feasibility of the mitral valve shear wave. This allowed for a notable difference as mentioned above (89% with dedicated settings vs 66% with general settings in healthy volunteers).

Another possible approach to the diastolic function through shear wave imaging would be a continuous or triggered multi-point determination of shear wave velocities during the cardiac cycle, as has already been done in experimental settings²⁵ by using externally-induced shear waves.

4. COMPARISON TO OTHER TECHNIQUES

Other research teams have focused on externally-induced shear waves, and showed significant findings^{15-17,25,26}. These externally-induced waves require a short burst (300

μs)¹⁶⁻¹⁷ of focused ultrasound (acoustic radiation force push) into the myocardium in order to induce a local excitation, that would then propagate as a shear wave in all directions. These bursts were triggered by an ECG and positioned in end-diastole, before the P wave. Then, using the same probe the shear waves were tracked with very high frame rates (around 5000 Hz), also in the parasternal position, but both in short and long axis, allowing for estimation of the local myocardial anisotropy^{15,16,26}.

In spite of the different excitation source, tracking method and the important difference in frame rates used, the two methods compare in several aspects:

- Shear waves are generated both naturally, by valve closure, and by acoustic radiation force. Since shear wave tracking by successive pulses during the whole heart cycle has been described²⁵, it is theoretically possible to measure instantaneous shear waves velocities throughout the cardiac cycle and compare the results that are simultaneous to the naturally-occurring shear waves. In practical terms this may prove difficult for several reasons. First, by using serial high energy bursts to induce shear waves the acoustic energy deposit is above regulations¹⁵. Second, the shear waves induced during the systolic period have lower amplitude²⁵, making their detection difficult with thoracic imaging. Third, generating actual systolic and diastolic stiffness maps needs a high sampling rate, which is actually technically achievable. Push-detection cycles in the study by Pernot *et al*²⁵ were performed in 5 ms and repeated every 7.5 ms, thus achieving a sampling rate of 133 measurements per second *ex vivo*. Such high repetition frequency of the push-detection sequence would surely exceed current acoustic safety limits for human exams, thus limiting translation to clinical application. To overcome this safety limitation, the *in vivo* heart rate could be temporarily slowed down by medication, allowing a lower sampling rate to still reach the same number of samples per cycle, or the trigger point could be moved progressively and data from several heart beats be stitched onto a single artificial heart beat. These are possible modalities to improve sampling rate per cycle while staying below acoustic safety limits.

- Externally-induced waves have the advantage of being controlled by the user, so independent from valve structure and mobility or transvalvular gradients. They can also be studied during the phases of the cardiac cycle when the stiffness of the LV is lowest and varies the least, being most closely related to the passive wall stiffness, i.e. in diastasis. Yet, generating and tracking these waves requires custom-designed ultrasound systems capable of inducing ultrasound push pulses and acquiring images at high frame rates. On the other hand, naturally-occurring shear waves are generated with each valve closure, without any external energy, and in the same patient their position within the heart cycle is expected to remain stable as long as the electrical activity remains

unchanged. However, their position in the cardiac cycle makes them less representative for the intrinsic properties of the myocardium during the true diastole (Chapter 9 and 10). Also, being generated by the valves, they are dependent on valve morphology, mobility, as well as pressure differences across the valves. It is theoretically possible that in significant mitral or aortic disease (stenosis or insufficiency) or very low transvalvular gradient states (severe systemic hypotension, advanced heart failure with low output) these waves are not detectable. This supposition has yet to be proven in future investigations.

- Externally induced shear waves have been proven to be diagnostic for the myocardial stiffness in normal and pathological myocardium^{16,17}. The studies demonstrated shear velocity values of 2.1 ± 1.3 m/s in healthy volunteers and 3.56 ± 1.71 m/s in HCM patients by triggering shear waves in end diastole, just before the P wave (these velocity values v were obtained by converting the reported elasticity values E^{17} , using $E = v^2$ with a tissue density of 1000 kg/m^3). In this thesis we demonstrate that naturally-occurring shear waves can also differentiate normal from pathological myocardial tissue (Chapters 10 and 11). The velocity values obtained were significantly higher than the ones obtained in the same type of population by externally-induced shear waves, corresponding to natural waves occurring in the myocardium during a partially contracted/relaxed state¹⁴.

- Tracking naturally occurring cardiac shear waves is already possible with present-day ultrasound scanners (this thesis), and a more precise quantification can be done with higher frame rates^{18,19}. High frame rate imaging by using plane wave compounding in order to detect natural or externally induced shear waves requires new technology, that is only now integrating in clinical cardiac ultrasound systems³⁸.

- An advantage of exploiting natural shear waves is that these SWs were found to have larger tissue velocity amplitudes^{13,14,18,39} (~ 4 cm/s) than the waves induced by an external acoustical force¹⁵ (~ 1 cm/s), likely leading to higher signal to noise ratios in TDI.

- However, the low frequency content of natural SWs^{18,22,23,35,39} compared to external sources^{15,25, 26,40,41} and thus the inherently larger wavelengths form a disadvantage of natural SWE measurements. Since the SWs can only be tracked over the limited length of a few centimeters of the interventricular septum (IVS), smaller fractions of the wavelength can be tracked for SWs with low frequencies, possibly leading to more measurement inaccuracy. Additionally, for 2D natural SWE measurements, the source of the SWs is not assured to be in plane with the field of view, as is the case for externally induced shear waves, and therefore out-of-plane propagation could also induce measurement inaccuracy^{39,42}. As explained in section 1 of this chapter, the parasternal long axis view,

by using very reproducible anatomical landmarks, is a good solution in order to avoid this type of error.

In our opinion, the two types of waves (externally induced versus natural) are not mutually exclusive as for their diagnostic yield. We anticipate that externally-induced shear waves will allow a precise quantification of the most-relaxed state of the myocardium in diastole, closely approximating the passive wall stiffness and maybe even its dynamics during the cardiac cycle. They would probably be the gold standard for cardiac shear wave elastography^{10,43}. Natural shear waves, being spontaneously present in almost every patient, would probably be used in the everyday echo lab due to their practical advantages (easy and fast to acquire, punctual measurement in a relatively fixed position during the cardiac cycle), making serial follow-up of patients readily available⁴². Further studies are however needed comparing these two modalities.

5. TRANSLATION INTO CLINICAL APPLICATION

Adequately addressing the challenges described in the Introduction would allow widespread clinical research. However, the final purpose would be to identify a new clinical ultrasound-based method allowing to better understand the *in vivo* physical properties of the left ventricular wall. To achieve this goal several other steps need to be taken:

- In order to validate shear wave imaging as a tool for clinical use, large standardization studies need to be performed. The recent evolution of deformation imaging from a research tool to a new clinical measurement of LV function⁴⁴ demonstrates such an effort of harmonization and standardization in echocardiography.
- Initial clinical studies of shear wave velocities show very promising results, at least regarding the velocity range^{14,17,19} and clear difference between normal and pathological tissue (Chapter 10) and different degrees of pathology (Chapter 11). Yet, in order to have high diagnostic yield and clinical relevance in early detection of disease, the shear wave velocity should be a continuum from normal to pathologic. A possible approach would be the creation of animal models of induced myocardial disease³⁹, allowing to serially test for a progressive degree of disease in a limited number of subjects. Further, establishing normal reference values for clinical use needs larger populations studies, in various pathologies, and especially in progressive states of disease.
- Full characterization of the myocardial properties throughout diastole may be performed by externally-induced shear wave imaging, by using for example a stitching

method, putting together measurements from several successive heart beats. This would potentially allow computing average velocity/stiffness values throughout diastole. An integrated time-velocity index may be more representative of the diastolic function than one punctual velocity determined in any point during diastole.

6. FUTURE PERSPECTIVES

There are several possible applications that could be developed based on the ultrasonic cardiac shear wave imaging:

Tissue characterization with echocardiography

Shear wave imaging offers the possibility of quantifying tissue stiffness in a specific region of the myocardium (Chapter 10), and even demonstrating variations in two adjacent segments of the wall (Chapter 11). This would potentially allow a quantitative estimation of the myocardial stiffness, that could for example be rendered in color-coded stiffness maps, in a similar manner to that presently used in parenchymatous organs¹².

3D/ multiplane shear wave imaging

One could imagine refining this method until being able to look three dimensionally at the way shear waves propagate into the heart⁴⁷, and reconstructing maps of myocardial stiffness in surface or in depth. A large part of this goal seems only restricted by the present state of technology and computing power, both of which are rapidly evolving. However, our experience so far with 3D imaging demonstrates that even for normal frame rates a reasonable resolution can only be achieved through stitching of multiple heart beats, by plane-by-plane reconstruction of the 3D volume. One possible solution is a volumetric plane wave, emitted simultaneously from all the crystals of the matrix probe, illuminating the whole volume in one emission, or compounding of few emissions in order to improve resolution. Theoretically this would solve the problem of 3D frame rate and achieve similar resolution to 2D compounded plane waves.

Other possible approaches to echocardiographic shear wave imaging

Experimental studies used intracardiac probes for in vivo high frame rate strain imaging⁴⁸. The intracardiac probes have to be brought in invasively and it is yet uncertain if intracardiac shear wave imaging⁴⁹ would bring any benefit as compared to the much better studied pressure/volume loops or simply cardiac output, pulmonary pressure and wedge pressure determination obtained through right heart catheterization.

Until now, very few studies were performed with transoesophageal high frame rate echocardiography⁵⁰. Although the gain in resolution may be significant in the near field (covering the atria), the study of the left ventricle in transesophageal echocardiography remains difficult because of its position away from the probe.

Another attractive perspective would be normalizing stiffness values in a specific myocardial area to the deformation indices derived from bidimensional strain. This might be more representative of the local interaction between stress and strain.

As presented in the previous chapters, tissue stiffness is a continuum, and results from a complex interaction between active and passive forces, pressure gradients and shape/volume variation. Most probably the stiffness itself will have to be normalized to the contribution of these forces, either by studying volume distension or pressure gradients, in a specific part of the cardiac cycle¹⁰.

7. CONCLUSION

In the first part of this thesis we demonstrate that left ventricular function can be assessed by using conventional echocardiographic imaging. Yet, the accurate estimation of the diastolic function of the left ventricle with echocardiography remains challenging, gives incomplete answers in a significant proportion of patients and has insufficient sensitivity for early detection of cardiac abnormalities. In an effort to overcome the gaps of our present day echocardiographic algorithms, we propose a new way of investigating the properties of the left ventricle, by using high frame rate shear wave imaging. Shear wave imaging offers a potential way of remotely “touching” the myocardium and measuring a marker for stiffness. We prove that cardiac shear wave imaging is feasible and can be used in order to answer relevant clinical questions.

We have now a new and more direct way of understanding the behavior of the cardiac muscle, and knowing its compliance to deformation forces^{10,42}. How much this resistance in itself may be characteristic of the function of the heart as a whole we do not yet know. This has still to be tested in theoretical models, in normal individuals and in pathological hearts, by directly comparing invasive pressure-volume loops with simultaneous stiffness determination through shear wave imaging. A large field of research opens before us, and hopefully in the coming years we will be able to gather evidence allowing to provide answers to this essential question.

REFERENCES

1. Edler I, Lindström K. The history of echocardiography. *Ultrasound Med Biol*. 2004;30(12):1565-644.
2. Nagueh SF, Smiseth OA, Appleton CP, Byrd BF 3rd, Dokainish H, Edvardsen T, Flachskampf FA, Gil- lebert TC, Klein AL, Lancellotti P, Marino P, Oh JK, Popescu BA, Waggoner AD. Recommendations for the Evaluation of Left Ventricular Diastolic Function by Echocardiography: An Update from the American Society of Echocardiography and the European Association of Cardiovascular Imaging. *Eur Heart J Cardiovasc Imaging*. 2016;17(12):1321-1360.
3. van Dalen BM, Strachinaru M, van der Swaluw J, Geleijnse ML. A simple, fast and reproducible echocardiographic approach to grade left ventricular diastolic function. *Int J Cardiovasc Imaging*. 2016. DOI 10.1007/s10554-015-0832-6
4. Lancellotti P, Galderisi M, Edvardsen T, Donal E, Goliash G, Cardim N, Magne J, Laginha S, Hagendorff A, Haland TF, Aaberge L, Martinez C, Rapacciuolo A, Santoro C, Iardi F, Postolache A, Dulgheru R, Mateescu AD, Beladan CC, Deleanu D, Marchetta S, Auffret V, Schwammenthal E, Habib G, Popescu BA. Echo-Doppler estimation of left ventricular filling pressure: results of the multicentre EACVI Euro-Filling study. *Eur Heart J Cardiovasc Imaging*. 2017;18(9):961-968. doi: 10.1093/ehjci/jex067.
5. Strachinaru M, van Dalen BM, Van Mieghem N, De Jaegere PP, Galema TW, Morissens M, Geleijnse ML. Relation between E/e' ratio and NT-proBNP levels in elderly patients with symptomatic severe aortic stenosis. *Cardiovasc Ultrasound*. 2015;13(1):29. doi: 10.1186/s12947-015-0021-8
6. Lang RM, Badano LP, Mor-Avi V, Afilalo J, Armstrong A, Ernande L, Flachskampf FA, Foster E, Gold- stein SA, Kuznetsova T, Lancellotti P, Muraru D, Picard MH, Rietzschel ER, Rudski L, Spencer KT, Tsang W, Voigt JU. Recommendations for cardiac chamber quantification by echocardiography in adults: an update from the American Society of Echocardiography and the European Associa- tion of Cardiovascular Imaging. *Eur Heart J Cardiovasc Imaging*. 2015;16(3):233-70. doi: 10.1093/ ehjci/jev014.
7. van Grootel RWJ, Strachinaru M, Menting ME, Vletter-McGhie JS, Roos-Hesselink JW, van den Bosch AE. In depth echocardiographic analysis of left atrial function in healthy adults using speckle tracking echocardiography and volumetric analysis. *Echocardiography*. 2018. doi: 10.1111/echo.14174.
8. Strachinaru M, Annis C, Catez E, Jousten I, Lutea ML, Pavel O, Morissens M. The mitral annular displacement by two-dimensional speckle tracking: a new tool in evaluating the left atrial func- tion. *J Cardiovasc Med (Hagerstown)*. 2016;17:344-53. doi: 10.2459/JCM.0000000000000346
9. van den Berg VJ, Strachinaru M, Akkerhuis KM, Baart S, Brankovic M, Constantinescu AA, Cornel JH, Manintveld OC, Victor Umans VAWM, Rizopoulos D, Geleijnse ML, Boersma E, van Dalen BM, Kardys I. Repeated Echocardiograms do not provide Incremental Prognostic Value to Single Echocardiographic Assessment in Minimally Symptomatic Patients with Chronic Heart Failure: Results of the Bio-SHIFT Study. *J Am Soc Echocardiogr*. 2019; DOI: 10.1016/j.echo.2019.04.419
10. Voigt JU. Direct Stiffness Measurements by Echocardiography: Does the Search for the Holy Grail Come to an End?. *JACC Cardiovasc Imaging*. 2018. pii: S1936-878X(18)30185-2. doi: 10.1016/j. jcmg.2018.02.004.

11. Sutherland GR, Bijnens B, McDicken WN. Tissue Doppler Echocardiography: Historical Perspective and Technological Considerations, *Echocardiography*. 1999;16:445-453.
12. Shiina T, Nightingale KR, Palmeri ML, Hall TJ, Bamber JC, Barr RG, Castera L, Choi BI, Chou YH, Cosgrove D, Dietrich CF, Ding H, Amy D, Farrokh A, Ferraioli G, Filice C, Friedrich-Rust M, Nakashima K, Schafer F, Sporea I, Suzuki S, Wilson S, Kudo M. WFUMB guidelines and recommendations for clinical use of ultrasound elastography: Part 1: basic principles and terminology, *Ultrasound Med Biol*. 2015;41:1126-47. doi: 10.1016/j.ultrasmedbio.2015.03.009.
13. Strachinaru M, Bosch JG, van Dalen BM, van Gils L, van der Steen AFW, de Jong N, Geleijnse ML, Vos HJ. Cardiac Shear Wave Elastography Using a Clinical Ultrasound System. *Ultrasound Med Biol*. 2017;43(8):1596-1606. doi: 10.1016/j.ultrasmedbio.2017.04.012.
14. Strachinaru M, Bosch JG, van Gils L, van Dalen BM, Schinkel AFL, van der Steen AFW, de Jong N, Michels M, Vos HJ, Geleijnse ML. Naturally occurring shear waves in healthy volunteers and hypertrophic cardiomyopathy patients. *Ultrasound Med Biol*. 2019. doi: 10.1016/j.ultrasmedbio.2019.04.004.
15. Couade M, Pernot M, Messas E, Bel A, Ba M, Hagege A, Fink M, Tanter M. In vivo quantitative mapping of myocardium stiffening and transmural anisotropy during the cardiac cycle, *IEEE Trans Med Imaging*, 2011;30:295–305
16. Villemain O, Correia M, Khraiche D, Podetti I, Meot M, Legendre A, Tanter M, Bonnet D, Pernot M. Myocardial Stiffness Assessment Using Shear Wave Imaging in Pediatric Hypertrophic Cardiomyopathy. *JACC Cardiovasc Imaging*. 2017. pii: S1936-878X(17)30888-4. doi: 10.1016/j.jcmg.2017.08.018.
17. Villemain O, Correia M, Mousseaux E, Baranger J, Zarka S, Podetti I, Soulat G, Damy T, Hagege A, Tanter M, Pernot M, Messas E. Myocardial Stiffness Evaluation Using Noninvasive Shear Wave Imaging in Healthy and Hypertrophic Cardiomyopathic Adults. *JACC Cardiovasc Imaging*. 2018. pii: S1936-878X(18)30140-2. doi: 10.1016/j.jcmg.2018.02.002.
18. Santos P, Petrescu A, Pedrosa J, Orłowska M, Komini V, Voigt JU, D'hooge J. Natural shear wave imaging in the human heart: normal values, feasibility and reproducibility. *IEEE Trans Ultrason Ferroelectr Freq Control*. 2018. doi: 10.1109/TUFFC.2018.2881493.
19. Petrescu A, Santos P, Orłowska M, Pedrosa J, Bézy S, Chakraborty B, Cvijic M, Dobrovie M, Delforge M, D'hooge J, Voigt JU. Velocities of Naturally Occurring Myocardial Shear Waves Increase With Age and in Cardiac Amyloidosis. *JACC Cardiovasc Imaging*. 2019. pii: S1936-878X(19)30057-9. doi: 10.1016/j.jcmg.2018.11.029.
20. Brekke B, Nilsen LC, Lund J, Torp H, Bjastad T, Amundsen BH, , Stoylen A, Aase SA. Ultra-high frame rate tissue Doppler imaging, *Ultrasound Med Biol*. 2014;40:222-31.
21. Keijzer LBH, Strachinaru M, Bowen DJ, Geleijnse ML, van der Steen AFW, Bosch JG, de Jong N, Vos HJ. Reproducibility of Natural Shear Wave Elastography Measurements. *Ultrasound Med Biol* (in press)
22. Keijzer LBH, Strachinaru M, Bosch JG, van Dalen BM, Heinonen I, Verweij MD, van der Steen AFW, de Jong N, Vos HJ. Longitudinal and Transversal Particle Motion Induced by Aortic Valve Closure in the Interventricular Septum. *IEEE IUS 2018* (abstr); http://sites.ieee.org/ius-2018/files/2018/09/IUS2019_AbstractBook_small.pdf
23. Kanai H. Propagation of spontaneously actuated pulsive vibration in human heart wall and in vivo viscoelasticity estimation, *IEEE Trans Ultrason Ferroelectr Freq Control*, 52 (2005), pp. 1931–1942.

24. Azhari H. Basics of biomedical ultrasound for engineers. Hoboken, NJ: John Wiley & Sons; 2010, p. 86-93; 236-243.
25. Pernot M, Couade M, Mateo P, Crozatier B, Fischmeister R, Tanter M. Real-time assessment of myocardial contractility using shear wave imaging. *J Am Coll Cardiol*. 2011;58:65-72.
26. Urban MW, Qiang B, Song P, Nenadic IZ, Chen S, Greenleaf JF. Investigation of the effects of myocardial anisotropy for shear wave elastography using impulsive force and harmonic vibration. *Phys Med Biol*. 2016;61(1):365-82. doi: 10.1088/0031-9155/61/1/365.
27. Strachinaru M, Annis C, Catez E, Jousten I, Lutea ML, Pavel O, Morissens M. The mitral annular displacement by two-dimensional speckle tracking: a new tool in evaluating the left atrial function. *J Cardiovasc Med (Hagerstown)*. 2016;17:344-53. doi: 10.2459/JCM.0000000000000346
28. Voigt JU, Lindenmeier G, Werner D, Flachskampf FA, Nixdorff U, Hatle L, Sutherland GR, Daniel WG. Strain rate imaging for the assessment of preload-dependent changes in regional left ventricular diastolic longitudinal function. *J Am Soc Echocardiogr*. 2002;15(1):13-9.
29. Pislaru C, Pellikka PA, Pislaru SV. Wave propagation of myocardial stretch: correlation with myocardial stiffness. *Basic Res Cardiol*. 2014;109(6):438. doi: 10.1007/s00395-014-0438-5
30. Pislaru C, Alashry MM, Thaden JJ, Pellikka PA, Enriquez-Sarano M, Pislaru SV. Intrinsic Wave Propagation of Myocardial Stretch, A New Tool to Evaluate Myocardial Stiffness: A Pilot Study in Patients with Aortic Stenosis and Mitral Regurgitation. *J Am Soc Echocardiogr*. 2017;30(11):1070-1080. doi: 10.1016/j.echo.2017.06.023.
31. Pislaru C, Ionescu F, Alashry M, Petrescu I, Pellikka PA, Grogan M, Dispenzieri A, Pislaru SV. Myocardial Stiffness by Intrinsic Cardiac Elastography in Patients with Amyloidosis: Comparison with Chamber Stiffness and Global Longitudinal Strain. *J Am Soc Echocardiogr*. 2019. pii: S0894-7317(19)30619-4. doi: 10.1016/j.echo.2019.04.418.
32. Strachinaru M, Geleijnse ML, de Jong N, van den Bosch AE, Michels M, Schinkel AFL, van der Steen AFW, Bosch JG, Vos HJ. Myocardial stretch post atrial contraction in healthy volunteers and hypertrophic cardiomyopathy patients. *Ultrasound Med Biol*. 2019;45(8):1987-1998. doi: 10.1016/j.ultrasmedbio.2019.04.031.
33. Pedrizzetti G, Martiniello AR, Bianchi V, D'Onofrio A, Caso P, Tonti G. Changes in electrical activation modify the orientation of left ventricular flow momentum: novel observations using echocardiographic particle image velocimetry. *Eur Heart J Cardiovasc Imaging*. 2016;17(2):203-9. doi: 10.1093/ehjci/jev137.
34. Voorneveld J, Keijzer LBH, Strachinaru M, Bowen DJ, Goei JSL, Ten Cate F, van der Steen AFW, de Jong N, Vos HJ, van den Bosch AE, Bosch JG. High Frame Rate echoPIV can Measure the High Velocity Diastolic Flow Patterns. *Circ Cardiovasc Imaging*. 2019;12(4):e008856. doi: 10.1161/CIRCIMAGING.119.008856.
35. Kanai H. Visualization of propagation of pulse vibration along the heart wall and imaging of its propagation speed. *Conf Proc IEEE Eng Med Biol Soc*. 2006;1:699-702.
36. Gaasch WH, Battle WE, Oboler AA, Banas JS Jr, Levine HJ. Left ventricular stress and compliance in man. With special reference to normalized ventricular function curves. *Circulation*. 1972;45(4):746-62.
37. Adler Y, Charron P, Imazio M, Badano L, Barón-Esquivias G, Bogaert J, Brucato A, Gueret P, Klingel K, Lionis C, Maisch B, Mayosi B, Pavie A, Ristic AD, Sabaté Tenas M, Seferovic P, Swedberg K, Tom-

- kowski W. 2015 ESC Guidelines for the diagnosis and management of pericardial diseases: The Task Force for the Diagnosis and Management of Pericardial Diseases of the European Society of Cardiology (ESC) Endorsed by: The European Association for Cardio-Thoracic Surgery (EACTS). *Eur Heart J*. 2015;36(42):2921-2964. doi: 10.1093/eurheartj/ehv318
38. Fadnes S, Wigen MS, Nyrnes SA, Lovstakken L. In Vivo Intracardiac Vector Flow Imaging Using Phased Array Transducers for Pediatric Cardiology. *IEEE Trans Ultrason Ferroelectr Freq Control*. 2017;64(9):1318-1326. doi: 10.1109/TUFFC.2017.2689799.
 39. Vos HJ, van Dalen BM, Heinonen I, Bosch JG, Sorop O, Duncker DJ, van der Steen AF, de Jong N. Cardiac Shear Wave Velocity Detection in the Porcine Heart. *Ultrasound Med Biol*. 2017. pii: S0301-5629(16)30412-4. doi: 10.1016/j.ultrasmedbio.2016.11.015.
 40. Hollender PJ, Wolf PD, Goswami R, Trahey GE. Intracardiac echocardiography measurement of dynamic myocardial stiffness with shear wave velocimetry. *Ultrasound Med Biol*, vol. 38, pp. 1271-1283, 2012.
 41. Pislaru C, Urban MW, Pislaru S V., Kinnick RR, Greenleaf JF. Viscoelastic properties of normal and infarcted myocardium measured by a multifrequency shear wave method: comparison with pressure-segment length method. *Ultrasound Med Biol* 2014b;40:1785-1795.
 42. Pernot M, Villemain O. In the Heart of Stiffness: Are Natural Heart Vibrations Reliable Enough to Assess Myocardial Stiffness, The New Holy Grail in Echocardiography? *JACC Cardiovasc Imaging*. 2019. pii: S1936-878X(19)30111-1. doi: 10.1016/j.jcmg.2019.01.012
 43. Cikes M, Tong L, Sutherland GR, D'hooge J. Ultrafast cardiac ultrasound imaging: technical principles, applications, and clinical benefits, *JACC Cardiovasc Imaging*. 2014;7:812-23.
 44. Voigt JU, Pedrizzetti G, Lysyansky P, Marwick TH, Houle H, Baumann R, Pedri S, Ito Y, Abe Y, Metz S, Song JH, Hamilton J, Sengupta PP, Kolias TJ, d'Hooge J, Aurigemma GP, Thomas JD, Badano LP. Definitions for a common standard for 2D speckle tracking echocardiography: consensus document of the EACVI/ASE/Industry Task Force to standardize deformation imaging. *Eur Heart J Cardiovasc Imaging*. 2015;16(1):1-11. doi: 10.1093/ehjci/jeu184.
 45. van der Steen AF. Myocardial integrated backscatter: the renaissance of an old parameter? *Eur J Echocardiogr*. 2000;1(1):2-4.
 46. Mor-Avi V, Lang RM, Badano LP, Belohlavek M, Cardim NM, Derumeaux G, Galderisi M, Marwick T, Nagueh SF, Sengupta PP, Sicari R, Smiseth OA, Smulevitz B, Takeuchi M, Thomas JD, Vannan M, Voigt JU, Zamorano JL. Current and evolving echocardiographic techniques for the quantitative evaluation of cardiac mechanics: ASE/EAE consensus statement on methodology and indications endorsed by the Japanese Society of Echocardiography. *Eur J Echocardiogr*. 2011;12(3):167-205. doi: 10.1093/ejechocard/jer021.
 47. B. Brekke, H. Torp, T. Bjåstad, A. Støylen and S. A. Aase. 3D Tissue Doppler imaging with ultra high frame rate. 2011 IEEE International Ultrasonics Symposium, Orlando, FL. 2011; pp. 717-720. doi: 10.1109/ULTSYM.2011.0174
 48. Grondin J, Wan E, Gambhir A, Garan H, Konofagou E. Intracardiac myocardial elastography in canines and humans in vivo. *IEEE Trans Ultrason Ferroelectr Freq Control*. 2015;62(2):337-49. doi: 10.1109/TUFFC.2014.006784.
 49. Hollender PJ, Wolf PD, Goswami R, Trahey GE. Intracardiac echocardiography measurement of dynamic myocardial stiffness with shear wave velocimetry. *Ultrasound Med Biol*. 2012;38(7):1271-83. doi: 10.1016/j.ultrasmedbio.2012.02.028.

50. Kwiecinski W, Bessière F, Colas EC, N'Djin WA, Tanter M, Lafon C, Pernot M. Cardiac shear-wave elastography using a transesophageal transducer: application to the mapping of thermal lesions in ultrasound transesophageal cardiac ablation. *Phys Med Biol.* 2015;60(20):7829-46. doi: 10.1088/0031-9155/60/20/7829



S

Heart failure is a clinical syndrome defined by the presence of typical symptoms (breathlessness, fatigue, ankle swelling), induced by an underlying functional cardiac abnormality, that results in an insufficient pump function or high intracardiac pressures at rest or during exertion. Despite numerous advances in the prevention, diagnosis and treatment of cardiac disease that lead to dysfunction, heart failure still prevails in 1-2% of the adult population in high income countries, and up to 10% of people over 70 years of age, and accounts for high rates of mortality and hospitalization.

However, recognizing the disease at this stage may be too late for possibly attempting a curative treatment that would restore the normal cardiac function. Before the clinical symptoms set on, patients do have unrecognized structural or functional abnormalities that prelude heart failure. Demonstrating such a structural (myocardial disease, valvular heart disease, etc.) or functional abnormality in the heart is thought to be essential to the early diagnosis and treatment. In the very early stages of the disease, such abnormality can be subtle or completely absent at rest, and present only during exertion, eliciting complicated investigations.

This thesis aims to prove that high frame rate echocardiography and cardiac shear wave imaging is feasible and can be used in order to detect the global or local stiffness of the heart walls which would be clinically relevant. This method could be used for the early detection of the subtle abnormalities that precede the onset of clinical heart failure. It is not the purpose of this thesis to propose a new technical solution, since the scientific effort was more directed towards the clinical and pathophysiological perspective. Taking advantage of an unforeseen technical ability of a clinical ultrasound system, we aim to demonstrate the importance and the clinical message of shear wave imaging in the heart. Hopefully this will trigger more efforts in the technical field and lead to a true clinical high frame rate application accessible to every cardiologist.

MAIN FINDINGS

In **Part One** we investigated current parameters used to estimate cardiac function with echocardiography. We demonstrate that the assessment of the diastolic function of the left ventricle with echocardiography remains challenging, gives incomplete answers in a significant proportion of patients and has insufficient sensitivity for early detection of cardiac abnormalities.

We demonstrate in **Chapter 2** in a group of 200 patients that in some cases it may be difficult to grade diastolic dysfunction with the ASE/EAE algorithm, since there may be

discrepancies in the assessed parameters. The locally developed algorithm to grade LV diastolic dysfunction was simpler, faster and yielded a higher diagnostic outcome as compared to the ASE/EAE algorithm.

The general message is that present day algorithms are very complicated and insufficiently precise in estimating the diastolic function of the left ventricle, because of the indirect nature of the parameters used and the theoretical assumptions made in order to validate each step.

One of the key parameters in diastology is the E/e' ratio. It represented a revolution in our understanding of the diastolic function based on more than filling patterns and flow indices.

Yet, **Chapter 3** demonstrates that it has only a moderate correlation with biomarkers of elevated intracardiac pressure, the best for the septal point E/e' ($r=0.584$, $P < 0.0001$). This correlation is influenced by the ejection fraction and the presence of co-morbidities (aortic or mitral regurgitation, annular calcifications, severe renal dysfunction, obesity or severe COPD).

Chapter 4 shows the major role of the diastolic dysfunction in the rise of the pulmonary pressure in an elderly population with severe aortic stenosis and co-morbidities, with an important impact on clinical decision and prognostic evaluation before and after the TAVI intervention.

Left atrial dilatation is predictive for complications in a multitude of cardiac diseases; therefore, adequate assessment is essential. Technological advances have made it possible to quantify LA function with Speckle Tracking Echocardiography (STE). In **Chapter 5** we assessed LA myocardial and volumetric function in a healthy cohort and investigated correlations with baseline characteristics. In this study we provided normal values for the three phasic functions of the LA, assessed with STE and volumetric function. Mean LA-strain was $39.7 \pm 6.2\%$, LA-SRe $-2.78 \pm 0.62 \text{ s}^{-1}$ and LA-SRa $-2.56 \pm 0.62 \text{ s}^{-1}$. Subjects were divided into 5 age decades (each 50% female). LA-strain and LA-SRe were lower in the oldest groups, whereas LA-SRa was higher. LA-SRa was higher in males ($-2.69 \pm 0.68 \text{ s}^{-1}$ vs $-2.42 \pm 0.52 \text{ s}^{-1}$).

The methods used to characterize the volume change and the deformation of the left atrium, as demonstrated in the previous chapter, are highly dependent on technical factors and may be difficult to use in a clinical environment. In **Chapter 6** we investigated the mitral annular displacement by speckle tracking as an alternative method

to studying the longitudinal left atrial function. There was a very strong correlation between three-dimensional volumetric function and mitral annular displacement, both for the reservoir ($r=0.78$; $P<0.0001$) and contractile ($r=0.76$; $P<0.0001$) functions. The correlation with the global longitudinal strain displayed an $r=0.87$, $P>0.0001$ for the reservoir and $r=0.81$, $P<0.0001$ for the contractile function. Mitral annular displacement was a very good discriminator for normal versus abnormal participants [area under the curve (AUC) for reservoir=0.872 and for contractile=0.843; $P<0.0001$], performing less well than three-dimensional (AUC reservoir=0.892 and contractile=0.915; $P<0.0001$) or deformation (AUC=0.921 and 0.903 respectively; $P<0.0001$), but better than pulsed TDI contractility (AUC=0.807; $P<0.0001$). Mitral annular displacement by speckle tracking is a reliable and fast method to evaluate left atrial function. Given the strength of the correlations with strain parameters, it could be used as a surrogate measure of the deformation of left atrium.

In **Chapter 7** we compared the prognostic value of a single 'baseline' echocardiographic estimation of systolic and diastolic function parameters with repeated echocardiography in stable chronic heart failure patients in the prospective Bio-SHiFT study cohort. Single baseline or repeatedly measured echocardiographic parameters (LV ejection fraction, diastolic LV diameter, systolic LV diameter, systolic left atrial diameter, E/A ratio and E/e' ratio) were associated with the endpoints. However all parameters remained stable on average during the 2.3 years follow-up in this, largely, minimally symptomatic CHF cohort and none of the trajectories from the investigated parameters showed worsening prior to the occurrence of clinical events (hospitalization for heart failure, LV assist device implantation, heart transplantation, and cardiovascular death). Thus, regular echocardiographic monitoring of systolic or diastolic LV function within this time-frame does not seem to carry incremental prognostic information over a single baseline measurement, suggesting that classical echocardiographic parameters of cardiac function have insufficient sensitivity for the early detection of subtle cardiac abnormalities.

In **Part two** we propose a new method of looking at the properties of cardiac muscle by using high frame rate echocardiography and shear wave imaging.

The propagation velocity of shear waves relates to tissue stiffness. In **Chapter 8** we prove that a regular clinical cardiac ultrasound system can determine shear wave velocity with a conventional unmodified tissue Doppler imaging (TDI) application, in tissue phantoms and *in vivo* in the parasternal view. The investigation was performed on tissue phantoms using a research platform capable of inducing and tracking shear waves and a clinical cardiac system able to achieve frame rates of 400-700 Hz in TDI by tuning the normal system settings. The research platform scanner was used as reference. Shear

wave velocities measured with TDI on the clinical cardiac system were very close to those measured by the research platform scanner, with a mean difference of 0.18 ± 0.22 m/s, and limits of agreement between -0.27 and $+0.63$ m/s, which can be considered reasonable for research purposes.

For the quantification of myocardial function, myocardial stiffness can potentially be measured non-invasively using shear wave elastography. However, using the method for clinical diagnosis requires high precision. In **Chapter 9** we tested the reproducibility of measuring propagation speeds of shear waves naturally induced by aortic and mitral valve closure with two different clinical systems (the unmodified clinical system used in the previous chapter versus a modified clinical system able to reach much higher frame rates and full access to the raw ultrasound data). In a group of healthy volunteers, the inter-scan and intra-scan variabilities were found to have similar ranges. Also, the propagation speeds obtained on different days were reproducible. We found different propagation speeds between the two clinical systems. Our analysis of the differences found suggested that the variations measured among healthy volunteers were mainly caused by measurement inaccuracies. In order to achieve clinically acceptable measurement precision averaging over multiple heartbeats should be used.

In **Chapter 10** we apply the clinical high frame rate tissue Doppler method to measure the propagation velocity of naturally occurring shear waves generated by aortic and mitral valves closure in healthy volunteers and patients with hypertrophic cardiomyopathy. In HCM, the mean velocity was 5.1 ± 0.7 m/s for the aortic shear wave (3.61 ± 0.46 m/s in matched volunteers, $p < 0.0001$) and 6.88 ± 1.12 m/s for the mitral shear wave (4.65 ± 0.77 m/s in matched volunteers, $p < 0.0001$). The very different propagation velocities in the two groups, practically without overlapping values, suggest that they can be used to assess differences between normal and pathologic myocardium. A threshold of 4 m/s for the aortic SW correctly classified pathologic myocardium with a sensitivity of 95% and specificity of 90%.

A local variation in stiffness is hypothesized to appear as a variation in the propagation velocity of naturally-occurring shear waves. In **Chapter 11** we demonstrate that *in vivo* myocardial shear wave imaging can detect a localized variation in myocardial tissue properties through a variation in propagation velocity. Elasticity maps of the myocardial tissue could be reconstructed in the future by automatic tracking algorithms.

In cardiac high-frame-rate color tissue Doppler imaging from the apical position, a wave-like pattern travels over the interventricular septum after atrial contraction. The propagation velocity of this myocardial stretch post-atrial contraction (MSPa) was also

proposed as a measure of left ventricular stiffness, in a purely relaxed state. In **Chapter 12** we investigated the MSPa in patients with hypertrophic cardiomyopathy compared with healthy volunteers. Our results suggest that this wave-like pattern does not simply behave like a longitudinal wave as suggested by other authors. In about 50% of the patients it displays an acceleration in the basal to mid-septum. The reason is hypothesized to be the reaching of maximal longitudinal myocardial distension in HCM patients. Despite the initial promising results, it may not be sensitive enough for direct stiffness estimation through linear equations.

Left ventricular flow patterns have been studied as potential early stage markers of cardiac dysfunction. A relatively new method of measuring flow patterns, named echo-particle image velocimetry (echoPIV), tracks the motion of ultrasound contrast agent microbubbles in the blood using echocardiography. However, the low frame rates (50-70 Hz) permitted by the current generation of clinical ultrasound scanners causes velocity magnitudes during filling and ejection to be severely underestimated. This is due to the relatively large displacement of the bubbles between frames. The recent feasibility of high frame rate (HFR) echocardiography, using diverging-wave transmission schemes, has allowed for frame rates of up to 100 times faster than conventional imaging methods. In **Chapter 13** we provide the first demonstration of echoPIV estimating the high velocity trans-mitral jet by using high temporal resolution in 2D, previously unobtainable through echoPIV with conventional frame rates.

In **Chapter 14 (Discussion)** we summarized the results of our research and analyzed the implications, the strengths and limitations of this new method, as well as future work needed to successfully translate it in clinical practice. We do not yet know how much the stiffness in itself may be characteristic of the function of the heart as a whole. Further, in order to have high diagnostic yield and clinical relevance in early detection of disease, the shear wave velocities should represent a continuum from normal to pathologic. This has still to be tested in theoretical models, in larger population studies in normal individuals and in pathological hearts.



S

Hartfalen is een klinisch syndroom en is gedefinieerd door het optreden van typische verschijnselen als kortademigheid, moeheid, en dikke enkels. Het wordt veroorzaakt door een onderliggend functionele afwijking van het hart, waardoor de pompfunctie onvoldoende is of de bloeddruk in het hart hoog is tijdens rust of inspanning. Ondanks vele verbeteringen in preventie, diagnose, en symptoombestrijding van hartziektes die tot de disfunctie kunnen leiden komt hartfalen nog altijd voor in 1 tot 2% van de volwassen bevolking in landen met hoge inkomsten, en komt zelfs voor in tot 10% van de mensen van 70 jaar of ouder. Hartfalen veroorzaakt grote kans op ziekenhuisopnames en sterfte.

Herkennen van hartfalen in de late fase van het syndroom kan echter te laat zijn voor een volledig herstel door behandeling gericht op het normaliseren van de hartfunctie. Reeds voordat de symptomen zichtbaar worden hebben patiënten al structurele of functionele afwijkingen voorafgaand aan het daadwerkelijke falen van het hart.

Het wordt algemeen aangenomen dat het aantonen van zulke structurele of functionele afwijkingen aan de hartspier, kleppen, etc. essentieel zullen zijn voor vroege herkenning en behandeling. In zeer vroeg stadium kunnen afwijkingen nog marginaal of zelfs afwezig zijn in rusttoestand, maar niet tijdens inspanning, wat vraagt om complex onderzoek.

Dit proefschrift heeft als doel om te bewijzen dat echocardiografie met hoge beeldfrequentie en *shear wave* afbeeldingstechnieken in het hart mogelijk zijn, en gebruikt kunnen worden voor het detecteren van globale en lokale stijfheid van de hartwand. De detectie zou klinisch relevant zijn. De methode kan mogelijk gebruikt worden voor het vroeg herkennen van subtiele afwijkingen die vooraf gaan aan het ontwikkelen van klinisch hartfalen. Het wetenschappelijk doel van dit proefschrift was niet om een nieuwe technologische methode te ontwikkelen maar juist het klinische en pathofysiologische aspect te onderzoeken. Gebruik makend van een onverwachte technische mogelijkheid van een klinisch ecosysteem om weefsel Doppler beelden te maken met zeer hoge beeldfrequentie, willen we het belang en het klinisch bericht verspreiden van de *shear wave* afbeeldingstechniek in het hart. We hopen hiermee verdere technische ontwikkelingen te stimuleren die uiteindelijk zullen leiden tot regulier klinisch gebruik van de hoge beeldfrequentie techniek in cardiologie.

BELANGRIJKSTE BEVINDINGEN

In **Deel 1** bestuderen we de huidige parameters waarmee hartfunctie wordt afgeschat in echocardiografie. We laten zien dat de beoordeling van de diastolische linker kamer functie een uitdaging blijft met echocardiografie, dat het incomplete antwoorden geeft

in een aanzienlijk deel van de patiëntenpopulatie en dat het onvoldoende gevoelig is voor vroege detectie van afwijkingen van het hart.

Hoofdstuk 2 laat in een groep van 200 patiënten zien dat in sommige gevallen het moeilijk is om een waardering van de diastolische dysfunctie te geven volgens het ASE/EAE algoritme, omdat er een discrepantie is tussen de gemeten parameters.

Retrospectief, het door ons ontwikkelde algoritme om de linker kamer diastolische dysfunctie te waarden was eenvoudiger, sneller in diagnose en had een betere diagnostische uitkomst in vergelijking met het ASE/EAE algoritme. Het belangrijkste bericht is dat huidige algoritmes complex zijn en onvoldoende nauwkeurig in het afschatten van de linker kamer diastolische functie, vanwege de indirecte relatie tussen de gebruikte parameters en kamer functioneren, en de theoretische aannames in de validatie van elke onderliggende stap.

Eén van de cruciale parameters in diastologie is de verhouding tussen diastolische piekinstroom bloedsnelheden en piek-snelheid van het weefsel rond de mitraal klep (E/e' ratio). Dit veroorzaakte een revolutie in het begrip van diastolische functie ten opzichte van de eerdere methode waarbij alleen naar bloedstroomsnelheden en -patronen werd gekeken. Desondanks laat **Hoofdstuk 3** zien dat er slechts een beperkte correlatie is met *biomarkers* die gerelateerd zijn aan verhoogde druk in de linker kamer. De hoogste correlatie heeft de E/e' ratio, gemeten septaal ($r= 0,384$; $P<0,0001$) De correlatie wordt beïnvloed door de ejectiefractie en de aanwezigheid van co-morbiditeit (klep-lekkage, calcificatie van het klepbed, nierfalen, obesitas, COPD).

Hoofdstuk 4 toont de belangrijke rol van de diastolische disfunctie bij de toename van de pulmonaledrukken bij een oudere patiënten populatie met ernstige aortaklep stenose en comorbiditeiten, met een belangrijke impact op de klinische traject en prognostische evaluatie voor en na de TAVI-interventie.

Dilatatie van de linker boezem heeft voorspellende waarde voor verschillende hartziekten, waaruit volgt dat goede beoordeling essentieel is. Technologische vooruitgang heeft ervoor gezorgd dat linker boezem functie kan worden gekwantificeerd met behulp van spikkel volgmethodode (speckle tracking) echografie.

In **Hoofdstuk 5** hebben we het linker boezem functioneren van de spier en het volume onderzocht van een gezond cohort, en we hebben de correlatie met basiswaardes bekeken. In deze studie hebben we normaalwaarden kunnen vastleggen voor de drie fasen in het functioneren van het linker boezem, bepaald met spikkel volgmethodode echografie

en volumetrische opnames. De gemiddelde linker-boezem rek (*strain*) was $39,7 \pm 6,2\%$, de rek snelheid (*strain rate*) in vroege diastole was $-2,78 \pm 0,62 \text{ s}^{-1}$ en de rek snelheid na boezem contractie was $-2,56 \pm 0,62 \text{ s}^{-1}$. De patiënten werden onderverdeeld in 5 leeftijdsgroepen (50%/50% man-vrouw verhouding). Rek en reksnelheid van de boezem in vroege diastole was lager in de oudste leeftijdscategorie, terwijl de boezemreksnelheid daarin hoger was. De reksnelheid was hoger bij mannen ($-2,69 \pm 0,68 \text{ s}^{-1}$ tegen $-2,42 \pm 0,52 \text{ s}^{-1}$).

De methodes waarmee volumeveranderingen en deformatie van het linker boezem worden gekarakteriseerd, zoals beschreven in voorgaande hoofdstuk, hangen sterk samen met technische factoren en zijn wellicht moeilijk te gebruiken in een klinische omgeving.

In **hoofdstuk 6** bekeken we de verplaatsing van de mitraal annulus met behulp van de spikkel volgmethode als alternatieve methode voor het bekijken van de longitudinale linker-boezem functie.

Er was een grote correlatie tussen volumetrisch functie en de verplaatsing van de mitraal annulus, zowel voor de reservoir-functie ($r=0,78$; $P<0,0001$) als de contractie-functie ($r=0,76$; $P<0,0001$). De correlatie tussen de globale longitudinale rek (*global longitudinal strain, GLS*) en reservoir functie was $r=0,87$, $P>0,0001$ en $r=0,81$, $P<0,0001$ met de contractiliteit. De mitraal annulus verplaatsing gaf een zeer goed onderscheid tussen normale en abnormale studiedeelnemers [oppervlak onder de curve (*AUC*) voor reservoir= $0,872$ en voor contractiliteit $0,843$; $P<0,0001$], met slechtere prestaties dan 3D echografie (*AUC* reservoir= $0,892$ en contractiliteit= $0,915$; $P<0,0001$) of deformatie-afbeelding (*AUC*= $0,921$ en $0,903$ respectievelijk; $P<0,0001$), maar beter dan gepulseerde *tissue Doppler imaging (TDI)* (*AUC* voor contractiliteit= $0,807$; $P<0,0001$). Verplaatsingsmetingen van de mitraal annulus met behulp van spikkel volgmethode is een betrouwbare en snelle methode om de linker boezem functie te analyseren. Vanwege de hoge correlatie met de meer algemene rek-methode, kan de verplaatsingsmethode gebruikt worden als surrogaat voor de deformatie-methode van de linker boezem.

In **Hoofdstuk 7** hebben we de voorspellende waarde van echocardiografische basiswaarden voor de schatting van systolische en diastolische functie vergeleken met herhaalde echografie in de prospectieve Bio-SHIFT studie cohort. De patiënten hadden stabiele chronisch hartfalen maar hadden over het algemeen weinig symptomen. Zowel initiële meetwaarden als repetitieve meetwaarden (Linker kamer ejectie fractie, diastolische and systolische linker kamer diameter, systolische linker boezem diameter, E/A ratio en E/e' ratio) waren gekoppeld aan de eindpunten van de studie. Tijdens de 2,3 jaar-durende looptijd van de studie bleven alle waardes gemiddeld stabiel voorafgaand

aan een klinische gebeurtenis (ziekenhuisopname voor hartfalen, implantatie van linker kamer hulpapparaat, harttransplantatie, of overlijden als gevolg van hart- of vaatziekte). Het lijkt erop dat het regulier echocardiografische monitoren van systolische en diastolische linker kamer functioneren in zo'n tijdsbestek geen voorspellende informatie toevoegt ten opzichte van de enkele startwaarde. Dit suggereert dat de conventionele echocardiografische parameters van hartfunctie onvoldoende gevoelig zijn voor vroege detectie van subtiele afwijkingen.

In **Deel 2** stellen we een nieuwe methode voor die kijkt naar de eigenschappen van de hartspier met behulp van echografie met hoge beeldfrequentie en *shear wave* afbeeldingstechnieken.

De propagatiesnelheid van *shear waves* zijn gerelateerd aan weefsel stijfheid. In **Hoofdstuk 8** laten we zien dat een reguliere klinisch echoscanner de snelheid van *shear waves* kan bepalen in de conventionele oorspronkelijke tissue Doppler imaging (TDI) mode in weefselfantomen en *in vivo* in parasternale probe-positie.

Het onderzoek was uitgevoerd op weefselfantomen, waarbij de *shear waves* werden geïnduceerd en gevolgd met een experimenteel echosysteem als referentie. Het klinische systeem kon beeldfrequenties tussen de 400 en 700 beelden per seconde halen in TDI mode via nauwkeurige instelling van afbeeldingsparameters. De *shear wave* snelheden gemeten met het klinisch systeem zaten dicht bij de waardes gemeten met het experimentele echosysteem, met een gemiddeld verschil van $0,18 \pm 0,22$ m/s, en zogenaamde limieten van overeenkomst tussen $-0,27$ en $+0,63$ m/s, wat als voldoende kan worden gezien voor onderzoeksdoeleinden.

De stijfheid van de hartspier, gemeten met niet-invasieve *shear wave* elastografie, kan mogelijk worden gebruikt voor kwantificatie van het functioneren van de hartspier. Klinische diagnose heeft echter een hoge precisie van een meting nodig. In **Hoofdstuk 9** hebben we de herhaalbaarheid bepaald van de uitkomst van *shear wave* propagatiesnelheden die op natuurlijke wijze ontstaan na het sluiten van de aortaklep en de mitraalklep. Dit hebben we onderzocht met twee klinische systemen: de ene is de reguliere klinisch echoscanner zoals hiervoor beschreven, de andere is een klinisch systeem dat door de fabrikant is aangepast om hogere beeldfrequenties op te nemen en de data onbewerkt op te slaan voor latere verwerking. In een groep van gezonde vrijwilligers hadden de inter-scan en intra-scan waardes een vrijwel gelijk bereik. Propagatiesnelheden waren herhaalbaar op verschillende dagen. We hebben verschillen gevonden in de waardes tussen de twee klinische systemen, die we verklaren uit verschillen in beeldfrequentie en in verwerkingsmethode van de beelden. Uit analyse van de verschillen

tussen de gezonde vrijwilligers bleek dat deze voornamelijk veroorzaakt worden door meetonzekerheid. Deze meetonzekerheid kan verkleind worden tot klinisch acceptabele waardes door over meerdere hartslagen te middelen.

In **Hoofdstuk 10** passen we de klinische hoge beeldfrequentie TDI toe op gezonde vrijwilligers en patiënten met hypertrofische cardiomyopathie (HCM) om de propagatiesnelheid te meten na het sluiten van de aortaklep en de mitraalklep. In HCM was de gemiddelde snelheid $5,1 \pm 0,7$ m/s voor de golf na sluiten van de aortaklep ($3,61 \pm 0,46$ m/s in leeftijds-passende groep van gezonden, $p < 0,0001$) en $6,88 \pm 1,12$ m/s voor de *shear wave* na mitraalklepsluiting ($4,65 \pm 0,77$ m/s in leeftijds-passende groep van gezonden, $p < 0,0001$). De significant verschillende snelheden tussen de twee groepen, vrijwel zonder overlappende waardes, suggereert dat ze gebruikt kunnen worden om verschillen te bepalen tussen normaal en pathologisch hartspierweefsel. Een drempelwaarde van 4 m/s voor de *shear wave* na sluiten van de aortaklep classificeerde pathologische hartspier met 95% gevoeligheid en 90% specificiteit.

Een lokale variatie in stijfheid zou moeten verschijnen als een lokale variatie in de propagatiesnelheid van de natuurlijk-voorkomende *shear waves*. In **Hoofdstuk 11** tonen we dit aan bij patiënten met lokaal littekenweefsel in de hartspier. Met deze techniek zou in de toekomst ook elasticiteitskaarten gemaakt kunnen worden met behulp van automatische volg-algoritmies.

In de apicale probe-positie wordt een golf-achtig patroon zichtbaar op het interventriculaire septum na de boezemcontractie in de hoge-beeldfrequentie TDI beelden. De propagatiesnelheid van dit patroon na boezemcontractie was al eerder geïntroduceerd in de literatuur als maat voor de linker-kamer stijfheid in ontspannen toestand. In **Hoofdstuk 12** hebben we dit patroon onderzocht in dezelfde groep patiënten met hypertrofische cardiomyopathie en gezonde vrijwilligers als in hoofdstuk 8. Onze resultaten suggereren dat dit patroon niet de eigenschappen heeft van een longitudinale golf, in tegenstelling tot wat eerdere studies suggereerden. In ongeveer de helft van de patiënten laat de golf-propagatie een acceleratie zien in het basaal-tot-midden gebied van de septale wand. Onze hypothese voor de reden van deze acceleratie is dat de maximale longitudinale rek van de linker kamer wordt bereikt in de HCM patiënten waardoor de momentane stijfheid zeer snel toeneemt. In tegenstelling tot eerdere hoopgevende resultaten lijkt de methode niet voldoende gevoelig voor stijfheidsmetingen tenzij deze acceleratie wordt meegenomen in de analyse.

Linker-kamer stromingspatronen zijn gemeten in eerdere studies om mogelijk vroege tekenen van dysfunctie van het hart te detecteren. Een relatief nieuwe manier van het

kwantificeren van de stromingspatronen, genaamd echo-deeltjes snelheidsafbeeldingstechniek (*echo-particle image velocimetry*, echoPIV) volgt de beweging van echografische contrast middelen in het bloed. De lage framerates (50 -75 Hz) van de huidige generatie van klinische echoscanners zorgt echter voor aanzienlijke onderschatting van stroomsnelheden. Dit komt door de relatief grote verplaatsing van de microbellen in het contrastmiddel tussen de opeenvolgende beelden. De recente mogelijkheden van hoge beeldfrequentie echografie, nu aangepast voor detectie van deze contrastmiddelen, geeft een beeldfrequentie die tot 100 keer hoger is dan op de conventionele scanners. In **Hoofdstuk 13** geven we hiermee een eerste voorbeeld van echoPIV waarbij we de snelheid schatten van de hoge-snelheids trans-mitrale pluim in 2D, wat niet mogelijk was met voorgaande conventionele beeldfrequenties.

De **discussie** vat de resultaten samen van ons onderzoek en analyseert de implicaties, sterktes en limitaties van deze nieuwe methode. Het bevat ook een vooruitblik op het mogelijk pad in de richting van klinische toepassing. We weten nog niet of stijfheid *an sich* een goede maat is voor het functioneren van het hart in zijn geheel. Verder, om hoge diagnostische opbrengst en klinische relevantie te hebben in de vroege detectie van hartfalen, moeten de *shear wave* snelheden een continu verloop hebben in de ontwikkeling van normaal naar pathologisch. Deze twee punten moet nog getest worden in theoretische modellen, in grotere controlegroepen, en in pathologische harten.



INTERNATIONAL JOURNALS

1. **Strachinaru M**, Morissens M, Latifyan S, Costescu I. Left atrial septal pouch thrombus assessed on three-dimensional transoesophageal echocardiography, *Eur Heart J Cardiovasc Imaging*. 2012;13(11): 967. doi: 10.1093/ehjci/jes122
2. **Strachinaru M**, Wauthy P, Sanoussi A, Morissens M, Costescu I, Catez E. The left atrial septal pouch as a possible location for thrombus formation. *J Cardiovasc Med (Hagerstown)*. 2013. doi: 10.2459/JCM.0b013e328360297e
3. **Strachinaru M**, Damry N, Nazeri A, Jousten I, Costescu I. Right-sided gothic aortic arch and Kommerell diverticulum. *Eur Heart J Cardiovasc Imaging*. 2013;14(9):864. doi: 10.1093/ehjci/jet043. Epub 2013 Mar 20.
4. **Strachinaru M**, Gazagnes MD, Mabiglia C, Costescu I. Coumadin ridge mass assessed on three-dimensional transoesophageal echocardiography. *Acta Cardiol*. 2013; 68(2):193-6.
5. **Strachinaru M**, Tran-Ngoc E, Damry N, Costescu I. An atypical evolution of tako-tsubo cardiomyopathy, *Acta Cardiol*. 2013;68(2):193-6
6. **Strachinaru M**, Damry N, Pavel O, Verbeet T. A short-lived valvular mass, *Eur Heart J*. 2014;35(18):1222. doi: 10.1093/eurheartj/ehf523
7. **Strachinaru M**, Papadopoulou B, Damry N, Laureys M, Samyn S. Contrast echocardiography detecting a rare abnormal venous connection, *European Heart Journal - Cardiovascular Imaging* 2015; doi: 10.1093/ehjci/jev062
8. **Strachinaru M**, van Dalen BM, Van Mieghem N, De Jaegere PP, Galema TW, Morissens M, Geleijnse ML. Relation between E/e' ratio and NT-proBNP levels in elderly patients with symptomatic severe aortic stenosis, *Cardiovasc Ultrasound*. 2015;13(1):29. doi: 10.1186/s12947-015-0021-8
9. **Strachinaru M**, Annis C, Catez E, Jousten I, Lutea ML, Pavel O, Morissens M. The mitral annular displacement by two-dimensional speckle tracking: a new tool in evaluating the left atrial function. *J Cardiovasc Med (Hagerstown)*. 2016;17:344-53. doi: 10.2459/JCM.0000000000000346
10. **Strachinaru M**, Damry N, Duttman R, Wauthy P, Catez E, Lutea M, Costescu I, Morissens M. Ultrasound Contrast Quantification for the Diagnosis of Intracardiac Masses. *JACC Cardiovasc Imaging*. 2016. pii: S1936-878X(15)00869-4. doi: 10.1016/j.jcmg.2015.06.025.
11. **Strachinaru M**, Wauthy P, Goffin C, Damry N. Rheumatic multiple valve disease and severe asymptomatic arterial occlusion. *Eur Heart J*. 2016. pii: ehw163.
12. **Strachinaru M**, Catez E, Jousten I, Pavel O, Janssen C, Morissens M, Gazagnes MD. The Left Atrial Septal Pouch as a Possible Risk Factor for Stroke. *Echocardiography*. 2016. doi: 10.1111/echo.13211.
13. **Strachinaru M**, Castro-Rodriguez J, Verbeet T, Gazagnes MD. The left atrial septal pouch as a risk factor for stroke: A systematic review. *Arch Cardiovasc Dis*. 2017. pii: S1875-2136(17)30026-8. doi: 10.1016/j.acvd.2017.01.001.
14. **Strachinaru M**, Bosch JG, van Dalen BM, van Gils L, van der Steen AFW, de Jong N, Geleijnse ML, Vos HJ. Cardiac Shear Wave Elastography Using a Clinical Ultrasound System. *Ultrasound Med Biol*. 2017;43(8):1596-1606. doi: 10.1016/j.ultrasmedbio.2017.04.012.

15. **Strachinaru M**, Huurman R, Schinkel AFL. Functional imaging in echocardiography can sometimes replace direct structure visualization. *Eur Heart J Cardiovasc Imaging*. 2019. doi: 10.1093/ehjci/jey180
16. **Strachinaru M**, Bosch JG, van Gils L, van Dalen BM, Schinkel AFL, van der Steen AFW, de Jong N, Michels M, Vos HJ, Geleijnse ML. Naturally occurring shear waves in healthy volunteers and hypertrophic cardiomyopathy patients. *Ultrasound Med Biol*. 2019. doi: 10.1016/j.ultrasmed-bio.2019.04.004.
17. **Strachinaru M**, Geleijnse ML, de Jong N, van den Bosch AE, Michels M, Schinkel AFL, van der Steen AFW, Bosch JG, Vos HJ. Myocardial stretch post atrial contraction in healthy volunteers and hypertrophic cardiomyopathy patients. *Ultrasound Med Biol*. 2019 May 30. pii: S0301-5629(19)30189-9. doi: 10.1016/j.ultrasmedbio.2019.04.031.
18. **Strachinaru M**, Kievit CM, Yap SC, Hirsch A, Geleijnse ML, Szili-Torok T. Multiplane/3D transesophageal echocardiography monitoring to improve the safety and outcome of complex transvenous lead extractions. *Echocardiography* 2019. doi: 10.1111/echo.14318.
19. **Strachinaru M**, MD, Ren B, van Dalen BM, Van Mieghem NM, De Jaegere PTT, van Gils L, Galema TW, Geleijnse ML. Determinants of changes in pulmonary artery pressure in patients with severe aortic stenosis treated by transcatheter aortic valve implantation. *Acta Cardiologica*. 2020 (in press)
20. Catez E, Barbraud C, Hunter K, **Strachinaru M**. Atypical presentation of tuberculous constrictive pericarditis: case report and review of the literature. *Acta Cardiol*. 2012;67(3):337-42
21. Catez E, Sina B, De Coodt P, Peperstraete B, Ngoc ET, Castro J, Morissens M, Flores G, **Strachinaru M**, Verbeet T. Management of atrial fibrillation in 2011, *Rev Med Brux*. 2011;32(4):328-41.
22. Verbeet T, Knecht S, Rondia G, Massin M, Ngoc ET, Vivian GF, Morissens M, Peperstraete B, Tatnga V, Catez E, **Strachinaru M**, Decoodt P, Castro J. Cryotherapy is a very effective and safe method for ablation of parahissian accessory pathways, *Acta Cardiologica* 2011; 66:1 (98-)
23. van Dalen BM, **Strachinaru M**, van der Swaluw J, Geleijnse ML. A simple, fast and reproducible echocardiographic approach to grade left ventricular diastolic function. *Int J Cardiovasc Imaging*. 2016. DOI 10.1007/s10554-015-0832-6
24. Boudart C, Tabolcea I, **Strachinaru M**, Castro J, Nosedá A, Gottignies P, Reper P. Acute coronary syndrome and platypnoea-orthodeoxia with thoracic and interauricular septal aneurysms. *Eur Rev Med Pharmacol Sci*. 2016;20(2):301-4.
25. de Groot-de Laat LE, Ren B, McGhie J, Oei FB, **Strachinaru M**, Kirschbaum SW, Akin S, Kievit CM, Bogers AJ, Geleijnse ML. The role of experience in echocardiographic identification of location and extent of mitral valve prolapse with 2D and 3D echocardiography. *Int J Cardiovasc Imaging*. 2016;32(8):1171-7. doi: 10.1007/s10554-016-0895-z.
26. den Uil CA, **Strachinaru M**, van der Hoven B, Meeder JHJ. Assessment of paravalvular leakage after transcatheter aortic valve implantation: add clinical signs to echocardiographic data. *Echo Res Pract*. 2017;4(4):I15-I16. doi: 10.1530/ERP-17-0041.
27. Schinkel AFL, Akin S, **Strachinaru M**, Muslem R, Soliman OII, Brugts JJ, Constantinescu AA, Manintveld OC, Caliskan K. Safety and feasibility of contrast echocardiography for the evaluation of patients with HeartMate 3 left ventricular assist devices. *Eur Heart J Cardiovasc Imaging*. 2018;19(6):690-693. doi: 10.1093/ehjci/jex177.

28. Costescu Strachinaru DI, Chaumont M, Gobin D, Sattar L, **Strachinaru M**, Karakike E, Roman A, Koponicki D. Hemophagocytic lymphohistiocytosis associated to Haemophilus parainfluenzae endocarditis- a case report. *Acta Clin Belg*. 2018;73(3):220-223. doi: 10.1080/17843286.2017.1341691
29. van Grootel RWJ, **Strachinaru M**, Menting ME, Vletter-McGhie JS, Roos-Hesselink JW, van den Bosch AE. In depth echocardiographic analysis of left atrial function in healthy adults using speckle tracking echocardiography and volumetric analysis. *Echocardiography*. 2018. doi: 10.1111/echo.14174.
30. van Velzen HG, van Grootel RWJ, van Slegtenhorst MA, **Strachinaru M**, Michels M. Five-Year Prognostic Significance of Global Longitudinal Strain in Individuals with a Hypertrophic Cardiomyopathy Gene Mutation without Hypertrophic Change. *Neth Heart J*. 2019. doi: 10.1007/s12471-019-1226-5.
31. Feyz L, Theuns DA, Bhagwandien R, **Strachinaru M**, Kardys I, Van Mieghem NM, Daemen J. Atrial fibrillation reduction by renal sympathetic denervation: 12 months' results of the AFFORD study. *Clin Res Cardiol*. 2019. doi: 10.1007/s00392-018-1391-3.
32. Voorneveld J, Keijzer LBH, **Strachinaru M**, Bowen DJ, Goei JSL, Ten Cate F, van der Steen AFW, de Jong N, Vos HJ, van den Bosch AE, Bosch JG. High Frame Rate echoPIV can Measure the High Velocity Diastolic Flow Patterns. *Circ Cardiovasc Imaging*. 2019;12(4):e008856. doi: 10.1161/CIRCIMAGING.119.008856.
33. van den Berg VJ, **Strachinaru M**, Akkerhuis KM, Baart S, Brankovic M, Constantinescu AA, Cornel JH, Manintveld OC, Victor Umans VAWM, Rizopoulos D, Geleijnse ML, Boersma E, van Dalen BM, Kardys I. Repeated Echocardiograms do not provide Incremental Prognostic Value to Single Echocardiographic Assessment in Minimally Symptomatic Patients with Chronic Heart Failure: Results of the Bio-SHIFT Study. *J Am Soc Echocardiogr*. 2019; DOI: 10.1016/j.echo.2019.04.419.
34. Keijzer LBH, **Strachinaru M**, Bowen DJ, Geleijnse ML, van der Steen AFW, Bosch JG, de Jong N, Vos HJ. Reproducibility of Natural Shear Wave Elastography Measurements. *Ultrasound Med Biol*. 2019; pii: S0301-5629(19)31502-9. doi: 10.1016/j.ultrasmedbio.2019.09.002.
35. Klimczak-Tomaniak D, van den Berg VJ, **Strachinaru M**, Akkerhuis KM, Baart SJ, Caliskan K, Manintveld OC, Umans VAWM, Geleijnse ML, Boersma H, van Dalen BM, Kardys I. Longitudinal patterns of NT-proBNP, troponin T and CRP in relation to the dynamics of echocardiographic parameters in heart failure patients. *Eur Heart J Cardiovasc Imaging*. 2019. doi: 10.1093/ehjci/jez242

NATIONAL JOURNALS

1. **Strachinaru M**. Alternative to hypolipemiant treatment – phytosteroles. *National Medical Journal* 2005 (article in Romanian);IX(1-2).
2. **Strachinaru M**, Costescu DI. Pulmonary stenosis in an elderly patient, *CARDIOLOGIE PRATIQUE* 2010; 933: ISSN 0766-3633.
3. **Strachinaru M**. Left atrium neoplastic invasion complicated by atrial fibrillation, *Journal de Cardiologie* 2012; 4: 247-248

BOOK CHAPTERS

1. Caliskan K, **Strachinaru M**, Soliman OI. Tricuspid Regurgitation in Patients with Heart Transplant. Practical Manual of Tricuspid Valve Disease, <https://link.springer.com/book/10.1007/978-3-319-58229-0>.
2. Soliman OI, McGhie J, Anwar AM, **Strachinaru M**, Geleijnse ML, ten Cate F. Tricuspid Valve Disease: Imaging Using Transthoracic Echocardiography. Practical Manual of Tricuspid Valve Disease, <https://link.springer.com/book/10.1007/978-3-319-58229-0>.



P

PhD training	Year	ECTS
Courses		
COEUR course Molecular Biology in Cardiovascular Research 2014	2014	0.5
COEUR course Patophysiology of Ischemic Heart Disease 2014	2014	0.5
COEUR course Intensive Care Research 2014	2014	0.5
COEUR course Cardiovascular Imaging and Diagnostics 2017	2017	0.5
Eendaagse training Begeleiden van aios (TtT III) 2018	2018	0.3
International conferences		
Belgian Society of Cardiology 33 rd Annual Scientific Meeting	2014	0.9
From Gout to Cardiovascular Disease: a Central Role for Uric Acid Bologna, Italy 2014	2014	0.9
EuroEcho-Imaging Congress Vienna, Austria 2014	2014	1.2
American Society of Echocardiography 26 th Annual Scientific Sessions Boston, USA 2015	2015	1.5
EuroEcho-Imaging Congress Seville, Spain 2015	2015	1.2
EuroEcho-Imaging Congress Leipzig, Germany 2016	2016	1.2
EuroEcho-Imaging Congress Lisbon, Portugal 2017	2017	1.2
EuroEcho-Imaging Congress Milan, Italy 2018	2018	1.2
ESC Congress Munich, Germany 2018	2018	1.5
NVVC Jubileumcongres 2019	2019	0.9
Heart Failure Congress – European Society of Cardiology Athens, Greece 2019	2019	1.2
ESC Congress Paris, France 2019	2019	1.5
Seminars and workshops		
Highlights of AHA congress 2017	2017	0.3
Nascholing NVvC Intensive Care	2017	0.3
LOK Belgian educational program for medical professionals 2017: High frame rate imaging - application clinique	2017	0.3
LOK Belgian educational program for medical professionals 2017: Chronic coronary occlusions	2017	0.3
LOK Belgian educational program for medical professionals 2017: Cardiology in the elderly: up to where to go?	2017	0.3
PhD training		
Echo avond "Beeldvorming bij patienten met ernstig hartfalen" 2018	2018	0.3
8 ^e regionale Hartfalen bijeenkomst 2018	2018	0.3
9 ^e regionale Hartfalen bijeenkomst 2018	2018	0.3
LOK Belgian educational program for medical professionals 2018: ARNI, 2 years after	2018	0.3
LOK Belgian educational program for medical professionals 2018: Cardiac revalidation programs	2018	0.3
Echocardiography workshop "Advanced heart failure, artificial heart implantation and heart transplantation" Bad Oeynhausen 2018	2018	1.2
Rechter Ventrikel falen oorzaak of gevolg van Tricuspidalisklep Insufficiëntie	2018	0.6
LOK Belgian educational program for medical professionals 2019: Stress echocardiography: state of the art	2019	0.3

Presentations

EuroEcho-Imaging Congress Vienna, Austria 2014	2014	0.8
Belgian Society of Cardiology 33 rd Annual Scientific Meeting	2014	0.5
EuroEcho-Imaging Congress Seville, Spain 2015	2015	0.3
American Society of Echocardiography scientific sessions Boston, USA 2015	2015	0.5
EuroEcho-Imaging Congress Leipzig, Germany 2016	2016	0.3
EuroEcho-Imaging Lisbon, Portugal 2017	2017	1.1
EuroEcho-Imaging Milan, Italy 2018	2018	0.8
IEEE IUS 2018 Kobe, Japan 2018	2018	0.3
Proceedings of the Sixteenth International Tissue Elasticity Conference Avignon, France 2018	2018	0.2
The 24th European symposium on Ultrasound Contrast Imaging Rotterdam, The Netherlands 2019	2019	0.2
7 th Dutch Bio-Medical Engineering Conference; Egmond aan zee, Netherlands 2019	2019	0.2

Lecturing

Short course on "Echocardiographic assessment of intracardiac masses" for residents 2016	2016	0.3
--	------	-----

PhD training

	Year	ECTS
Lecture ECHO avond ASZ 2016: Intracardiale massa's en cardiale emboliebronnen: diagnostiek middels (contrast)echocardiografie, cardio CT en cardio MRI.	2016	0.6
Short course on "TEE Evaluation of the Patient for Cardiac Source of Embolism" for residents 2016	2016	0.3
Lecture COEUR course Cardiovascular Imaging and Diagnostics 2017: Valvular and ischemic disease –US	2017	0.6
Lecture LOK (Lokale kwaliteitsgroep) educational program Belgium 2017: High frame rate imaging - application clinique	2017	0.6
Short course on "3D Echocardiography" for sonographers 2017	2017	0.3
Lecture symposium Rechter Ventrikel falen oorzaak of gevolg van Tricuspidalisklep Insufficiëntie 2018: "Challenges" van TV imaging met echocardiografie	2018	0.6
Short course on "Technical aspects of echocardiography" for sonographers 2018	2018	0.3
Short course on "Update on LVAD/ heart transplant echocardiography" for heart failure specialists 2018	2018	0.3
Research colloquium UMC Utrecht 2019: Shear wave imaging and high frame rate echocardiography	2019	0.6
	Total	31.4

C



Mihai Strachinaru was born on the 11th of May 1976 in Iasi, Romania. Upon completing secondary school he moved to Bucharest where he completed his Medical Doctor (MD) degree, finishing in the top of his year in 2001. He then went on to train in Cardiology at the “Carol Davila” University of Medicine and Pharmacy Bucharest until 2007. During this period he developed a keen interest in cardiac non-invasive imaging, with a special interest in echocardiography. He then moved on to work as a cardiologist in France (2008-2009), Belgium (2009-2016) and The Netherlands (2016-2019). He currently holds Romanian, French and European certifications in transthoracic and transesophageal echocardiography.

His research interests cover both the clinical and the fundamental aspects of cardiac imaging. Beside the clinical duties, the last 5 years were dedicated to the research work that led tot his thesis.

